HYDRODYNAMIC STUDIES IN TWO AND

THREE–PHASE SLURRY BUBBLE COLUMN REACTORS

Volume II

A Dissertation

by

JAMES G. DALY

Submitted to the Office of Graduate Studies of
Texas A&M University
in partial fulfillment of the requirements for the degree of

DOCTOR OF PHILOSOPHY

August 1990

Major Subject: Chemical Engineering

HYDRODYNAMIC STUDIES IN TWO AND

THREE–PHASE SLURRY BUBBLE COLUMN REACTORS

Volume II

A Dissertation

by

JAMES G. DALY

Approved as to style and content by:

_____

Dragomir B. Bukur
(Chair of Committee)

_____

Ahmed M. Gadalla
(Member)

_____

Albert T. Watson
(Member)

_____

Fred R. Best
(Member)

_____

Raymond W. Flumerfelt
(Head of Department)

August 1990

TABLE OF CONTENTS

LIST OF TABLES

Volume II

LIST OF FIGURES

Figure   Page

Figure   Page

Figure   Page

Volume II

CHAPTER IV
AXIAL SOLIDS DISTRIBUTION

Knowledge of axial solids distribution is essential to properly design a slurry bubble column reactor. The distribution of solid particles in a bubble column reactor has an effect on reactant conversion and may affect product selectivity (Bukur and Kumar, 1986; Smith and Ruether, 1985). Operating conditions (i.e. gas and slurry velocity), physical properties of the liquid medium, particle size and density, and column diameter influence the axial distribution of solid particles in a slurry bubble column reactor.

In this study, the effect of particle size and type, column diameter, slurry velocity and gas velocity on axial solids distribution was examined. The semi—infinite dispersion model presented by Smith and Ruether (1985) was used to analyze our results. The theory (semi—infinite dispersion model), a summary of the average solids concentrations in the bubble column and storage tank during each run, and results (i.e. axial solids distributions and axial solids dispersion coefficients) from our studies are discussed.

Semi—Infinite Dispersion Model

Several variations of the one—dimensional sedimentation dispersion model, based on different frames of reference, are available in the literature. The model presented by Parulekar and Shah (1980) is based on the cross—sectional area of the column; whereas, the models by Cova (1966), Kato et al. (1972), Smith and Ruether (1985), and O'Dowd et al. (1987), are based on the cross—sectional area occupied by the slurry phase alone (i.e. the area associated with the gas phase is not included). More recently, Murray and Fan (1989) developed a mechanistic model to describe the solids distribution in slurry bubble columns. In the present analysis, the model presented by Smith and Ruether (1985) was used to analyze our experimental data. Their one—dimensional dispersion

model is given by

$$\frac{\delta}{\delta x}\left[\frac{-E_s}{H_{exp}}\frac{\delta C_s}{\delta x}\right] + \frac{\delta}{\delta x}\left[\left[\frac{u_{s\ell}}{(1-\epsilon_g)} - \Phi_\ell u_p\right]C_s\right] = H_{exp}\frac{\delta c_s}{\delta t} \qquad (4.1)$$

where x is the dimensionless height above the distributor (based on the expanded height, H_{exp}), E_s is the axial solids dispersion coefficient, C_s is the solids concentration in the slurry, $u_{s\ell}$ is the average slurry flow rate, u_p is the hindered settling velocity of the solid particles, Φ_ℓ is the volume fraction of liquid in the slurry, and t is the time. The solids concentration in the slurry, C_s is defined as

$$C_s = \omega_s\rho_{s\ell} \qquad (4.2)$$

where ω_s is the weight fraction of solids and $\rho_{s\ell}$ is the density of the slurry.

Since the volume fraction of liquid in the slurry, Φ_ℓ, does not vary significantly with axial position (less than 3% for our experiments), an average value may be used and is defined as:

$$\overline{\Phi_\ell} = (1 - \frac{\overline{C_s}}{\rho_s}) \qquad (4.3)$$

where ρ_s is the density of the solids and $\overline{C_s}$ is the average solids concentration in the slurry and is given by

$$\overline{C_s} = \frac{\sum\limits_i C_{s_{ij}}V_{ij}}{V_T} \qquad i = 1 \text{ to } 5 \text{ and } j = i+1 \qquad (4.4)$$

where V_T is the total volume of slurry, V_{ij} is the volume of slurry between pressure ports i and j (see Figure 2.9) and $C_{s_{ij}}$ is the solids concentration in the slurry between pressure ports i and j. Note, j = 6 corresponds to the top of the column. The total volume of slurry is

$$V_T = h_{exp}(1 - \epsilon_g) \qquad (4.5)$$

where h_{exp} is the expanded height of the dispersion and ϵ_g is the average gas holdup in the column. The volume of slurry between pressure ports i and j is

$$V_{ij} = \Delta h_{ij}(1 - \epsilon_{g_{ij}}) \qquad i = 1 \text{ to } 5 \text{ and } j = i+1 \qquad (4.6)$$

where Δh_{ij} is the distance between pressure ports i and j and $\epsilon_{g_{ij}}$ is the axial gas holdup in the i,j section of the column.

For batch experiments (i.e. $u_{s\ell} = 0$) at steady state (no time derivatives), and assuming no dependency of Φ_ℓ on height, Eq. 4.1 reduces to

$$\frac{\delta}{\delta x}\left[\frac{-E_s}{H_{exp}}\frac{\delta C_s}{\delta x}\right] - \frac{\delta}{\delta x}\left[\overline{\Phi_\ell} u_p C_s\right] = 0 \qquad (4.7)$$

Equation 4.7 may be integrated twice to yield:

$$C_s = C_1 + C_2 \exp\left[-H_{exp}\overline{\Phi_\ell}\frac{u_p}{E_s}x\right] \qquad (4.8)$$

For the semi–infinite dispersion model, the boundary conditions are given by: $C_s = 0$ as x approaches infinity and $C_s = C_s^B$ for x=0, where C_s^B is the concentration of solids at the bottom of the dispersion. Application of these boundary conditions to Eq. 4.8 yields:

$$C_s = C_s^B \exp\left[-H_{exp}\overline{\Phi_\ell}\frac{u_p}{E_s}x\right] \qquad (4.9)$$

Solids concentration vs. axial position data can now be used to obtain estimates of $\frac{u_p}{E_s}$ and the concentration of solids at the bottom of the column, C_s^B, using regression analysis.

For continuous slurry flow, the solution to Eq. 4.1 is:

$$C_s = (C_s^B + a)\exp\left[-(u_p\overline{\Phi_\ell} - u_{s\ell}')\frac{H_{exp}}{E_s}x\right] - a \qquad (4.10)$$

where $a = \frac{u_{s\ell}' C_s^f}{\overline{\Phi_\ell} u_p - u_{s\ell}}$ and $u_{s\ell}' = \frac{u_{s\ell}}{(1-\epsilon_g)}$. The quantity C_s^f is the concentration of solids in the feed (or storage tank). It is assumed that no settling occurs in the feed stream (i.e.,

at x<0, $u_p = 0.0$ and $\frac{\delta C_s}{\delta x} = 0.0$). In developing Eqs. 4.9 and 4.10, it was assumed that the gas holdup did not vary with axial position. The assumption of an axially uniform gas holdup holdup profile leads to the assumptions of a constant (i.e. no axial variation) dispersion coefficient and a constant hindered settling velocity. With the exception of experiments in which foam was produced, axial gas holdup profiles were fairly uniform (see Figures 2.14 and 2.15). The model also assumes a uniform particle size.

A variety of approaches may be used to obtain values for u_p, E_s, and C_s^B (see Eq. 4.10). Kato et al. (1972) assumed that E_s and u_p were not affected by slurry velocity, $u_{s\ell}$. They used the quantity $\frac{u_p H_{exp}}{E_s}$ obtained from batch experiments (see Eq. 4.9) together with two points taken from a smoothed plot of concentration versus axial position (continuous experiment) to obtain a value for $\frac{u'_{s\ell} H_{exp}}{E_s}$, from which E_s was calculated. Then substituting the values of E_s and H_{exp} into $\frac{u_p H_{exp}}{E_s}$, a value for u_p was obtained. On the other hand, Smith and Ruether (1985), used non–linear regression analysis of Eq. 4.10 to obtain E_s, u_p, and C_s^B.

For batch experiments, u_p and E_s are not separable, and in order to obtain axial dispersion coefficients, one must assume values for the hindered settling velocity of the solids, u_p. There are various correlations available in the literature for estimating the hindered settling velocity (e.g. Kato et al., 1972; Smith and Ruether, 1985; Zigrand and Sylvester, 1980; and O'Dowd et al., 1987). The correlations proposed by Kato et al., Smith and Ruether, and O'Dowd et al. are all of the form

$$u_p = a u_t^b u_g^c \overline{\Phi}_\ell^{-d} \qquad (4.11)$$

where u_t is the terminal rise velocity of a single particle in an infinite medium. The numerical values of constants (a, b, c, and d) in Eq. 4.10 are (1.33, 0.75, 0.25, 2.5) for Kato et al., (1.91, 0.8, 0.26, 3.5) for Smith and Ruether, and (1.69, 0.8, 0.23, 1.28) for O'Dowd et al. correlation.

Several correlations have been presented in the literature for predicting axial dispersion coefficients. The correlation proposed by Kato et al. is:

$$Pe_p = \frac{13Fr_g(1 + 0.009Re_pFr_g^{-0.8})}{1 + 8Fr_g^{0.85}} \tag{4.12}$$

The equation presented by Smith and Ruether is:

$$Pe_p = 9.6\left[\frac{Fr_g^6}{Re_g}\right]^{0.114} + 0.019Re_p^{1.1} \tag{4.13}$$

and the equation presented by O'Dowd et al. for an unbaffled bubble column is:

$$Pe_p = 7.7\left[\frac{Fr_g^6}{Re_g}\right]^{0.098} + 0.019Re_p^{1.1} \tag{4.14}$$

where $Pe_p = \frac{u_gd_{col}}{E_s}$, $Re_g = \frac{u_gd_{col}\rho_\ell}{\mu_\ell}$, $Fr_g = \frac{u_g}{\sqrt{gd_{col}}}$, and $Re_p = \frac{d_p\rho_\ell u_t}{\mu_\ell}$. The terms containing Re_p in Eqs. 4.12 to 4.14 are correction factors which take into account particle size. Due to insufficient data with different size particles, O'Dowd et al., used the correction factor presented by Smith and Ruether. Murray and Fan (1989) also presented an empirical correlation for predicting axial solids dispersion coefficients, E_s; however, their correlation does not take into account the effect of column diameter.

Summary of Solids Concentrations in the Column and Storage Tank

As mentioned in Chapter II, slurry samples were withdrawn from the storage tank and column during three–phase experiments. Table 4.1 contains the nominal solids concentration for each run, as well as the range of average solids concentration in the column and in the storage tank during each run. Also shown in Table 4.1 is the total amount of solids charged in the storage tank and the total amount of solids accounted for during each experiment. The experiment numbers given in the first column of Tables

4.1a (0.05 m ID column) and 4.1b (0.21 m ID column) correspond to the experiment numbers given in Tables 2.4 and 2.5, respectively.

For experiments conducted with small particles, the solids concentrations measured in both the storage tank and column were usually within 3 % (absolute) of the desired (or nominal) concentration. However, very low solids concentrations were observed in both the storage tank and bubble column during our initial continuous experiments with large iron oxide particles (experiments 19 and 20 in Table 4.1a) in the 0.05 m ID column. Following these experiments, the entire system was inspected and approximately 50% of the initial amount of solids charged in the storage tank was recovered in the expansion unit. The expansion unit was modified to reduce the amount of settling (see Figure 4.1). Partitions were added inside the expansion unit to minimize the surface area available for the deposition of solids. Experiments 26 and 27 were conducted with large iron oxide particles at superficial slurry velocities of 0.02 and 0.005 m/s following the modification of the expansion unit. There was some settling of solids during these experiments; however, the amount of settling was substantially less than that previously observed (i.e. the solids concentration in the column was 18 − 19 %). During experiment 27 ($u_{s\ell}$ = 0.005 m/s), the overflow line from the expansion unit to the calibration chamber (see Figure 4.1) plugged during the last gas velocity (i.e. u_g = 0.02 m/s), and the solids concentration in column dropped considerably (i.e. ω_s (column) = 19.2% at u_g = 0.04 m/s and 9.3 % at u_g = 0.02 m/s). Also, during this same experiment solids concentrations in the storage tank were very low (i.e. 6.9 − 8.4 wt%). Similar results were obtained during the experiment with SASOL wax and large iron oxide particles at a slurry flow rate of 0.005 m/s (see results for experiment 33 in Table 4.1a).

Solids accountability (large particles) was substantially better for experiments conducted in the large diameter column, with the exception of experiments 15 and 16 (see Table 4.1b). The solids concentration in these two experiments (both in the column and

Table 4.1a. Summary of Solids Concentrations for Experiments in the 0.05 m ID Bubble Column

EXP. No.	u_ℓ (m/s)	SOLIDS[a]	NOMINAL CONC (WT %)	AVG CONC IN COLUMN (WT %)	AVG CONC IN TANK (WT %)	AMOUNT CHARGED (g)	AMOUNT ACCOUNTED TANK+COLUMN (g)
4	0.005	1	10	9.5–10.0	N/A	1900	N/A
5	0.02	1	10	8.9–9.5	N/A	1900	N/A
6	0.0	1	10	9.5–10.2	N/A	1900	N/A
7	0.005	1	20	16.4–17.4	15.8–17.4	3910	3000–3100
8	0.02	1	20	17.3–17.7	16.9–18.3	3910	3400–3600
9	0.0	1	20	18.5–19.1	19.4	3910	3200
10	0.005	1	30	28.4–28.9	27.9–29.3	7282	6220–6300
11	0.02	1	30	28.5–29.3	27.6–28.6	7282	6300–6500
12	0.0	1	30	29.2–29.6	28.5–29.1	7282	6325–6370
13[e]	0.005	2	10	3.0–5.0	3.0–5.0	1765	200–650
14	0.005	3	10	9.2–10.5	8.6–9.4	1766	1410–1580
15	0.005	3	20	18.9–20.0	18.8–19.2	4284	3600–3800
16	0.02	3	20	17.2–18.6	18.1–19.1	4284	3400–3700
17	0.0	3	20	18.0–20.0	17.68	4284	3300–3400
18	0.005	3	30	26.3–28.1	25.1–27.1	7926	5100–5500
19	0.005	2	10	2.5–3.6	1.2–1.7	1816	230–370
20	0.02	2	10	5.3–6.5	4.2–5.2	1816	680–840
21	0.0	2	20	21.4–24.0	21.2	4103	3871–3960
22	0.0	4	20	7.5–8.2,20.2[b]	18.3	2800	2741
25	0.0	2	20	10,16–17[c]	19.3	4540	4120
26	0.02	2	20	17.8–19.5	15.6–17.0	4540	3600–3730
27	0.005	2	20	9,21–22.6[d]	6.9–8.4	4540	1790–2710
28	0.0	4	20	17.8–18.7	19.4	3280	3050
31	0.005	1	20	17.0–21.3	17.2–18.2	3936	3180–3540
32	0.0	2	20	18.3–22.6	18.5	3973	3820
33	0.005	2	20	14.6–18.3	9.9–10.8	3973	2032–2086
34[e]	0.005	2	20	N/A	N/A	3973	N/A

[a] 1: 0 – 5 μm iron oxide
    2: 20 – 44 μm iron oxide
    3: 0 – 5 μm silica
    4: 20 – 44 μm silica
[b] 20 wt% at u_g = 0.12 m/s
[c] 10 wt% at u_g = 0.02 m/s
[d] 9 wt% at u_g = 0.02 m/s
[e] Pump shut down during the experiment

Table 4.1b. Summary of Solids Concentration for Experiments
in the 0.21 m ID Bubble Column

EXP. No.	u_ℓ (m/s)	SOLIDS[a]	NOMINAL CONC (WT %)	AVG CONC IN COLUMN (WT %)	AVG CONC IN TANK (WT %)	AMOUNT CHARGED (g)	AMOUNT ACCOUNTED TANK+COLUMN (g)
6	0.0	1	10	9.7–10.1	9.2	13620	13260
7	0.0	1	20	18.0–19.9	20.6	30418	30640
8	0.005	1	20	20.2–20.7	20.4–20.9	30418	28550–29940
9	0.02	1	20	20.2–21.2	20.9–21.2	30418	28400–30300
10	0.0	1	20	19.0–21.2	20.3	30418	29680
11	0.005	1	20	20.3–21.0	19.7–21.1	30418	28500–29140
12	0.0	1	20	20.4–22.1	19.5	30418	27310
13	0.0	1	30	29.0–30.7	28.7–29.9	47216	45800–44970
14	0.005	30	29.3–30.3	29.5–30.0	47216	39400–43400	
15[b]	0.005	2	10	6.4–8.5	7.1–7.5	14272	8210–10120
16[b]	0.02	2	10	0.6–7.7	2.2–8.6	14272	1900–5160
17	0.0	2	20	17.2–22.2	21.1	41016	41467
18	0.005	2	20	20.9–24.9	18.0–20.9	41016	34310–39770
19	0.02	2	20	22.7–23.7	20.7–22.4	41016	40410–41100
20	0.0	2	20	18.5–22.9	N/A	41016	N/A
21	0.0	2	20	14.9,23.0–24.6[c]	N/A	41016	N/A
22	0.0	2	30	36.5–37.4	29.4	68710	63823
23	0.005	2	30	34.1–35.1	30.5–32.1	68710	59750–69240
24	0.02	2	30	33.1–36.6	32.4–34.9	68710	59750–69240
26	0.0	4	20	23.7–26.7	23.8	37355	39400
27	0.005	4	20	19.0–20.1	19.9–21.6	37355	31900–34100
28	0.02	4	20	18.5–23.0	19.5–21.8	37355	31970–34400
29	0.005	4	30	33.6–35.4	33.4–34.0	60764	60890–62470
33	0.0	2	20	13.0[c],20.4–21.2	N/A	30645	N/A
34	0.005	2	20	17.2–20.7	13.7–17.4	30645	21550–27704
35	0.005	2	20	15.8[c],19.9–21.5	14.4,18.0–19.7	33709	25320–35650

[a] 1: 0 – 5 μm iron oxide
2: 20 – 44 μm iron oxide
4: 20 – 44 μm silica
[b] Poor solids suspension in the storage tank
[c] Low solids concentrations at u_g = 0.02 m/s was due to settling in the bottom of the column
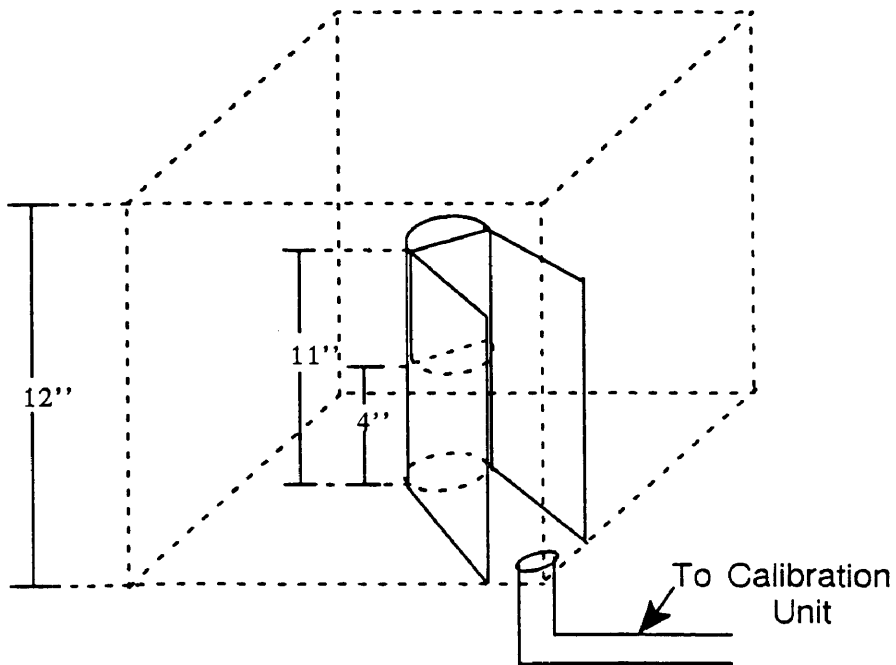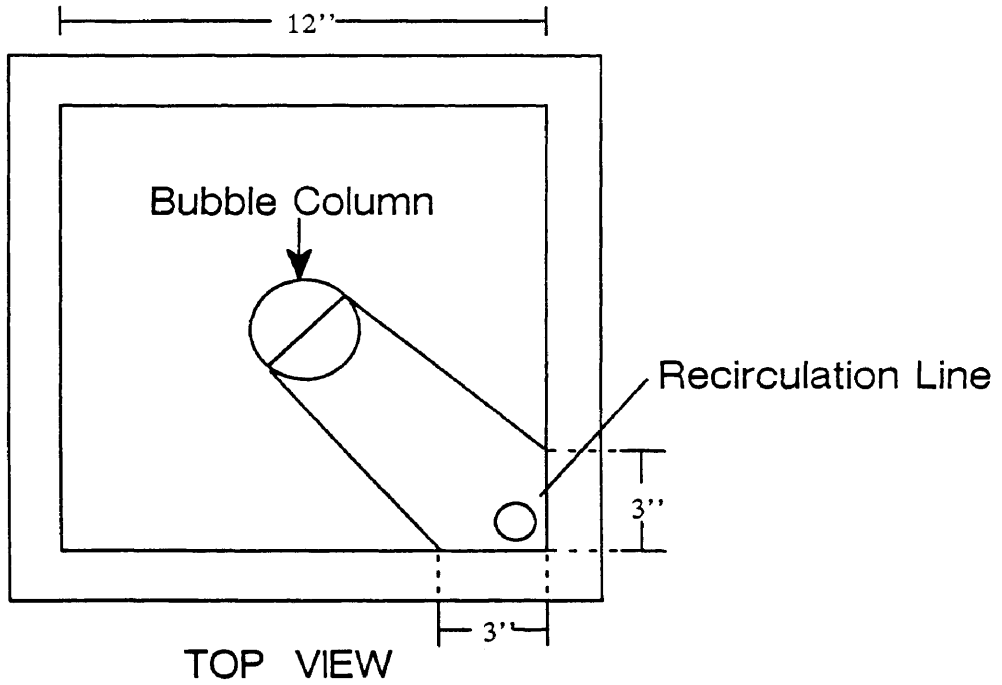
FIGURE 4.1. Schematic diagram of modified expansion unit.

storage tank) was considerably lower than the nominal wt% solids. After these runs, the system was shut down and inspected. It was found that the majority of solids had settled at the bottom of the storage tank. In order to improve mixing in the storage tank, a new propeller was installed. Following this modification, solids concentrations in the storage tank and bubble column were similar to the desired (or nominal) concentration. During three of the experiments with large particles (i.e. experiments 21, 33, and 35 in Table 4.1b), solids settled in the bottom of the column at a gas velocity of 0.02 m/s. Since we were unable to account for these solids, the measured solids concentrations in both the bubble column and storage tank were low at this gas velocity.

Following each batch of experiments, the slurry (wax + solids) was removed from the system and weighed. For experiments in the small column, approximately 90 − 95% of the slurry charged was recovered. And, for experiments in the large column, approximately 95 − 99% of the slurry charged was recovered.

Results and Discussion

Solids concentration profiles obtained from batch experiments in the 0.05 m ID column with large (i.e. 20 − 44 μm) iron oxide and silica particles were analyzed using the one−dimensional sedimentation dispersion model to obtain axial solids dispersion coefficients, E_s. Due to operational problems with both the pump (i.e. inability to maintain a constant flow rate) and settling of solids in the expansion unit, solids concentration data from experiments conducted in the continuous mode of operation in the small column were not analyzed. Data from both batch and continuous (one) experiments in the 0.21 m ID column with large particles were analyzed to obtain axial solids dispersion coefficients.

Regardless of the slurry flow rate, particle type, or column diameter, axial solids distributions were fairly uniform at all gas velocities for experiments conducted with

small (i.e. $0 - 5$ μm) particles. Figures 4.2a and 4.2b show axial solids concentrations (wt%) from batch experiments conducted with slurries containing 20 wt% small iron oxide and small silica particles, respectively, in the 0.05 m ID column. The decrease in axial solids concentration at a height of 2.2 m is due to the inability of the foam to suspend the solids. Solids concentrations from a batch experiment with $0 - 5$ μm iron oxide particles (20 wt%) in the 0.21 m ID column are shown in Figure 4.2c. Axial solids concentrations for experiments with small particles varied by less than 2 wt% (actual) across the entire column during all continuous experiments.

Solids concentration profiles from batch experiments with 20 wt% $20 - 44$ μm iron oxide and silica particles in the 0.05 m ID column are shown in Figures 4.3a and 4.3b, respectively. During these experiments, significant gradients in the axial solids distribution were observed. Our results from the continuous experiments with large iron oxide particles show that a slight upward slurry velocity (0.02 m/s) significantly improves the suspension of solids (see Figure 4.3c). During this experiment, there were some problems with the pump, and the actual slurry velocity ranged from approximately 0.01 to 0.03 m/s. However, these results indicate that solids suspension, which does not show any noticeable improvement when gas velocity is increased (see Figures 4.3a and 4.3b) improves significantly with the introduction of a small upward slurry flow. This is expected since the terminal settling velocity for large iron oxide particles is about 0.001 m/s and that for silica particles is 0.0004 m/s. Both of these values are well below the slurry circulation velocity ($0.01 - 0.03$ m/s).

Figures 4.4a and 4.4b show solid concentration profiles for batch experiments conducted with large iron oxide particles in the 0.21 m ID bubble column with the perforated plate (PP) and bubble cap (BC) distributors, respectively. Axial solids concentration profiles from experiments with the PP and BC distributors were similar. Solids concentration gradients in the small column for batch experiments with large particles (see
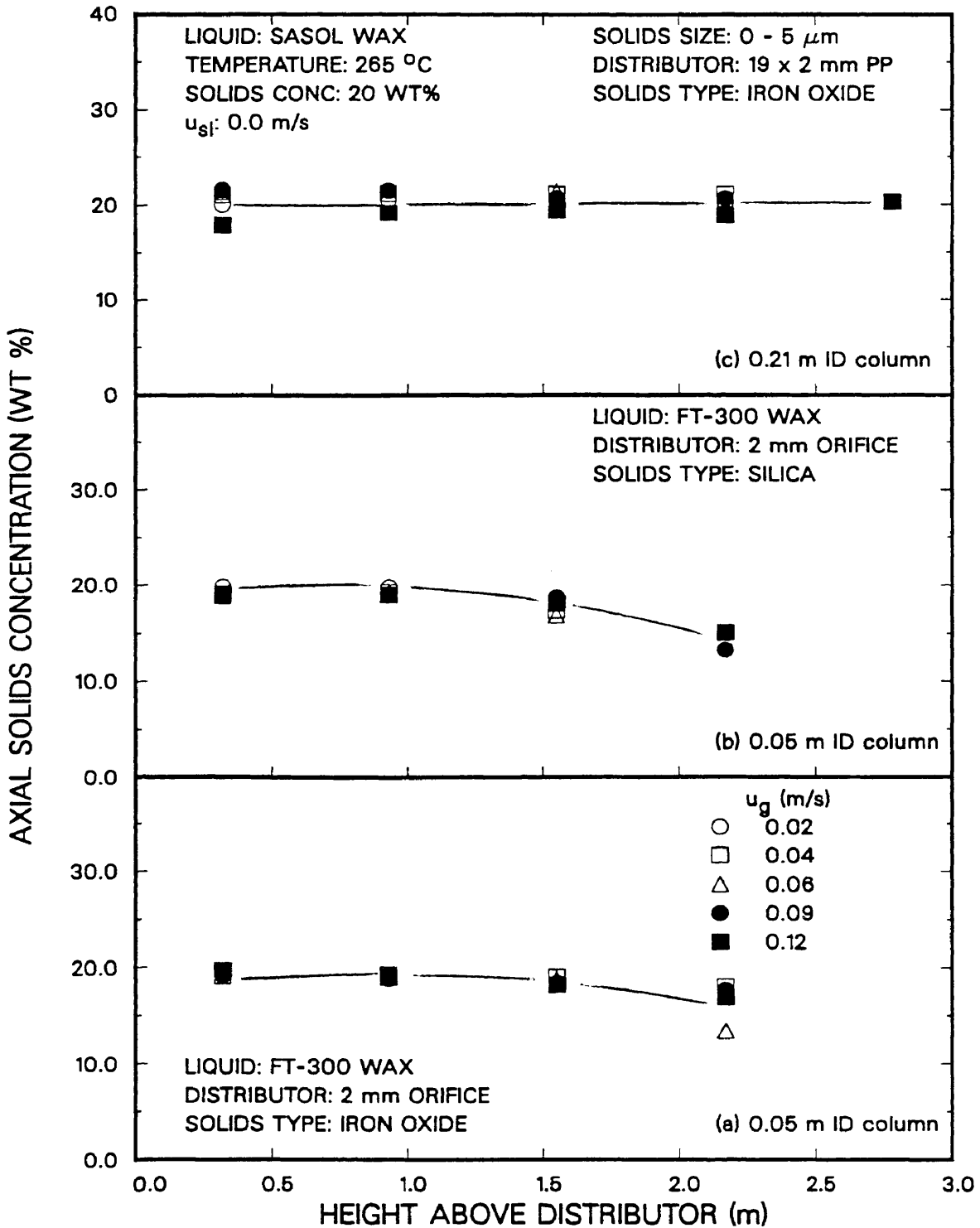
Figure 4.2. Effect of axial position and superficial gas velocity on solids concentrations (20 wt%, 0 - 5 μm particles, u_{sl} = 0.0 m/s; (a) iron oxide, 0.05 m ID column; (b) silica, 0.05 m ID column; (c) iron oxide, 0.21 m ID column).
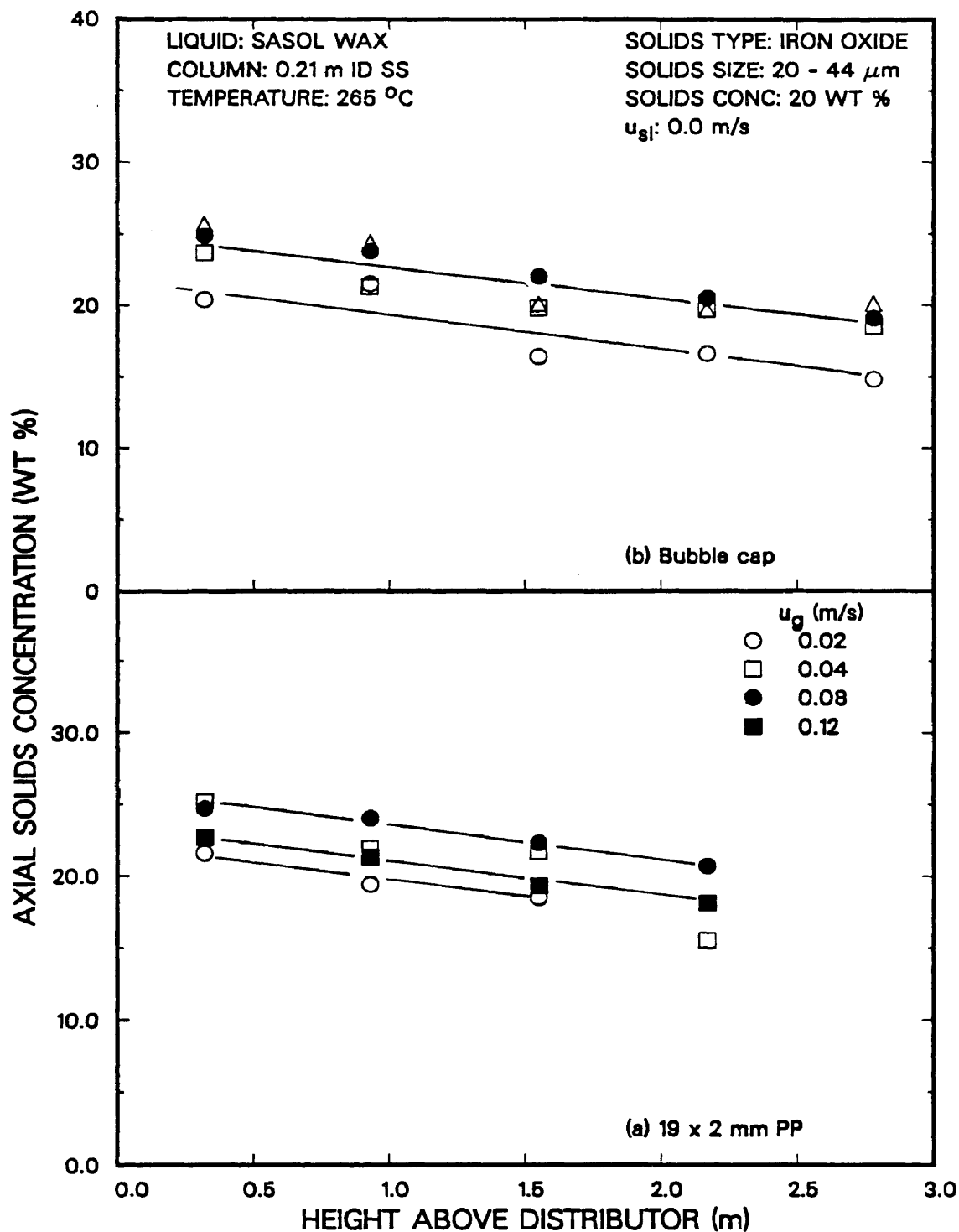
Figure 4.4. Effect of axial position and superficial gas velocity on solids concentrations (20 wt% 20 - 44 μm iron oxide particles, 0.21 m ID bubble column, u_{sl}=0 m/s; (a) 19 x 2 mm PP distributor; (b) bubble cap distributor).

Figures 4.3a and 4.3b) were steeper than those observed in the large column for experiments conducted in the batch mode of operation with large particles (see Figures 4.4a and 4.4b). This trend is expected since intense circulation patterns develop in the large diameter column which help to suspend the solid particles. A similar trend was observed with large silica particles in the 0.05 and 0.21 m ID columns.

Solids concentration profiles were fairly uniform for experiments conducted with both large iron oxide and large silica particles in the continuous mode of operation in the 0.21 m ID column. For experiments conducted with a slurry velocity of 0.02 m/s, the solids concentration profiles were essentially uniform (i.e. ω_s varied by less than 2 wt% (actual) across the entire column). During the experiment conducted with 30 wt% large iron oxide particles at a slurry velocity of 0.005 m/s, a slight solids concentration gradient was observed (see Figure 4.5a). Results from other experiments with large iron oxide particles at a superficial slurry velocity of 0.005 m/s also indicated a slight decrease in solids concentration with increase in height above the distributor; however, during these runs, the solids concentration profiles in the column below a height of 2.2 m fluctuated with axial position (see Figure 4.5b). Thus, the only data (i.e. axial solids concentrations) from a continuous experiment that were analyzed, were from the experiment conducted with 30 wt% large iron oxide particles at a slurry velocity of 0.005 m/s.

Axial solids dispersion coefficients for iron oxide and silica were estimated using solids distribution profiles from batch mode experiments in both the 0.05 m and 0.21 m ID bubble columns via Eq. 4.9. A total of three batch experiments with large iron oxide particles were conducted in the 0.05 m ID bubble column, two with FT-300 wax as the liquid medium and the other with SASOL wax as the liquid medium. Two batch mode experiments were also conducted in the small diameter column with large silica particles suspended in FT-300 wax. A total of four batch mode experiments with large
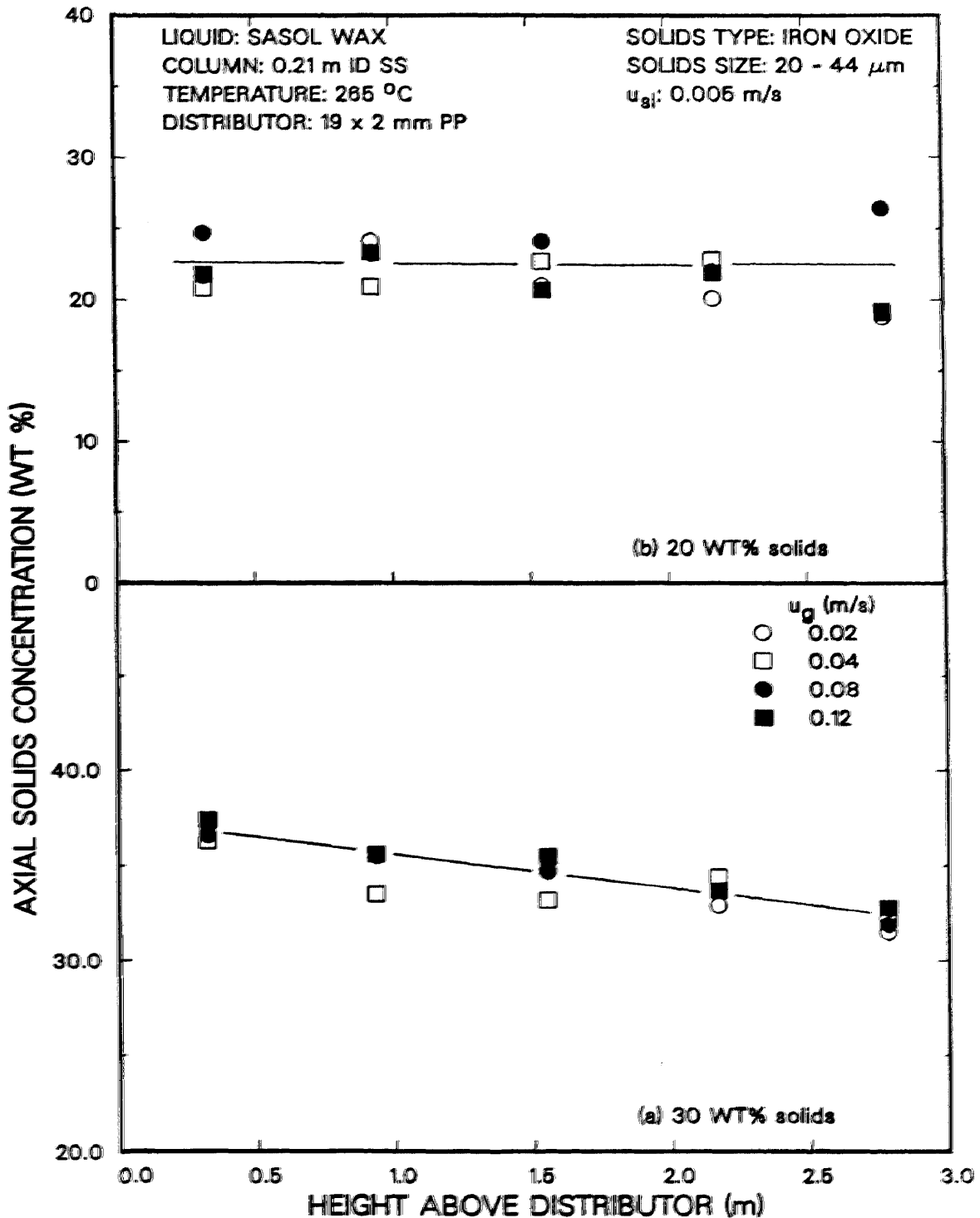
Figure 4.5. Effect of axial position and superficial gas velocity on solids concentrations (20 - 44 μm iron oxide particles, 0.21 m ID bubble column, u_{gl}=0.005 m/s; (a) 30 wt %; (b) 20 wt %).

iron oxide particles were conducted in the large diameter column, three with SASOL wax and the other with FT–300 wax as the liquid medium.

Figure 4.6 shows the effect of superficial gas velocity on the quotient $\frac{u_p}{E_s}$, which was estimated by fitting solids concentration (g/cc) vs. normalized axial height data to Eq. 4.9. Figures 4.6a and 4.6b correspond to values of $\frac{u_p}{E_s}$ obtained from batch experiments in the small diameter column with large iron oxide and large silica particles, respectively. Figure 4.6c shows results from batch experiments with large iron oxide particles in the 0.21 m ID column. Values of $\frac{u_p}{E_s}$ obtained from different experiments with large silica particles in the 0.05 m ID column were similar (Figure 4.6b); whereas, there was some variation in the values of $\frac{u_p}{E_s}$ obtained from different experiments with large iron oxide particles in the small column, particularly at a gas velocity of 0.02 m/s (Figure 4.6a). u_p / E_s values obtained from different experiments with large iron oxide particles in the large column were comparable (see Figure 4.6c).

As noted earlier, for batch mode experiments, the terms u_p and E_s are not separable, and hindered settling velocities must be assumed in order to estimate the dispersion coefficients. Hindered settling velocities and axial solids dispersion coefficients were obtained from the experiment conducted at a superficial slurry velocity of 0.005 m/s with 30 wt%, 20 – 44 μm iron oxide particles in the large diameter column using non–linear regression analysis (NLIN on SAS) of the experimental data (i.e. fit data (solids concentration vs. normalized height) to Eq. 4.10). The solids concentration of the feed, C_s^f, was assumed to be equal to the average solids concentration in the storage tank. The values of u_p from this experiment agreed with the values predicted using the correlation presented by Kato et al. (1972); whereas, the correlations presented by Smith and Ruether (1985) and O'Dowd et al. (1987) overestimated the hindered settling velocities (see Figure 4.7). Thus, the correlation presented by Kato et al. (Eq.
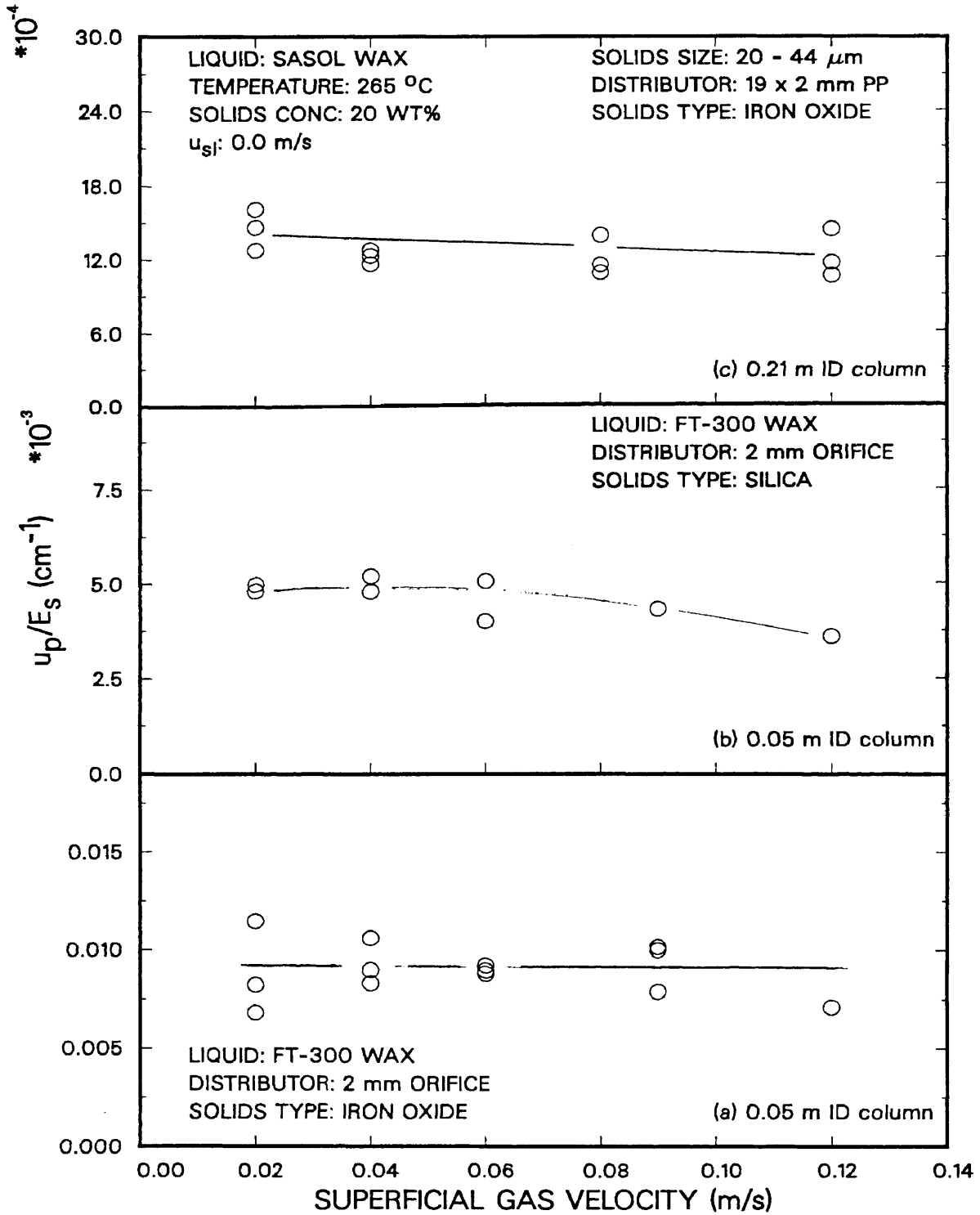
Figure 4.6. Effect of superficial gas velocity on u_p/E_s (20 - 44 μm particles, u_{sl} = 0.0 m/s; (a) iron oxide, 0.05 m ID column; (b) silica, 0.05 m ID column; (c) iron oxide, 0.21 m ID column).

LIQUID: SASOL WAX   DISTRIBUTOR: 19 x 2 mm PP
COLUMN ID: 0.21 m   SOLIDS TYPE: IRON OXIDE
TEMPERATURE: 265 °C   SOLIDS SIZE: 20 - 44 μm
u_{sl}: 0.005 m/s   SOLIDS CONC: 30 WT%

KATO et al. (1982)
SMITH AND RUETHER (1985)
O'DOWD et al. (1987)

SUPERFICIAL GAS VELOCITY (m/s)

u_p (cm/s)
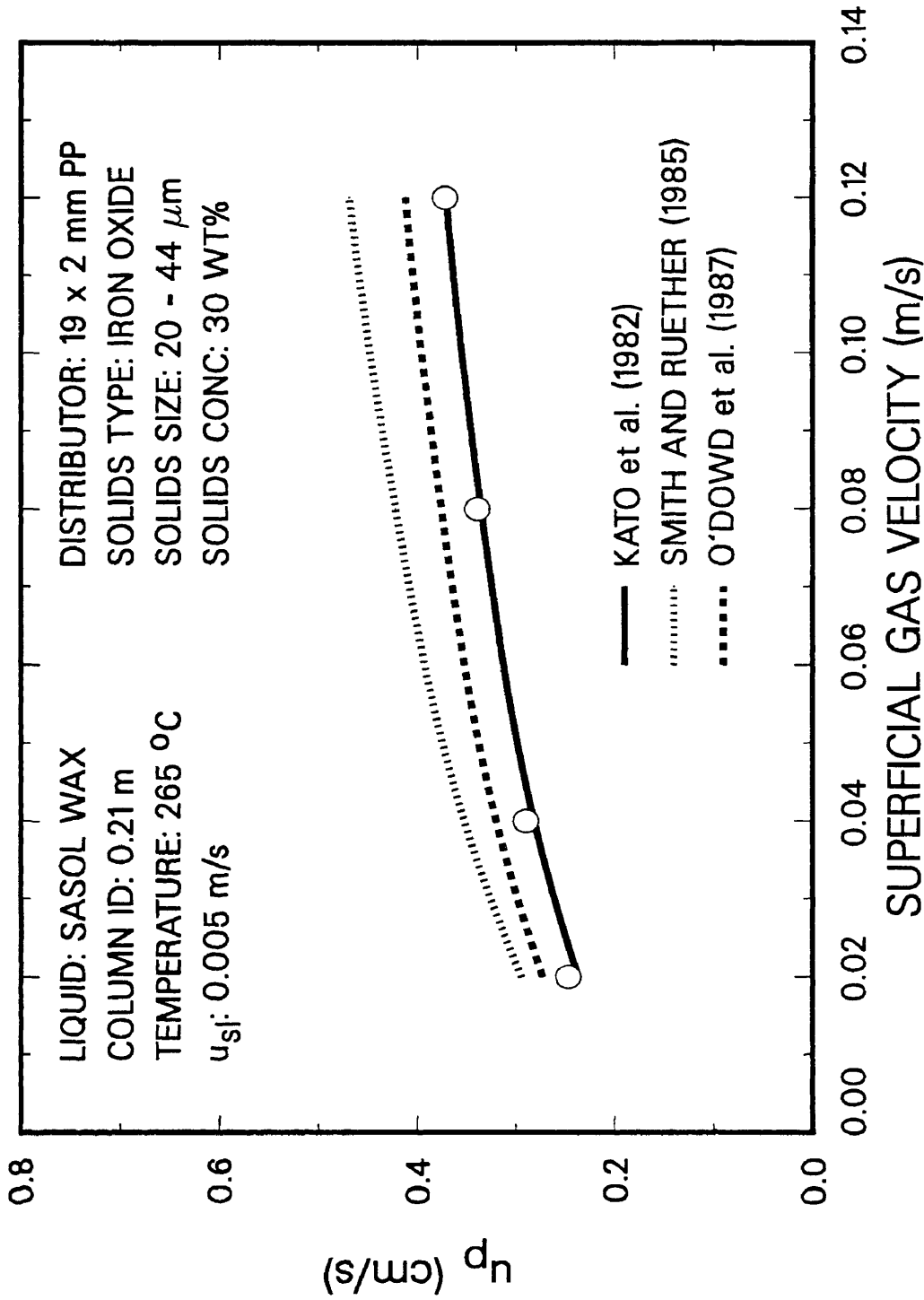
Figure 4.7. Effect of superficial gas velocity on hindered particle settling velocity
for 20 - 44 μm iron oxide particles in SASOL reactor wax.

4.11) was used to calculate the hindered settling velocities needed to obtain the axial solids dispersion coefficients for experiments conducted in the batch mode of operation.

Axial solids dispersion coefficients, E_s, for batch experiments in both columns were calculated using $\frac{u_p}{E_s}$ (from least square fit of experimental data) and u_p (from Kato et al.'s correlation). The following correlation for the particle Pectlet number, Pe_p, which is similar to the ones presented by Smith and Ruether (1985) (Eq. 4.13) and O'Dowd et al. (1987) (Eq. 4.14) was developed

$$Pe_p = 8.4\left[\frac{Fr_g^6}{Re_g}\right]^{0.107} = \frac{u_g d_{col}}{E_s}\tag{4.15}$$

for $0.014 < Fr_g < 0.271$ and $283 < Re_g < 7140$. The estimated parameters (i.e. 8.4 and 0.107) in Eq. 4.15 are comparable to those given by Smith and Ruether (9.6 and 0.114) and O'Dowd et al. (7.7 and 0.098).

Figures 4.8a and 4.8b show results for axial dispersion coefficients from experiments conducted with large particles in both the 0.05 m and 0.21 m ID columns, respectively, together with the predicted dispersion coefficients obtained using Eq. 4.15. The correlation overestimates the measured axial solids dispersion coefficients at gas velocities greater than 0.06 m/s in the large diameter column and underestimates the axial dispersion solids coefficients in the small diameter column at gas velocities less than 0.06 m/s. Axial solids dispersion coefficients obtained from the experiment in the large diameter column with the bubble cap distributor were consistently lower than those obtained from experiments with the perforated plate distributor at high gas velocities.

Figure 4.9 compares predicted and measured axial solids concentrations (g/cc). The predicted solids concentrations were obtained using Eq. 4.15 to predict the axial solids dispersion coefficient, E_s, and Kato et al.'s (1972) correlation to predict the hindered settling velocity, u_p. These quantities were then used in Eq. 4.9 to obtain the solids concentration at a given axial location for batch mode experiments. The solids
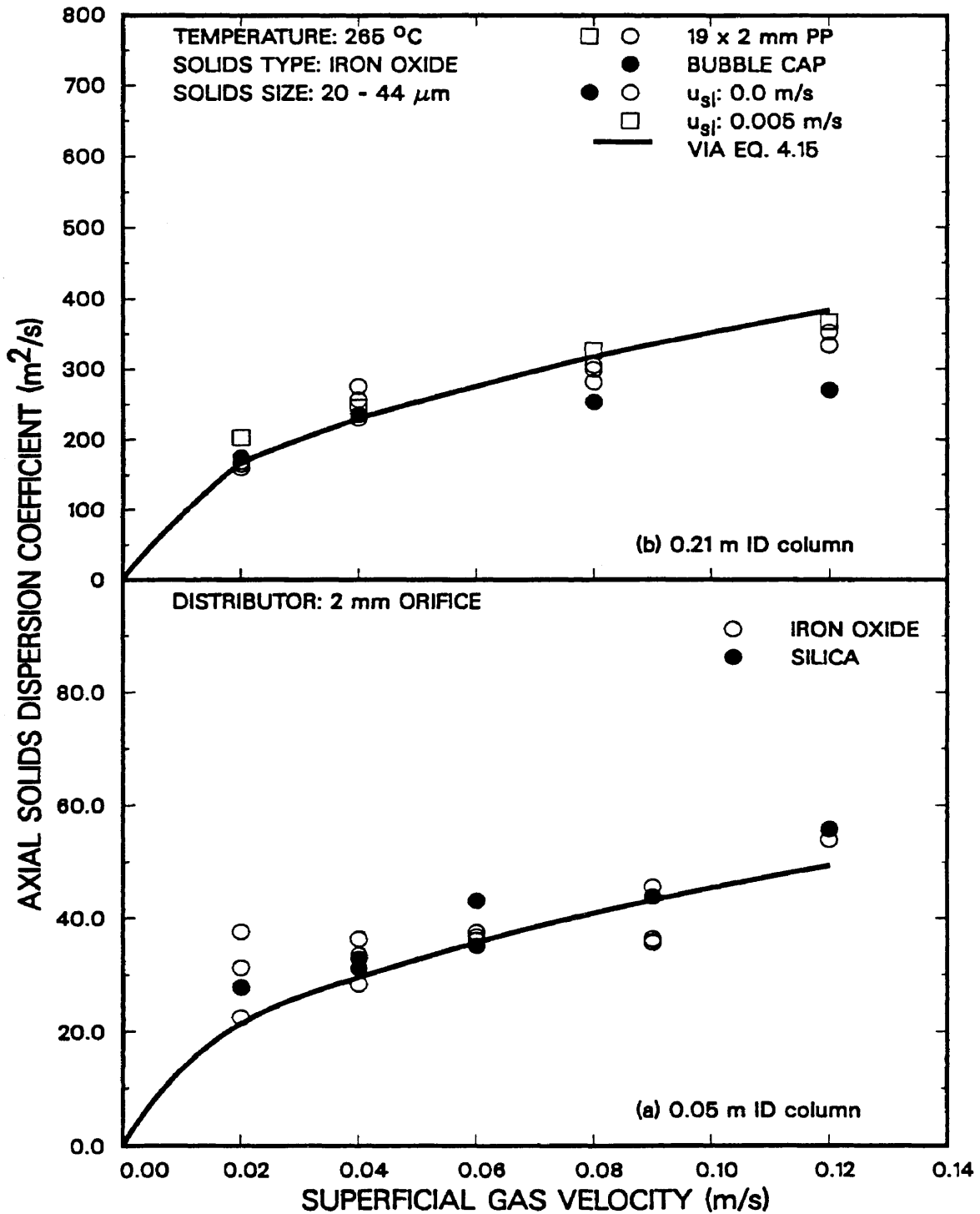
Figure 4.8. Effect of superficial gas velocity on axial solids dispersion coefficients
((a) 0.05 m ID column, (b) 0.21 m ID column).
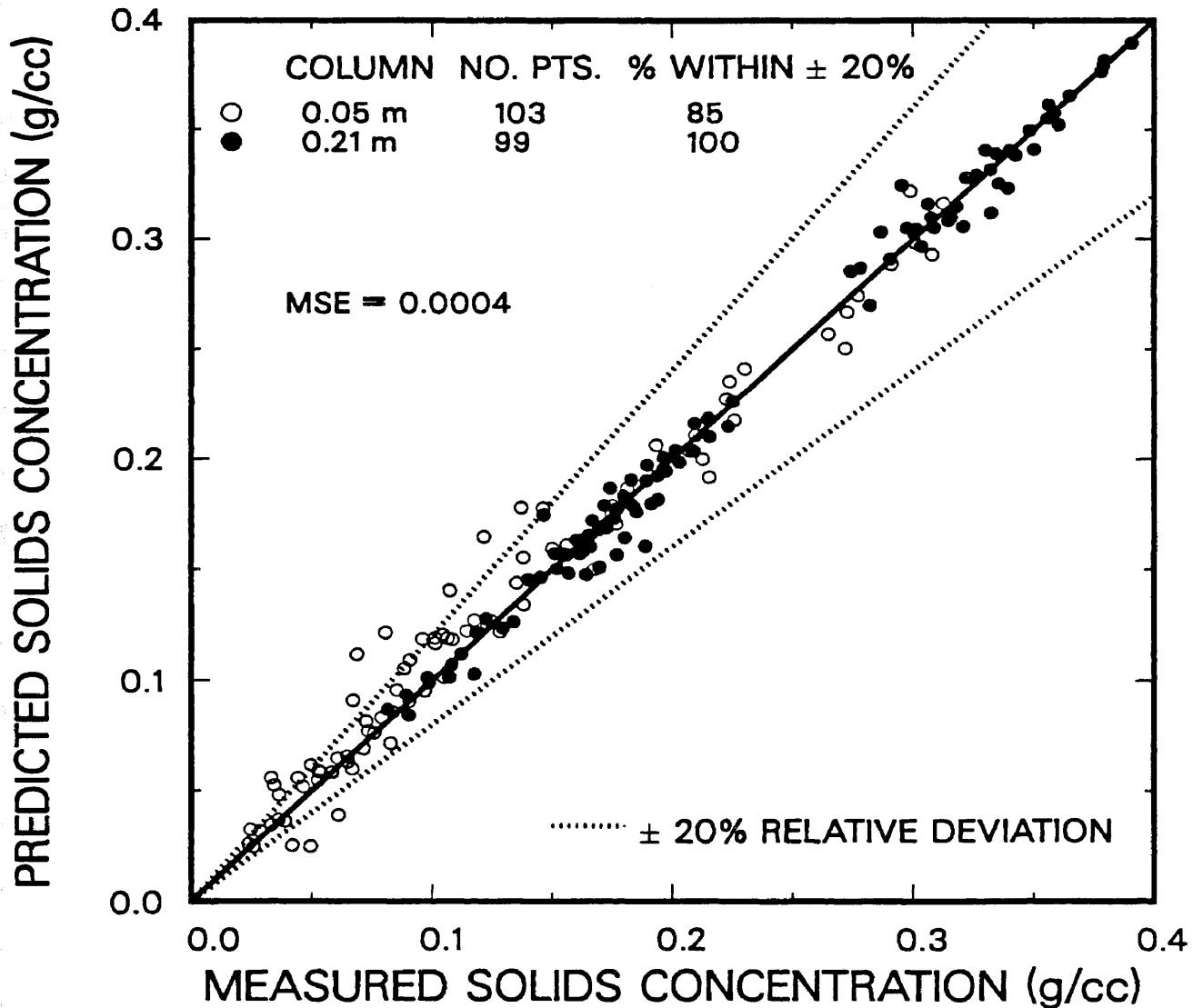
Figure 4.9. Parity plot of measured versus predicted solids concentrations; (20 - 44 μm iron oxide and silica particles; u_{sl} = 0.0 m/s and 0.005 m/s - 0.21 m ID column only).

concentration at the bottom of the column, C_s^B, was assumed to be the same as that obtained in the original analysis. For the experiment conducted in the continuous mode, the solids concentration profile was obtained using Eq. 4.10 with C_s^B and C_s^f being the same as determined in the original analysis. As shown in Figure 4.9 there is excellent agreement between the predicted and measured solids concentrations in both the small and large diameter columns.

As mentioned previously, no attempt was made to obtain axial solids dispersion co-efficients for experiments conducted in the batch mode of operation with small particles because of the uniform solids concentration profiles. Theoretical solids concentration profiles for iron oxide and silica at gas velocities of 0.01, 0.12, and 0.30 m/s (Figures 4.10a and 4.10b, respectively) were determined. These profiles were obtained using the normalized (with respect to the solids concentration at the bottom of the column, C_s^B) form of Eq. 4.9. The axial solids dispersion coefficients were obtained from Eq. 4.15 and the hindered settling velocity were calculated from Eq. 4.11 using the constants given by Kato et al. (1972). The expanded height, H_{exp} was assumed to be 3 m. As shown in Figure 4.10, the solids concentration profiles for both iron oxide and silica are fairly uniform, and show very little effect of gas velocity. Similar trends were observed with our experimental data (see Figures 4.2a and 4.2b).

The effect of particle size (iron oxide) on the theoretical solids concentration distribution at gas velocities of 0.01, 0.12, and 0.30 m/s is shown in Figures 4.11a, 4.11b, and 4.11c, respectively. Particle sizes of 3 and 30 μm are representative of the average size of the particles used in the present study. The predicted trends (i.e. increasing solids concentration gradient with increasing particle size) are in agreement with those obtained from our experiments (symbols in Figure 4.11b). An increase in gas velocity decreases the concentration gradient along the height of the bubble column. However,
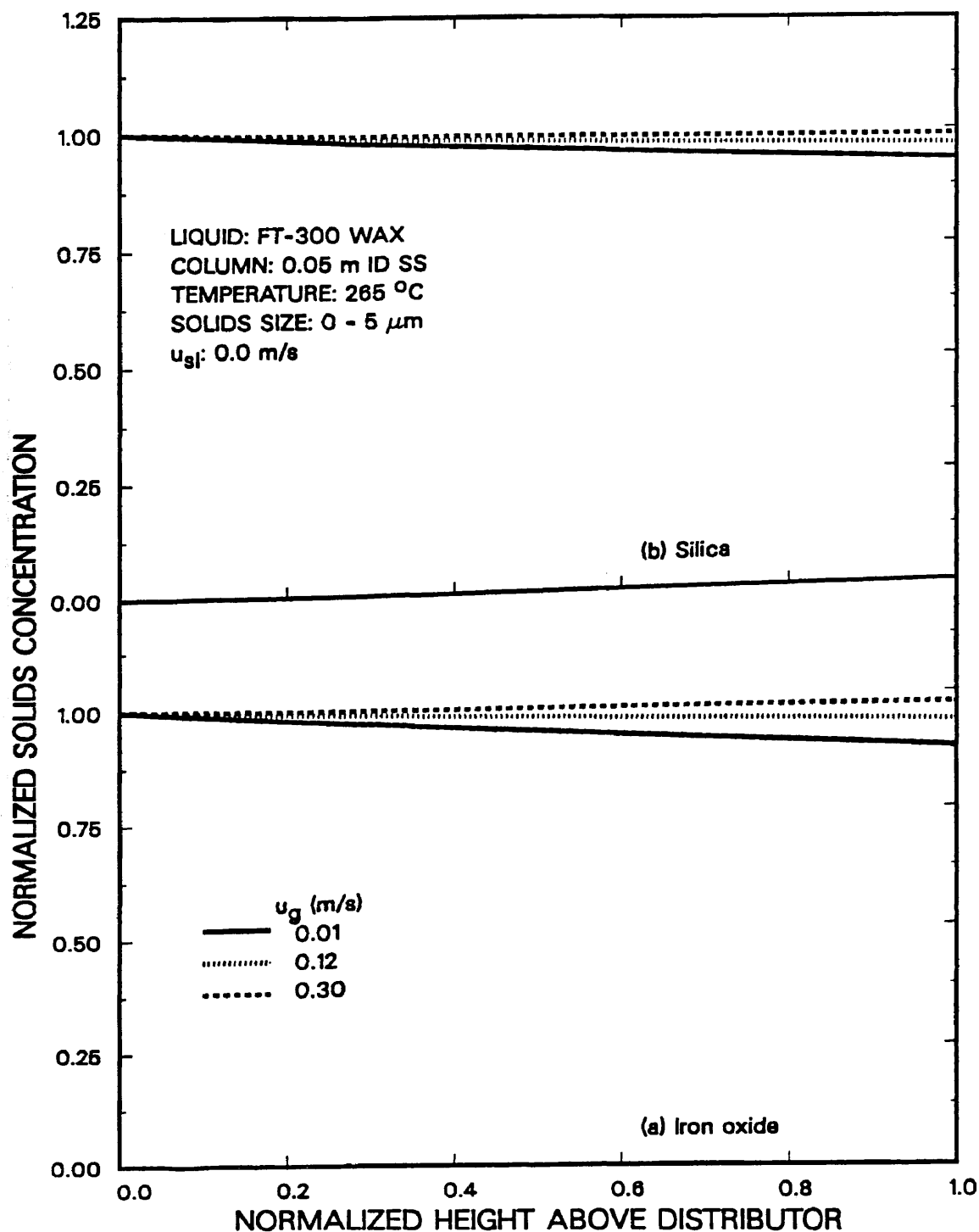
Figure 4.10. Effect of superficial gas velocity on axial solids concentrations
(0 - 5 μm particles; 0.05 m ID bubble column; u_{sl}=0 m/s;
(a) iron oxide (b) silica).
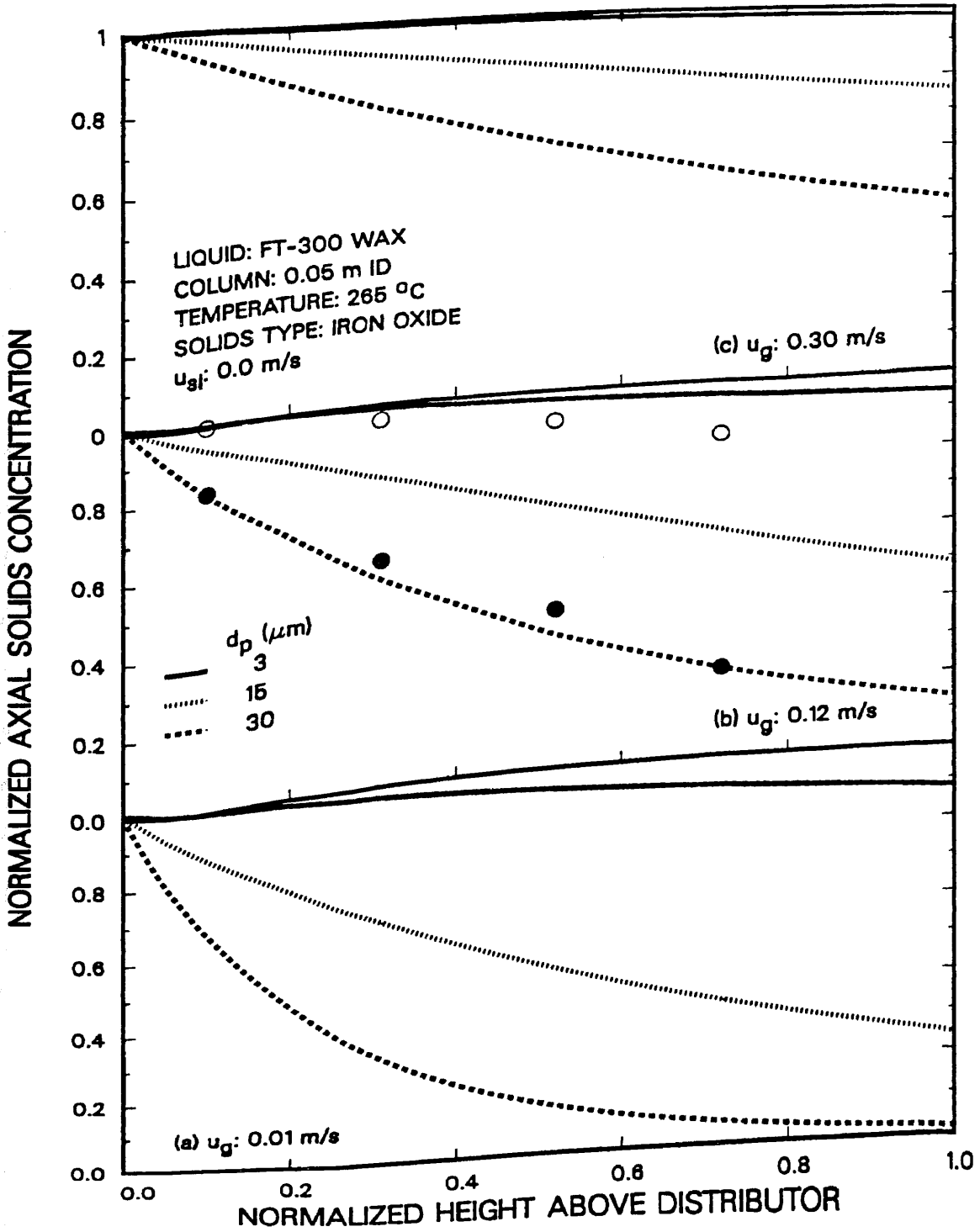
Figure 4.11. Effect of particle size and superficial gas velocity on axial solids concentrations.

even for a gas velocity of 0.30 m/s, there is still approximately a 58 % decrease in the solids concentration along the height of the reactor for 30 μm particles.

Figures 4.12a and 4.12b show the effect of slurry flow rate on solids (20 − 44 μm iron oxide particles) suspension in both the 0.05 and 0.21 m ID bubble columns, respectively. Also shown in Figure 4.12 are data obtained from batch experiments in the small and large diameter columns. The results presented in Figure 4.12 were obtained from Eq. 4.10, using Eq. 4.15 to estimate E_s and Eq. 4.11 to estimate u_p (Kato et al.'s constants). The solids concentrations were normalized with respect to the concentration at the bottom of the column, C_s^B. There is excellent agreement in the solids concentration obtained from the theory and those measured experimentally in both columns ($u_{s\ell} = 0$ m/s). At a slurry velocity of 0.02 m/s in the small column, the solids concentration profile is essentially uniform, which agrees with the results from our study (see Figure 4.3c). The theory predicts that a concentration gradient will exist in the small diameter column at a slurry velocity of 0.005 m/s with large iron oxide particles (see Figure 4.12a). However, due to operational problems with our pump, we were not able to obtain data at this slurry velocity. In the large diameter column, there is very little effect of slurry flow rate on axial solids distribution; whereas, in the small diameter column, there is a significant effect. At a slurry velocity of 0.02 m/s, the solids concentration profile in both columns is essentially uniform.
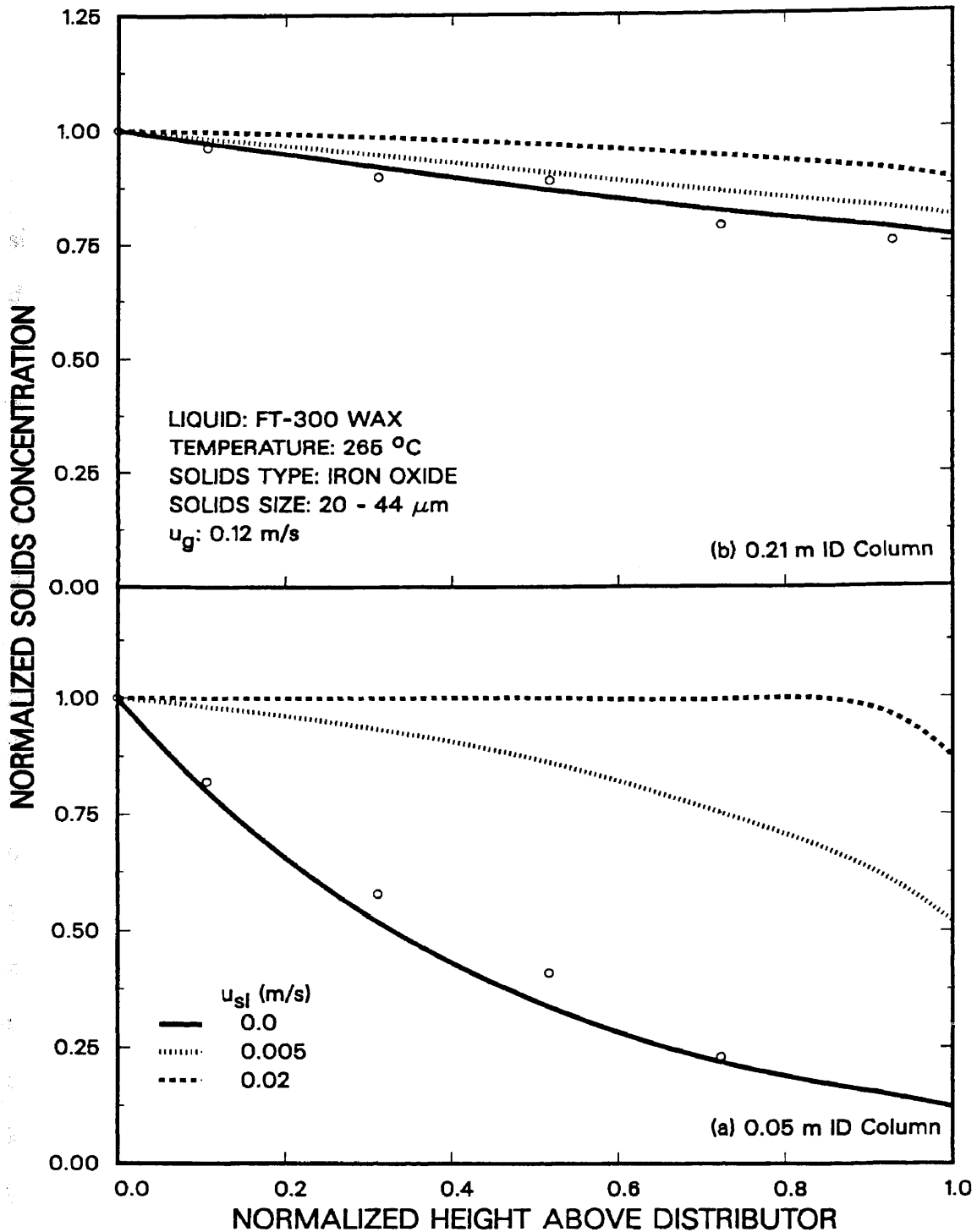
Figure 4.12. Effect of column diameter and superficial slurry velocity on axial solids concentrations.

CHAPTER V

BUBBLE SIZE DISTRIBUTIONS

The overall mass transfer rate per unit volume of the dispersion in a bubble column is governed by the liquid–side mass transfer coefficient ($k_\ell a$), assuming that the gas–side resistance is negligible. In a bubble column reactor, the variation in $k_\ell a$ is primarily due to variations in the interfacial area (Fan, 1989). Assuming spherical bubbles, the specific gas–liquid interfacial area is related to the gas holdup, ϵ_g and the Sauter mean bubble diameter, d_s, by

$$a_s = \frac{6\epsilon_g}{d_s} \tag{5.1}$$

Thus, a precise knowledge of the gas holdup and bubble size distribution is needed to determine the specific gas–liquid interfacial area.

Extensive work on bubble size measurements in two–phase systems has been reported in the literature, and has been reviewed by several authors (e.g. Buchholz and Schugerl, 1979; Shah et al., 1982; Saxena et al., 1988); however, the majority of these studies pertain to air–water systems. Bubble size measurements with molten wax as the liquid medium are rather limited (e.g. Calderbank et al., 1963; Quicker and Deckwer, 1981; O'Dowd et al., 1987; Bukur et al., 1987a,c; Patel et al., 1989) and there is some disagreement between bubble size data reported in these studies. Previous work with this medium has dealt primarily with overall gas holdup and its dependence on operating conditions and system parameters (e.g. Deckwer et al., 1980; Kuo, 1985; Sanders et al., 1986; Bukur et al., 1985, 1987a; Bukur and Daly, 1987). The general consensus is that some molten wax systems depict an unique behavior, namely, an abundance of very small bubbles is present and high gas holdups are obtained in comparison to pure hydrocarbons having similar physical properties. The resulting specific gas–liquid inter–facial areas could be an order of magnitude greater than those of pure hydrocarbons

(Quicker and Deckwer, 1981). The findings from bubble size measurement studies with molten waxes are summarized below.

Calderbank et al. (1963) used a light transmission technique to measure interfacial areas of Krupp wax at 265 °C for gas velocities less than 0.06 m/s in a 0.05 m ID column equipped with a ball and cone type sparger. When these data, together with the average gas holdup values reported by them, are used in Eq. 5.1, Sauter mean bubble diameters in the range 2 − 3 mm are obtained. Zaidi et al. (1979) and Deckwer et al. (1980) reported a much lower d_s value, 0.7 mm, for paraffin wax using photography in 0.041 and 0.1 m ID columns equipped with 75 μm porous plate spargers (T = 250 − 270 °C, $u_g \leq 0.03$ m / s). Quicker and Deckwer (1981) measured d_s values for FT−300 wax in a 0.095 m ID column equipped with a 0.9 mm nozzle. Sauter mean bubble diameters, determined by the photographic method, at 170 °C ranged from 1.3 mm (u_g = 0.01 m/s) to 0.6 mm (u_g = 0.035 m/s). More recently, O'Dowd et al. (1987) obtained d_s values for a P−22 wax, and for reactor wax from run 7 in Mobil's pilot plant slurry reactor (Unit CT−256) using the hot wire anemometer technique at 250 °C and 1.48 MPa. Their d_s values, from a 0.022 m ID column equipped with a 1 mm orifice plate, for the two waxes were in the range 2.7 to 3.9 mm for $u_g \leq 0.02$ m/s, and are comparable to values reported by Calderbank et al. (1963).

The lower d_s values from the studies conducted by Zaidi et al., Deckwer et al., and Quicker and Deckwer, cannot be attributed to the limitation of the photographic technique (i.e. its bias towards small bubbles in the vicinity of the wall). This is because all of these studies were conducted in the homogeneous bubbling regime ($u_g \leq 0.035$ m/s) where the dispersion is expected to be radially uniform. A possible cause for the difference could be the behavior of the medium itself. We have shown in our laboratory that, despite similar physical properties, different waxes have dissimilar hydrodynamic behavior (Bukur et al., 1987a,c).

Numerous techniques have been used to measure bubble size distributions. Some of the techniques which are commonly employed are photography, hot wire anemometry, electrical conductivity, and light transmission. More recently, the dynamic gas disengagement (DGD) technique, originally developed by Sriram and Mann, 1977, has been employed (e.g. Vermeer and Krishna, 1981; Kuo, 1985; Bukur et al., 1987a,c; Patel et al., 1989). This technique was used in the present study.

The approach presented by Sriram and Mann has been used by several researchers to determine the holdup structure of the dispersion. In most cases, the dispersion was assumed to consist of one or two dominant bubble sizes. Vermeer and Krishna (1981) applied this approach to the nitrogen–turpentine 5 system. They assumed a bimodal distribution with large bubbles forming the transport portion of the holdup and small, slow rising, bubbles forming the entrained portion. Based on this assumption, they considered the initial part of the disengagement profile to be dictated solely by the large bubbles, with the small bubbles disengaging only after all of the large bubbles have left the system. They used the resulting disengagement profiles to estimate the contribution to the gas holdup by the two bubble classes. Schumpe and Deckwer (1982), and Godbole et al. (1982, 1984) conducted experiments with highly coalescing CMC (carboxymethyl cellulose) systems and used bimodal bubble size distributions to determine the holdup structure of the dispersion by dynamic gas disengagement. For such systems, they showed that the contribution of small bubbles to the overall gas holdup is negligible. In similar experiments with different concentrations of surfactants added to the CMC solution, Godbole et al. (1984) showed that the contribution of small bubbles to the overall gas holdup increased with increasing surfactant concentration (i.e. decreasing coalescence rates), while the contribution due to large bubbles remained virtually unchanged. In experiments conducted with alcohol solutions (noncoalescing media) by Kelkar et al. (1983), similar results were obtained when the holdup structure

was determined using the dynamic gas disengagement technique assuming a bimodal bubble size distribution. For these solutions, the contribution to overall gas holdup by small bubbles was even greater than that due to large bubbles.

More recently, Schumpe and Grund (1986) have presented results for the air–water system, with an emphasis on some of the problems associated with the DGD technique and have proposed corrective measures which to some extent can alleviate these problems. The problems analyzed by the authors include the subjectivity involved in obtaining an accurate disengagement profile during large bubble disengagement, the "waterfall" effect or downward flow of liquid during bubble disengagement and its impact on the rise velocity of small bubbles, and errors introduced by bubbles entering the dispersion as the pressure in the plenum chamber equilibrates with the hydrostatic pressure of the dispersion, following the interruption of the gas supply. The authors assumed a bimodal bubble size distribution in their analysis and presented the gas holdup structure as well as bubble rise velocities for the two bubble classes. The problems associated with obtaining accurate disengagement profiles were also discussed by Lee et al. (1985), who developed a digital sensor with a computer interface that greatly improved accuracy and reproducibility of the measured disengagement profile.

Researchers at Mobil (Kuo, 1985) were the first to discretize Sriram and Mann's original equation without introducing any new assumptions other than a noncontinuous distribution. They applied the resulting equations to disengagement profiles obtained from experiments using molten wax as the liquid medium at low gas velocities and assumed either unimodal or bimodal bubble size distributions. The quantities estimated in their study included the gas holdup structure, bubble rise velocities, and bubble sizes.

The dynamic gas disengagement technique offers several advantages over the previously mentioned techniques. Bubble size distributions obtained from DGD are based

on the entire dispersion; whereas, all other techniques mentioned above are local measurement techniques. We have shown previously (Bukur et al., 1987a,c and Patel et al., 1990) that the bubble size distribution is a function of radial position (i.e. larger bubbles rise through the center of the column). Thus, when employing any of the "probe" techniques or even photography, measurements must be made at numerous radial positions to obtain an accurate estimate of the Sauter mean bubble diameter. The major drawback with DGD is the fact that bubble sizes are not measured directly.

The purpose of this study was to determine bubble size distributions, and consequently specific gas–liquid interfacial areas for FT–300 wax and SASOL reactor wax in both the 0.05 and 0.21 m ID bubble columns. A description of the DGD technique, the theory associated with DGD, and results from experiments conducted with waxes (FT–300 and SASOL) are presented. Also, results for Sauter mean bubble diameters and specific gas–liquid interfacial areas are presented for an experiment conducted with tap water in the 0.05 m ID stainless steel bubble column.

Experimental Techniques for Measurement of the Disengagement Profile

The DGD technique requires an accurate measurement of the rate at which the gas–liquid dispersion drops once the gas flow to the bubble column is shut off. As mentioned previously, one of the problems associated with this technique is determination of the rate at which the liquid level drops during the initial period of disengagement. The majority of previous studies (transparent systems) utilized a video camera/VCR system to measure the rate at which the dispersion dropped once the gas flow was shut off. During large bubble disengagement, the top of the dispersion is not well defined because of splashing caused by the disengagement of large bubbles. In the current study, a video camera/VCR system could not be used since measurements were made in stainless steel columns. Thus, pressure transducers were used to measure the rate at which the

liquid level dropped during the disengagement process. The use of pressure transducers not only enables one to use this technique in opaque systems, but also reduces the subjectivity involved in estimating the rate at which the liquid level drops during large bubble disengagement. In our previous studies (Bukur et al., 1987a,c; Patel et al., 1990), DGD was used to obtain bubble size distributions for a variety of waxes in the 0.05 and 0.23 m ID glass bubble columns. During these studies, the rate at which the liquid level dropped, once the gas flow had been interrupted, was recorded with a video camera/VCR system.

The primary difference in the analysis of data obtained from different forms of data acquisition (i.e. video system vs. pressure transducers) is the frame of reference. Analysis of data obtained from visual observations (i.e. video system) is based on the cross–sectional area of the liquid in the gas/liquid dispersion; whereas, analysis of data obtained from pressure transducers is based on the cross–sectional area of the dispersion. For the former, the volume of liquid in the dispersion remains constant, but the total volume of the dispersion changes (Patel et al., 1989); whereas, for the latter, the total volume of the dispersion below the pressure transducer remains constant but the volume of the liquid varies.

Theory

In the following analysis, we will assume that the dispersion is axially homogeneous and no bubble–bubble interactions occur once the gas flow is interrupted. These are the same assumptions as those used by Sriram and Mann (1977). Deviations from these assumptions may occur in strongly coalescing systems (e.g. air–water system) at high gas flow rates. The assumption of axial homogeneity may also be violated with noncoalescing systems in which there is a high concentration of fine bubbles at the top of the dispersion.

For simplicity, we have assumed a bimodal distribution; however, equations are also presented for multimodal distributions. The dispersion for a bimodal distribution may be partitioned into three fractions representing the liquid volume, total volume of large bubbles, and total volume of small bubbles. Under the assumption of axial homogeneity, the dispersion, just before gas flow is cut off, may be represented by Figure 5.1. Since information is not obtained for the dispersion above the pressure transducer, no distinction is made between large and small bubbles in this region. The volumes of the three components are proportional to the respective holdup fractions. The disengagement process may be envisioned as either a constant rate process, case I, where the small and large bubbles disengage independent of one another, or as an interactive process, case II, where the disengagement of large bubbles retards the disengagement rate of small bubbles. Even though the latter case is interactive, it does not account for bubble–bubble interaction (i.e. coalescence and breakup). A third, although less likely possibility, is the case where the disengagement rate of small bubbles is enhanced by the disengagement of large bubbles. This could occur if small bubbles adhere to the surface of large bubbles and disengage along with them. The actual disengagement process is expected to lie between the two extremes described above (i.e. case I and case II).

Case I.   Constant Rate Disengagement Process

Before analyzing this case, it is important to define the constant rate disengagement process. Under this condition, the volumes representing the large and small bubbles (Figure 5.1) move away from the bottom of the column (disengage) at constant rise velocities. Furthermore, if we assume each volume to be a column of gas with a constant cross sectional area, then this constancy is preserved during the time it takes that column of gas to disengage. At any time during the first period of disengagement (Figure 5.2), the volume of liquid passing below the pressure transducer (V_ℓ) must be the same as the volume of gas associated with the small (V_s) and large (V_L) bubbles which rise
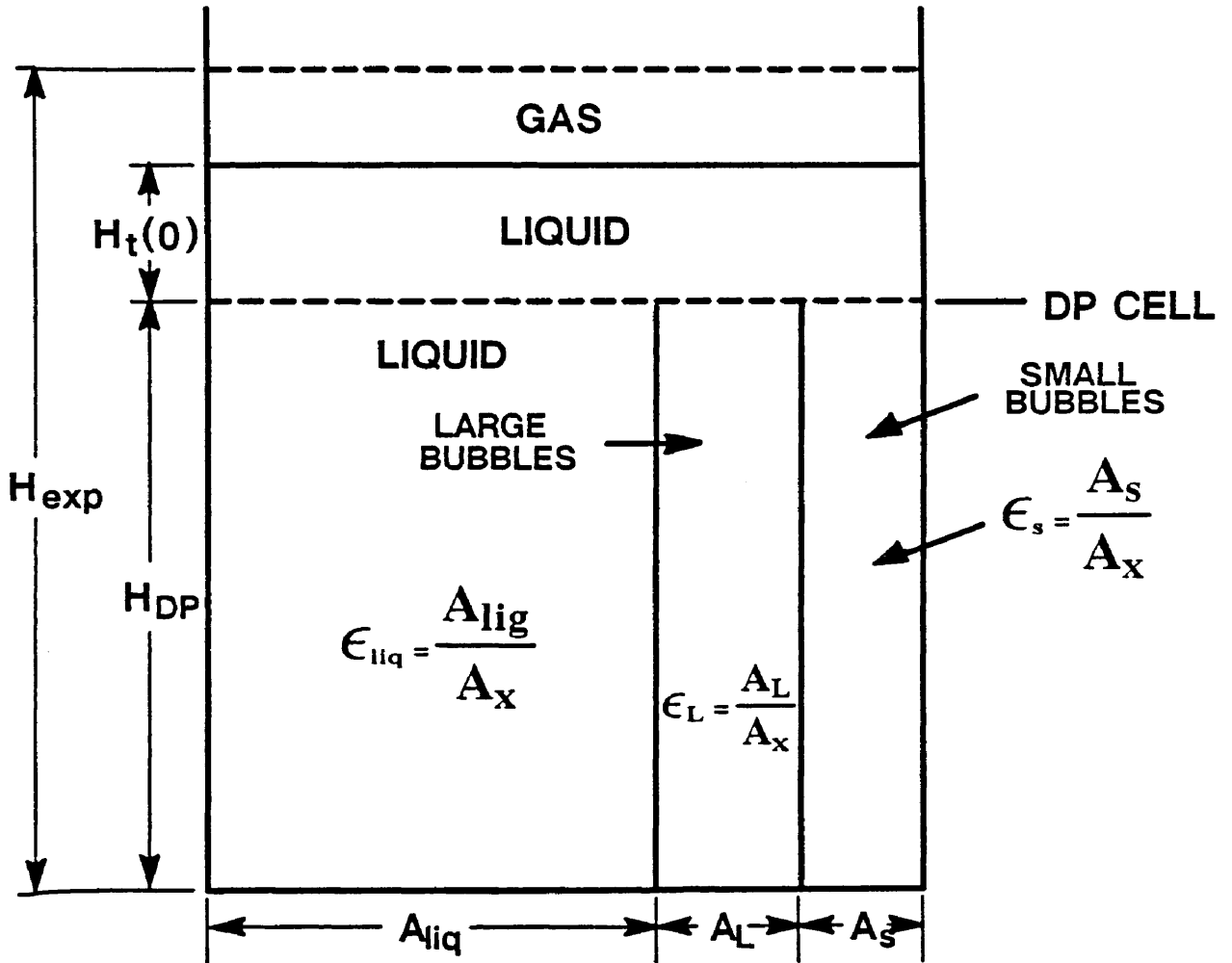
Figure 5.1. Dispersion prior to disengagement (t = 0).
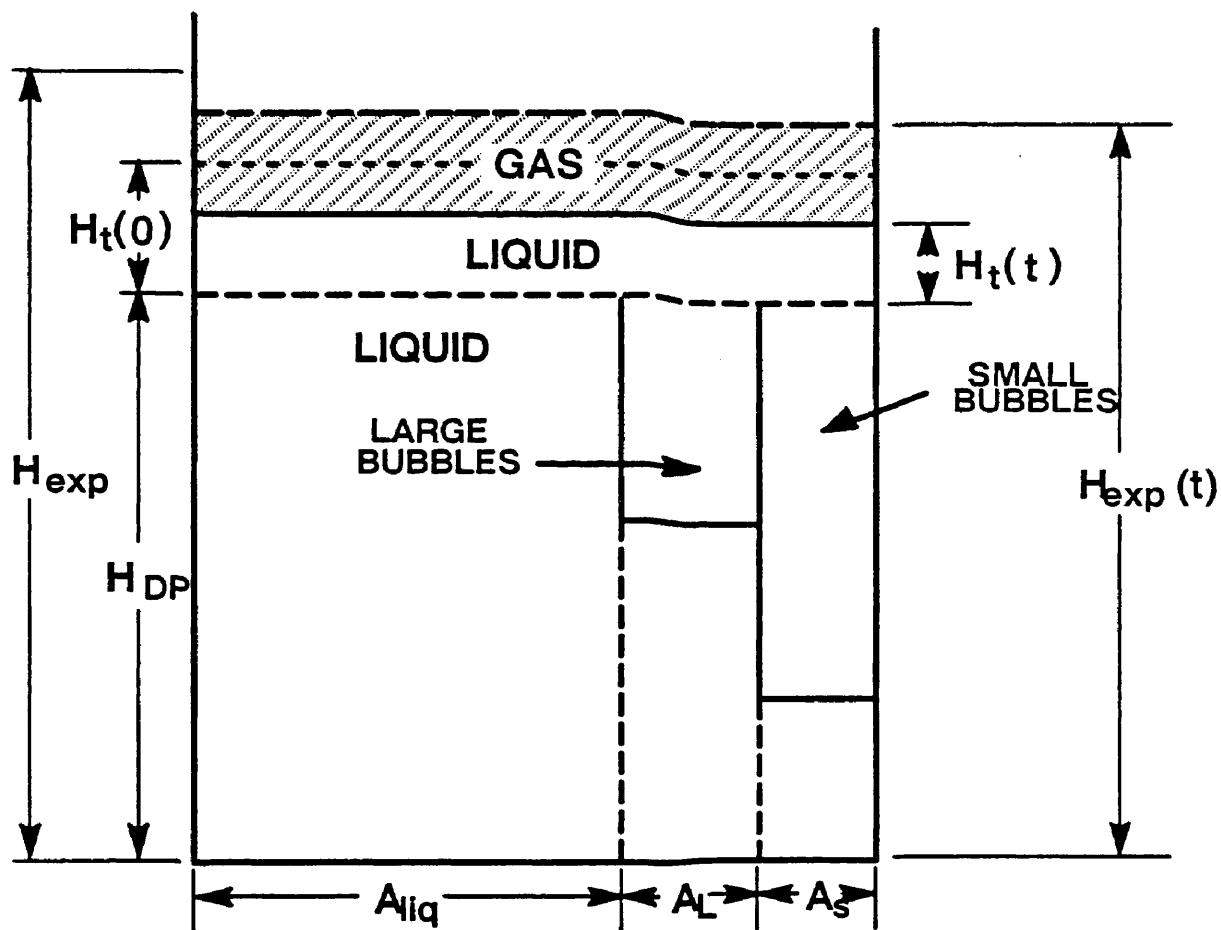
Figure 5.2. Dispersion during the constant rate disengagement process (Period 1).

above the pressure transducer. Thus, at any time t, a volume balance between the liquid entering and gas exiting is

$$V_\ell(t) = V_s(t) + V_L(t) \tag{5.2}$$

Furthermore, by the definition of the constant rate disengagement process, the distance between the rear of the small or large bubble swarm would simply be the product of the respective rise velocity and the time elapsed since the initiation of the disengagement process.

The volume of liquid passing below the pressure transducer at any time t may be expressed as

$$V_\ell(t) = V_o - V(t) \tag{5.3}$$

where V_o is the volume of liquid above the pressure transducer immediately prior to interruption of the gas flow and $V(t)$ is the volume of liquid above the pressure transducer during the disengagement process at time t. Substituting Eq. 5.3 into Eq. 5.2 and expressing volumes in terms of heights yields upon rearrangement

$$H_t(t)A_x = H_t(0)A_x - t[u_{bs}A_s + u_{bL}A_L] \tag{5.4}$$

where $H_t(t)$ is the height of liquid above the pressure transducer at time t, $H_t(0)$ is the initial (i.e. at steady state) height of liquid above the pressure transducer, A_x is the cross–sectional area of the column, u_{bs} is the rise velocity of small bubbles, A_s is the cross–sectional area of the column of small bubbles (see Figure 5.1), u_{bL} is the rise velocity of large bubbles, A_L is the cross–sectional area of the column of large bubbles, and t is the time. The cross–sectional area of bubbles of size i ($i = s$ or L) divided by the cross–sectional area of the column represents the volume fraction of gas corresponding to bubbles of size i. Thus, dividing Eq. 5.4 by A_x yields

$$H_t(t) = H_t(0) - t[u_{bs}\epsilon_{gos} + u_{bL}\epsilon_{goL}] \tag{5.5}$$

where ϵ_{gos} is the volume fraction of small bubbles at steady state conditions and ϵ_{goL} is the volume fraction of large bubbles at steady state conditions. The above equation is valid as long as large bubbles are present below the pressure transducer (i.e. for $t < H_{DP}/u_{bL}$, where H_{DP} is the height of the pressure transducer above the distributor).

Similarly, a balance equation for the liquid entering the section of the column below the pressure transducer during the second period of disengagement (Figure 5.3) may be written as

$$V_{\ell}(t) = H_t(t_1)A_x - H_t(t)A_x = u_{bs}A_s(t - t_1) \qquad t \geq H_{DP}/u_{bL} \qquad (5.6)$$

where t_1 corresponds to the time at which all large bubbles passed by the pressure transducer (i.e. $t_1 = H_{DP}/u_{bL}$), $H_t(t)$ is the height of liquid above the pressure transducer at time t and $H_t(t_1)$ is the height of liquid above the pressure transducer at the beginning of period 2 (i.e. small bubble disengagement). Dividing Eq. 5.6 by the cross-sectional area of the column, A_x yields upon rearrangement

$$H_t(t) = H_t(t_1) - u_{bs}\epsilon_{gs}(t - t_1) \qquad t \geq H_{DP}/u_{bL} \qquad (5.7)$$

For a multimodal distribution, the following expression is used to describe the rate at which the level drops during the disengagement of bubbles of size j

$$H_t(t) = H_t(t_k) - \sum_{i=j}^{n} u_{bi}\epsilon_{gi}(t - t_k) \qquad k = j-1, \quad t_k < t < H_{DP}/u_{bj} \qquad (5.8)$$

where n is the total number of bubble classes. Note $j = 1$ corresponds to the first period of disengagement and $j = n$ corresponds to the last period of disengagement (i.e. disengagement of the smallest bubbles). Also, for $k = 0$ (i.e. $j = 1$), $t = 0$.
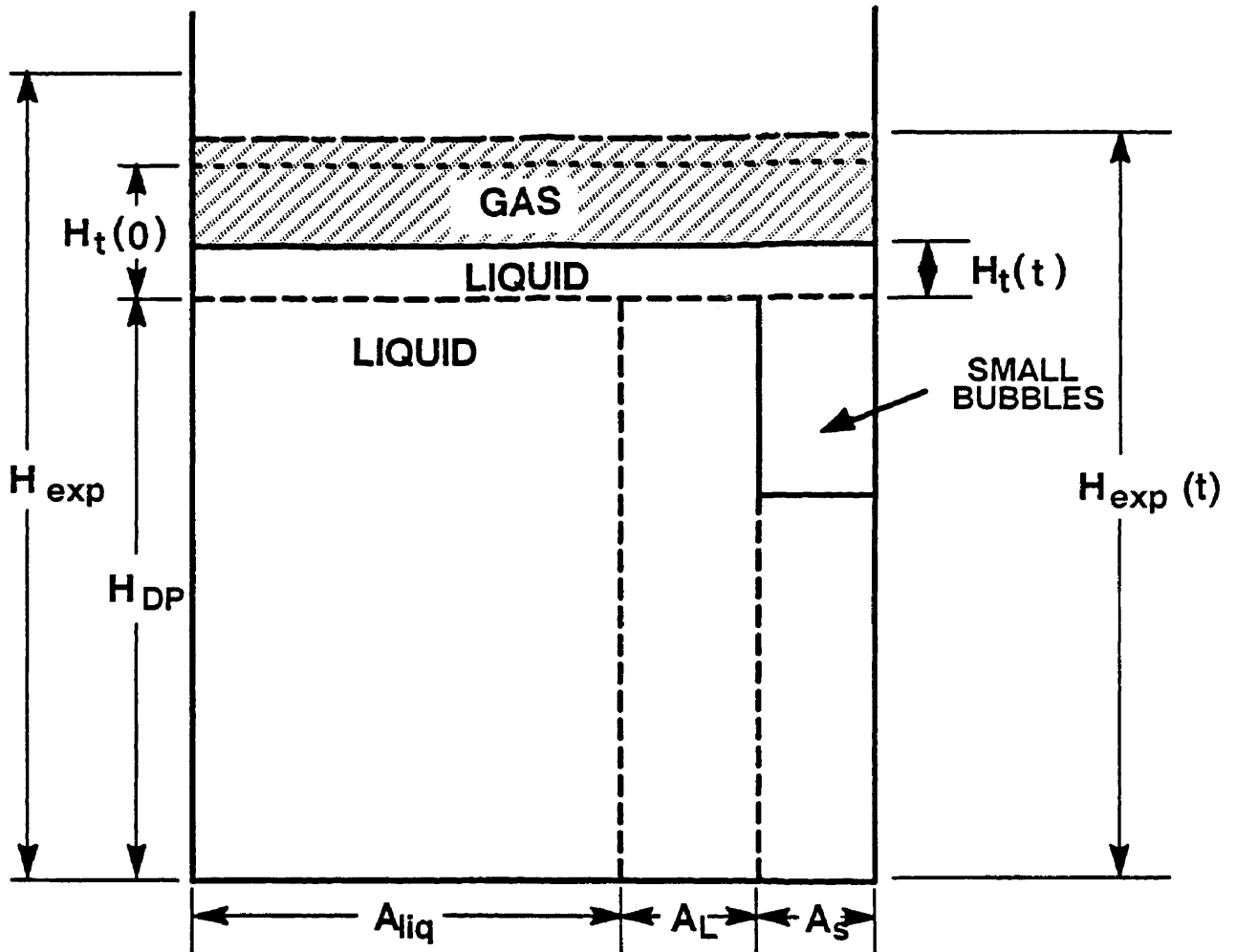
Figure 5.3. Dispersion during the constant rate disengagement process (Period 2).

Estimating Bubble Rise Velocities and Gas Holdups During Constant Rate Disengagement

Equation 5.8 implies that a plot of height of liquid above the pressure transducer, $H_t(t)$, versus time, t, should yield a series of straight lines (Figure 5.4) which may be used to determine the rise velocities and volume fractions of bubbles in the dispersion. Since we assumed that the bubbles disengaged from the bottom of the column at a constant rate, the rise velocity associated with bubbles of size j is simply

$$u_{bj} = \frac{H_{DP}}{t_j} \qquad (5.9)$$

where t_j is the time at which the last bubble of size j, passed above the pressure transducer. Once the rise velocities of the bubbles are determined, the gas holdup corresponding to bubbles of size j can be obtained from Eq. 5.8, and is expressed as follows

$$\epsilon_{goj} = \frac{-S_j - \sum_{i=j+1}^{n} u_{bi}\epsilon_{goi}}{u_{bj}} \qquad (5.10)$$

where S_j is the slope of the disengagement curve corresponding to the disengagement of bubbles in period j (see Figure 5.4). Eq. 5.10 is solved recursively beginning with j = n (i.e. last period of disengagement). Note, for j=n, $\epsilon_{gon} = -S_n/u_{bn}$.

Case II.   Interactive Disengagement Process

The disengagement process is defined to be interactive when the disengagement of one class of bubbles affects the disengagement of another class. This type of disengagement may occur for highly coalescing systems in which the slug flow regime occurs. Once again, for simplicity, we have assumed a bimodal bubble size distribution in order to illustrate the theory. Based on visual observations of the flow pattern in the 0.05 m ID glass column with tap water as the liquid medium, large slugs, intermittantly spaced were present. At a gas velocity of 0.04 m/s, slug lengths in the range 10 to 15 cm were
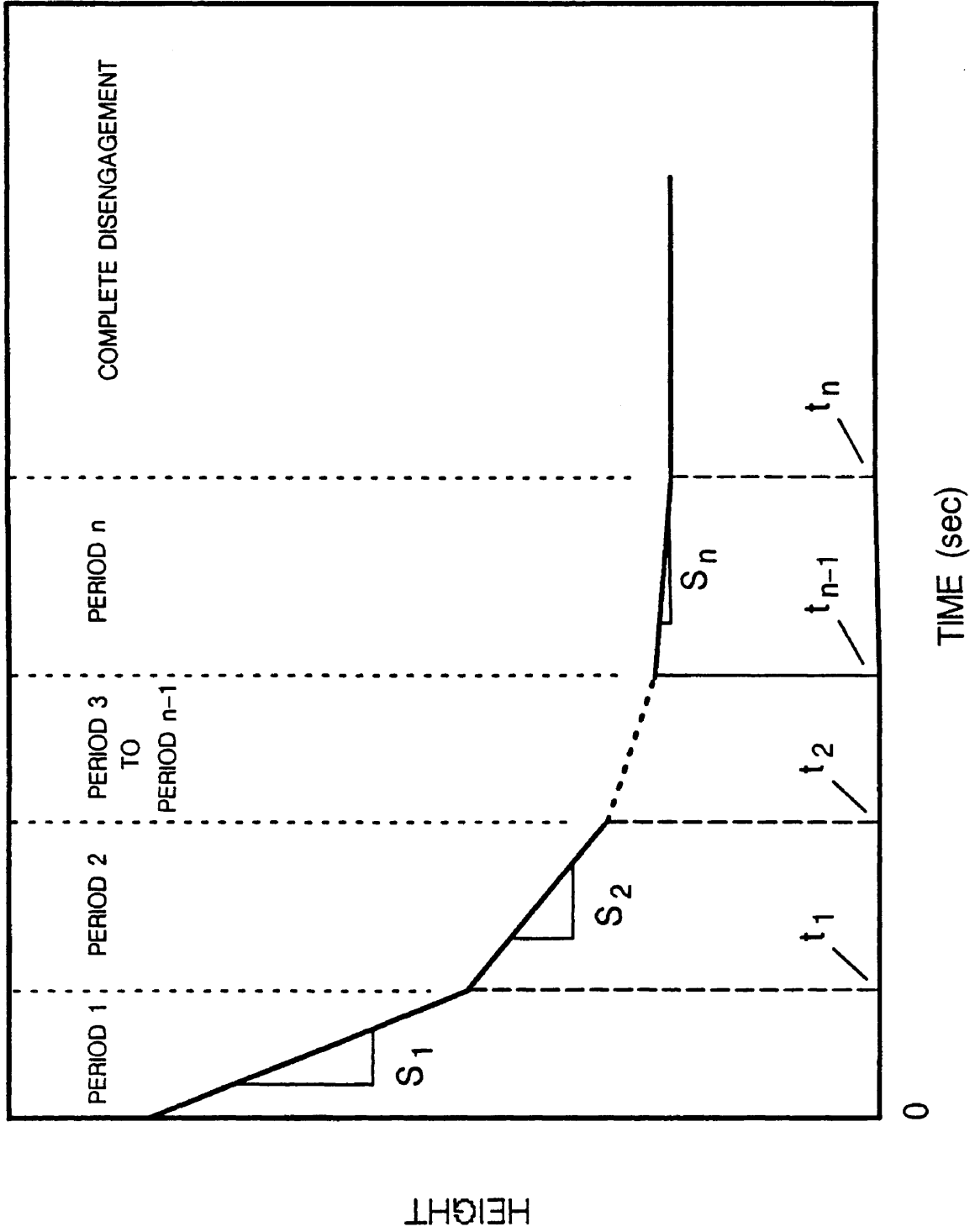
Figure 5.4. Plot of height vs. time for a multimodal distribution (constant rate process).

observed, and at a gas velocity of 0.09 m/s, slugs lengths in the range 10 to 25 cm in length were observed. Figure 5.5 is a schematic representation of the flow field during steady state flow. As one can see, the slugs are separated by sections which contain both small bubbles and liquid. Thus, intuitively, one would expect to observe a stepwise decrease in the disengagement curve during large bubble disengagement, followed by a monotonic decrease in the disengagement curve following large bubble disengagement.

There are several approaches one may use in modeling this type of disengagement process. In the present analysis, we consider three possible types of interactions between the large and small bubbles during large bubble disengagement.

Type 1. Interactive Disengagement

For the first case, we assume the following: (1) the volume fraction of small bubbles is uniform throughout the dispersion (i.e. volume fraction of small bubbles in the liquid is axially uniform) at the beginning of the disengagement process , (2) both small bubbles and large bubbles disengage from the bottom of the column at a constant rate, (3) slugs do not form a continuous column of gas, but rather, individual slugs are separated by dispersion containing liquid and small bubbles, and (4) the slip velocity between the liquid and small gas bubbles in the dispersion between slugs remains constant.

Assumption (3) implies that during the disengagement of large bubbles, the change in the liquid height above the pressure transducer will not be continuous. That is, there will be a sharp drop in the liquid level as the slug passes, followed by a slight decrease in the liquid level due to small bubbles disengaging from the dispersion immediately below the slug, until the next slug disengages, at which time, there will be another sharp drop in the liquid level. This process will continue until all the slugs have passed by the pressure transducer. Thus, two equations are needed to describe the disengagement process during large bubble disengagement. First, we will consider what happens as a slug rises past the transducer. Figure 5.6 is a schematic representation of the slug and
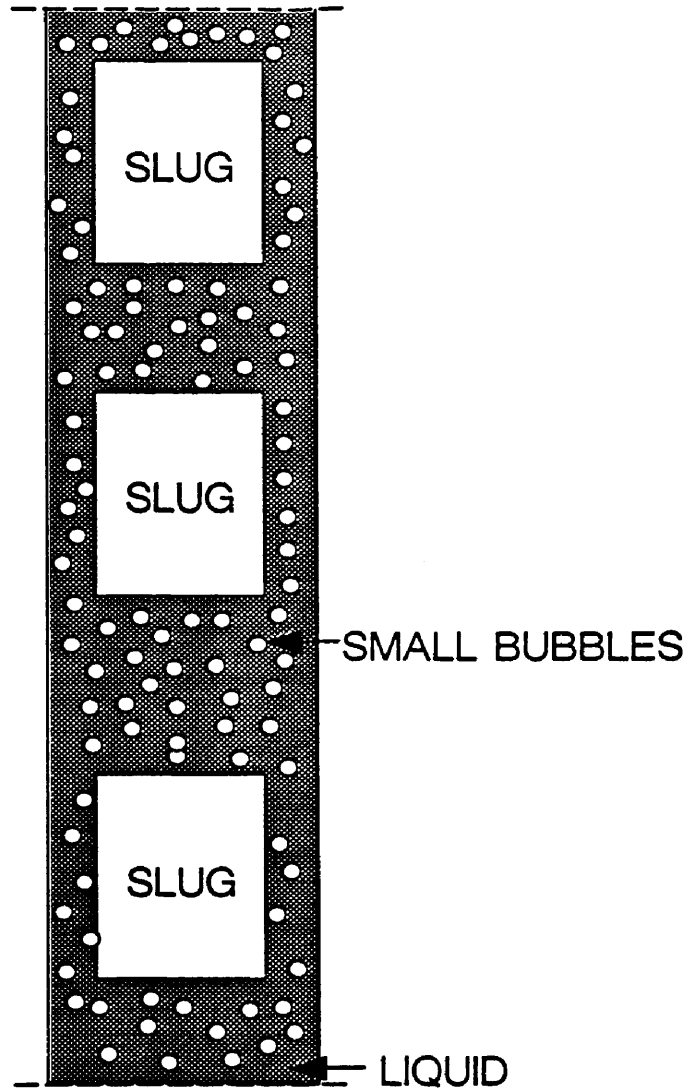
Figure 5.5. Schematic representation of slug flow in the small column with tap water as the liquid medium.
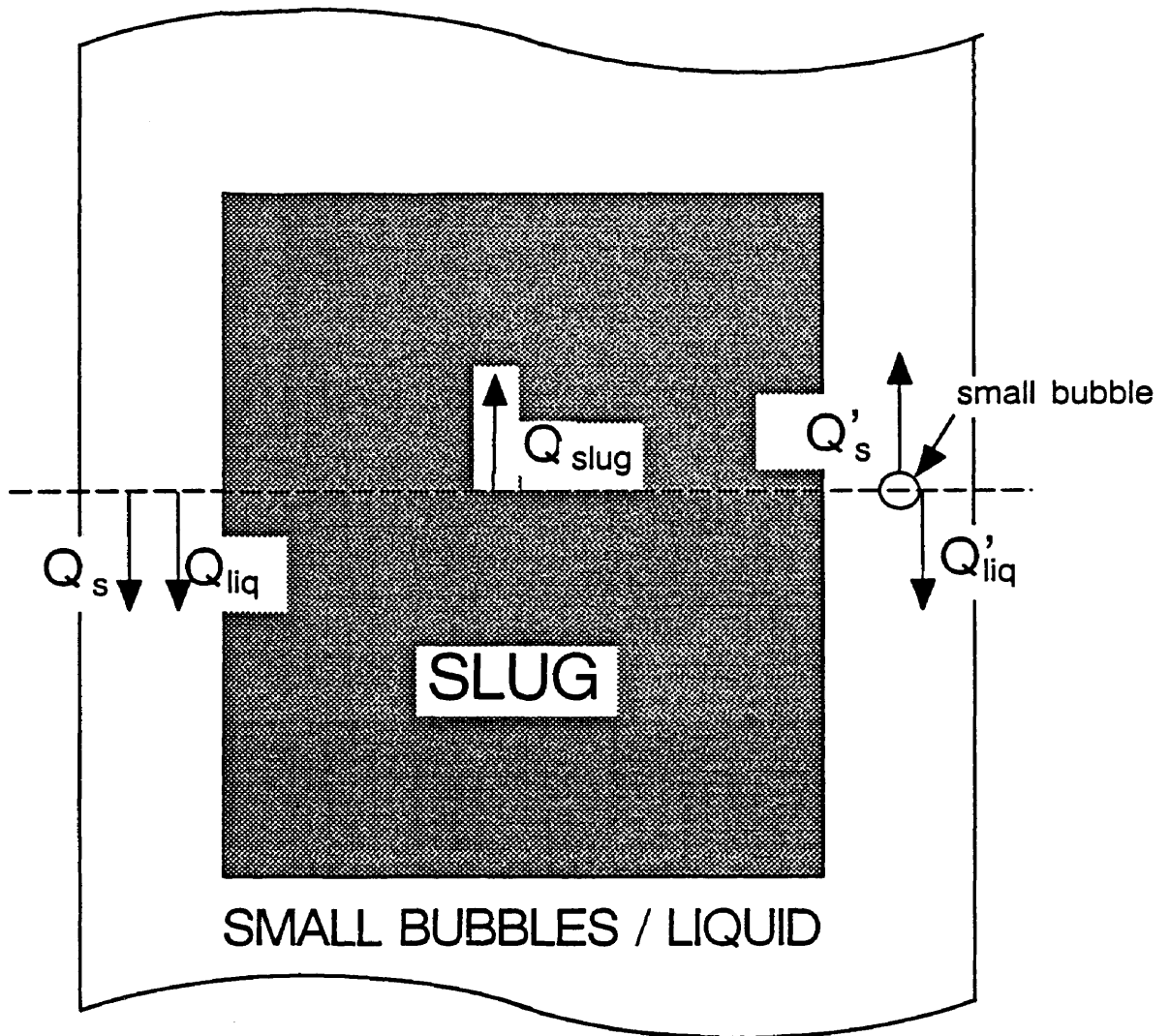
Figure 5.6. Schematic representation of the flow about a slug.

the dispersion surrounding the slug. In regions where slugs are present, gas is moving upward in the form of a slug, and both liquid and gas (small bubbles) are moving downward to fill the void left by the slug. However, the small bubbles do not flow downward at the same rate at which the liquid does, but in essence they flow downward at a slower rate due to their buoyancy. Thus, a volume balance in the region of a slug yields

$$Q_{slug} = (Q_{liq} + Q'_{liq}) + (Q_s - Q'_s) \tag{5.11}$$

where Q_{slug} is the volumetric flow rate of the slug in the upward direction, $(Q_{lig} + Q'_{liq})$ is the net downward flow of liquid, and $(Q_s - Q'_s)$ is the net downward flow of small bubbles. Thus, the net downward flow of liquid, Q_{netliq} is

$$Q_{netliq} = Q_{slug} - Q_s + Q'_s \tag{5.12}$$

The volumetric flow rate of the slug in the upward direction is simply the rise velocity of the slug times the cross sectional area occupied by the slug

$$Q_{slug} = u_{bL} A_{slug} \tag{5.13}$$

Similarly, the volumetric flow rate of gas in the downward direction due to the displacement of dispersion caused by the slug, Q_s, is

$$Q_s = u_{bL} A_{slug} \epsilon_{gs} \tag{5.14}$$

where ϵ_{gs} is the gas holdup of small bubbles in the dispersion surrounding the slug, which is assumed to remain constant throughout the entire disengagment of all slugs. An finally, the volumetric flow rate of small bubbles in the upward direction, due to their buoyancy, Q'_s, is

$$Q'_s = u_{bs}(A_x - A_{slug})\epsilon_{gs} \tag{5.15}$$

where u_{bs} is the rise velocity of the small bubbles and A_x is the cross-sectional area of the column. Combining Eqs. 5.13, 5.14, and 5.15, the volumetric rate at which the liquid level drops may be expressed as

$$Q_{netliq} = u_{BL}A_{slug} + [u_{bs}(A_x - A_{slug}) - u_{bL}A_{slug}]\epsilon_{gs} \qquad (5.16)$$

Thus, at any time during which a slug rises above the pressure transducer, the volume of liquid displaced is

$$V_{liq}(t) = u_{BL}A_{slug}(t - t_{start}) + [u_{bs}(A_x - A_{slug}) - u_{bL}A_{slug}]\epsilon_{gs}(t - t_{start}) \qquad (5.17)$$

where t is the time elapsed since the gas flow to the column was shut off and t_{start} is the time at which the slug reaches the pressure transducer. The volume of liquid displaced, $V_{liq}(t)$, may be expressed as

$$V_{liq}(t) = (H_t(t_{start}) - H_t(t))A_x \qquad (5.18)$$

where $H_t(t_{start})$ is the height of liquid (based on the cross-sectional area of the column) above the pressure transducer immediately prior to the passage of the slug and $H_t(t)$ is the height of liquid above the pressure transducer at time t during the passage of the slug. Thus, combining Eqs. 5.17 and 5.18 and rearranging the terms, the expression for the height of liquid above the pressure transducer during the passage of a slug is

$$H_t(t) = H_t(t_{start}) - u_{BL}f_{slug}(t - t_{start}) - [u_{bs}f_s - u_{bL}f_{slug}]\epsilon_{gs}(t - t_{start}) \qquad (5.19)$$

where f_{slug} is defined as $\frac{A_{slug}}{A_x}$ and f_s is defined as $\frac{A_x - A_{slug}}{A_x}$.

Since the dispersion immediately behind the slug is composed of small bubbles and liquid, only small bubbles rise above the pressure transducer until the next slug reaches the transducer. During this period, the volume of liquid which passes below the pressure transducer, $V'_{liq}(t)$, is

$$V'_{liq}(t) = u_{bs}\epsilon_{gs}(t - t_{slug})A_x \qquad (5.20)$$

The volume of liquid displaced by the small gas bubbles is

$$V'_{liq}(t) = (H_t(t_{slug}) - H_t(t))A_x \qquad (5.21)$$

where $H_t(t_{slug})$ is the height of liquid above the pressure transducer at the time the slug immediately above this section of dispersion passed by the pressure transducer, $H_t(t)$ is the height of liquid above the pressure transducer at any time t during the period in which only small bubbles are allowed to disengage, and t_{slug} is the time at which the slug immediately above the dispersion of liquid and small bubbles passed by the pressure transducer. Combining Eqs. 5.20 and 5.21, and rearranging the terms yields the following expression for the height of liquid above the pressure transducer at any time t during the period between slug disengagement in which only small bubbles disengage

$$H_t(t) = H_t(t_{slug}) - u_{bs}\epsilon_{gs}(t - t_{slug}) \qquad (5.22)$$

Thus, Eqs. 5.19 and 5.22 may be used to describe the disengagement process during slug disengagement.

Once all slugs have passed above the pressure transducer, the only bubbles remaining below the transducer are small bubbles. Thus, a single equation may be used to describe the rate at which the liquid level drops throughout this entire period. The expression used to describe the rate at which the liquid level drops is

$$H_t(t) = H_t(t_{lastslug}) - u_{bs}\epsilon'_{gs}(t - t_{lastslug}) \qquad (5.23)$$

where $H_t(t_{lastslug})$ is the height of liquid above the pressure transducer at the instant the last slug disengaged and ϵ'_{gs} is the volume fraction of small gas bubbles in the dispersion which is disengaging. Note: ϵ'_{gs} does not equal ϵ_{gs}. The quantity ϵ_{gs} is the volume fraction of small bubbles in the dispersion (does not include slug volume) during steady state operation.

Hence, Eqs. 5.19 and 5.22, together with Eq. 5.23 may be used to describe the disengagement process for slug flow in highly coalescing media.

Type 2. Interactive Disengagement

In deriving the equations presented above, we assumed that once a slug rises above a given section of the column, the dispersion immediately below that section is no longer affected by the slug. Thus, in between slugs, we assumed small bubbles rose above the pressure transducer without any resistance (see Eq. 5.22). However, in actuality, the dispersion immediately below the slug is affected by downward force of the liquid passing around the slug. This will retard the rate at which the small bubbles rise above the pressure transducer in between the passage of slugs. The extreme case would be that no small bubbles rise above the pressure transducer in between the passage of slugs. For this case, Eq. 5.22 becomes

$$H_t(t) = H_t(t_{slug}) \qquad (5.24)$$

Equations 5.19 and 5.23 remain the same, with the exception of the value of ϵ'_{gs}. For this type of disengagement, ϵ'_{gs} would be greater than the value of ϵ'_{gs} obtained for Type 1 interactive disengagement.

Type 3. Interactive Disengagement

The third possibility is that the volume of small bubbles which pass below the pressure transducer during the passage of a slug equals the volume of small bubbles that rise above the pressure transducer in between the passage of slugs. Since we are assuming the total drop in the liquid level during the entire slug disengagment period is due solely to the volume of liquid displaced by the slugs, the overall change in the liquid level during slug disengagement is

$$H_t(t_{lastslug}) = H_t(t_{start}) - u_{BL} \epsilon_{goL}(t_{lastslug}) \qquad (5.25)$$

where ϵ_{goL} is the volume fraction of large bubbles (slugs) below the pressure transducer at steady state conditions. Once all slugs have risen past the pressure transducer, the rate at which the liquid level drops is simply

$$H_t(t_{end}) = H_t(t_{lastslug}) - u_{bs}\epsilon_{gos}(t_{end}) \qquad (5.26)$$

Estimating Bubble Rise Velocities During Interactive Disengagement

For the three types of interactive disengagement, rise velocities are calculated in the same manner. Once breakpoints (i.e. end of slug disengagement and end of small bubble disengagement) are determined, rise velocities may be calculated using

$$u_{bL} = H_{DP} / t_{lastslug} \qquad (5.27)$$

and

$$u_{bs} = H_{DP} / t_{end} \qquad (5.28)$$

where $t_{lastslug}$ is the time at which the last slug rose past the pressure transducer, t_{end} is the time the last small bubble rose past the pressure transducer, and H_{DP} is the height of the pressure transducer. Note, Eqs. 5.27 and 5.28 are identical to Eq. 5.9 (i.e. rise velocities are the same whether interactive disengagement or constant rate disengagement is assumed).

Estimating Gas Holdups During Type 1 Interactive Disengagement

The three quantities needed to determine the volume fraction of small bubbles are ϵ_{gs}, ϵ'_{gs}, and A_{slug}. For this type of disengagement process, these three quantities could be determined explicitly provided the disengagement curve was well behaved (i.e. no oscillations) during the period between slugs (i.e. during the period described by Eq. 5.22). Assuming that Type 1 disengagement accurately describes the disengagement process, then the slope, S_1, of the disengagement curve between successive slugs should

be identical. Once this slope is known, the quantity ϵ_{gs} may be calculated directly via Eq. 5.22

$$\epsilon_{gs} = \frac{-S_1}{u_{bs}} \qquad (5.29)$$

Then, the slope of the disengagement curve while a slug passes the pressure transducer, S_2, together with ϵ_{gs} may be used to estimate the quantity A_{slug} via Eq. 5.19 and is

$$A_{slug} = \frac{A_x(S_2 + u_{bs}\epsilon_{gs})}{-u_{bL}(1 - \epsilon_{gs}) + u_{bs}\epsilon_{gs}} \qquad (5.30)$$

And, the last quantity which is needed, ϵ'_{gs}, is estimated from the slope, S_3, of the disengagement curve once all slugs have passed above the pressure transducer (see Eq. 5.23). Thus, ϵ'_{gs} is

$$\epsilon'_{gs} = \frac{-S_3}{u_{bs}} \qquad (5.31)$$

Once these three quantities are known, the volume fraction of small bubbles may be calculated. Recall that the definition of gas holdup is the volume of gas in the dispersion divided by the total volume of the dispersion. The total volume of the dispersion, V_T is simply

$$V_T = H_{DP}A_x \qquad (5.32)$$

The volume of gas associated with the small bubbles below the pressure transducer at steady state is calculated in a three step process. First, we must determine the volume of small bubbles, V_{sb}, which entered the region below the pressure transducer as a slug moves past the pressure transducer. This volume is given by (See Eq. 5.16)

$$V_{sb_i} = (u_{bs}f_s - u_{bL}f_{slug})\epsilon_{gs}A_x\Delta t_i \qquad (5.33)$$

where V_{sb_i} is the volume of small bubbles displaced by slug i, and Δt_i is the time taken for slug i to rise above the pressure transducer. Thus, the total volume of small bubbles

which enters the dispersion below the pressure transducer while the slugs exit the system is

$$V_{sb_{slug}} = \sum_i V_{sb_i} \qquad i = 1 \text{ to } n \tag{5.34}$$

where n is the total number of slugs. The next step is to determine the volume of small bubbles which rise above the pressure transducer in between the passage of slugs. This volume may be estimated via Eq. 5.22 and is

$$V_{sb_j} = u_{bs}\epsilon_{gs}A_x\Delta t_j \tag{5.35}$$

where Δt_j is the time difference between successive slugs. Thus the total volume of small bubbles which leave during the period between consecutive slugs is

$$V_{sb_{between}} = \sum_j V_{sb_j} \qquad j = n \text{ or } n-1 \tag{5.36}$$

where n is the total number of slugs which have disengaged. And finally the volume of small bubbles which rise past the pressure transducer during the last period of disengagement (see Eq. 5.23) is

$$V_{sb_{last}} = u_{bs}\epsilon'_{gs}A_x\Delta t_{last} \tag{5.37}$$

where Δt_{last} is the length of time associated with the last period of disengagement. Thus, the total volume of small bubbles located below the pressure transducer under steady state conditions is

$$V_{sb_{total}} = V_{sb_{slug}} + V_{sb_{between}} + V_{sb_{last}} \tag{5.38}$$

The gas holdup associated with small bubbles at steady state, ϵ_{gos}, is simply

$$\epsilon_{gos} = \frac{V_{sb_{total}}}{V_T} \tag{5.39}$$

The volume fraction of large bubbles (or slugs) at steady state conditions, ϵ_{goL} is calculated using the average gas holdup and the gas holdup of small bubbles

$$\epsilon_{goL} = \epsilon_g - \epsilon_{gos} \qquad (5.40)$$

where ϵ_g is simply the total height of liquid displaced during the entire disengagement process divided by the height of the pressure transducer. A sample calculation including the sensitivity of the technique to f_{slug} is presented in Appendix D.

Estimating Gas Holdups During Type 2 Interactive Disengagement

For type 2 interactive disengagement, the process of determining the volume fraction of small bubbles in the dispersion below the pressure transducer is not as simple. During the first period of disengagement, there are two unknown quantities (i.e. ϵ_{gs} and A_{slug}). Based on the assumptions of type 2 disengagement, there is only one equation (i.e. Eq. 5.19) which includes the two terms mentioned above. Thus, one of the quantities must be estimated. We assumed that the slug diameter was approximately 0.65 times the column diameter. This implies that the cross sectional area of the slug is half as large as the cross sectional area of the column. Thus, the quantities f_s and f_{slug} (see Eq. 5.19) are both 0.5. Having assumed a value for A_{slug}, one may now calculate ϵ_{gs} using the slope of the line associated with a slug passing the pressure transducer, S_2 (see Eq. 5.19)

$$\epsilon_{gs} = \frac{S_2 + u_{bL}f_{slug}}{u_{bL}f_{slug} - u_{bs}f_s} \qquad (5.41)$$

Then, the volume of small bubbles entering the dispersion below the pressure transducer due to the disengagement of a slug is

$$V_{sb_i} = (u_{bs}f_s - u_{bL}f_{slug})\epsilon_{gs}A_x\Delta t_i \qquad (5.42)$$

where V_{sb_i} is the volume of small bubbles displaced by slug i, and Δt_i is the time taken for slug i to rise above the pressure transducer. The total volume of small bubbles which enter the dispersion while the slugs exit the system is

$$V_{sb_{slug}} = \sum_i V_{sb_i} \qquad i = 1 \text{ to } n \qquad (5.43)$$

where n is the total number of slugs. Since no small bubbles leave or enter the dispersion below the pressure transducer during the period between slugs, $V_{sb_{between}}$ is 0. The remaining calculations are the same as those presented in Eqs. 5.37 to 5.40. A sample calculation is presented in Appendix D.

Estimating Gas Holdups During Type 3 Interactive Disengagement

This is the simplest case to analyze. Since we assumed that the volume of small bubbles in the dispersion below the pressure transducer was the same at the beginning and end of slug disengagement, the total volume of small bubbles in the dispersion at steady state is equal to the total volume of liquid displaced during the small bubble disengagement period. Thus, the steady state volume fraction of small bubbles is simply

$$\epsilon_{gos} = \frac{H_t(lastslug) - H_t(end)}{H_{DP}} \qquad (5.44)$$

where $H_t(lastslug)$ is the height of the liquid above the pressure transducer at the instant the last slug rose past the pressure transducer and $H_t(end)$ is the height of the liquid above the pressure transducer after the last small bubble rose past the transducer. The volume fraction of large bubbles is calculated from Eq. 5.40. A sample calculation is presented in Appendix D.

Estimating Bubble Diameters and the Specific Gas-Liquid Interfacial Area

Bubble rise velocities are estimated from the analysis presented above. However, this analysis does not take into account any radial variations in the rise velocities due to the presence of circulation patterns. This limitation of the DGD technique has

been acknowledged in previous studies (e.g. Sriram and Mann, 1977; Schumpe and Grund, 1986), although no effort has been made to introduce any corrective measures. Based on our visual observations using DGD in the glass columns, the dispersion is fairly uniform once all the large bubbles have disengaged. However, during large bubble disengagement, it is possible that strong circulation patterns still exist in the column and the large bubble rise velocities obtained from DGD may not be accurate.

Bubble sizes are estimated from the terminal rise velocity by using appropriate correlations. The correlations used to determine the bubble sizes in the present study are presented in Table 5.1. For the range of rise velocities not covered by these correlations, bubble diameters were obtained by interpolation. Figure 5.7a shows the curve used to determine bubble sizes for FT–300 wax at 265 °C, with the broken line indicating the interpolated region. The correlations by Abou–el–Hassan (1983) and Clift et al. (1978) were used to estimate bubble diameters. The ranges of applicability for these correlations were satisfied for all cases, except for the wax density at 265 °C. At this temperature, the densities of the waxes used in this study (i.e. FT–300 and SASOL) were in the range 660 – 680 kg / m^3, and they are slightly below the range of applicability of the Abou–el–Hassan correlation. These same correlations were used to estimate bubble sizes for the experiment conducted with tap water (see Figure 5.7b).

Once the bubble sizes are known, the Sauter mean bubble diameter may be calculated. The definition of the Sauter mean bubble diameter assumes spherical bubbles and is given by

$$d_s = \frac{\sum_{i=1}^{N} n_i d_{Bi}^3}{\sum_{i=1}^{N} n_i d_{Bi}^2} \tag{5.45}$$

Table 5.1. Correlations for Estimating Bubble Size from Bubble Rise Velocity

Reference	Correlation	Range of applicability
Clift et al. (1978)	$u_b = \left[\dfrac{2.14\sigma_\ell}{\varrho d_b} + 0.505 g d_b\right]^{0.5}$	$d_b > 1.3\ mm$
Abou-el-Hassan (1983)	$V = 0.75[log(F)]^2$ $V = velocity\ number$ $= \dfrac{u_b d_b^{2/3}\varrho_\ell^{2/3}}{\mu_\ell^{1/3}\sigma_\ell^{1/3}}$ $F = flow\ number$ $= \dfrac{g d_b^{8/3}(\varrho_\ell - \varrho_g)\varrho_\ell^{2/3}}{\mu_\ell^{4/3}\sigma_\ell^{1/3}}$	$710 \leq \varrho_\ell \leq 1180\ kg/m^3$ $0.233 \leq \mu_\ell \leq 59\ mPa.s$ $0.015 \leq \sigma_\ell \leq 0.072\ N/m$ $0.1 \leq V \leq 40$ $1 \leq F \leq 10^6$
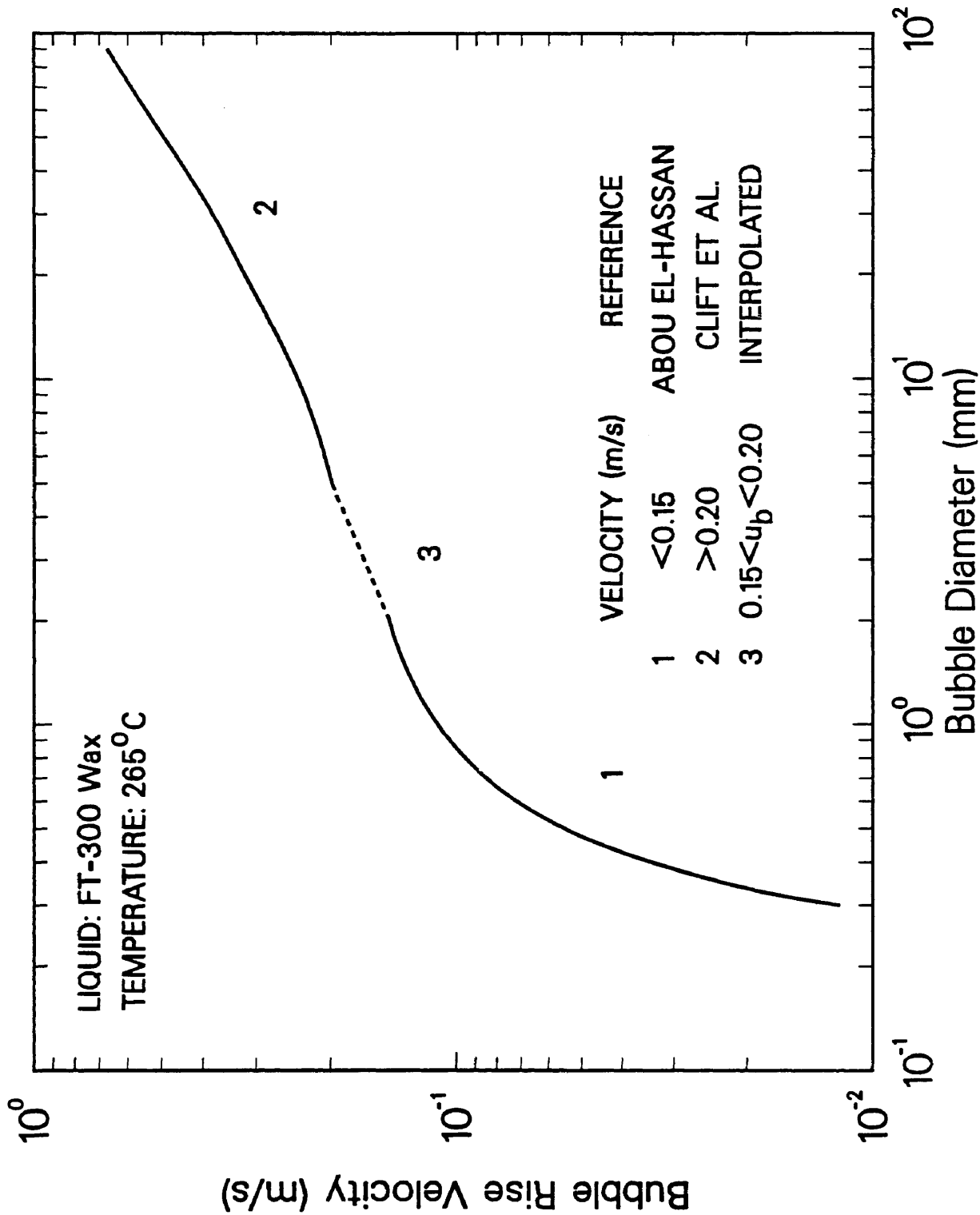
Figure 5.7a. Bubble rise velocity vs. bubble diameter correlation for FT-300 wax.
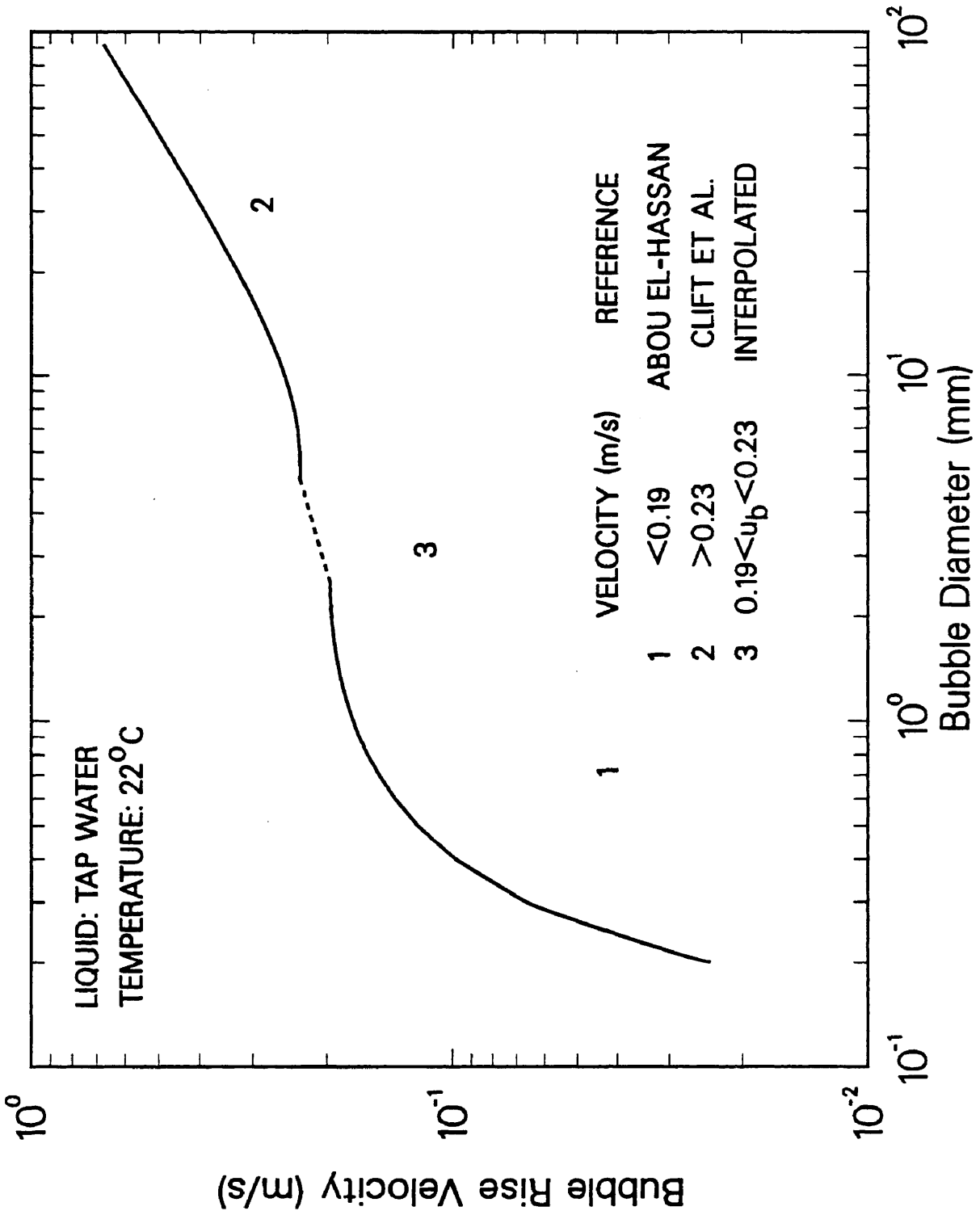
Figure 5.7b. Bubble rise velocity vs. bubble diameter correlation for tap water.

where N is the total number of bubble classes, and n_i is total number of bubbles of size d_{Bi}. The number of bubbles of size d_{Bi} may be estimated as follows. The overall gas holdup may be defined as

$$\epsilon_g = \sum_{i=1}^{N} \epsilon_{gi} = \frac{\sum_{i=1}^{N} n_i V_i}{V_t} \tag{5.46}$$

Thus, the number of bubbles in a given bubble class may be written as

$$n_i = \frac{\epsilon_{gi} V_T}{V_i} \tag{5.47}$$

where V_i is the volume corresponding to a bubble of size d_{Bi} and V_T is the total volume of the dispersion below the pressure transducer. Since the volume of an individual bubble is $\pi d_{Bi}^3 / 6$ and the total volume of the dispersion below the pressure transducer is $\pi d_{col}^2 H_{DP} / 4$, Eq. 5.47 may be rewritten as

$$n_i = \frac{3\epsilon_{gi} d_{col}^2 H_{DP}}{2 d_{Bi}^3} \tag{5.48}$$

Substituting the expression for n_i (Eq. 5.48) into the definition of the Sauter mean bubble diameter, Eq. 5.45, the following expression for the Sauter mean bubble diameter is obtained upon rearrangement

$$d_s = \frac{\epsilon_g}{\sum_{i=1}^{N} \epsilon_{gi} / d_{Bi}} \tag{5.49}$$

Data Acquisition and Reduction Procedures for Experiments with Wax

Pressure transducers located at heights of 0.6, 1.3, and 1.9 m above the distributor were used to measure the rate at which the liquid level dropped during the disengagement process. By obtaining data at different heights, knowledge of the axial variation in bubble size distribution may be obtained. After achieving steady state at a given gas velocity ($\approx$ 1.5 hours), the gas flow to the column was shut off using a solenoid

valve and the change in the output voltage from the pressure transducer indicators was recorded via the data acquisition system described in Chapter II. Based on our previous work (Bukur et al., 1987a) disengagment was complete within 2 minutes; thus, during the present studies, disengagement data (i.e. output voltages) were acquired for approximately 2 minutes at a sampling frequency of 10 Hz once the gas flow to the column was terminated. The output voltage from each pressure indicator was converted to pressure (inches of water) using the calibration curves (see Chapter II)

$$P \text{ (inches of water)} = SLOPE * (OUTPUT\ VOLTAGE) + INT \qquad (5.50)$$

The pressure, P, may be expressed in "inches of wax" by

$$P \text{ (inches of wax)} = \frac{P \text{ (inches of water)}}{s_\ell} \qquad (5.51)$$

where s_ℓ is the specific gravity of wax. Numerically, the pressure (inches of wax) corresponds to the height of liquid wax above a given pressure transducer.

Typical output voltage versus time data at heights of 0.6, 1.3, and 1.9 m above the distributor from the batch experiment with FT–300 in the 0.05 m ID column at a superficial gas velocity of 0.06 m/s are shown in Figures 5.8a, 5.8b, and 5.8c, respectively. The disengagement profiles at heights of 1.3 and 1.9 m are well defined, but their is a significant amount of oscillations in the disengagement curve acquired at a height of 0.6 m above the distributor. The variation in the disengagement curve at a height of 0.6 m are due to oscillations in the pressure caused by the disengagement of large bubbles from the dispersion. Due to the uncertainty in the disengagement curve at a height of 0.6 m, data obtained at this height were not analyzed.

The original disengagement curve was smoothed by dividing it into 120 equally spaced intervals. This was done by averaging the output voltage for every ten data
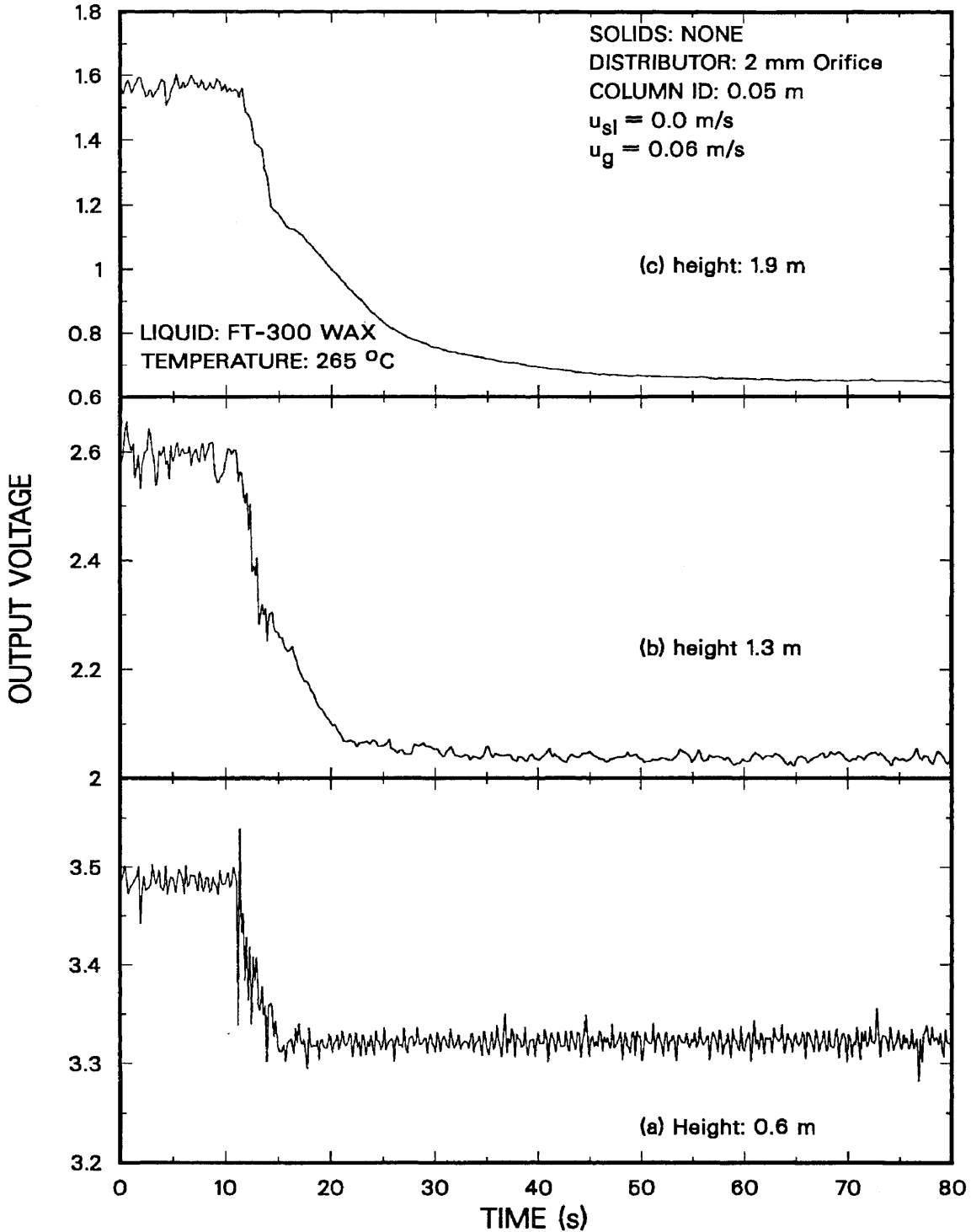
Figure 5.8. Raw pressure transducer signal for DGD analysis from the experiment with FT-300 wax in the small diameter column at heights of (a) 0.6 m; (b) 1.3 m; and (c) 1.9 m above the distributor.

points, with the exception of the five points at the beginning and end of the disengagement curve. Following this, the slope between successive points were calculated. If successive slopes varied by less than 0.5 %, then the slopes of the two lines were assumed to be the same, and the point common to both lines was omitted, thus reducing the number of bubble classes by one. In general, this reduced the 120 bubble classes to approximately 10 to 20. The output voltage of each data point was then converted to height (inches of wax) by use of Eqs. 5.50 and 5.51. These data (i.e. height vs time) were used to calculate bubble rise velocities and gas holdups for each bubble class via Eqs. 5.9 and 5.10, respectively. Once bubble rise velocities were obtained, bubble sizes were calculated using the correlations presented in Table 5.1. The Sauter mean bubble diameter was obtained from Eq. 5.49. Finally, the specific gas–liquid interfacial area was calculated from Eq. 5.1 using the gas holdup of the dispersion below the pressure transducer.

Data Acquisition and Reduction Procedures for the Experiment with Water

The interactive disengagement process was used to model the data obtained from the experiment with tap water conducted in the 0.05 m ID bubble column. Data were collected at heights of 1.3 and 1.9 m above the distributor. Based on our previous work (Patel et al., 1989), the time required for complete disengagement (air/water system) is less than 20 sec. Thus, data was collected for 20 sec at a sampling frequency of 50 Hz. The height of water above a given pressure transducer at any time t during the disengagment process, was obtained using Eq. 5.50 and the output voltage data from the pressure transducer indicator.

Height of water (inches) versus time data from the experiment with tap water at a height of 1.9 m above the distributor are shown in Figure 5.9. During large bubble disengagement, there is a non–continuous change in the liquid level with time. The
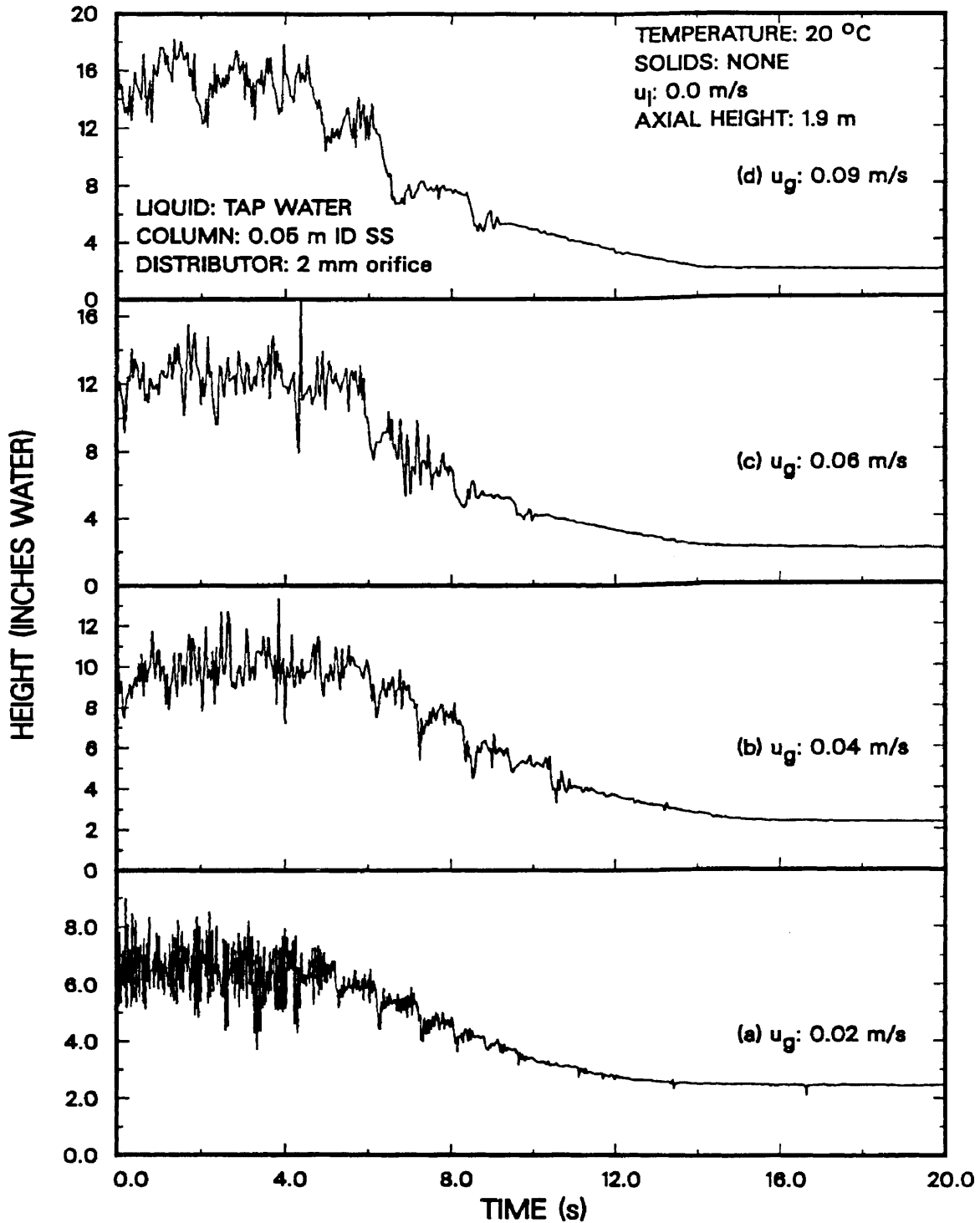
Figure 5.9. Effect of superficial gas velocity on disengagement (Tap water).

data from this experiment were analyzed assuming both type 2 and type 3 interactive disengagment. Once the rise velocities and gas holdup associated with the two bubble classes were calculated (see Appendix D for sample calculations), bubble sizes were obtained using the correlations presented in Table 5.1. The Sauter mean bubble diameters were obtained using Eq. 5.49 and the specific gas–liquid interfacial areas were calculated using Eq. 5.1.

Discussion of Results

Dynamic gas disengagement results will be divided into two main sections. In the first section, results from experiments with both FT–300 and SASOL wax are discussed, whereas in the second section, results from the experiment with tap water in the small diameter column are presented.

Results from Experiments with Wax

Dynamic gas disengagement measurements were carried out in the two stainless steel columns (0.05 m ID and 0.21 m ID, 3 m tall) during some of the two–phase experiments conducted in the batch mode of operation. DGD data were acquired during two experiments with SASOL wax (experiments 1 and 5 in Table 2.5) and one experiment with FT–300 wax (experiment 30 in Table 2.5) in the large diameter column, and during one experiment with SASOL wax (experiment 29 in Table 2.4) and one experiment with FT–300 wax (experiment 23 in Table 2.4) in the small diameter column. The 2 mm orifice plate distributor was used in the 0.05 m ID column and the 19 x 2 mm distributor was employed in the 0.21 m ID column. All disengagement data for wax were analyzed assuming Case I disengagement.

Figures 5.10 and 5.11 show the disengagement curves at heights of 1.3 and 1.9 m above the distributor plotted as normalized differential height versus time for FT–300
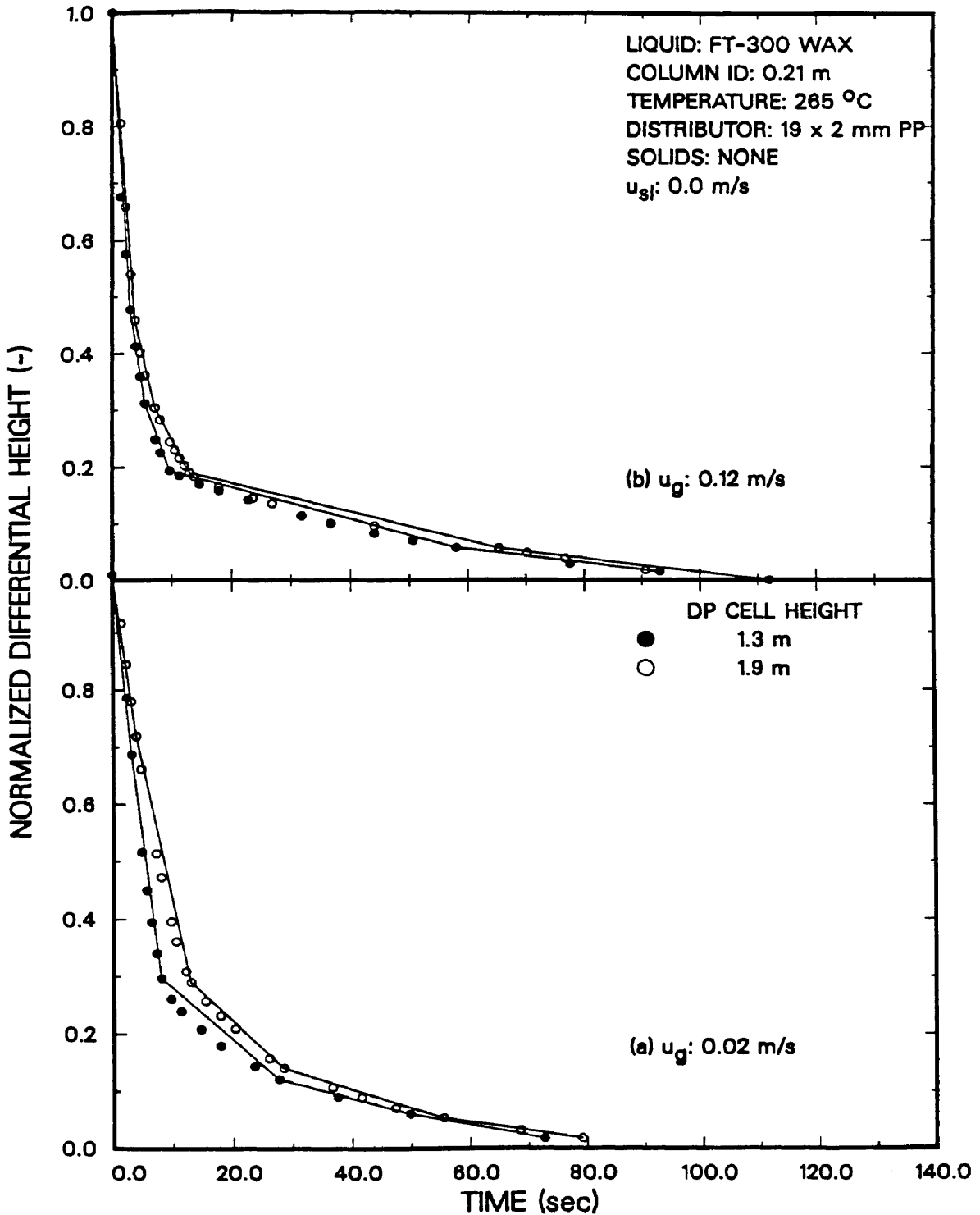
Figure 5.10. Effect of axial position on disengagement (FT-300 wax, (a) $u_g = 0.02$ m/s; (b) $u_g = 0.12$ m/s).
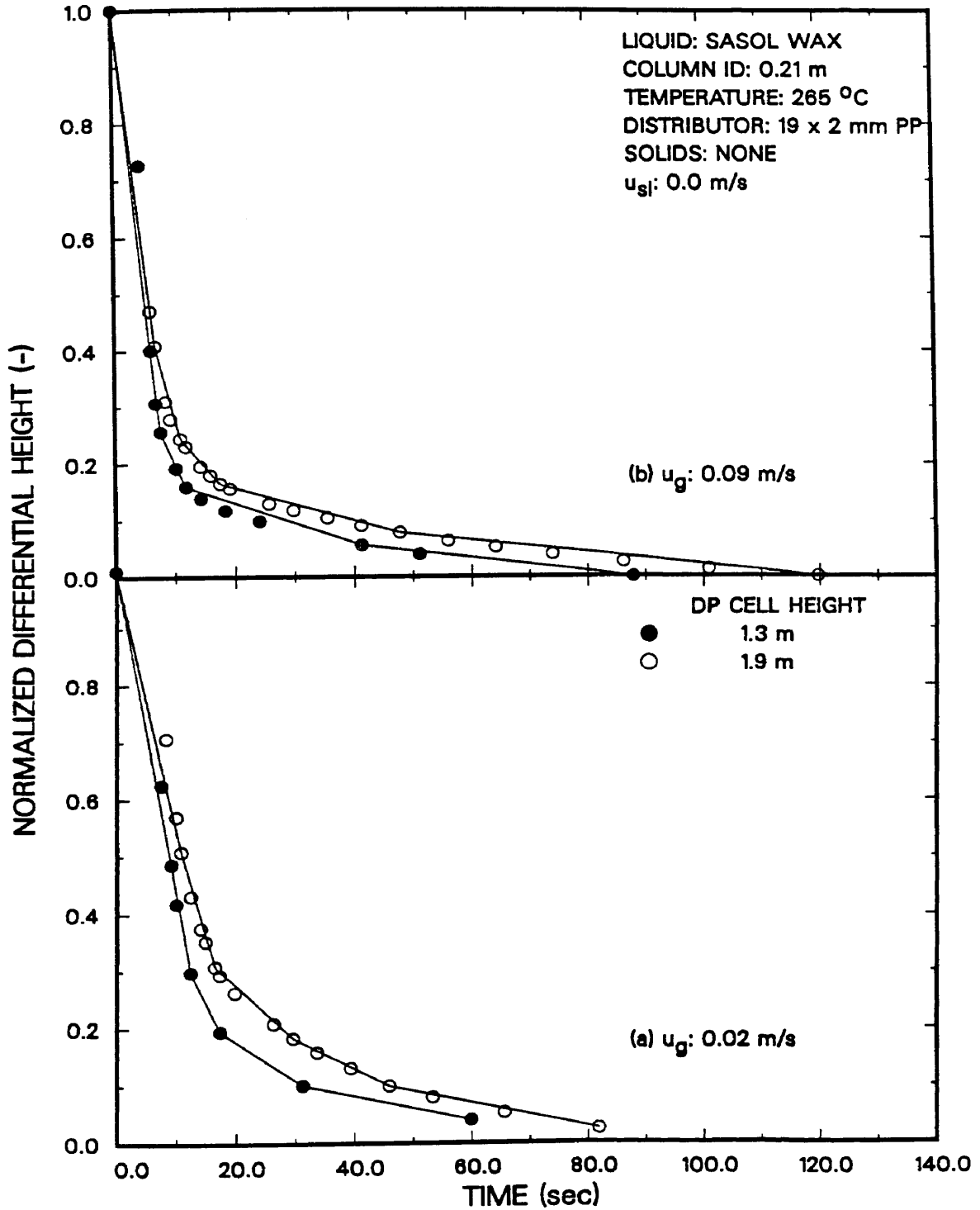
Figure 5.11. Effect of axial position on disengagement (SASOL wax. (a) u_g = 0.02 m/s; (b) u_g = 0.09 m/s).

wax and SASOL wax, respectively. The normalized differential height is defined as

$$\text{Norm. Diff. Height} = \frac{H_t(t_i) - H_t(t_n)}{H_t(0) - H_t(t_n)} \qquad i = 1 \text{ to } n \qquad (5.52)$$

where $H_t(t_n)$ is the height of the liquid above the pressure transducer at the instant the last small bubble rises above the pressure transducer, $H_t(0)$ is the height of liquid above the pressure transducer immediately prior to interrupting the gas flow (i.e. at steady state conditions), and $H_t(t_i)$ is the height of liquid above the pressure transducer when the last bubble of size d_{Bi} passes above the pressure transducer. The data from experiments in the large column were also analyzed by dividing the disengagement curve into five intervals (i.e. five bubble classes, lines on Figures 5.10 and 5.11) to see what effect the number of bubble classes used has on the Sauter mean bubble diameter and specific gas–liquid interfacial area. If the dispersion is axially uniform, then the major breakpoints on the two curves (i.e. at heights of 1.3 and 1.9 m) would occur at the same normalized differential height. Also, if bubbles are rising at the same velocity as they rise past heights of 1.3 and 1.9 m, then the curve associated with the DP cell located at 1.9 m should be shifted to the right of the curve associated with the DP cell located 1.3 m. Both the trends mentioned above were observed in all experiments with wax in both the large and small diameter columns.

The gas holdups presented throughout this discussion, unless otherwise noted, correspond to the gas holdup of the dispersion below the measurement location. These gas holdups were obtained using Eq. 2.27, with n = 3 (for data obtained at a height of 1.3 m above the distributor) and n = 4 (for data obtained at a height of 1.9 m above the distributor). The specific gas liquid interfacial areas and Sauter mean bubble diameters are based on the holdup of the dispersion below the measurement location. Tables 5.2, 5.3, and 5.4 summarize the results obtained from experiments in the large diameter column with FT–300 wax and SASOL reactor wax (decreasing and increasing order of

Table 5.2a. DGD Results from the Experiment with FT–300 Wax at a Height of 1.3 m (0.21 m ID Stainless Steel Bubble Column, 265 °C)

u_g (m/s)	ϵ_{go} (-)	u_{bs} (m/s)	u_{bm} (m/s)	u_{bl} (m/s)	f_l (-)	d_s (mm)	d_s^* (mm)	a_s (m^{-1})	a_s^* (m^{-1})
0.02	0.093	0.017	0.168	0.51	0.13	0.92	0.96	607	581
0.04	0.118	0.015	0.168	0.51	0.23	0.95	1.01	745	701
0.08	0.181	0.014	0.126	0.51	0.45	1.12	1.12	970	970
0.12	0.199	0.013	0.137	0.51	0.55	1.33	1.30	898	920

Table 5.2b. DGD Results from the Experiment with FT–300 Wax at a Height of 1.9 m (0.21 m ID Stainless Steel Bubble Column, 265 °C)

u_g (m/s)	ϵ_{go} (-)	u_{bs} (m/s)	u_{bm} (m/s)	u_{bl} (m/s)	f_l (-)	d_s (mm)	d_s^* (mm)	a_s (m^{-1})	a_s^* (m^{-1})
0.02	0.102	0.024	0.151	0.57	0.13	0.92	0.97	665	631
0.04	0.121	0.020	0.162	0.57	0.23	0.92	0.99	789	733
0.08	0.184	0.017	0.142	0.57	0.54	1.26	1.32	876	836
0.12	0.196	0.017	0.151	0.57	0.57	1.37	1.45	858	811

* Denotes values from analysis of all points.

Table 5.3a. DGD Results from the Experiment with SASOL Wax (Decreasing Gas Velocity) at a Height of 1.3 m (0.21 m ID Stainless Steel Bubble Column, 265 $^{\circ}$C)

u_g (m/s)	ϵ_{go} (-)	u_{bs} (m/s)	u_{bm} (m/s)	u_{bl} (m/s)	f_l (-)	d_s (mm)	d_s^* (mm)	a_s (m^{-1})	a_s^* (m^{-1})
0.02	0.069	0.023	0.190	0.38	0.34	1.30	1.20	318	345
0.04	0.094	0.015	0.150	0.38	0.56	1.30	1.30	434	434
0.06	0.124	0.013	0.130	0.51	0.63	1.50	1.50	496	496
0.09	0.152	0.015	0.150	0.51	0.65	1.60	1.70	570	540

Table 5.3b. DGD Results from the Experiment with SASOL Wax (Decreasing Gas Velocity) at a Height of 1.9 m (0.21 m ID Stainless Steel Bubble Column, 265 $^{\circ}$C)

u_g (m/s)	ϵ_{go} (-)	u_{bs} (m/s)	u_{bm} (m/s)	u_{bl} (m/s)	f_l (-)	d_s (mm)	d_s^* (mm)	a_s (m^{-1})	a_s^* (m^{-1})
0.02	0.074	0.024	0.174	0.38	0.33	1.10	1.10	404	404
0.04	0.109	0.024	0.174	0.38	0.60	1.30	1.40	503	467
0.06	0.130	0.015	0.113	0.45	0.65	1.40	1.50	557	520
0.09	0.154	0.016	0.133	0.56	0.67	1.60	1.60	578	578

* Denotes values from analysis of all points.

Table 5.4a. DGD Results from the Experiment with SASOL Wax (Increasing Gas Velocity) at a Height of 1.3 m (0.21 m ID Stainless Steel Bubble Column, 265 $^{\circ}$C)

u_g (m/s)	ϵ_{go} (-)	u_{bs} (m/s)	u_{bm} (m/s)	u_{bl} (m/s)	f_l (-)	d_s (mm)	d_s^* (mm)	a_s (m^{-1})	a_s^* (m^{-1})
0.02	0.079	0.031	0.152	0.52	0.25	1.00	1.00	474	474
0.04	0.100	0.030	0.176	0.51	0.45	1.10	1.20	545	500
0.06	0.141	0.031	0.164	0.57	0.52	1.20	1.24	705	682
0.09	0.156	0.031	0.178	0.57	0.50	1.25	1.28	749	731

Table 5.4b. DGD Results from the Experiment with SASOL Wax (Increasing Gas Velocity) at a Height of 1.9 m (0.21 m ID Stainless Steel Bubble Column, 265 $^{\circ}$C)

u_g (m/s)	ϵ_{go} (-)	u_{bs} (m/s)	u_{bm} (m/s)	u_{bl} (m/s)	f_l (-)	d_s (mm)	d_s^* (mm)	a_s (m^{-1})	a_s^* (m^{-1})
0.02	0.083	0.047	0.171	0.43	0.30	1.20	1.30	415	383
0.04	0.122	0.031	0.150	0.49	0.45	1.20	1.20	610	610
0.06	0.145	0.034	0.150	0.49	0.50	1.23	1.25	707	696

* Denotes values from analysis of all points.

velocities), respectively. The experiment with FT–300 wax was conducted employing a decreasing order of gas velocities. The results presented in the tables for rise velocities, u_{bi}, and fractions of large bubbles f_L were based on the five bubble class analyses. The rise velocity of large bubbles was taken as the largest rise velocity, and the rise velocity of small bubbles was taken as the smallest rise velocity. The medium bubble rise velocity corresponds to the rise velocity of the middle bubble class. Sauter mean bubble diameters and specific gas–liquid interfacial areas are presented assuming five bubble classes and using all points. The Sauter mean bubble diameters and specific gas–liquid interfacial areas were comparable using both types of analyses. Similar results were obtained in the small column with SASOL and FT–300 wax (see Tables 5.5 and 5.6).

Figure 5.12 compares Sauter mean bubble diameters, specific gas liquid interfacial areas and gas holdups at a height of 1.3 m above the distributor for the experiments conducted in the large column (from 5 bubble classes analysis). The specific gas-liquid interfacial area and Sauter mean bubble diameters are based on the gas holdup of the dispersion below the pressure transducer. The gas holdup values from the experiment with FT–300 wax were slightly higher than those obtained from either of the experiments with SASOL wax (see Figure 5.12c). As shown in Figure 5.12a, the Sauter mean bubble diameters for the experiment conducted with FT–300 wax were consistently lower than those for the experiment conducted with SASOL reactor wax employing a decreasing order of gas velocities. In particular, Sauter mean bubble diameters ranged from approximately 1.0 to 1.3 mm for the experiment conducted with FT–300 wax as opposed to 1.3 to 1.6 mm for the experiment conducted in a decreasing order of gas velocities with SASOL reactor wax. However, the Sauter mean bubble diameters from the experiment conducted in an increasing order of gas velocities with SASOL reactor wax were comparable (slightly higher) to those obtained from the experiment conducted with FT–300 wax. The difference in Sauter mean bubble diameters is caused

Table 5.5a. DGD Results from the Experiment with FT–300 Wax (Increasing Gas Velocity) at a Height of 1.3 m (0.05 m ID Stainless Steel Bubble Column, 265 ^{o}C)

u_g (m/s)	ϵ_{go} (-)	u_{bs} (m/s)	u_{bm} (m/s)	u_{bl} (m/s)	f_l (-)	d_s (mm)	d_s^* (mm)	a_s (m^{-1})	a_s^* (m^{-1})
0.02	0.077	0.031	0.152	0.52	0.25	1.38	1.28	334	361
0.04	0.128	0.030	0.176	0.51	0.45	0.94	1.10	768	698
0.06	0.161	0.031	0.164	0.57	0.52	1.22	1.26	790	767
0.09	0.151	0.031	0.178	0.57	0.50	1.27	1.32	570	686

Table 5.5b. DGD Results from the Experiment with FT–300 wax (Increasing Gas Velocity) at a Height of 1.9 m (0.05 m ID Stainless Steel Bubble Column, 265 ^{o}C)

u_g (m/s)	ϵ_{go} (-)	u_{bs} (m/s)	u_{bm} (m/s)	u_{bl} (m/s)	f_l (-)	d_s (mm)	d_s^* (mm)	a_s (m^{-1})	a_s^* (m^{-1})
0.02	0.086	0.047	0.171	0.43	0.30	1.09	1.12	471	461
0.04	0.137	0.031	0.150	0.49	0.45	0.90	1.01	902	814
0.06	0.181	0.034	0.150	0.49	0.50	0.90	0.97	1200	1120
0.09	0.200	0.034	0.150	0.49	0.50	1.49	1.38	808	870

* Denotes values from analysis of all points.

Table 5.6a. DGD Results from the Experiment with SASOL Wax (Increasing Gas Velocity) at a Height of 1.3 m (0.05 m ID Stainless Steel Bubble Column, 265 °C)

u_g (m/s)	ϵ_{go} (–)	u_{bs} (m/s)	u_{bm} (m/s)	u_{bl} (m/s)	f_l (–)	d_s (mm)	d_s^* (mm)	a_s (m^{-1})	a_s^* (m^{-1})
0.02	0.052	0.031	0.152	0.52	0.25	1.40	1.45	220	215
0.04	0.088	0.030	0.176	0.51	0.45	1.80	1.78	290	297
0.06	0.110	0.031	0.164	0.57	0.52	1.81	1.83	350	361
0.09	0.137	0.031	0.178	0.57	0.50	2.10	2.21	390	372

Table 5.6b. DGD Results from the Experiment with SASOL Wax (Increasing Gas Velocity) at a Height of 1.9 m (0.05 m ID Stainless Steel Bubble Column, 265 °C)

u_g (m/s)	ϵ_{go} (–)	u_{bs} (m/s)	u_{bm} (m/s)	u_{bl} (m/s)	f_l (–)	d_s (mm)	d_s^* (mm)	a_s (m^{-1})	a_s^* (m^{-1})
0.02	0.086	0.047	0.171	0.43	0.30	1.30	1.32	400	391
0.04	0.110	0.031	0.150	0.49	0.45	1.60	1.52	410	434
0.06	0.129	0.034	0.150	0.49	0.50	1.60	1.61	480	481
0.09	0.157	0.034	0.150	0.49	0.50	2.00	2.30	420	410

* Denotes values from analysis of all points.
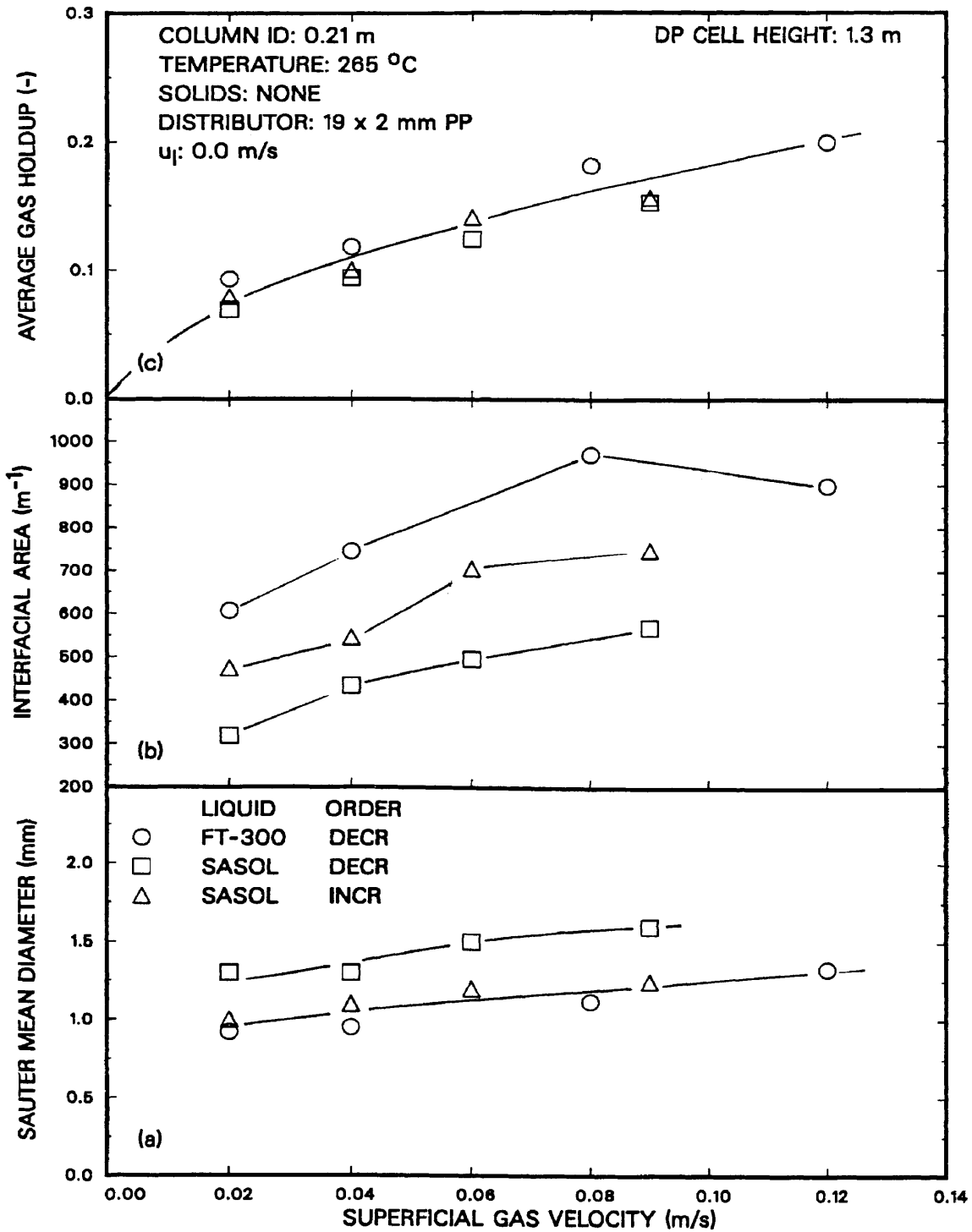
Figure 5.12. Effect of superficial gas velocity and wax type on (a) Sauter mean bubble diameter, (b) specific gas-liquid interfacial area, and (c) gas holdup in the 0.21 m ID column at a height of 1.3 m above the distributor.

by differences in the fraction of large bubbles. For example, at a gas velocity of 0.09 m/s, the fraction of large bubbles for the experiment conducted in an increasing order of gas velocities was 0.50 whereas it was 0.65 for the experiment conducted in a decreasing order of velocities with SASOL reactor wax (see Tables 5.3a and 5.4a). These results indicate that bubble size distribution is affected by the operating procedure. Specific gas liquid interfacial areas obtained from the three experiments were substantially different. There was almost a 100 % increase in a_s between the experiment conducted with FT–300 wax and the experiment conducted in a decreasing order of gas velocities with SASOL reactor wax. Similar results were obtained at a height of 1.9 m above the distributor (see Figure 5.13).

Figures 5.14 and 5.15 show results from experiments in the small diameter column at heights of 1.3 and 1.9 m above the distributor. As shown in Chapter II, FT–300 wax produces foam and as a result, the gas holdups with FT–300 wax are considerably larger than those produced with SASOL reactor wax (see Figures 5.14c and 5.15c). These higher gas holdups result in lower Sauter mean bubble diameters (Figures 5.14a and 5.15a), except at a gas velocity of 0.02 m/s, where the Sauter mean bubble diameters obtained for both waxes are comparable. This is expected, since homogeneous bubbly flow exists in the column at this velocity. As the gas velocity is increased to 0.04 m/s, the gas holdup from the experiment with FT–300 is significantly greater than that from the experiment with SASOL wax. This difference is holdup is due primarily to the presence of fine bubbles which accumulate in the uppermost region of the dispersion. This increase in the number of small bubbles associated with FT–300 wax results in a lower Sauter mean bubble diameter (see Figures 5.14a and 5.15a). Specific gas–liquid interfacial areas are shown in Figures 5.14b and 5.15b.

Figure 5.16 shows axial gas holdups from the experiments conducted with FT–300 wax and SASOL wax, at gas velocities of 0.02, 0.04, and 0.09 m/s. Axial gas holdup
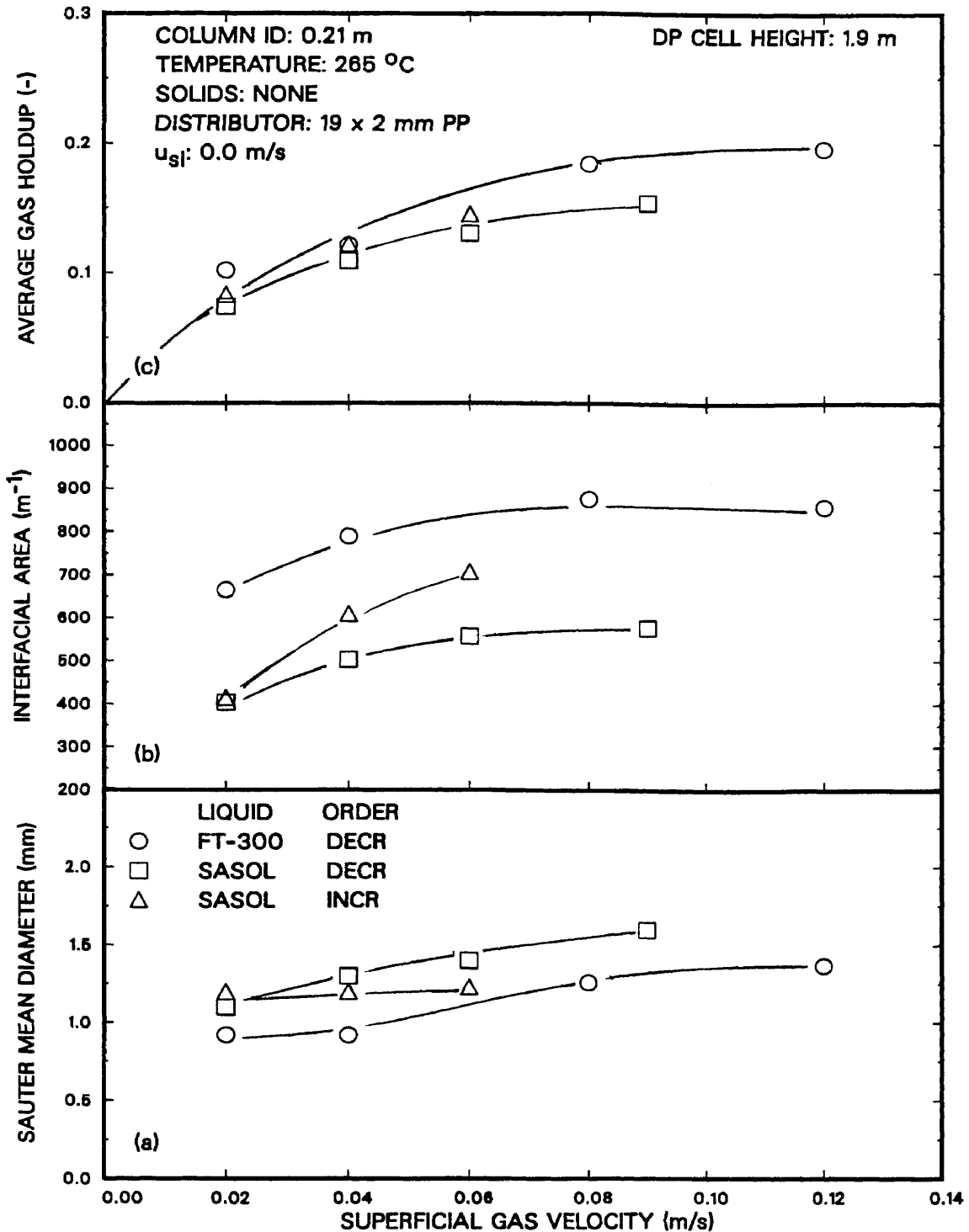
Figure 5.13. Effect of superficial gas velocity and wax type on (a) Sauter mean bubble diameter, (b) specific gas-liquid interfacial area, and (c) gas holdup in the 0.21 m ID column at a height of 1.9 m above the distributor.
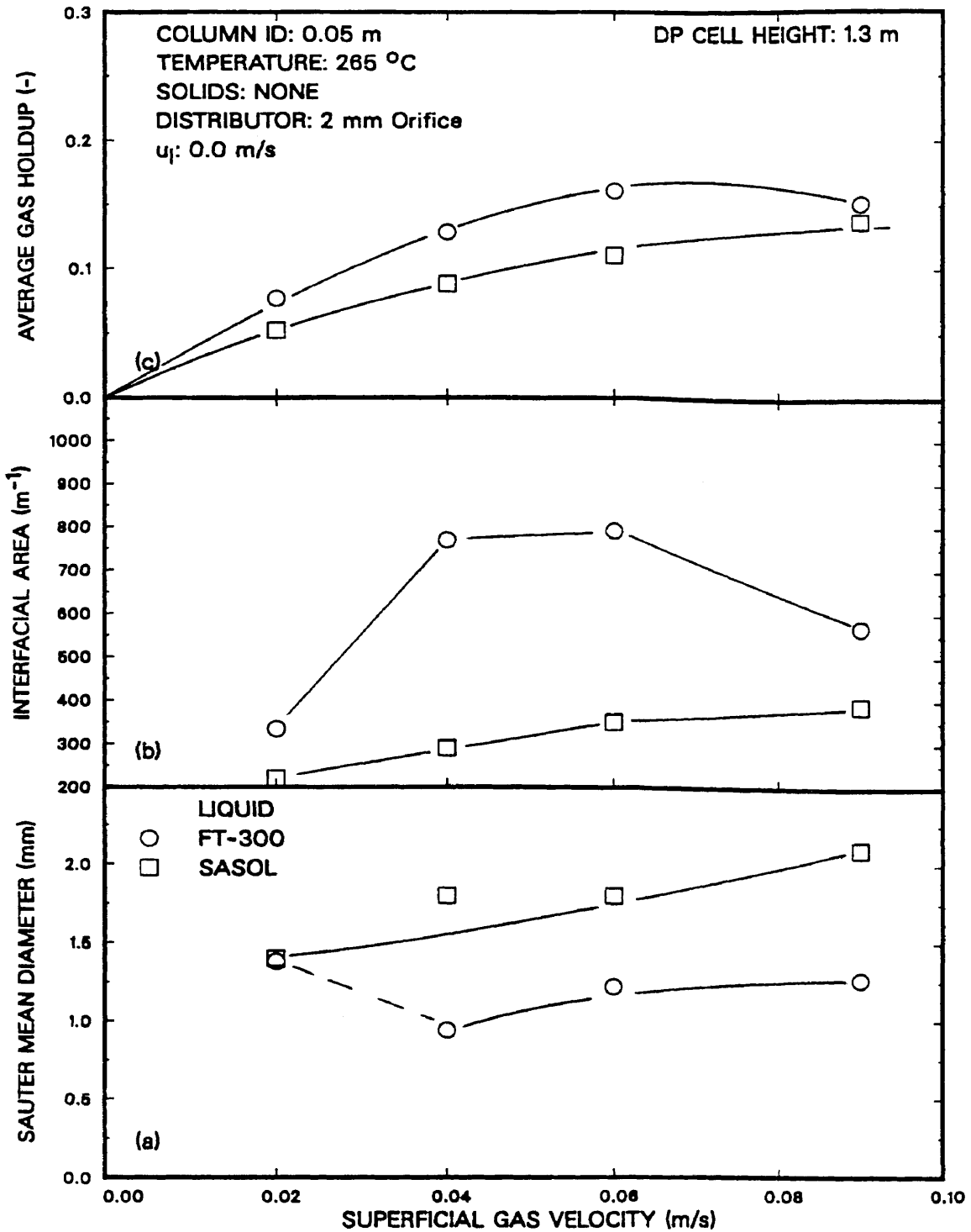
Figure 5.14. Effect of superficial gas velocity and wax type on (a) Sauter mean bubble diameter,
(b) specific gas-liquid interfacial area, and (c) gas holdup in the 0.05 m ID column
at a height of 1.3 m above the distributor.
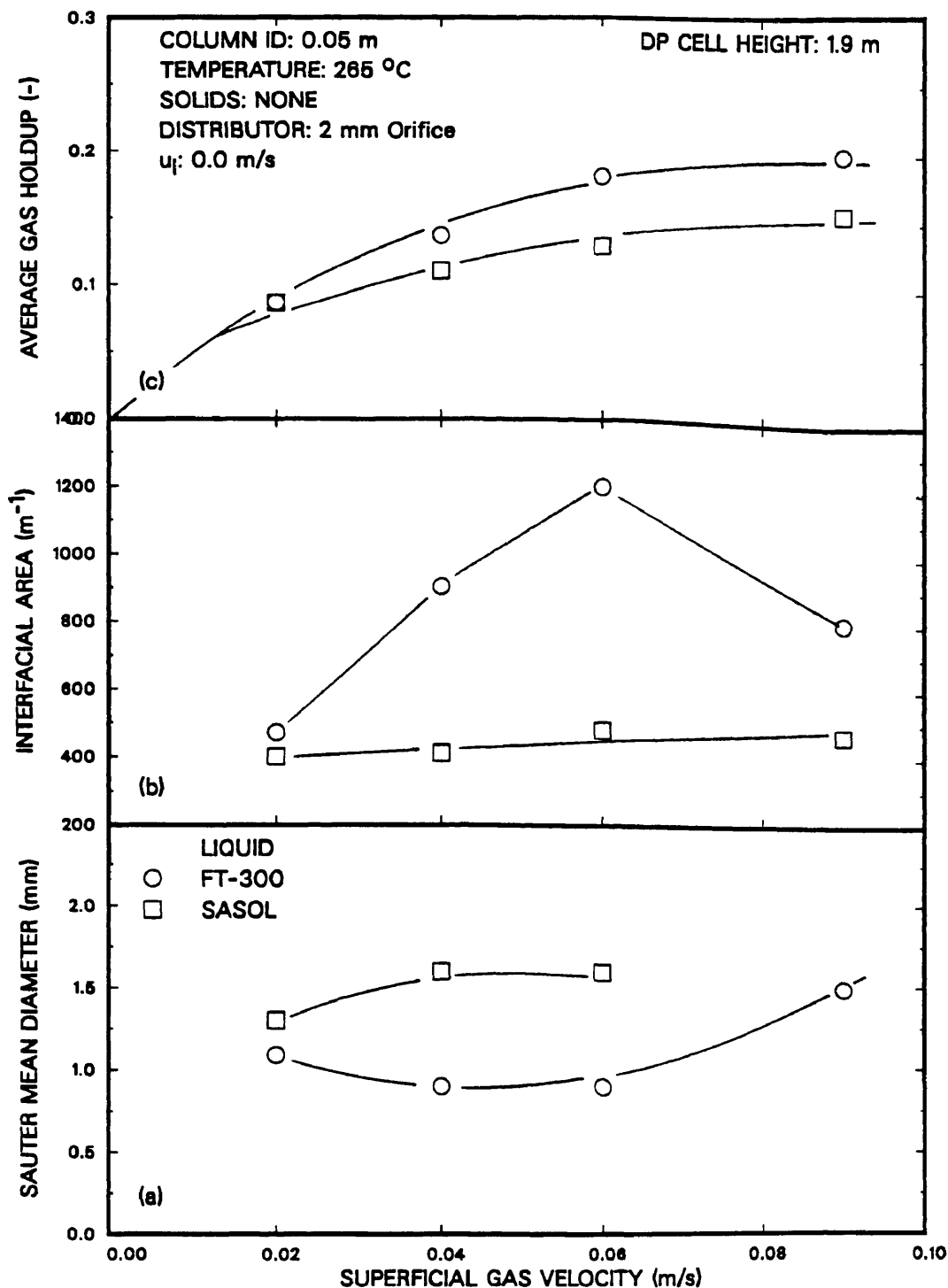
Figure 5.15. Effect of superficial gas velocity and wax type on (a) Sauter mean bubble diameter, (b) specific gas-liquid interfacial area, and (c) gas holdup in the 0.05 m ID column at a height of 1.9 m above the distributor.
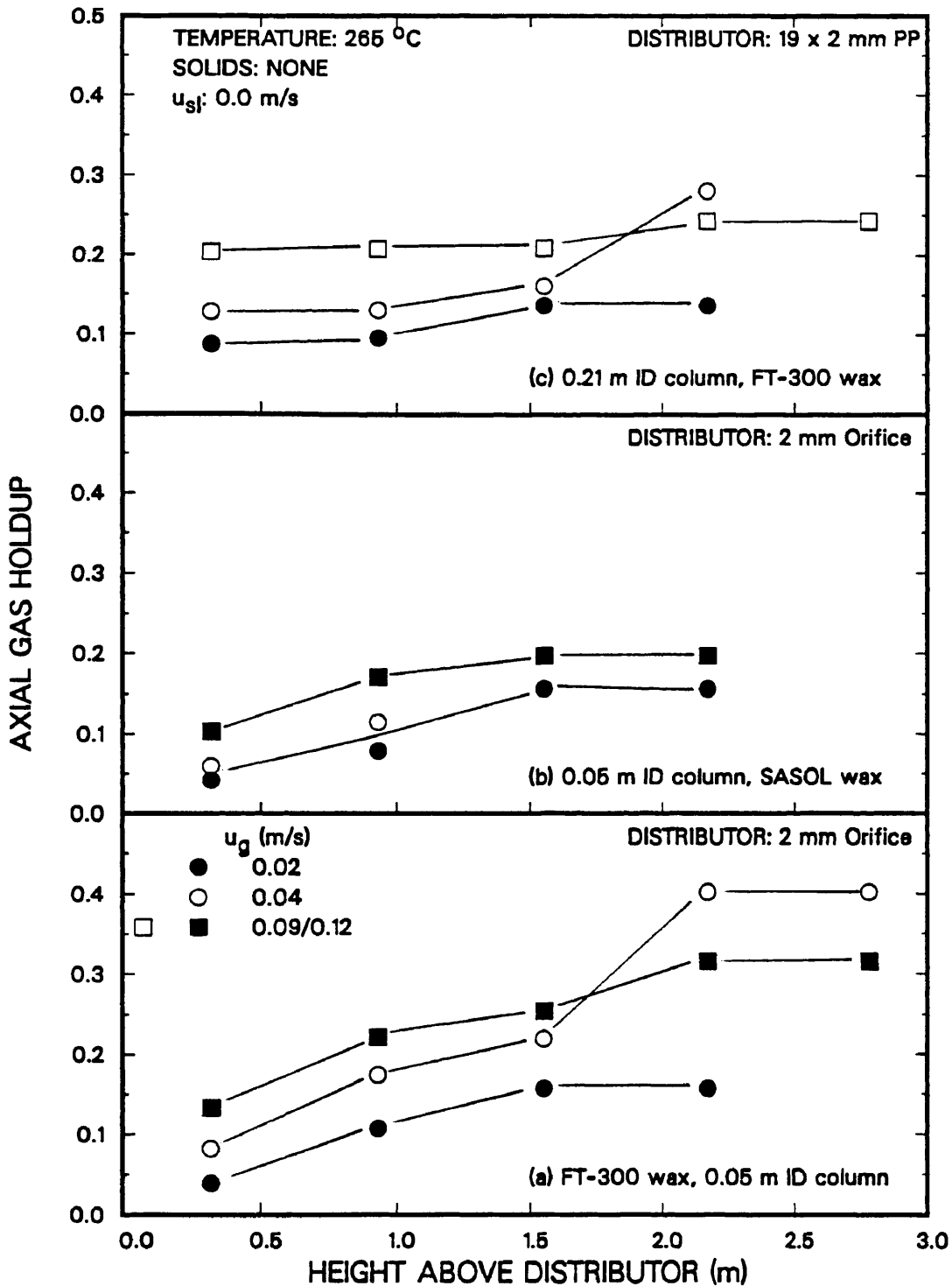
Figure 5.16. Effect of superficial gas velocity on axial gas holdup ((a) 0.05 m ID column, FT-300 wax; (b) 0.05 m ID column, SASOL wax; (c) 0.21 m ID column, FT-300 wax).

profiles from the experiment with SASOL wax show a slight increase in gas holdup with increasing height above the distributor (see Figure 5.16b). However, for the experiment with FT–300 wax, the gas holdup in the uppermost region of the column at a gas velocity of 0.04 m/s increases significantly compared to the holdup at lower heights. In particular, at a height of 1.6 m above the distributor, the gas holdup is approximately 0.2; whereas, at a height of 2.2 m above the distributor, the gas holdup is approximately 0.4. At a gas velocity of 0.09 m/s, the foam layer which was present at a gas velocity of 0.04 m/s dissipates and there is a gradual increase in holdup with increasing height above the distributor. With the exception of a gas velocity of 0.02 m/s, the gas holdups with FT–300 wax are higher than those with SASOL wax, particularly at a gas velocity of 0.04 m/s, and as a result, the Sauter mean bubble diameters from the experiment with FT–300 wax are lower than those obtained from the experiment with SASOL reactor wax. The results from this study with FT–300 wax and SASOL reactor wax indicate that the Sauter mean bubble diameter is directly related to the gas holdup (i.e. the higher the gas holdup, the lower the Sauter mean bubble diameter). However, in our studies with other waxes (in the small diameter column) it was found that it is possible to have similar holdup values but significantly different Sauter mean bubble diameters (Bukur et al., 1987c; Patel et al., 1990).

Effect of Axial Position

Figure 5.17 shows the effect of height above the distributor on gas holdup and Sauter mean bubble diameter. The gas holdup values shown in this figure correspond to the average gas holdup below the given pressure transducer. Figures 5.17a and 5.17b show results from the experiments conducted in the large diameter column, and Figures 5.17c and 5.17d show results from experiments conducted in the small diameter column. In the large diameter column, we did not observe a significant difference in gas holdup with axial position, and as a result, there is excellent agreement in gas holdups
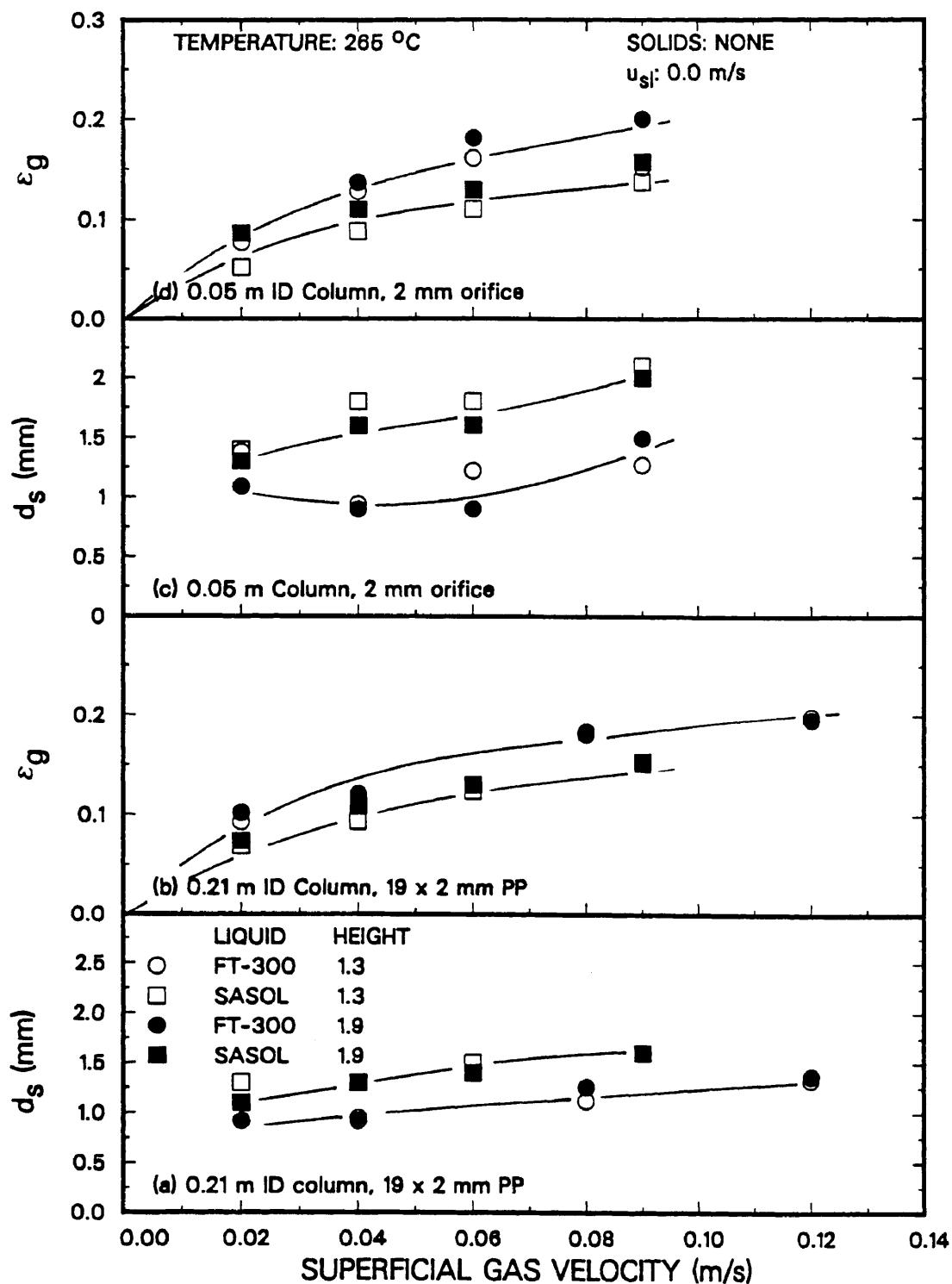
Figure 5.17. Effect of axial position on (a and c) Sauter mean bubble diameter and (b and d) gas holdup in 0.05 and 0.21 m ID bubble columns with wax (decreasing gas velocity - SASOL wax, 0.21 m ID column).

and Sauter mean bubble diameters obtained at heights of 1.3 and 1.9 m above the distributor. However, in the small column, gas holdup increases with increasing height above the distributor, and as a result, gas holdups are slightly higher at a height of 1.9 m as compared to a height of 1.3 m. This increase in gas holdup with increasing height above the distributor results in slightly lower Sauter mean bubble diameters at a height of 1.9 m.

Effect of Column Diameter

Figures 5.18a and 5.18b show the effect of column diameter on the Sauter mean bubble diameter for experiments conducted with FT–300 wax and SASOL reactor wax (decreasing gas velocities) in the 0.05 and 0.21 m ID bubble columns at a height of 1.9 m above the distributor. Sauter mean bubble diameters for experiments conducted with FT–300 wax were similar in both columns for gas velocities less than 0.09 m/s (see Figure 5.18a). This is expected, since very small bubbles are formed with FT–300 at low gas velocities, and as a result, the Sauter mean bubble diameters are similar. At gas velocities greater than 0.09 m/s, the Sauter mean bubble diameter remains fairly constant in the large diameter column. Results from our previous experiments conducted in the small diameter glass column (Patel et al., 1990) indicate that the Sauter mean bubble diameter increases with increasing gas velocity between gas velocities of 0.09 and 0.12 m/s. The differences in trends with increasing gas velocities are due to differences in flow regimes in the 0.21 and 0.05 m ID columns. In the small diameter column, the slug flow regime exists; whereas, in the large diameter column, the churn–turbulent flow regime exists.

The Sauter mean bubble diameters were consistently higher in the small diameter column compared to the large diameter column for the experiments conducted with SASOL wax (see Figure 5.18b). The primary reason for differences in the Sauter mean bubble diameters is due to differences in the flow regimes. The large diameter column
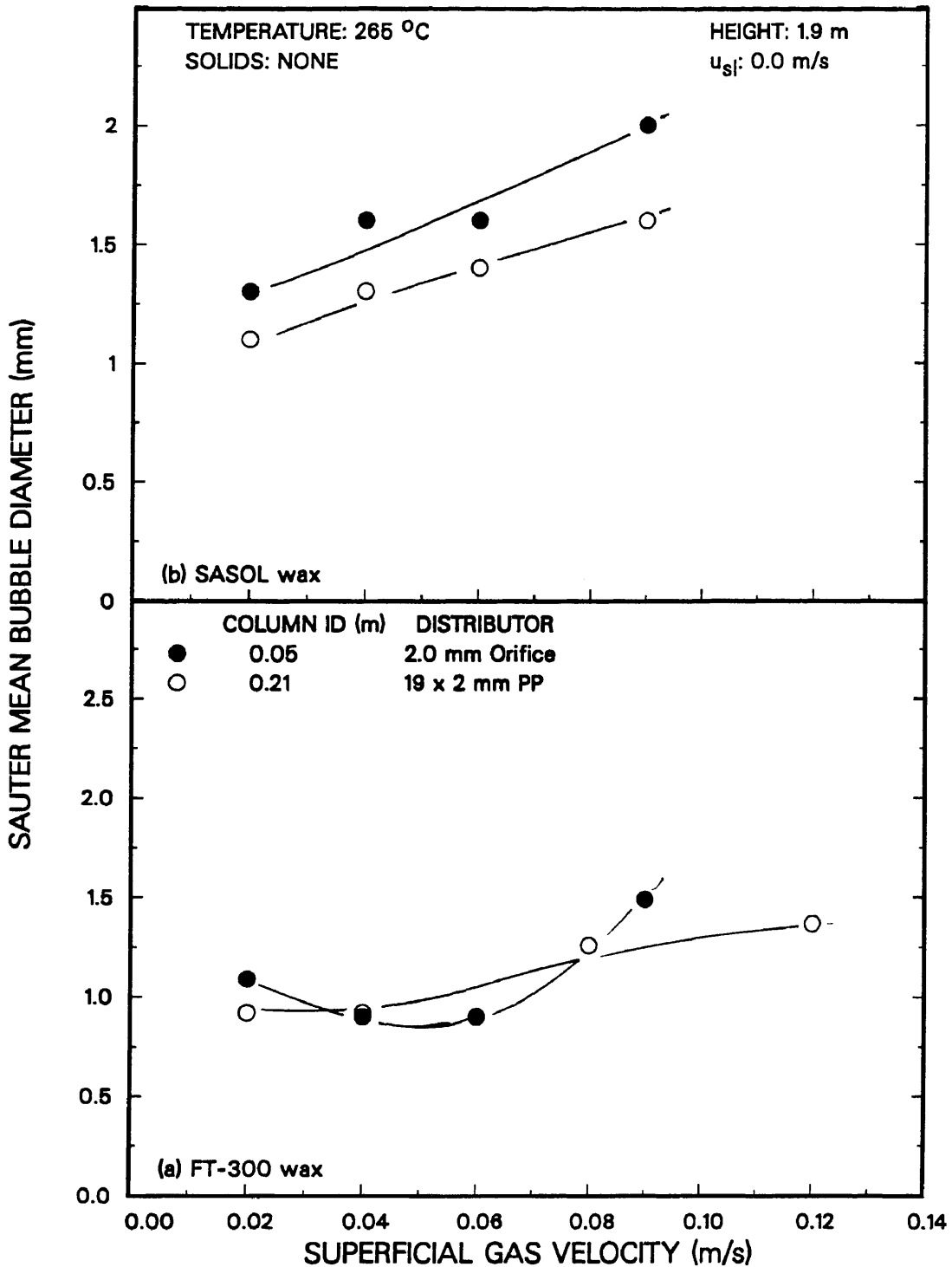
Figure 5.18. Effect of column diameter on Sauter mean bubble diameter for (a) FT-300 wax and (b) SASOL reactor wax - decreasing gas velocity in 0.21 m ID column.

operates in the churn—turbulent flow regime and the small diameter column operates in the slug flow regime. The increase in turbulence associated with the large diameter column results in the formation of smaller bubbles.

Comparison of Results Obtained in the Glass and Stainless Steel Bubble Columns

The dynamic gas disengagement technique was used to obtain bubble size distributions in both the stainless steel and glass bubble columns. A VCR/video camera system was used to measure the disengagement profile during experiments conducted in the glass column (Bukur et al., 1987a,b; Patel et al., 1990); whereas, pressure transducers were used to measure the disengagement rate in the stainless steel columns. Since disengagement profiles in the glass column were measured for the entire dispersion, only results obtained at a height of 1.9 m above the distributor in the stainless steel columns are used for comparison. Figure 5.19 compares values of d_s and gas holdup from experiments conducted in the large diameter glass and stainless steel columns with FT—300 wax. Results from two experiments in the glass column are shown. There was excellent agreement in Sauter mean bubble diameters in the glass and stainless steel columns when gas holdups were comparable. However, during one experiment in the glass column, a substantial amount of foam was produced and the values of d_s were markedly lower than those obtained in either of the other two experiments.

Figure 5.20 compares d_s values and gas holdups from experiments conducted in the small diameter glass and stainless steel columns. For the experiment conducted in the stainless steel column, the average gas holdup in the entire column, as well as the gas holdup in the column below a height of 1.9 m is shown. The overall gas holdup is substantially greater than that below a height of 1.9 m, indicating the presence of foam in the upper region of the column. While the overall gas holdups in the two columns (glass and stainless steel) were similar for gas velocities greater than 0.02 m/s, the Sauter mean bubble diameters are significantly different. This difference is a result
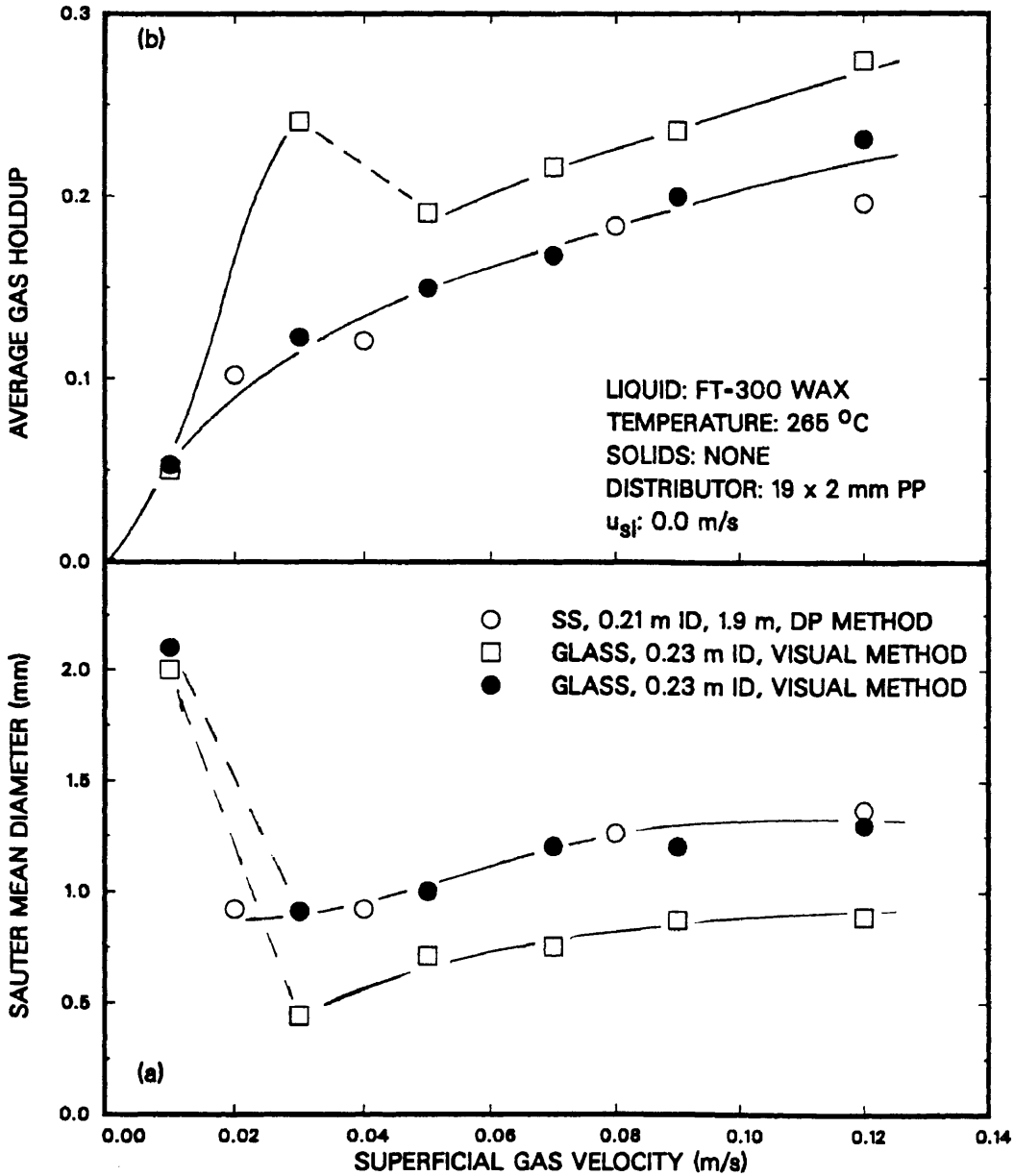
Figure 5.19. Comparison of (a) Sauter mean bubble diameters and (b) gas holdup obtained in the 0.21 m ID stainless steel column (DP method, 1.9 m) and the 0.23 m ID glass column (visual method) with FT-300 wax.
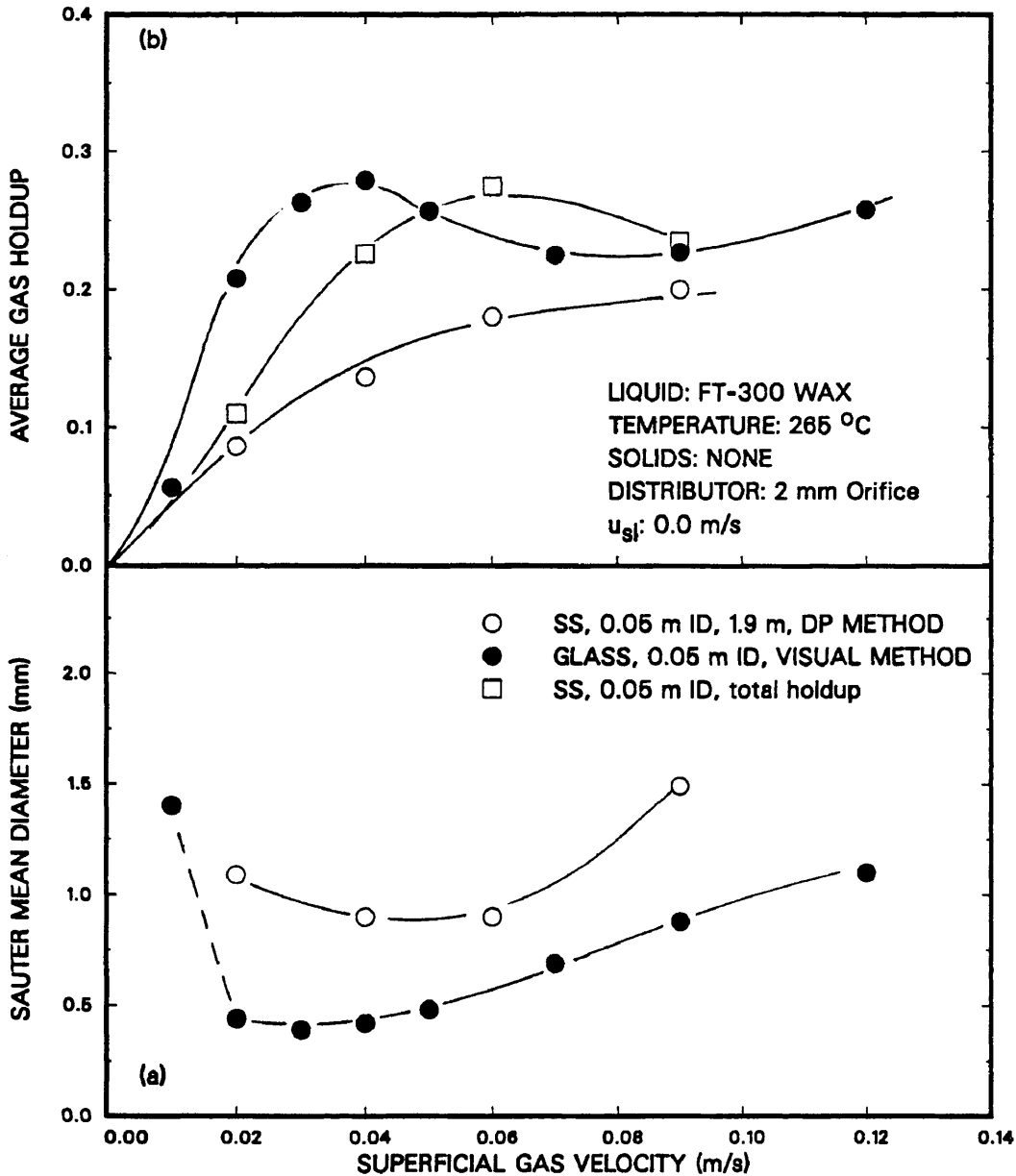
Figure 5.20 Comparison of (a) Sauter mean bubble diameters and (b) gas holdup obtained in the 0.05 m ID stainless steel column (DP method, 1.9 m) and the 0.05 m ID glass column (visual method) with FT-300 wax.

of the data acquisition technique. For the experiment in the glass column, d_s is based on the entire dispersion; whereas, in the stainless steel column, d_s, is based only on the dispersion below a height of 1.9 m. This illustrates one of the problems associated with the DGD technique (i.e. a non–uniform axial gas holdup). For the FT–300 wax system in the small diameter column, the gas holdup remains fairly uniform in the lower region of the column, but increases significantly in the uppermost region of the column for gas velocities between 0.02 and 0.09 m/s. The disengagement rate in the glass column was obtained by recording the drop in dispersion level with time via a VCR/video camera system. Thus, the disengagement profile was based on the entire dispersion. However, in the stainless steel column, the disengagement profile was based only on the dispersion below a given pressure transducer. Hence, the assumption of axial homogeneity is violated for measurements in the glass column, but not for measurements in the stainless steel column. If there is a significant amount of small bubbles located in the uppermost region of the column, which do not disengage continuously (e.g. stable foam), then there will be a bias towards small bubbles which results in a lower Sauter mean bubble diameter. Measurements made with the pressure transducers do not take into account the small bubbles in the uppermost region of the dispersion. However, these bubbles should be included in the overall Sauter mean bubble diameter. Thus, the actual values of d_s are probably within the range of values shown in Figure 5.20.

Figure 5.21 compares Sauter mean bubble diameters and gas holdups obtained from experiments conducted with SASOL wax in the small diameter glass and stainless steel columns. As stated earlier, SASOL wax does not produce foam, and as a result, the axial gas holdups remained fairly uniform. Thus, it is not surprising that Sauter mean bubble diameters and gas holdups measured using different techniques in the two columns (i.e. video/VCR - glass column; pressure transducers - stainless steel column) are in excellent agreement.
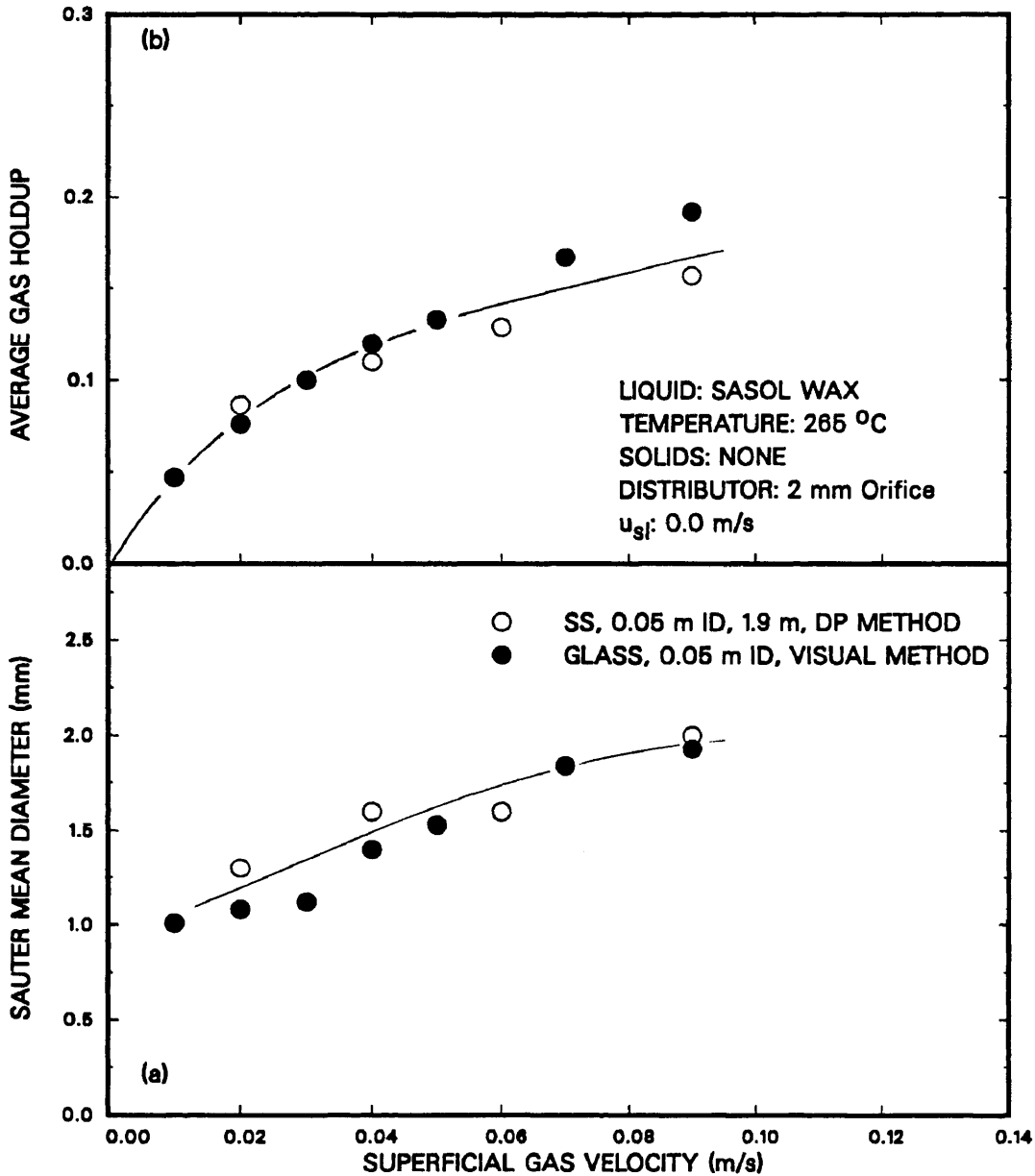
Figure 5.21. Comparison of (a) Sauter mean bubble diameters and (b) gas holdup obtained in the 0.05 m ID stainless steel column (DP method, 1.9 m) and the 0.05 m ID glass column (visual method) with SASOL wax.

DGD Results for the Air — Water System

The DGD data obtained from the experiment with tap water in the 0.05 m ID bubble column with the 2 mm orifice plate distributor were analyzed assuming Type 2 and Type 3 interactive disengagement. Figures 5.22a to 5.22d show the disengagement curves at a height of 1.9 m above the distributor for gas velocities of 0.02, 0.04, 0.06, and 0.09 m/s, respectively. As shown in Figure 5.22, a non–continuous decrease in the liquid level with time was observed at all gas velocities during the initial stages of disengagement followed by a linear change in the liquid level above the transducer with time during the second period of disengagement. This type of behavior indicates the presence of two dominant bubble classes, namely large bubbles (or slugs) and small bubbles. At low gas velocities the number of large bubbles is significantly greater than the number of large bubbles at higher gas velocities. For example, at a gas velocity of 0.02 m/s, there are approximately six large bubbles indicated by the six "steps" in the disengagement curve (see Figure 5.22a), but at a gas velocity of 0.09 m/s, there are only three "steps" in the disengagment curve. Also, the change in height with each "step" increases with increasing gas velocity. This type of behavior (i.e. a decrease in the number of large bubbles with increasing gas velocity and an increase in the volume of large bubbles with increasing gas velocity) indicates that as the gas velocity is increased, coalescence takes place and larger, less frequent slugs are formed. This decrease in the frequency of large bubbles with increasing gas velocity is in qualitative agreement with results from pressure fluctuation measurements with wax (see Chapter VI), where it is shown that the dominant bubble frequency decreases with increasing gas velocity.

As seen in Figure 5.22, the level fluctuates significantly between the passage of slugs, and thus Type 1 interactive disengagement may not be used, since the change in height with time during these periods must be known. For analysis assuming Type
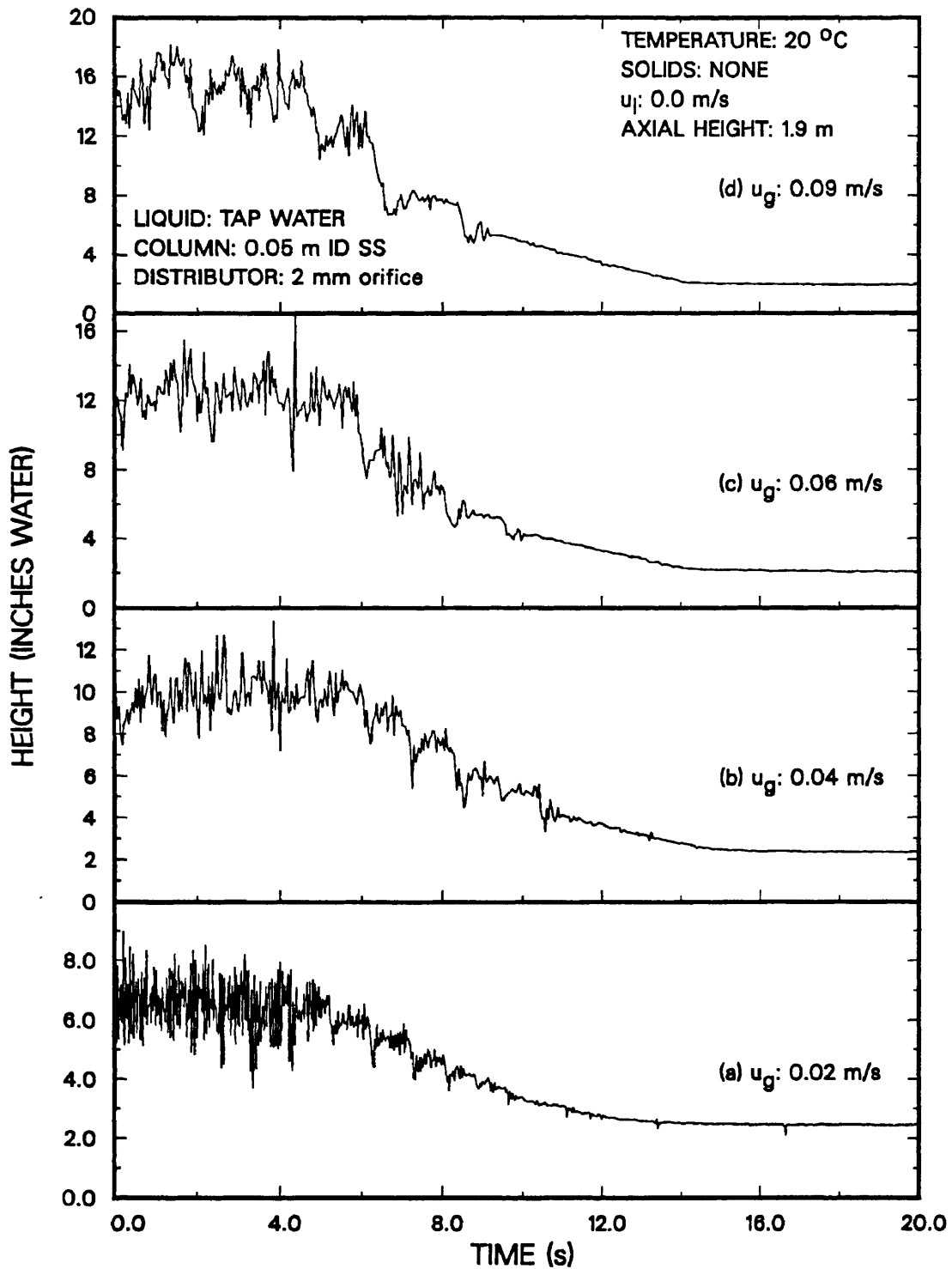
Figure 5.22. Effect of superficial gas velocity on disengagement (Tap water).

2 disengagment, it was previously mentioned that the volume fraction of the cross-sectional area of the column occupied by the slug was assumed to be one–half of the cross–sectional area of the column. Note, that the change in the liquid level detected by the pressure transducer is based on the cross–sectional area of the column. During experiments in the small diameter glass column at a gas velocity of 0.09 m/s, the slug lengths were observed to range from 10 to 20 cm (Patel et al., 1989). From Figure 5.22, the largest drop in the liquid level was approximately 4 inches (10.2 cm). Thus, if the actual slug length was 20 cm, then the value of f_{slug} is approximately 0.5 (see Eq. 5.41).

Figures 5.23a, 5.23b, and 5.23c compare the effect of gas velocity on d_s, a_g, and ϵ_g, respectively, assuming both Type 2 and Type 3 interactive disengagement(d_s and a_g only) at heights of 1.3 and 1.9 m above the distributor. There is not a significant difference in the Sauter mean bubble diameter predicted using the two models. However, the d_s values are consistently lower for Type 3 disengagement. This is expected since Type 3 disengagement assumes that no additional small bubbles have entered the dispersion below the DP cell; whereas, during Type 2 disengagement it is assumed that some small bubbles enter the dispersion below the DP cell. Thus, the volume fraction of small bubbles is greater for Type 3 disengagement, which results in a lower Sauter mean bubble diameter. The gas holdups, interfacial areas and Sauters are comparable at both heights. The rise velocities of large and small bubbles and the volume fraction of large bubbles, as well as the gas holdups, Sauter mean bubble diameters, and interfacial areas presented in Figure 5.23 are given in Table 5.7.

Comparison of Results Obtained in the Glass and Stainless Steel Bubble Columns

Figure 5.24 compares values of d_s and ϵ_g obtained in the present study to those previously obtained in the small diameter glass column. The data presented for the small glass column were obtained using a video camera/VCR system assuming interactive
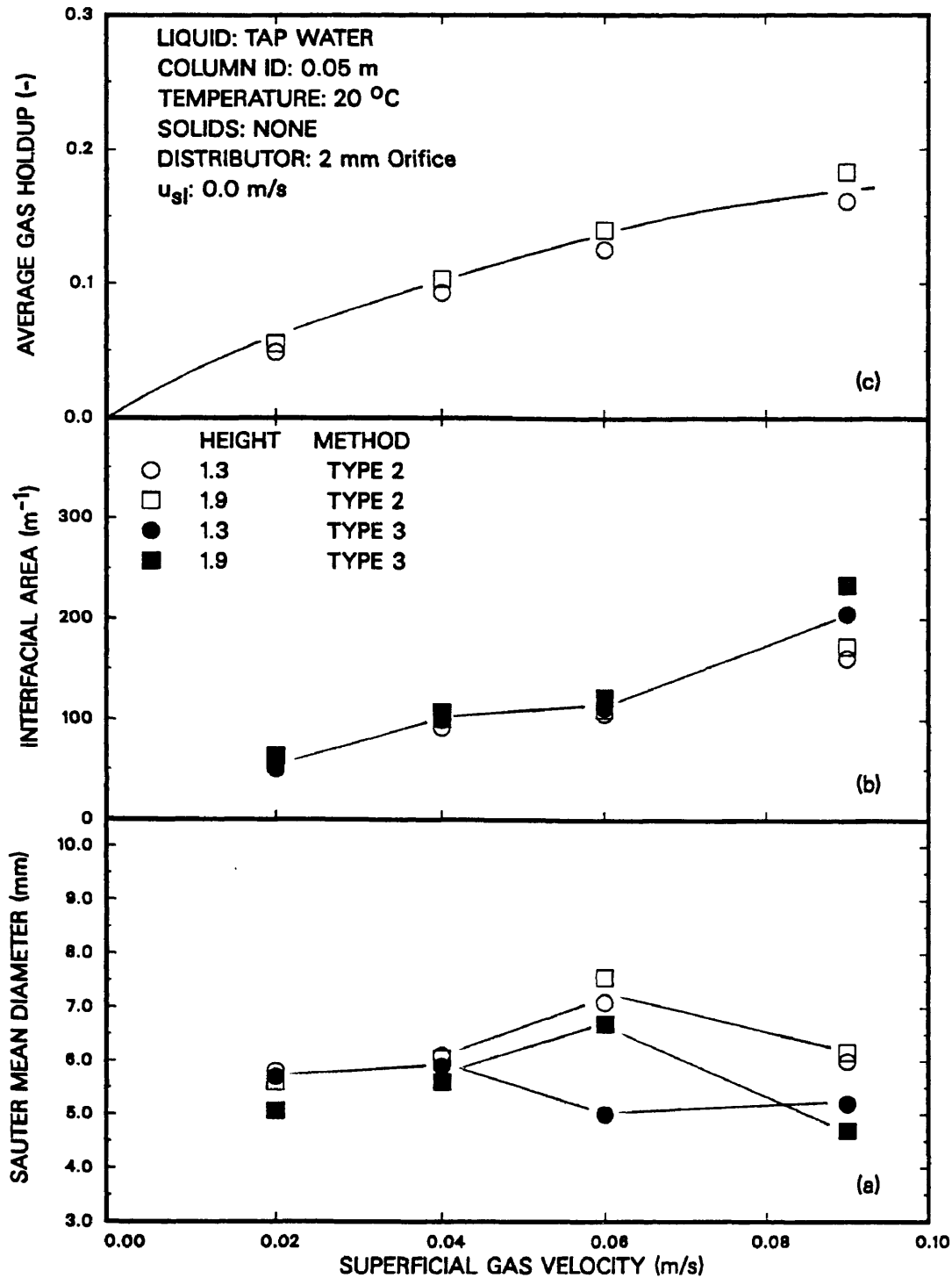
Figure 5.23. Effect of axial position and disengagement model on (a) Sauter mean bubble diameter, (b) specific gas-liquid interfacial area, and (c) gas holdup in the 0.05 m ID column with tap water as the liquid medium.

Table 5.7a. DGD Results from the Experiment with Tap Water at a Height of 1.3 m (0.05 m ID Stainless Steel Bubble Column)

u_g (m/s)	ϵ_{go} (-)	u_{bs} (m/s)	u_{bl} (m/s)	f_l^a (-)	f_l^b (-)	d_s^a (mm)	d_s^b (mm)	a_s^a (m^{-1})	a_s^b (m^{-1})
0.02	0.049	0.192	0.35	0.77	0.75	5.8	5.7	50	51
0.04	0.093	0.191	0.35	0.77	0.74	6.1	5.9	92	99
0.08	0.125	0.211	0.45	0.80	0.68	7.1	5.0	106	112
0.12	0.161	0.197	0.48	0.74	0.70	6.0	5.2	161	205

Table 5.7b. DGD Results from the Experiment with Tap Water at a Height of 1.9 m (0.05 m ID Stainless Steel Bubble Column)

u_g (m/s)	ϵ_{go} (-)	u_{bs} (m/s)	u_{bl} (m/s)	f_l^a (-)	f_l^b (-)	d_s^a (mm)	d_s^b (mm)	a_s^a (m^{-1})	a_s^b (m^{-1})
0.02	0.055	0.196	0.57	0.77	0.74	5.6	5.1	58	63
0.04	0.103	0.189	0.57	0.81	0.79	6.1	5.6	100	107
0.08	0.140	0.190	0.57	0.85	0.83	7.1	6.7	110	122
0.12	0.183	0.192	0.57	0.81	0.74	6.0	4.7	173	234

[a]Type 2 interactive disengagement
[b]Type 3 interactive disengagement
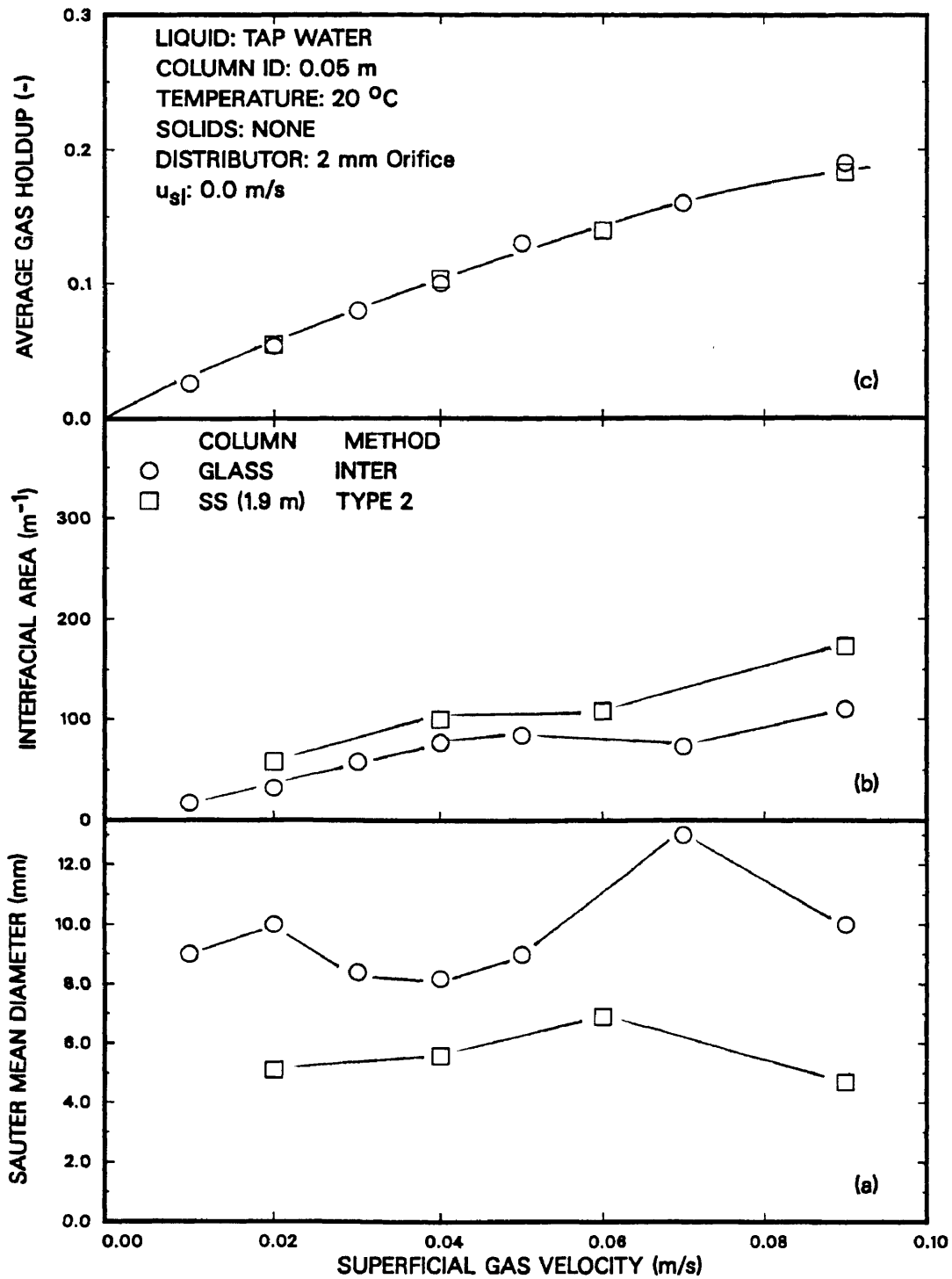
Figure 5.24. Comparison of (a) Sauter mean bubble diameters, (b) specific gas-liquid interfacial areas, and (c) gas holdups obtained in the 0.05 m ID stainless steel and glass columns with tap water as the liquid medium.

disengagement similar to Type 2. Details of the analysis of data from the glass column are presented elsewhere (Patel et al., 1989). There is an excellent agreement in the gas holdup values obtained from the two experiments; however, the values of the Sauter mean bubble diameters are different. For the experiment conducted in the glass column, the Sauter mean bubble diameter fluctuated around a value of 9 mm for all gas velocities employed; whereas, the value of d_s obtained from the experiment in the stainless steel column fluctuated around a value of 5 mm for all gas velocities. The differences in the estimated Sauter mean bubble diameters are probably caused by differences in the data acquisition and analysis techniques. The sizes of the small bubbles and large bubbles were essentially the same in both studies; however, the volume fraction of large bubbles obtained from the study in the glass column was approximately 0.9 whereas it was 0.8 for the study in the stainless steel column. This difference in the volume fractions of large bubbles is responsible for the differences in the estimated Sauter mean bubble diameters. Recall, that in our glass column studies, the disengagment rate was measured by following the rate at which the dispersion level dropped with time. Interactive disengagment analysis for data from the small diameter glass column, assumes that small bubbles do not disengage from the system throughout the large bubble disengagment period. If some small bubbles that are near the top of the dispersion disengage from the system during large bubble disengagement, then the volume fraction of large bubbles will be overestimated. This might explain the differences in Sauter mean bubble diameters obtained using the two techniques (i.e. video camera/VCR vs. pressure transducers).

Comparison of Results with Correlations from the Literature

There are several correlations in the literature which may be used to predict the Sauter mean bubble diameter. Two of the more widely used correlations are those given by Akita and Yoshida (1974) and Hughmark (1967). The correlation presented

by Hughmark is

$$d_s = 0.00635\left(\frac{\sigma}{0.072}\right)^{0.6}\left(\frac{1000}{\rho_\ell}\right)^{0.2} \tag{5.53}$$

and the correlation presented by Akita and Yoshida is

$$d_s = 26D_{col}\left(\frac{D_{col}^2\rho_\ell g}{\sigma}\right)^{-0.5}\left(\frac{D_{col}^3\rho_\ell^2 g}{\mu_\ell^2}\right)^{-0.12}\left(\frac{u_g}{\sqrt{gD_{col}}}\right)^{-0.12} \tag{5.54}$$

The surface tension of the tap water used in this study was 68 g/s^2. The density was assumed to be 1 g/cm^3 and the viscosity was taken as 0.01 g/cm-s. Figure 5.25 compares the Sauter mean bubble diameters obtained from this study with those predicted using the correlations presented above. Also shown in Figure 5.25 are the Sauter mean bubble diameters obtained from the experiment conducted in the glass column. The values of the Sauter mean bubble diameter obtained from experiments in the stainless steel column compare favorably with those predicted using Hughmark's correlation. Akita and Yoshida's correlation predicts slightly higher Sauter mean bubble diameters than those obtained in the stainless steel column at low gas velocities. However, for gas velocities $\geq$ 0.06 m/s, d_s predicted by Akita and Yoshida's correlation begins to approach the values obtained in the present study. The values of d_s obtained in from the experiment in the glass column are in good agreement with those predicted using Akita and Yoshida's correlation for gas velocities less than 0.05 m/s; however, they are consistently higher than those predicted using either correlation for gas velocities greater than 0.05 m/s.
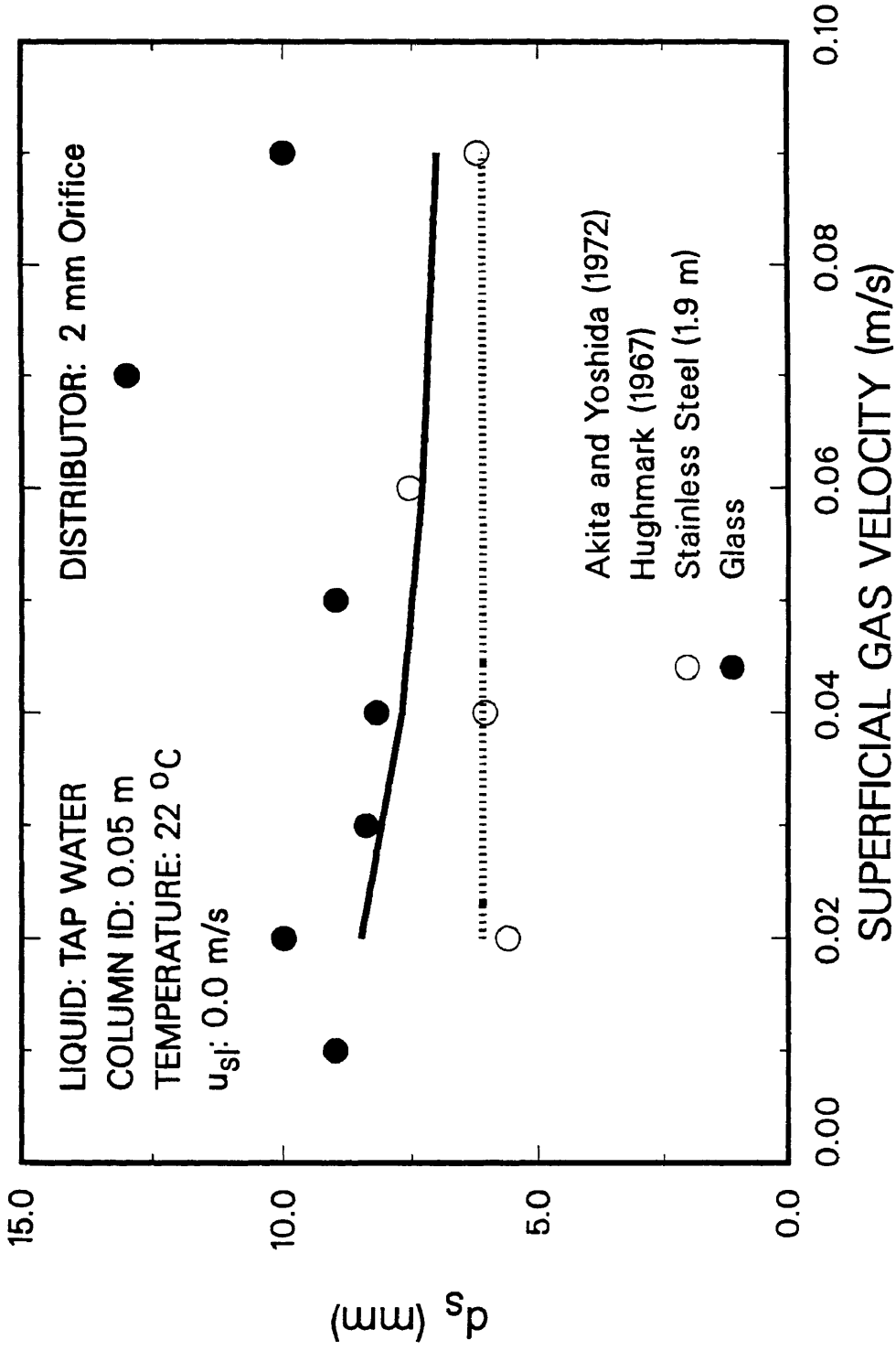
Figure 5.25. Comparison of Sauter mean bubble diameters with correlations from the literature for tap water.

CHAPTER VI

FLOW REGIME CHARACTERIZATION

Pressure signals and nuclear density gauge signals were recorded during several experiments in both the 0.05 m ID and 0.21 m ID bubble columns. Statistical analysis of the pressure fluctuations and density gauge fluctuations was used to determine flow regimes and flow regime transitions. Wall pressure measurements were made at heights of 0.08, 0.61, 1.22, 1.83, and 2.44 m above the distributor during experiments conducted in both columns. In the 0.05 m ID bubble column, density gauge measurements were made at a fixed height (1.5 m above the distributor); whereas, in the large diameter column, density gauge measurements were made at heights of 0.9, 1.5, and 1.7 m above the distributor. We developed the necessary software that would allow us to do time series analysis of the signals on the Zenith-248 AT compatible computer in our laboratory. The same computer is also interfaced to the data acquisition system (see Chapters II and III) that was used to record the pressure and density gauge fluctuations.

Theoretical Background

Statistical analysis of pressure fluctuations has been used in the past to determine transitions between flow regimes in both two–phase and three–phase bubble columns and fluidized beds. Various techniques may be used to determine flow regimes and flow regime transitions. The two most commonly used designs involving pressure transducers are: (1) measurement of absolute pressure fluctuations and (2) measurement of differential pressure fluctuations. For analysis of systems which operate in the slug flow regime, differential pressure fluctuations can provide more detailed information, and a more accurate measure of the transition from bubbly to slug flow, slug flow to annular flow, and annular flow to mist flow. Differential pressure measurements have generally been limited to two–phase systems (e.g., Ishigai et al., 1965a,b; Lin and Hanratty, 1987;

Matsui, 1984; Miyazaki, et al. 1973; Akagawa, et al. 1971a, b, c). These measurements may be used to determine instantaneous fluctuations in void fraction. The signals returned from differential transducers have the same characteristics as those obtained from a nuclear density gauge or a probe.

Surface pressure fluctuations may be detected with various types of pressure measurement equipment (e.g., pitot tubes, surface mounted transducers, microphones, transducers connected by an external tube, etc.). One drawback associated with surface mounted and tube mounted transducers is that they respond to fluctuations occurring not only in the boundary layer, but also to fluctuations beyond the boundary layer. The tube mounted transducers also suffer from signal delay governed by the length of the tube and the velocity of sound in the medium (Lee, 1983). With tube mounted transducers, it is usually difficult to obtain data over the entire range of frequencies. In general, data obtained from tube mounted transducers will be limited to low frequency fluctuations in the system. For our purpose, this should be sufficient since we are interested in detecting the onset of slug flow.

As discussed by Glasgow et al. (1984), the passage of a buoyant bubble can produce three distinct response characteristics: (1) sound of approach (observable if rapidly rising bubbles are present), (2) pressure field around the object, and (3) wake or vortex street behind the object. Our pressure transducers will only detect fluctuations caused by changes in the pressure field as a bubble passes the surface of the tube (i.e. low frequency oscillations). Even if our system was sensitive enough to detect fluctuations caused by the wakes of bubbles, it would be very difficult, if not impossible, to distinguish between these fluctuations and those created by the pressure field around the bubble.

Three different statistical techniques are commonly employed to determine flow regimes and flow regime transitions from pressure transducer measurements. The statistical analysis involves the use of the power spectral density function (psd), the mean

square error of the pressure fluctuations (MSE), and the probability density function (pdf). The pdf is used extensively in the analysis of signals obtained from differential transducers, nuclear density gauges, and probes. Flow regimes and flow regime transitions cannot be determined directly from pdf's for data obtained from absolute pressure measurements (e.g. Fan et al., 1981; Matsui, 1984,1986; Akagawa et al., 1971a,b,c).

For data from differential pressure measurements and nuclear density gauge measurements, the pdf has significantly different characteristics for different flow regimes. In bubbly flow the pdf is concentrated near a pressure difference (or count rate) corresponding to low gas hold–up. However, when slugs begin to appear, two peaks (or regions) are observed on the pdf curve, one corresponding to low hold–up and the other corresponding to high hold–up. The low hold–up region corresponds to the liquid slugs and the high hold–up region corresponds to the gas slugs. In annular flow, the low hold–up peak disappears and only the peak corresponding to high gas hold–up is observed (Matsui, 1984).

As mentioned previously, the pdf of an absolute pressure signal cannot be used as a direct measure of flow regime transitions. However, the pdf of an absolute pressure signal will broaden as turbulence increases (Patel, 1985). In other words, the variance of the pressure fluctuations in the column changes with gas and liquid velocities, and this change is reflected by an increase or decrease in the variance of the pdf. Two quantities which have found some use in determining flow regime transitions and changes in turbulence are the mean square error (MSE) and root mean square (RMS) of the pressure fluctuations. The MSE is defined as:

$$MSE = \frac{\left[\sum(P_i - \overline{P})^2 / N\right]^{1/2}}{\overline{P}} \quad i = 1, \ldots, N \qquad (6.1)$$

where N is the total number of data points, P_i is the pressure corresponding to data point i, and $\overline{P}$ is the average pressure defined as:

$$\overline{P} = \frac{\sum P_i}{N} \qquad i = 1, \ldots, N$$

Fan et al. (1984) had reasonable success in using this quantity to determine flow regime transitions in a three–phase fluidized bed. Lee (1983) used the RMS, defined as :

$$RMS = (MSE)(\overline{P}) \qquad (6.2)$$

to obtain a qualitative description of turbulence in an air lift bubble column.

Two other statistical quantities which are sometimes used are the autocorrelation function and the power spectral density function (psd). The psd is the Fourier transform of the autocorrelation function. The autocorrelation function is the normalized autocovariance function. The autocovariance function gives an indication of how the dependence between adjacent values in a stochastic process changes with lag (u) and is defined as (Jenkins and Watts, 1968):

$$\gamma_{xx}(u) = E[(x(t) - \mu)(x(t + u) - \mu)] = cov[x(t), x(t + u)] \qquad (6.3)$$

where E[y] is the expected value of y, cov is the covariance, μ is the mean of the time series, x is the measured quantity (pressures for our case), and u is the lag between observations. The autocorrelation function is given by:

$$\rho_{xx}(u) = \frac{\gamma_{xx}(u)}{\gamma_{xx}(0)} \qquad (6.4)$$

where $\gamma_{xx}(u)$ is the autocovariance function evaluated at lag u and $\gamma_{xx}(0)$ is the autocovariance function evaluated at lag 0, or more simply, the variance of the time series. Thus, the RMS is the square root of the autocovariance function evaluated at lag 0, and the MSE is the square root of the autocovariance function evaluated at lag 0 divided

by the mean of the time series (or, for our case, the mean of the pressure fluctuations or density gauge fluctuations).

Fourier transforms are used to approximate the time series. A series of periodic functions may be used to approximate a non–periodic signal. One such series is the Fourier series, in which the periodic functions are sines and cosines. Thus, the Fourier series may be used to approximate the actual pressure signal. In essence, we are fitting the raw signal to a Fourier series. From this type of a fit, we gain information on the periodicity of the signal. Fourier series have the important property that an approximation consisting of a given number of terms achieves the minimum mean square error between the signal and approximation, and also, since they are orthogonal, the coefficients may be determined independently of one another. The sample spectrum is the Fourier transform of the sample autocovariance function. It shows how the average power or variance of the signal is distributed over frequency. Fourier analysis breaks down when applied to time series because it is based on the assumption of fixed amplitudes, frequencies, and phases. Thus, the sample spectrum of a time series can be quite erratic in nature. However, if we treat the sample spectrum as a random variable, and examine its moments, we will be able to explain the erratic behavior. The power spectrum is defined as the first moment, or mean, of the sample spectrum. The power spectral density function is a normalized version of the power spectrum. The psd is the Fourier transform of the autocorrelation function and is defined by (Jenkins and Watts, 1968):

$$P(f) = \int_{-\infty}^{\infty} \rho_{xx}(u)\exp(-j2\pi fu)du \qquad (6.5)$$

Thus, all three quantities (i.e., RMS or MSE, autocorrelation and psd) are related. For our data, we will only use the MSE and psd to show qualitatively, the transitions between flow regimes for various experimental data.

Taitel et al. (1981) presented various correlations for the prediction of flow regime transitions in two–phase gas–liquid flow. By treating our three–phase system as a two–phase system (i.e., using slurry properties in place of liquid properties), we can use Taitel et al.'s correlations to obtain approximate values for the transitions between bubbly and slug flow in the 0.05 m ID bubble column. According to Taitel et al., for our system and range of operating conditions in the 0.05 m ID bubble column, there are two possible flow regimes which can exist, bubbly and slug flow. Taitel et al. also present a correlation for describing the entrance region in which mixing (i.e. churn flow) will exist due to the incoming gas (i.e., in the lower section of the column there will be churn flow, but towards the top of the column slug flow will exist).

According to Taitel et al., bubbly flow will not exist if the following correlation is satisfied:

$$\left[\frac{\rho_{s\ell}^2 g D_{col}^2}{(\rho_{s\ell} - \rho_g)\sigma}\right]^{1/4} \leq 4.36 \tag{6.6}$$

where $\rho_{s\ell}$ is the density of the slurry, D_{col} is the column diameter, ρ_g is the density of the gas, and σ is the surface tension of the liquid. Note that in their original correlation they used the density of the liquid and not the density of the slurry. For the small diameter bubble column, the quantity on the left hand side of Eq. 6.6 ranges from approximately 5.2 to 5.5. Thus, for our system, according to Taitel et al., it is possible to observe the bubbly regime.

Assuming that the transition to slug flow occurs when the gas hold–up is approximately 25 %, Taitel et al. propose that the following correlation can be used to determine the transition to slug flow:

$$U_{s\ell} = 3.0 U_g - 1.15 \left[\frac{g(\rho_{s\ell} - \rho_g)\sigma}{\rho_{s\ell}^2}\right]^{1/4} \tag{6.7}.$$

where $U_{s\ell}$ is the superficial slurry velocity and U_g is the superficial gas velocity at which the transition takes place. For the various systems and operating conditions used in

this study, the transition from the bubbly to slug flow regime should occur between gas velocities of 0.048 and 0.056 m/s.

Taitel et al. also present a correlation for predicting the entry region over which churn flow will exist. In this region, it is assumed that short Taylor bubbles are created. Two of these coalesce to form a "large" Taylor bubble (or slug). The entry region is the region in which this coalescence takes place and is defined by:

$$\frac{l_e}{D_{col}} = 40.6\left[\frac{U_m}{\sqrt{gD_{col}}} + 0.22\right] \tag{6.8}$$

For our system, the entry length, l_e ranges from approximately 0.7 m at a gas velocity of 0.06 m/s to 1.0 m at a gas velocity of 0.12 m/s. Thus, if Taitel et al.'s correlations (i.e., Eqs. 6.7 and 6.8) hold true for our system, we should observe a transition to slug flow between gas velocities of 0.04 and 0.06 m/s for all experiments, and furthermore, we should not observe slugs in the lower (0.7 to 1.0 m) section of the bubble column.

The range of gas velocities at which the transition from bubbly to slug flow occurs based on the correlations presented by Taitel et al., agrees with the range of velocities predicted by Deckwer et al., 1980 (see Figure 2.12). Based on the flow regime map presented by Deckwer et al., the transition from the bubbly to churn–turbulent flow regime in the 0.21 m ID bubble column occurs between gas velocities of 0.04 and 0.07 m/s.

Discussion Of Results

Wall pressure fluctuations and nuclear density gauge fluctuation measurements were made in both the small diameter and large diameter stainless steel bubble columns. Raw output (i.e. voltages) from the density gauges and pressure transducers were recorded on the Zenith AT personal computer. The data were then analyzed to obtain the MSE, pdf, and psd. The spectral density functions, psd, were obtained using the IMSL routine PFFT.

Figures 6.1a and 6.1b show typical raw signals from the nuclear density gauge obtained during experiments in the 0.05 m ID bubble column at gas velocities of 0.02 and 0.06 m/s, respectively. The large peaks in each figure correspond to the passage of large bubbles across the beam path of the density gauge. The regularity of the large peaks is significantly different at the two gas velocities. At 0.02 m/s, the large peaks appear randomly and also are less frequent; however, at a gas velocity of 0.06 m/s, they appear at an increased regularity, and also have a relatively higher intensity (amplitude) than those at 0.02 m/s. This regularity indicates the presence of slugs in the dispersion at a gas velocity of 0.06 m/s. At the lower gas velocity (0.02 m/s), the bubbles are smaller and are randomly dispersed in the flow field. Additionally, the lower amplitude of the oscillations at this gas velocity is indicative of the larger liquid fraction at 0.02 m/s relative to that at 0.06 m/s. Figure 6.2 shows typical density gauge fluctuations during experiments in the 0.21 m ID column. The large peaks in Figures 6.2a and 6.2b correspond to the passage of large bubbles through the beam of radiation at gas velocities of 0.02 and 0.12 m/s, respectively. The fluctuations at a gas velocity of 0.02 m/s in the 0.21 m ID column appear similar to those in the 0.05 m ID column at the same velocity. However, at a gas velocity of 0.12 m/s in the 0.21 m ID column, peaks appear randomly; whereas, in the 0.05 m ID column the peaks occur regularly during slug flow (see Figure 6.1b). This non–regularity in peaks at a relatively high gas velocity indicates the presence of the churn–turbulent flow regime. At a gas velocity of 0.12 m/s, the amplitude of the peaks is higher than at a gas velocity of 0.02 m/s, thus indicating the presence of either larger bubbles or swarms of bubbles at this velocity.

Figures 6.3 and 6.4 show typical probability density functions of the pressure signals in the 0.05 and 0.21 m ID column, respectively. Figures 6.3a and 6.4a correspond to the homogeneous bubbly regime. The homogeneous bubbly regime is characterized by a narrow density distribution function. As the gas flow is increased, the pressure variation
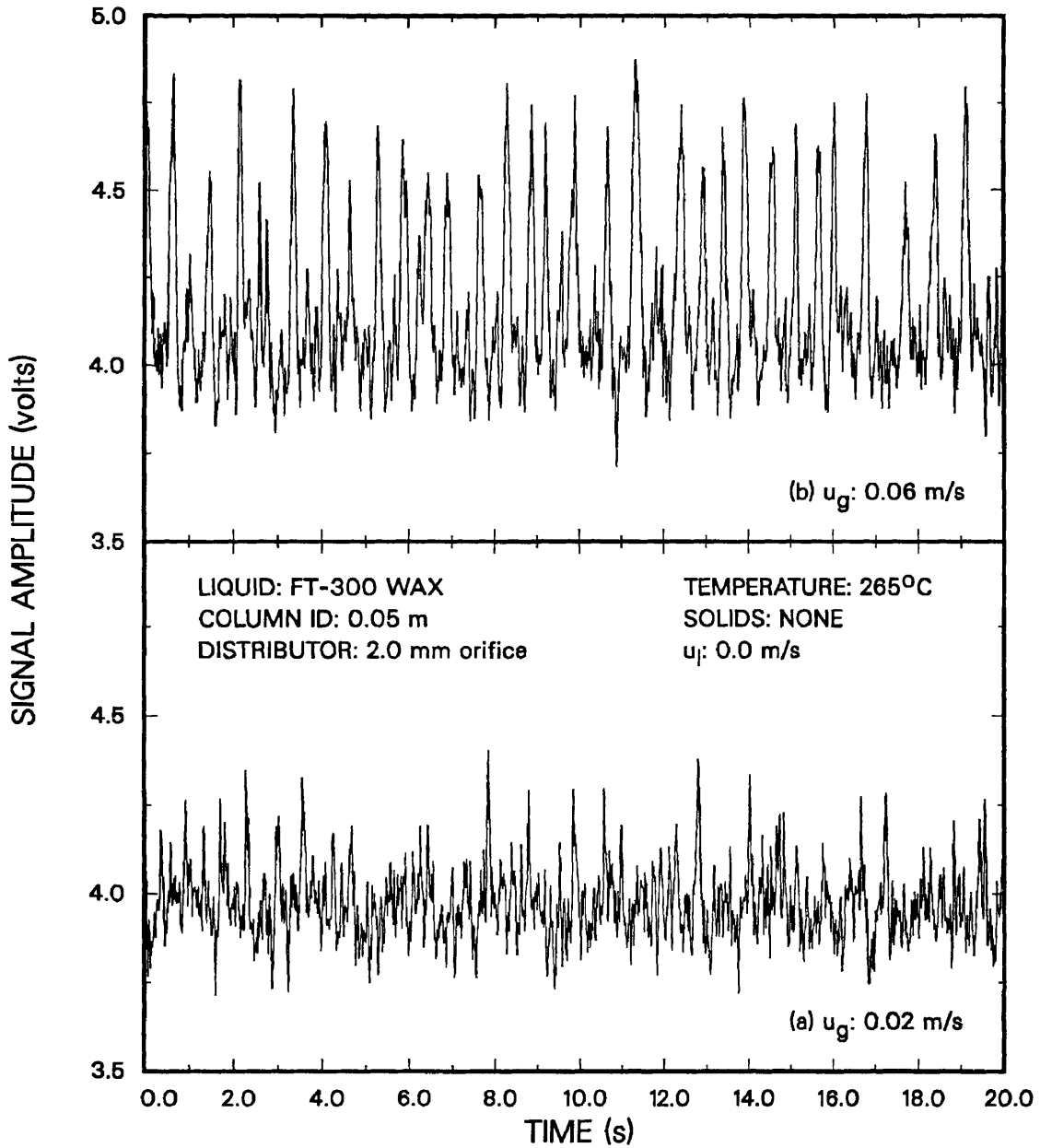
Figure 6.1. Typical raw signals from the nuclear density gauge apparatus during experiments in the 0.05 m ID bubble column.
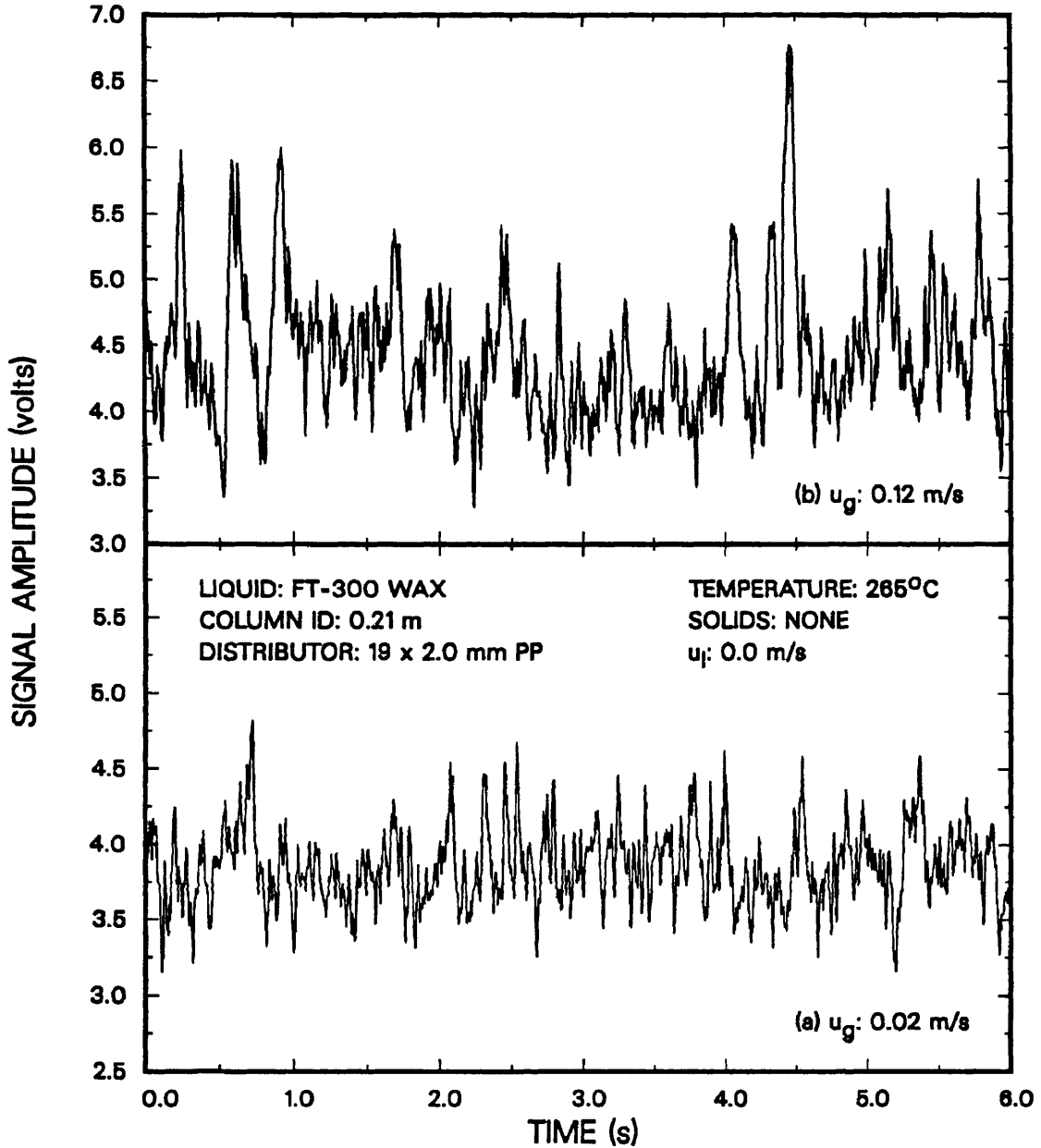
Figure 6.2. Typical raw signals from the nuclear density gauge apparatus during experiments in the 0.21 m ID bubble column.
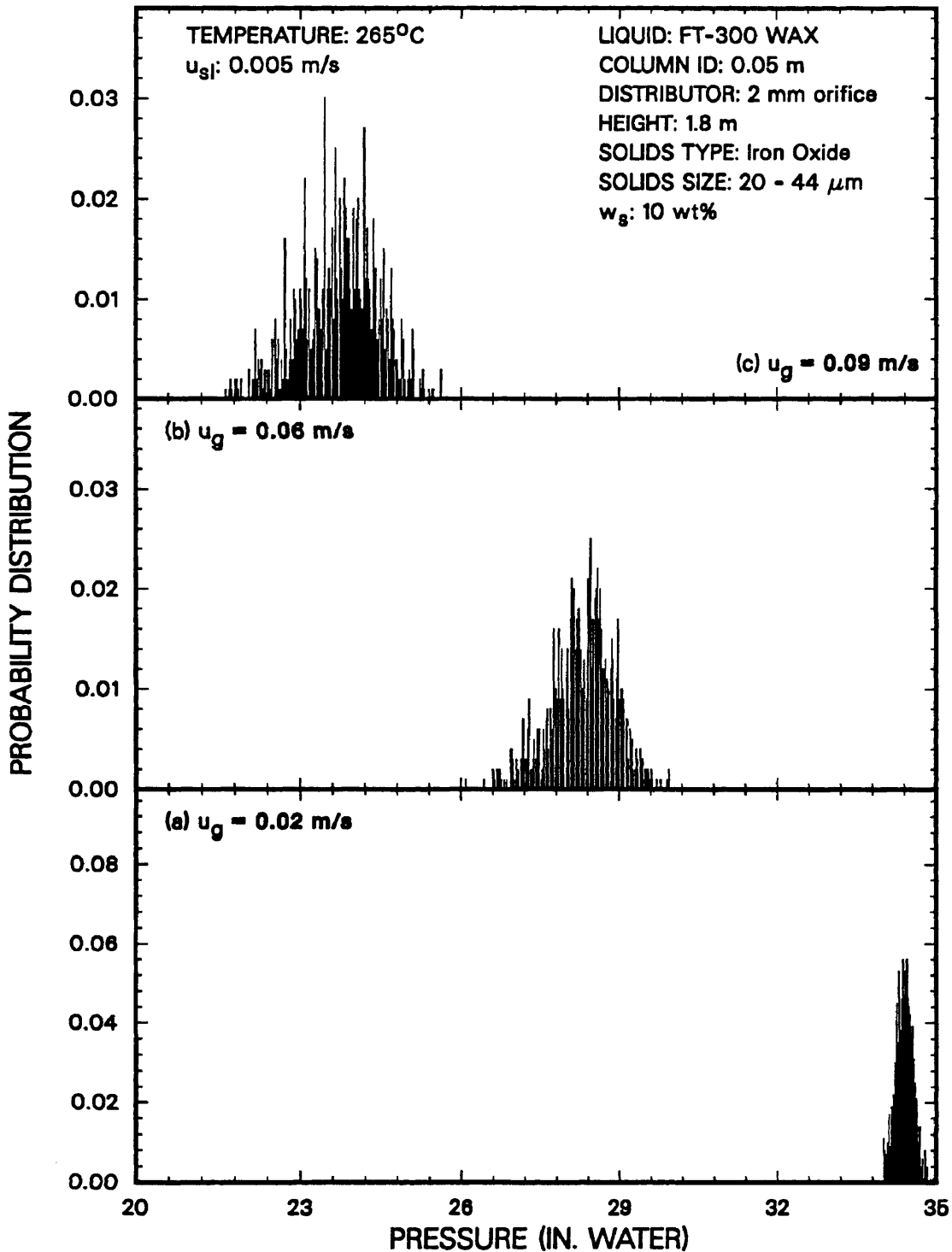
Figure 6.3. Effect of superficial gas velocity on the probability density function from the pressure transducer in the 0.05 m ID bubble column at a height of 1.8 m above the distributor.
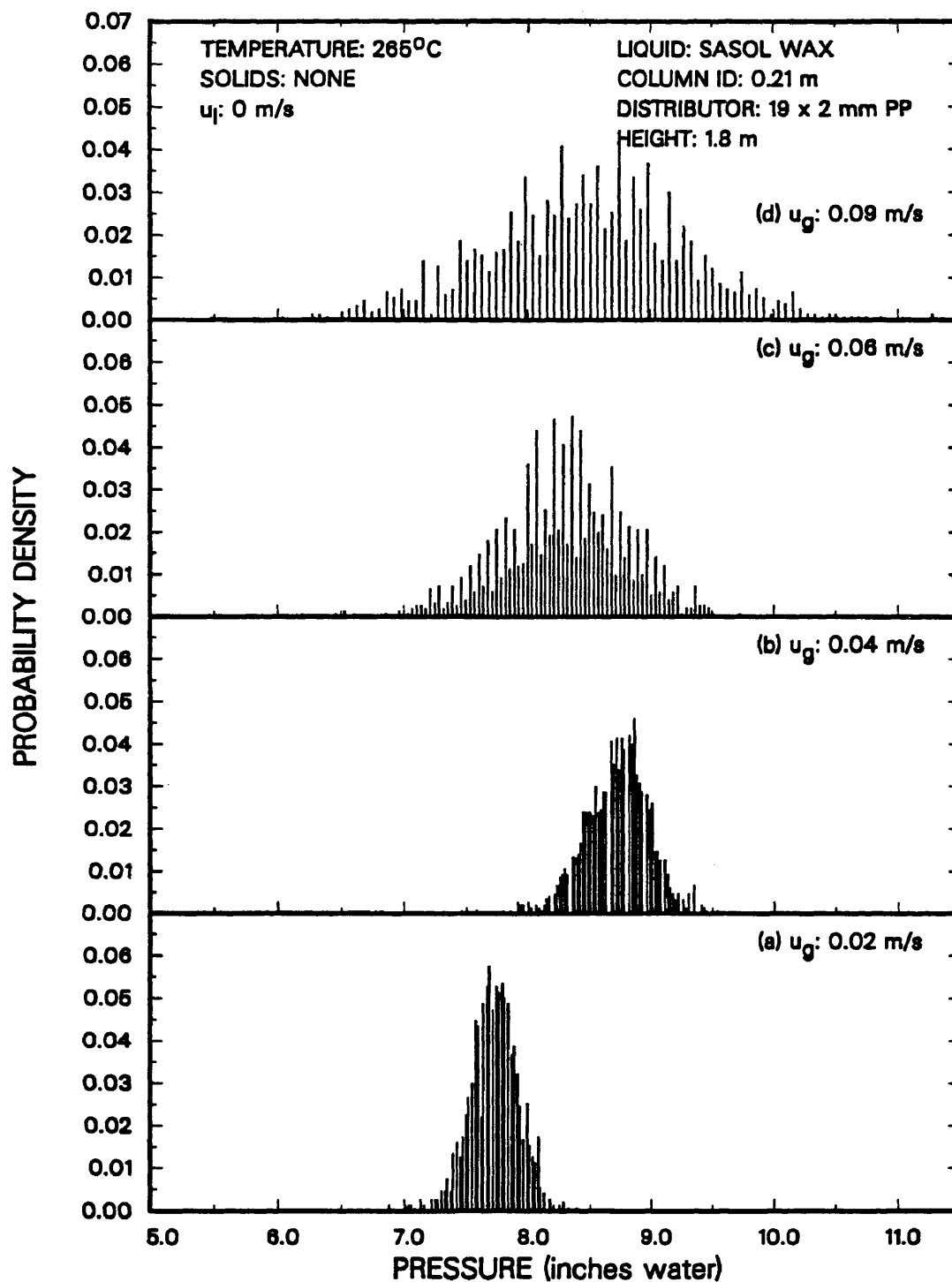
Figure 6.4. Effect of superficial gas velocity on the probability density function
from the pressure transducer in the 0.21 m ID bubble column at a height
of 1.8 m above the distributor.

increases. As the gas flow is increased to 0.04 m/s, the variation in pressure begins to increase in the 0.21 m ID column (see Figure 6.4b). This slight increase may correspond to the transition regime between bubbly and churn–turbulent flow. At gas velocities of 0.06 and 0.09 m/s in both columns, the variation in pressure increases significantly, indicating the presence of slug flow in the small diameter column and churn–turbulent flow in the large diameter column.

Typical probability density functions from the nuclear density gauges, associated with experiments in the small diameter and large diameter bubble columns, are shown in Figures 6.5 and 6.6, respectively. As mentioned previously, nuclear density gauge fluctuations correspond to fluctuations in gas holdup. The distribution at a gas velocity of 0.02 m/s in both columns has the shape of a normal distribution and can be associated with the homogeneous bubbly regime. As the gas velocity is increased in the small diameter column, the Gaussian distribution becomes skewed to the right (e.g. $u_g=0.04$ m/s). At a gas velocity of 0.06 m/s, the formation of a second peak is evident at the right hand end of the distribution, and this is exemplified at 0.09 m/s (see Figures 6.5c and 6.5d). An increase in peak intensity corresponds to an increase in the volume fraction of gas. Thus, the second peak at gas velocities of 0.06 and 0.09 m/s corresponds to the presence of slugs. In the large diameter column at gas velocities of 0.08 and 0.12 (see Figures 6.6b and 6.6c, respectively), the distribution becomes skewed to the right also. However, the second peak is not formed. This is expected, since in the churn–turbulent flow regime, the passage of large bubbles is not as regular as it is in the slug flow regime.

Flow Regime Transitions Based on the MSE

MSE were calculated from the raw pressure signal data for all runs conducted in the 0.05 m ID column. In general, the MSE increased with increasing gas velocity and with increasing height above the distributor, but decreased with increasing liquid velocity.
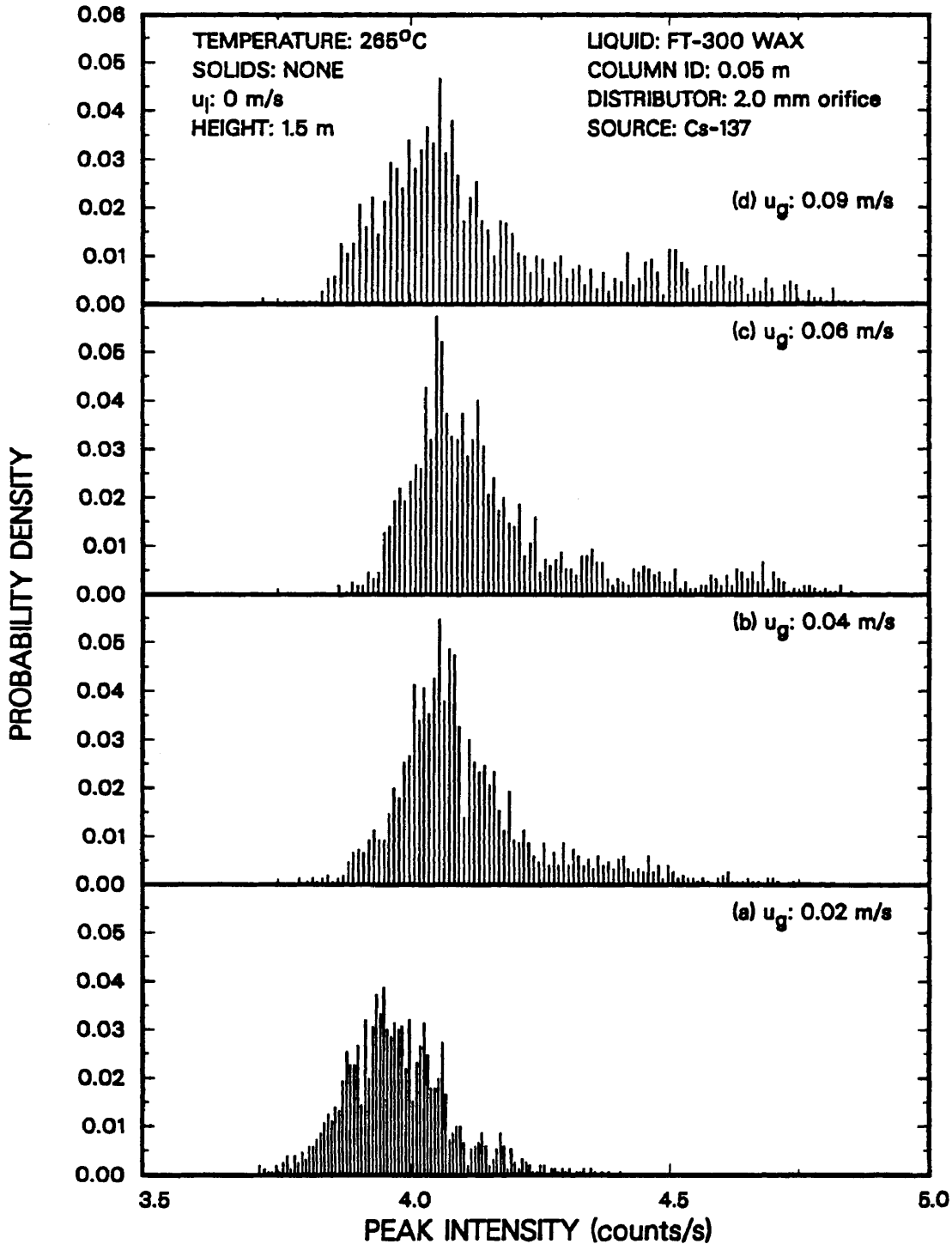
Figure 6.5. Effect of superficial gas velocity on the probability density function from the nuclear density gauge using the Cesium-137 source in the 0.05 m ID bubble column at a height of 1.5 m above the distributor.
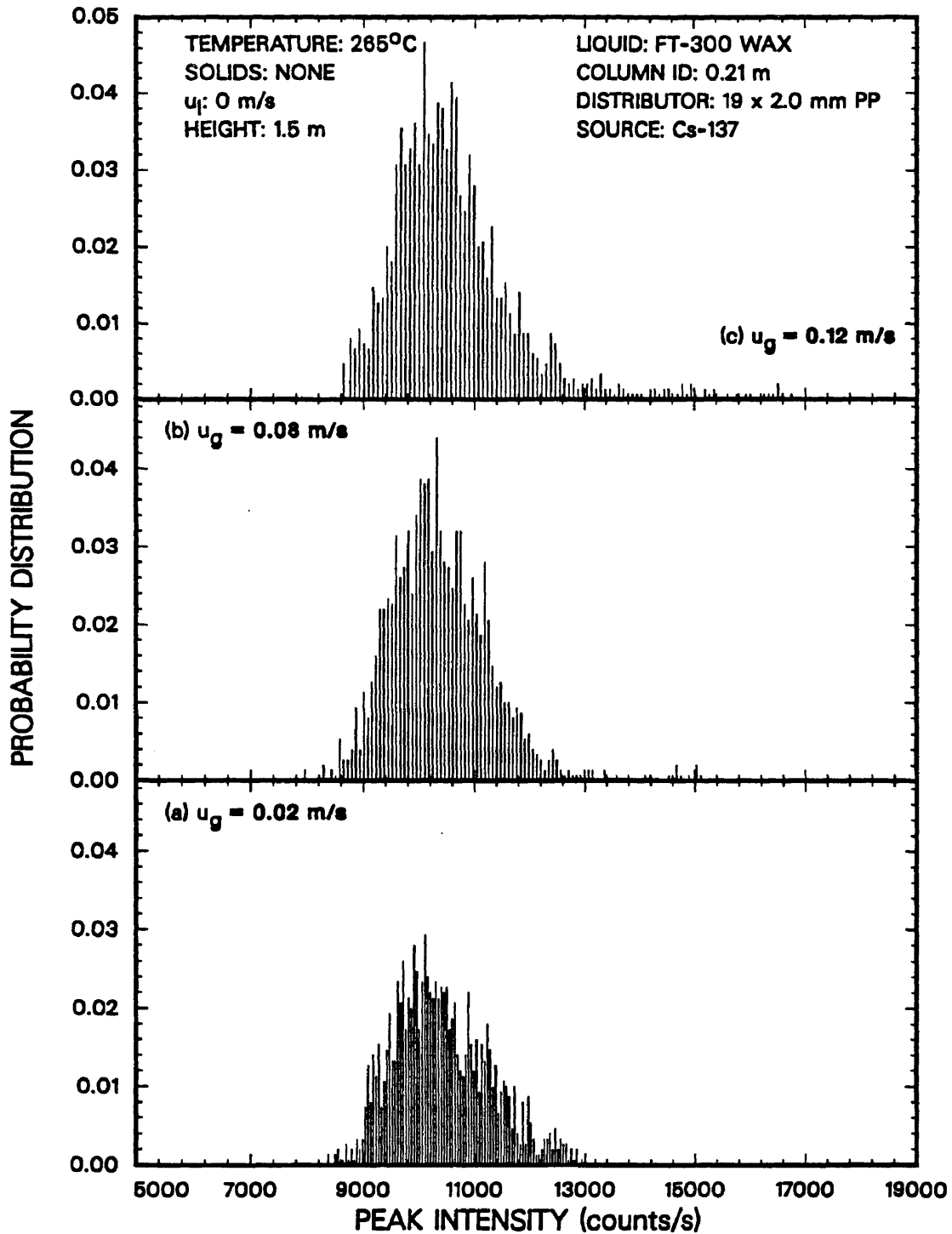
Figure 6.6. Effect of superficial gas velocity on the probability density function from the nuclear density gauge using the Cesium-137 source in the 0.21 m ID bubble column at a height of 1.5 m above the distributor.

Figure 6.7 shows the MSE obtained at a height of 1.2 m for experiments conducted with 0 − 5 μm silica particles at slurry velocities of 0, 0.005, and 0.02 m/s. At low gas velocities (i.e., u_g ≤ 0.06 m/s, the MSE of the pressure fluctuations is essentially the same for all three experiments. However, at gas velocities of 0.09 and 0.12 m/s the MSE of the pressure fluctuations are significantly different for the various experiments. The MSE for the experiment conducted in the batch mode of operation is significantly higher than those for the other two runs, which were conducted in the continuous mode of operation. This increase in MSE for the batch experiment may be attributed to an increase in turbulence at the top of the dispersion due to fluctuations caused by slugs exiting the slurry. The MSE for the experiment conducted using a superficial slurry velocity of 0.005 m/s was higher than that for the experiment conducted using a superficial slurry velocity of 0.02 m/s. Increasing the liquid velocity causes a decrease in pressure fluctuations. This decrease in the variance of pressure fluctuations with increasing slurry flow rate may be attributed to two factors: (1) the relative velocity between the gas and slurry decreases with increasing slurry velocity and (2) the static height of the slurry above a given pressure port does not fluctuate as much during a continuous run as it does during a batch run. In Figure 6.7 there is a distinct change in the slope of the curves between gas velocities of 0.02 to 0.04 m/s and 0.06 to 0.12 m/s (i.e. the slopes of curves between gas velocities of 0.06 and 0.12 m/s are greater than the slopes of the curves between gas velocities of 0.02 and 0.04 m/s).. This change in slope may be attributed to a change in the flow regime from bubbly to slug flow. It appears that the transition occurs somewhere between gas velocities of 0.04 and 0.06 m/s for all three experiments. Similar trends were observed in all other experiments conducted. This result agrees with the transition velocities predicted from Taitel et al.'s correlation (i.e., Eq. 6.7).
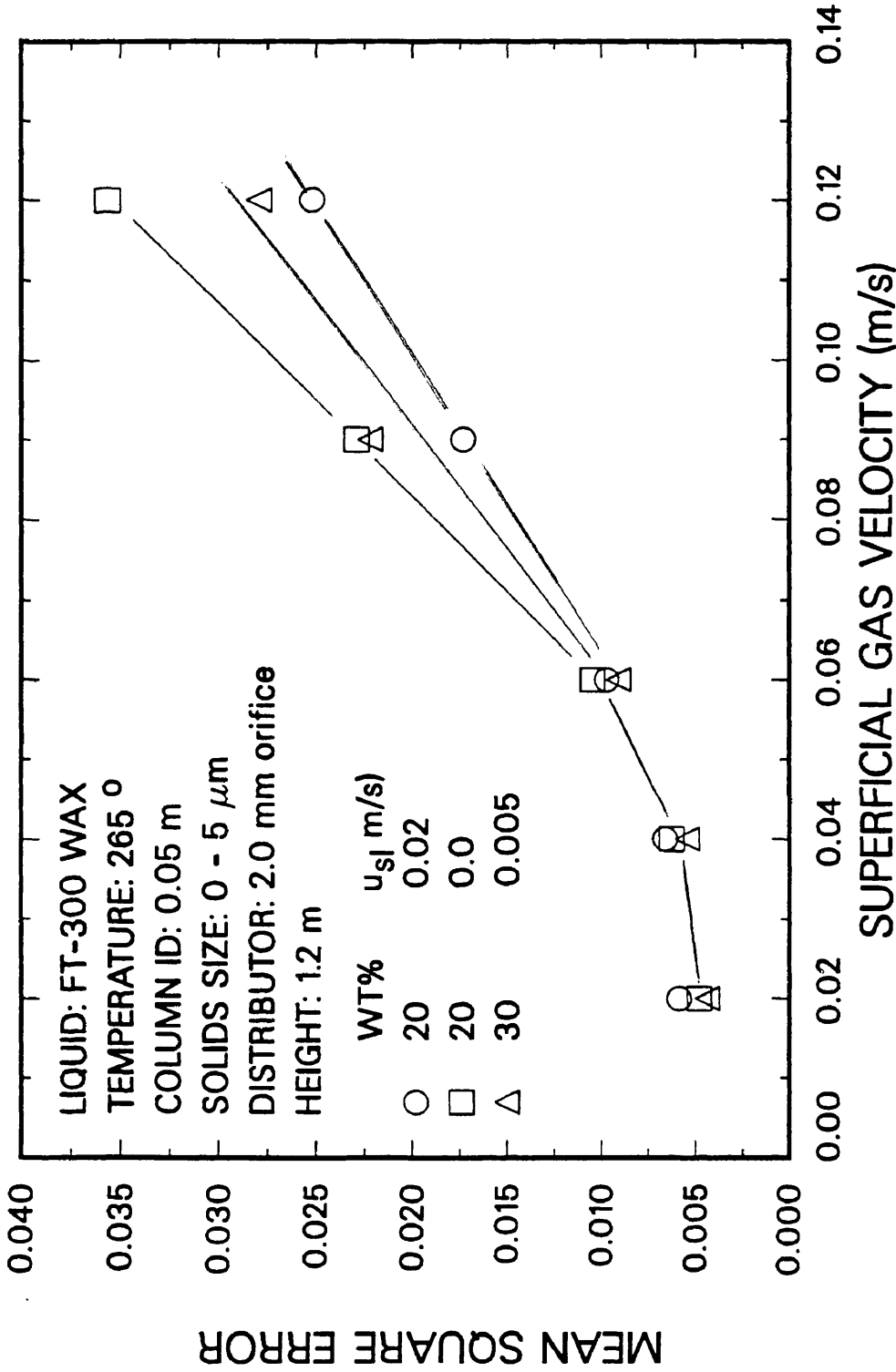
Figure 6.7. Effect of slurry flow rate on the mean square error of pressure fluctuations at the wall (FT-300 wax, 265 °C, 0 - 5 μm silica, 0.05 m ID column, 1.2 m above the distributor).

Figure 6.8 shows the effect of height above the distributor on the MSE at various gas velocities for the batch experiment shown in Figure 6.7. In general, the MSE increases with increasing u_g for all pressure transducers. One interesting trend was the decrease in the MSE between heights of 0.08 and 0.6 m above the distributor. We cannot be certain of the cause for the decrease in MSE at gas velocities of 0.09 and 0.12 m/s. One possible explanation is that the increase in oscillations at a height of 0.08 m is due to the increase in turbulence near the distributor caused by the increase in the gas velocity. The sharp changes in the slope of the MSE curve between heights of 0.6 and 1.2 m at gas velocities of 0.06, 0.09, and 0.12 m/s indicates that slugs begin appearing in the column somewhere between these heights. At gas velocities of 0.02 and 0.04 m/s, there is a slight change in the slope of the MSE curve between heights of 1.2 and 1.8 m, indicating the presence of large bubbles. This result agrees with the prediction of Eq. 6.8, i.e., slugs will not develop in the bottom part of the column.

Figure 6.9 show the effect of superficial gas velocity on the MSE of the pressure fluctuations for the same experiment. At heights of 0.08 and 0.6 m, we do not observe a transition to slug flow; however, the change in slope of the MSE curve for at a height of 1.2 m between gas velocities of 0.04 and 0.06 m/s indicates a transition to slug flow between these velocities. On the other hand, the slope of the MSE curve at a height of 1.8 m above the distributor does not change significantly, indicating that large bubbles are present at all velocities at this height.

Results obtained from experiments with large iron oxide particles showed similar trends in the MSE with gas velocity and height above the distributor. In general, for all experiments in which pressure fluctuations were obtained, the transition between bubbly and slug flow occurred somewhere between gas velocities of 0.04 and 0.06 m/s. Also, slugs were not observed below a height of 0.6 m above the distributor.
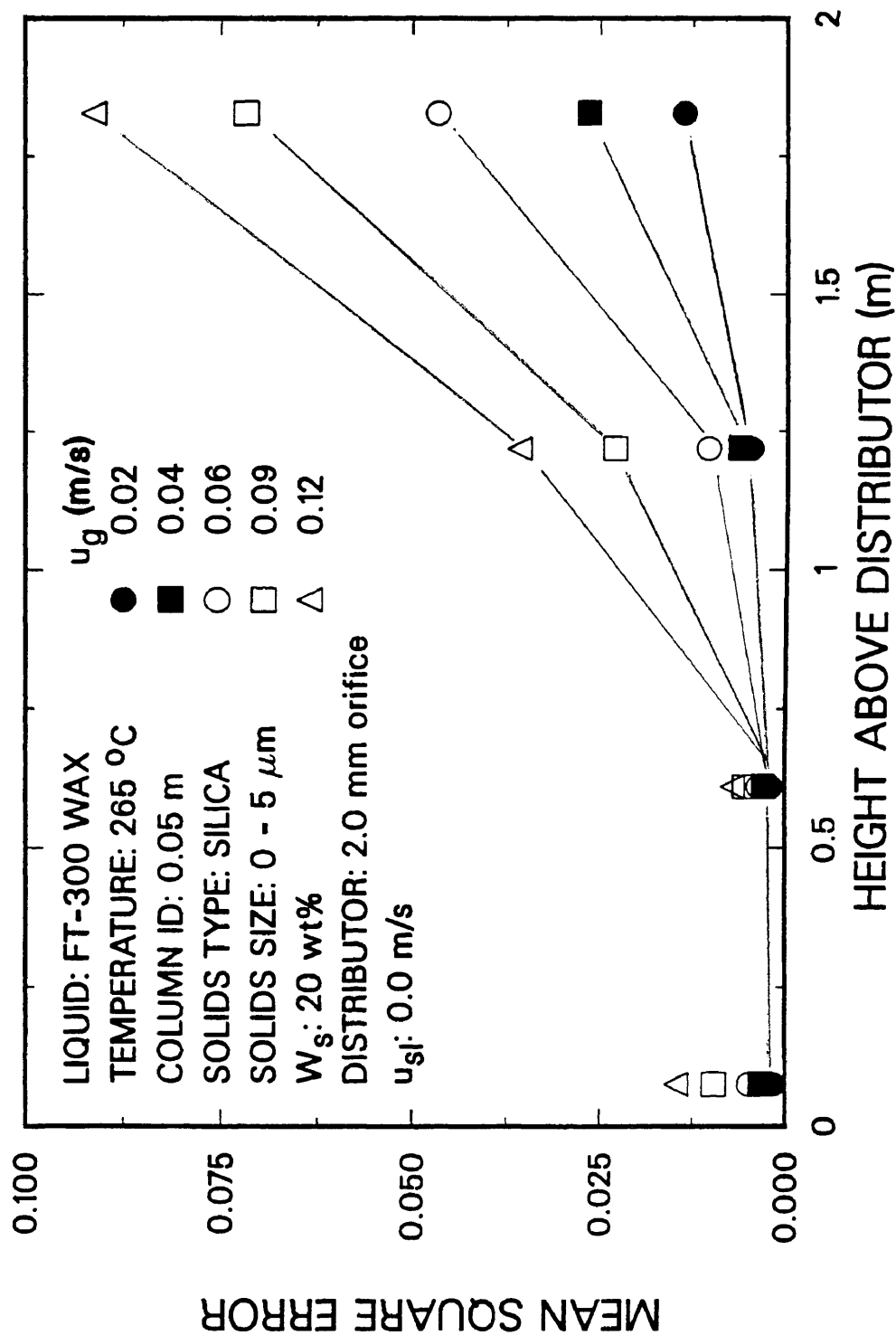
Figure 6.8. Effect of height above the distributor on the mean square error of pressure fluctuations at the wall (FT-300 wax, 265 °C, 20 wt% 0 - 5 μm silica, 0.05 m ID column, u_{sl} = 0.0 m/s).
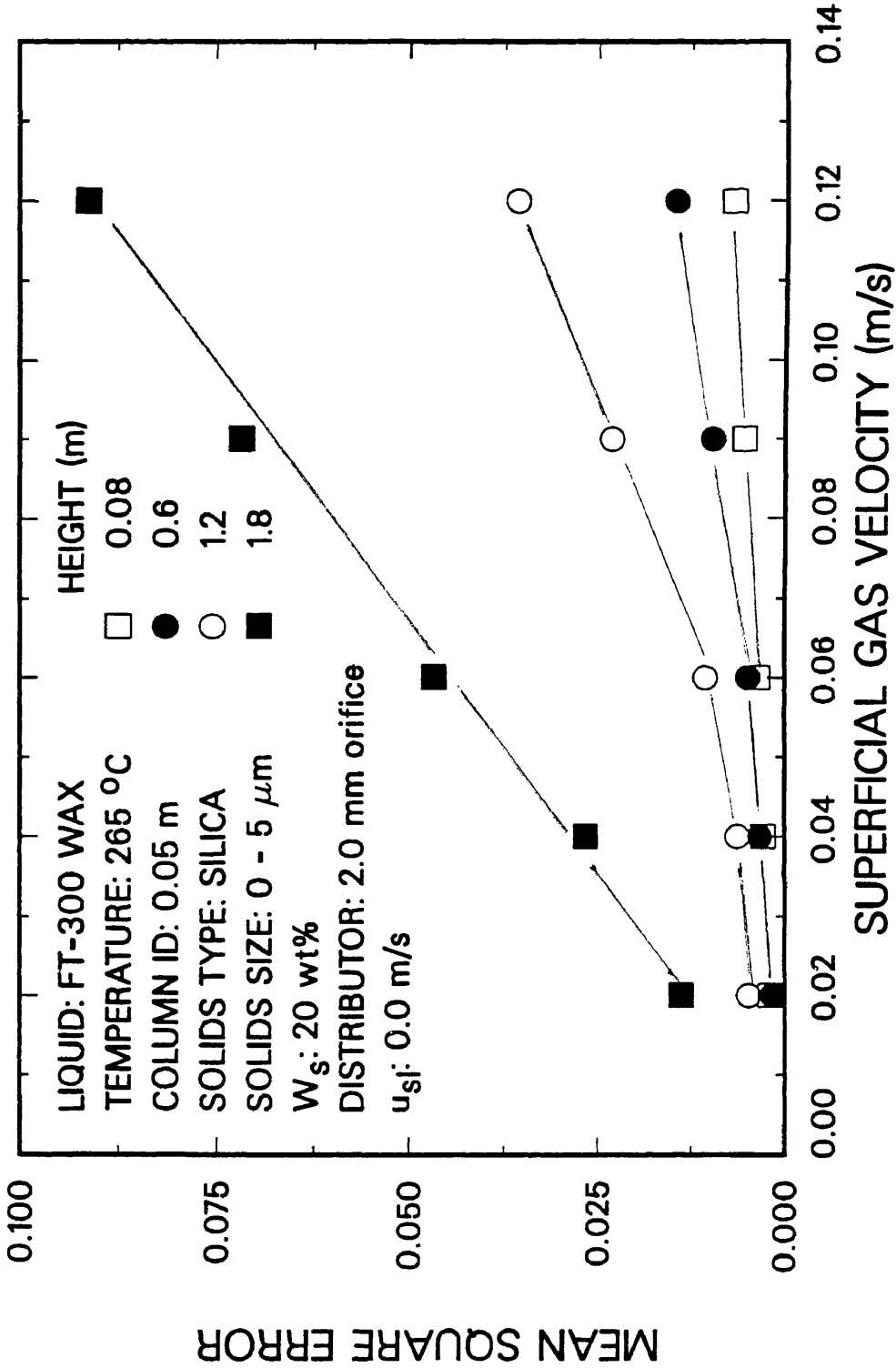
Figure 6.9. Effect of superficial gas velocity on the mean square error of pressure fluctuations at the wall (FT-300 wax, 265 °C, 20 wt% 0 - 5 μm silica, 0.05 m ID column, u_{sl} = 0.0 m/s).

MSE were calculated from both nuclear density gauge signals and raw pressure signals in the 0.21 m ID column for several experiments. In general, the MSE increased with increasing gas velocity but decreased slightly with increasing height above the distributor. Figure 6.10 shows the effect of superficial gas velocity on MSE for nuclear density gauge fluctuations at liquid velocities of 0.005 and 0.02 m/s using the perforated plate distributor and 0.005 m/s using the bubble cap distributor with SASOL reactor wax. An increase in the MSE of nuclear density fluctuations indicates an increase in the variation of gas holdup. For the experiments with the perforated plate distributor there is essentially no effect of liquid flow rate on MSE. However, the MSE of the density gauge fluctuations from the experiment conducted with the bubble cap distributor were significantly lower than those obtained during the experiments with the perforated plate distributor at gas velocities of 0.06 and 0.09 m/s. The lower MSE associated with the bubble cap distributor indicate the presence of a more uniform distribution (i.e. fewer larger bubbles). These results help substantiate the claim that smaller bubbles are formed with the bubble cap distributor due to its geometry. MSE from all experiments were essentially the same at gas velocities of 0.02 and 0.04 m/s. There is a change in the slope of the curves between gas velocities of 0.04 and 0.06 m/s for the experiments conducted with the perforated plate distributor and between gas velocities of 0.06 and 0.09 m/s for the experiment conducted with the bubble cap distributor. The change in slope indicates the transition from the homogeneous bubbly regime to the churn–turbulent flow regime. Similar trends were observed in other experiments. The transition velocities from the bubbly to churn–turbulent flow regime are within the range of velocities given by Deckwer et al. (1980).

Figure 6.11 shows the effect of axial position on the MSE of the pressure fluctuations for the batch experiment conducted with SASOL wax in the 0.21 m ID column. At gas velocities of 0.02 and 0.04 m/s, the MSE of the pressure fluctuations was essentially

313
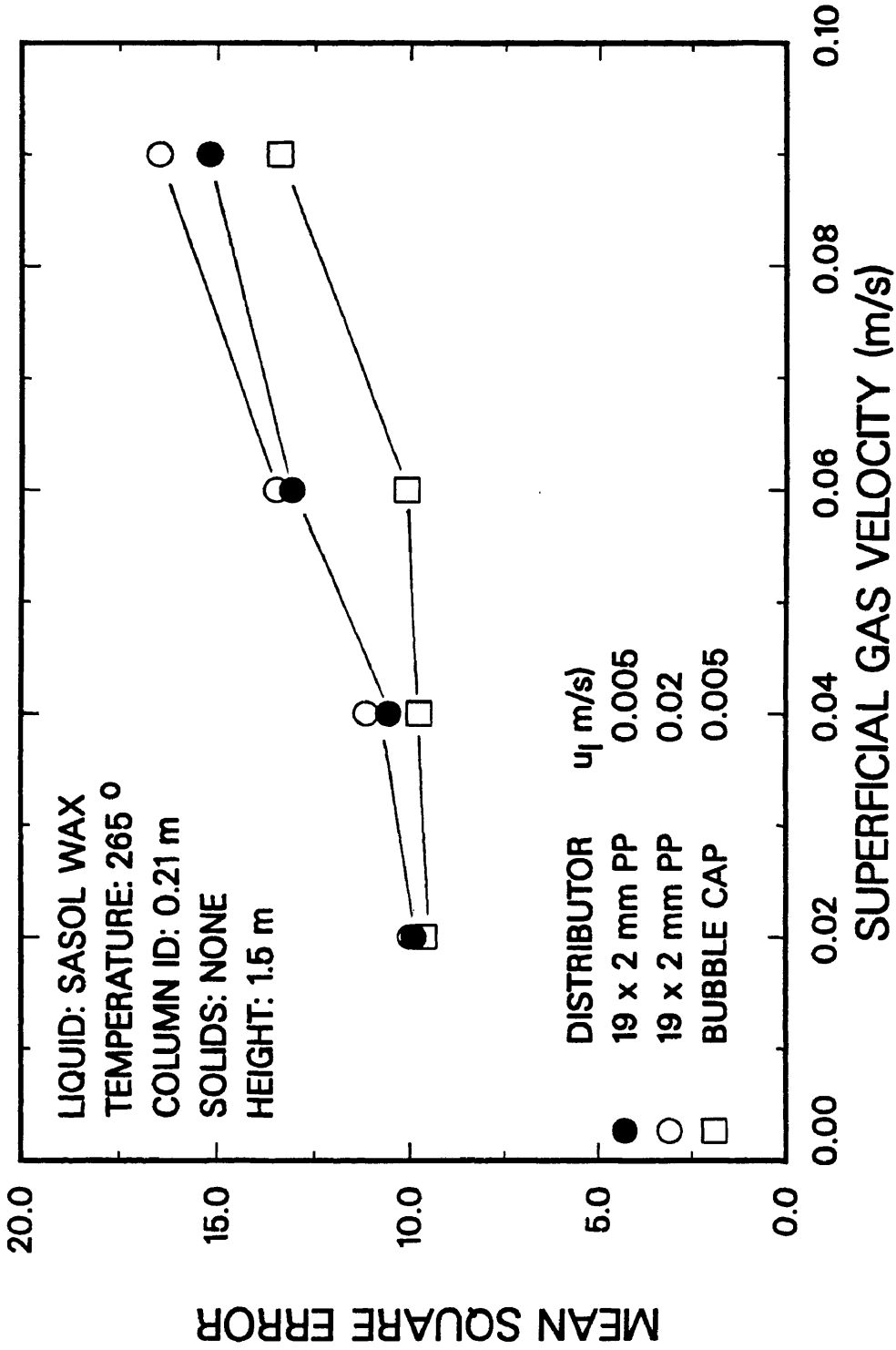
Figure 6.10. Effect of slurry flow rate and distributor on the mean square error of nuclear density gauge fluctuations (SASOL wax, 265 °C, 0.21 m ID column, Cesium-137 source, 1.5 m above the distributor).
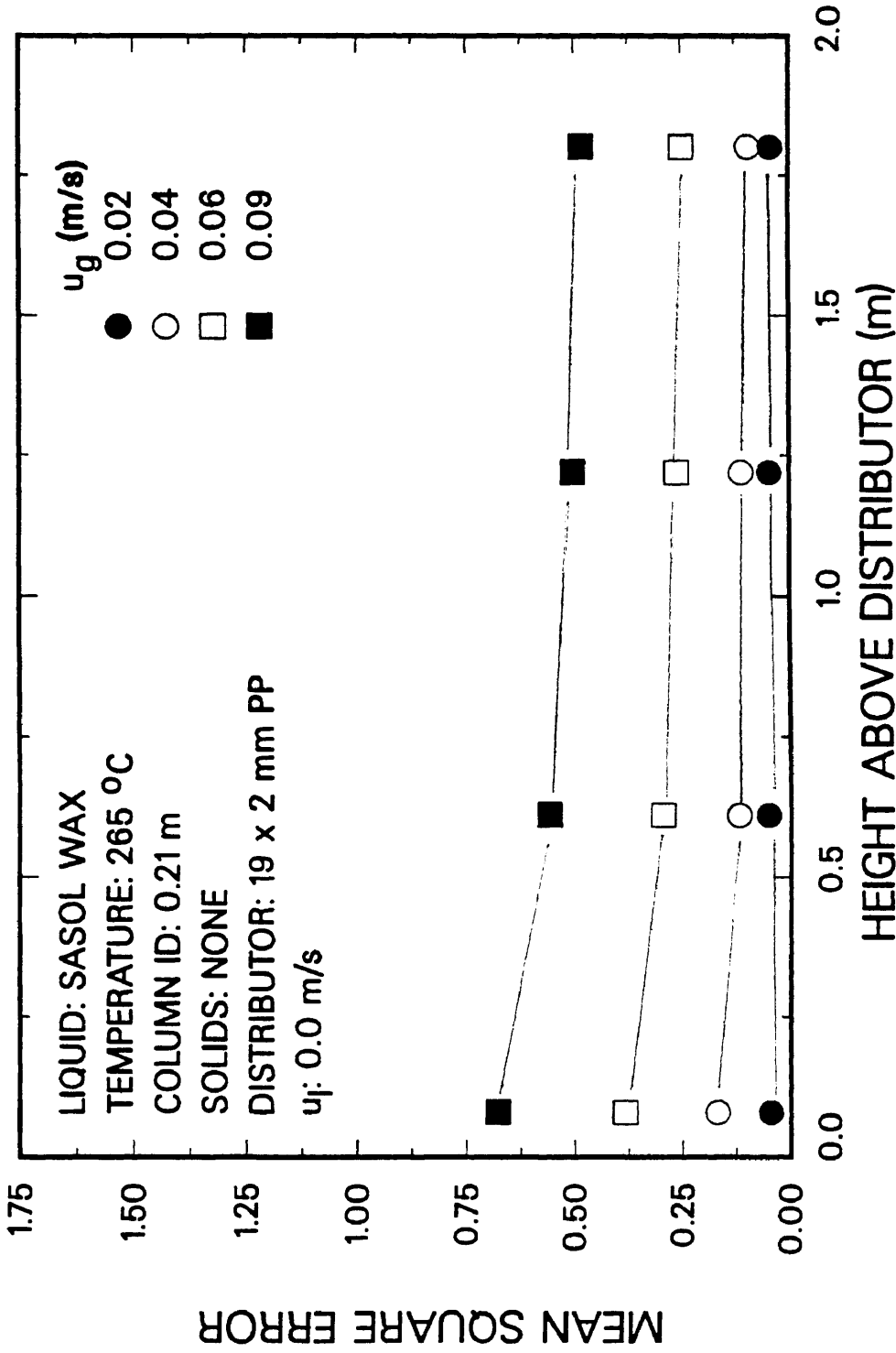
Figure 6.11. Effect of height above the distributor on the mean square error of pressure fluctuations at the wall (SASOL wax, 265 °C, 0.21 m ID column, u_l = 0.0 m/s).

the same at all heights, indicating the presence of the homogeneous bubbly regime. At gas velocities of 0.06 and 0.09 m/s, we observed a slight decrease in the MSE of the pressure fluctuations between heights of 0.08 and 0.6 m above the distributor. A similar trend was observed in the small diameter column (see Figure 6.8). However, in the small diameter column, the MSE increased significantly between heights of 0.6 and 1.2 m above the distributor, but in the large diameter column, it remained essentially constant. The lack of variation in the MSE with column height indicates that there is a minimal amount of axial variation in the flow patterns. We also observed uniform axial gas holdup profiles and bubble size distributions in the large diameter column, which agrees with these results. This type of behavior is representative of the churn–turbulent flow regime.

The effect of superficial gas velocity on the MSE of pressure fluctuations is shown in Figure 6.12 for the batch experiment with SASOL wax in the 0.21 m ID column. As expected, there is an increase in the MSE with increasing gas velocity. The change in slope between gas velocities of 0.04 and 0.06 m/s may be attributed to the transition from the bubbly to the churn–turbulent flow regime. These results are in agreement with those obtained from MSE analysis of nuclear density fluctuations.

Flow Regime Transitions Based on the PSD

Pressure signals and nuclear density gauge signals required high pass filtering. Slow changes in the mean of the signal, unrelated to higher frequency hydrodynamic phenomena, gave rise to a heavy low frequency bias in the psd and autocorrelation functions (Weimer et al., 1985) . To avoid this, the first difference of the time series corresponding to the fluctuations was used before spectra were obtained. The first difference is defined as (Jenkins and Watts, 1968):

$$P'_t = P_{t+\Delta t} - P_t \qquad (6.9)$$
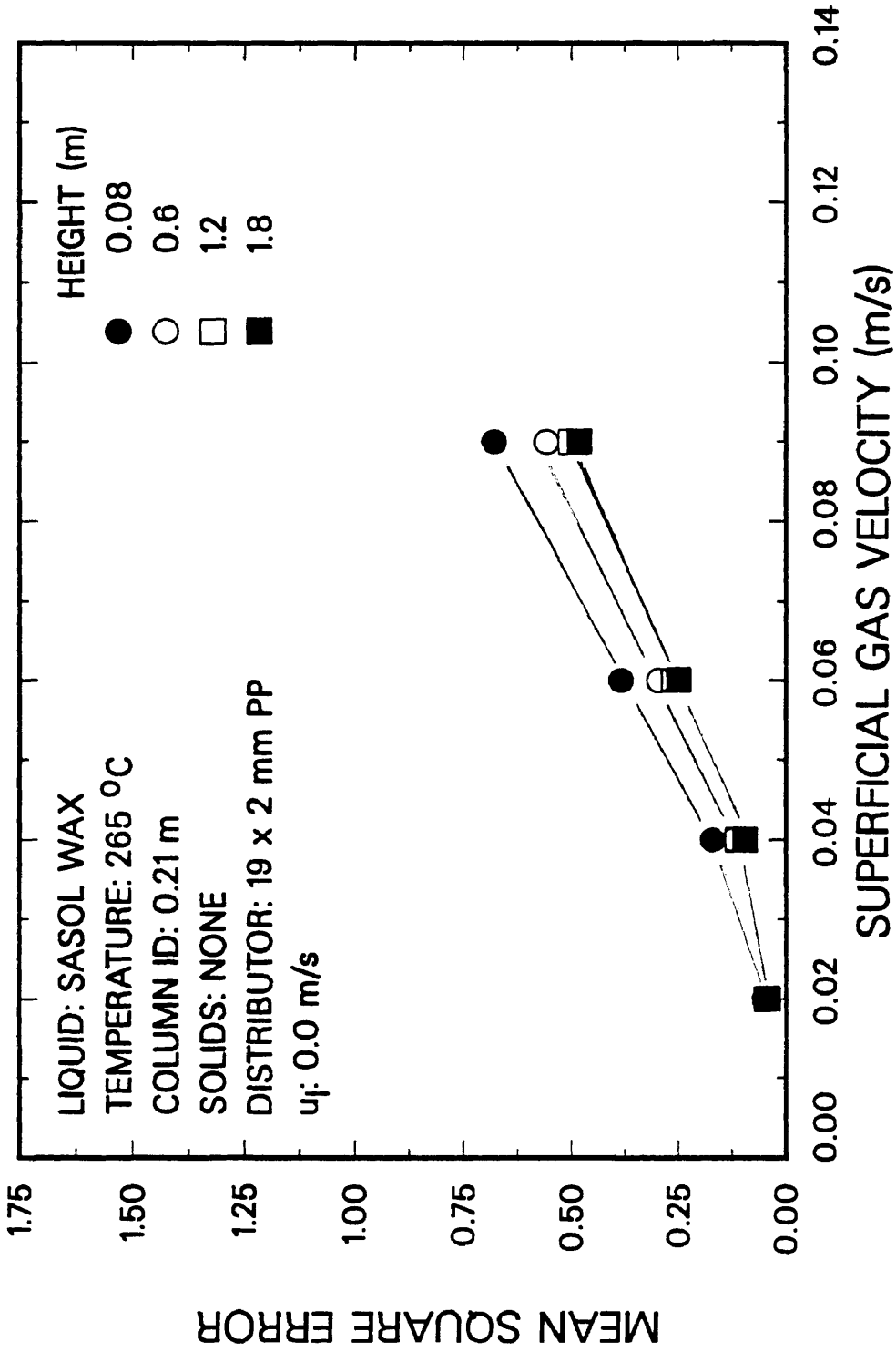
Figure 6.12. Effect of superficial gas velocity on the mean square error of pressure fluctuations at the wall (SASOL wax, 265 °C, 0.21 m ID column, u_l = 0.0 m/s).

where P corresponds to the pressure or nuclear density gauge signal and Δt corresponds to the time difference between two successive measurements. For example, if data was acquired at a rate of 100 Hz, then Δt would correspond to 0.01 sec. The psd was obtained from the new time series, P'_t. The psd of data from experiments with small silica particles and large iron particles in the small diameter column were obtained. The results from these calculations were used to determine flow regime transitions and slug frequencies. Likewise, the psd of data from experiments in the large diameter column in the absence of solids were obtained. These results were used to determine the transition from the bubbly to churn–turbulent flow regime.

Figure 6.13 show spectra of pressure signals obtained at a height of 1.8 m at different gas velocities in the 0.05 m ID column at a superficial slurry velocity of 0.02 m/s. The psd are fairly broad at a gas velocity of 0.02 and 0.04 m/s, with frequencies ranging from 2.5 to 10 Hz. For $u_g \geq 0.06$ m/s, the dominant frequency is in the range 2.5 to 5 Hz. The shift in frequency is indicative of the onset of slug flow between gas velocities of 0.04 and 0.06 m/s. Also, the intensity of the psd increases with increasing gas velocity; a similar trend was observed with the MSE (i.e. MSE increased with increasing gas velocity).

The spectra from transducers at heights of 0.6, 1.2, and 1.8 m above the distributor at a gas velocity of 0.12 m/s for the batch experiment conducted with 20 wt% 20 – 44 μm iron oxide particles in the 0.05 m ID column are shown in Figure 6.14. The dominant frequency observed at a height of 0.6 m above the distributor is 5 Hz; whereas, the dominant frequency at heights of 1.2 and 1.8 m is 2.5 Hz. This shift from 5 Hz to at the bottom of the column to 2.5 Hz at the top of the column is an indication of coalescence which may be taking place. Similar results were observed for the batch experiment with small silica (see Figure 6.15). For experiments conducted in the glass column we observed slug frequencies in the range 2 to 3 Hz at the top of the column
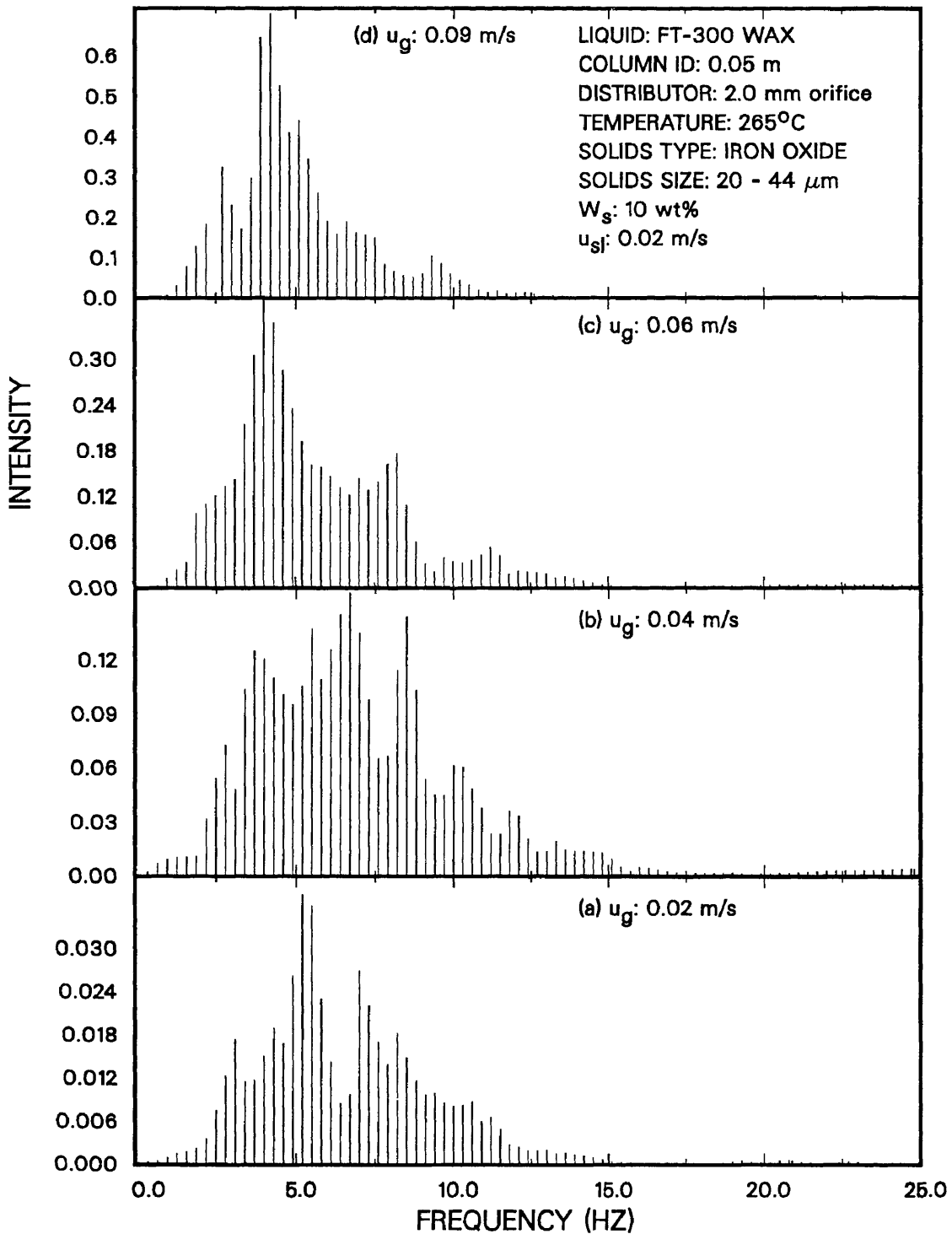
Figure 6.13. Effect of superficial gas velocity on the power spectral density function for pressure fluctuations at the wall (FT-300 wax, 265 °C, 0.05 m ID column, 10 wt% 20 - 44 μm iron oxide, u_{sl} = 0.02 m/s, height = 1.8 m).
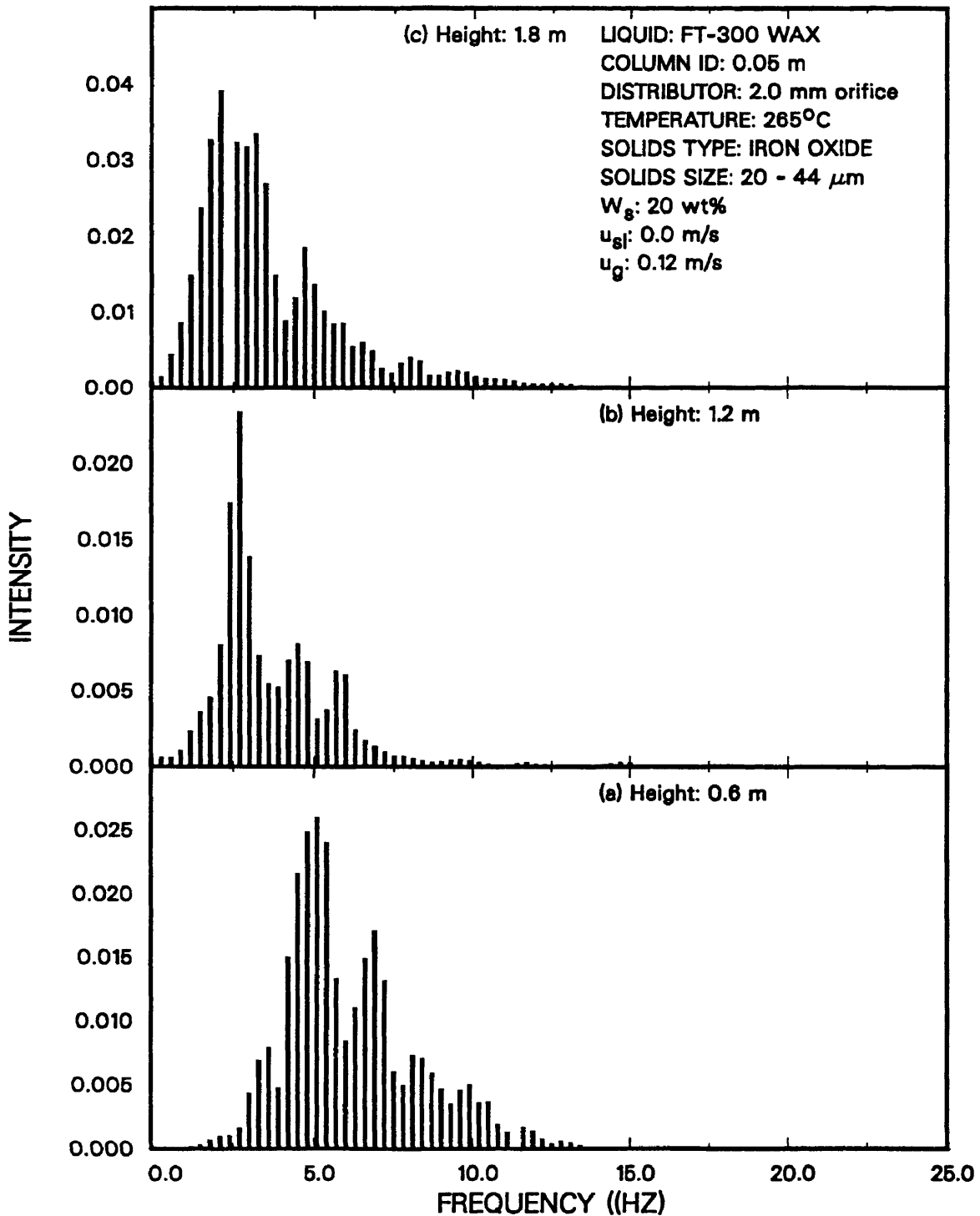
Figure 6.14. Effect of height above the distributor on the power spectral density function for pressure fluctuations at the wall (FT-300 wax, 265 °C, 0.05 m ID column, 20 wt% 20 - 44 μm iron oxide, u_{sl} = 0.0 m/s, u_g = 0.12 m/s).
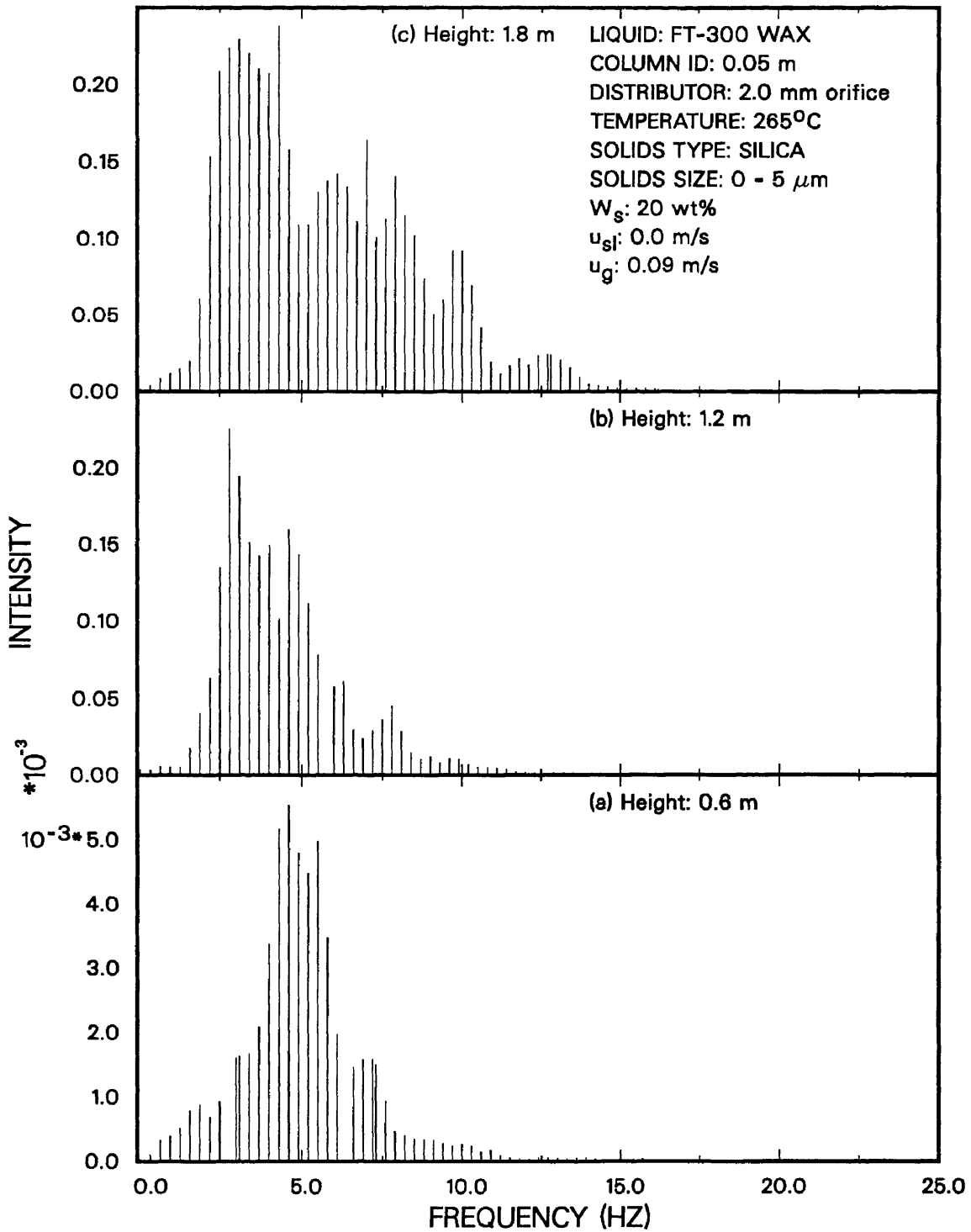
Figure 6.15. Effect of height above the distributor on the power spectral density function for pressure fluctuations at the wall (FT-300 wax, 265 °C, 0.05 m ID column, 20 wt% 0 - 5 μm silica, u_{sl} = 0.0 m/s, u_g = 0.09 m/s).

for gas velocities of 0.07, 0.09, and 0.12 m/s. At the bottom of the column, we have more frequent, smaller slugs, whereas, towards the top of the column, two small slugs coalesce to form a single large slug. This type of behavior has been observed visually in our two—phase experiments conducted in the glass column. This also agrees with the description proposed by Taitel et al. (1981) which was used in their correlation for determining the entry region over which churn flow exists.

Thus, for experiments conducted in the small stainless steel column in the batch mode of operation, the dominant slug frequency is approximately 2.5 Hz at the top of the column. Coalescence of small slugs to form large slugs occurs between a height of 0.6 m and 1.2 m above the distributor.

Figure 6.16 shows the effect of superficial gas velocity on the psd of the nuclear density gauge fluctuations from the batch experiment with FT—300 wax (without solids) in the small diameter column at gas velocities of 0.02, 0.04, 0.06, and 0.09 m/s. The four plots at the four different gas velocities indicate the progressive movement of the dominant frequency to the left (towards lower values) with an increase in gas velocity. These results show that the spectra are narrower at higher gas velocities (u_g=0.06 and 0.09 m/s) than they are at lower velocities. This behavior in the frequency spectrum is indicative of the change in flow regime in the bubble column. At low gas velocities, the homogeneous bubbly regime prevails and goes through a transition before approaching the slug flow regime at a gas velocity of 0.06 m/s. The dominant frequency at a gas velocity of 0.02 m/s is in the range 7.5 to 10 Hz, and shifts to the range 2.5 to 5 Hz at 0.04 m/s, and finally approaches 2.5 Hz as slug flow develops at 0.06 m/s. The definite shift in the dominant frequency observed between gas velocities of 0.04 and 0.06 m/s which was observed in all experiments indicates that slug flow begins somewhere between these two velocities. As mentioned previously, the same transition region was observed in experiments with the silica particles using MSE analysis (see Figure 6.9).
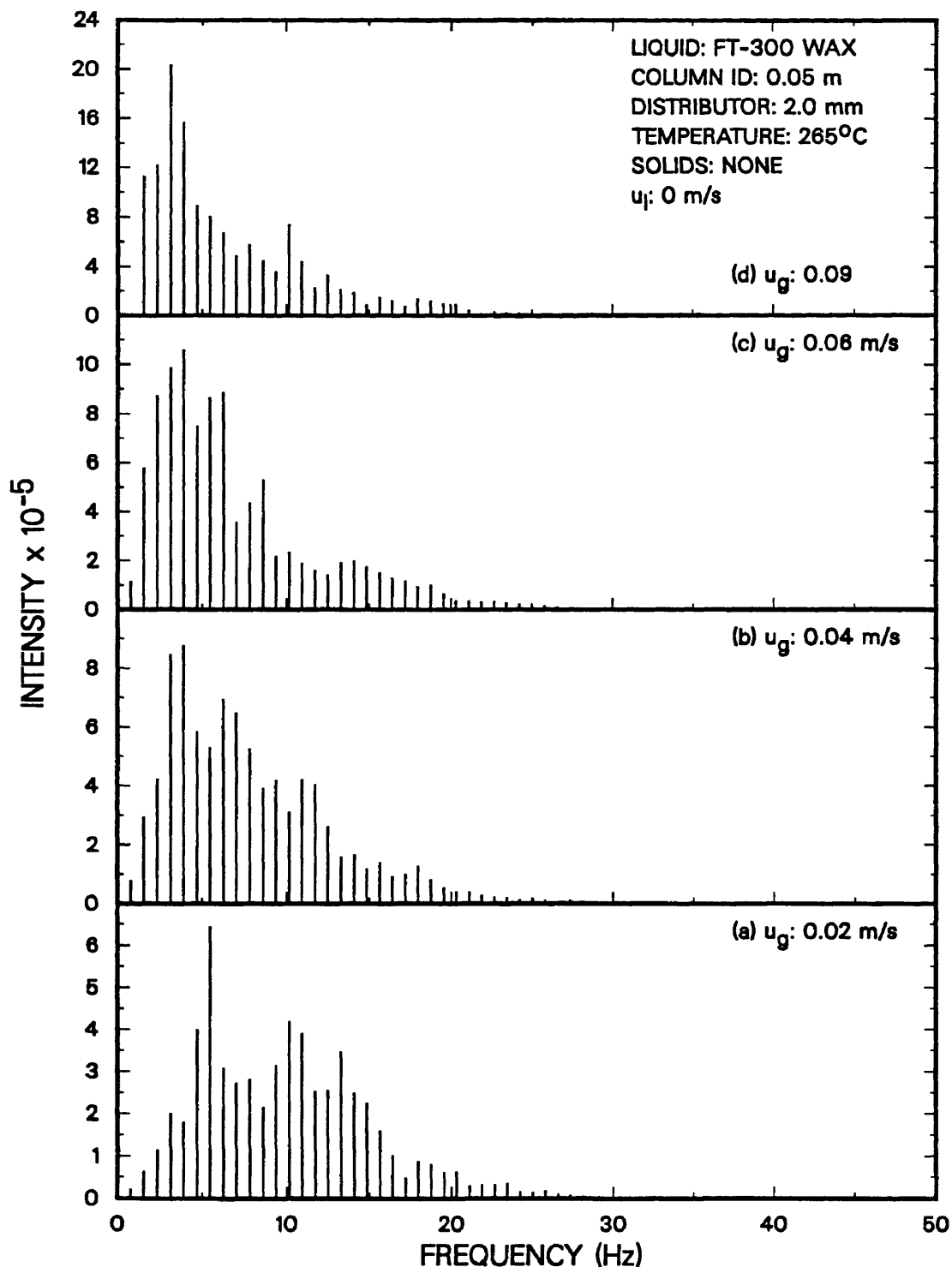
Figure 6.16. Effect of superficial gas velocity on the power spectral density function from the nulcear density gauge (FT-300 wax, 265 °C, 0.05 m ID column u_l = 0.0 m/s, Cesium-137, height = 1.5 m).

Hence, both MSE and psd analysis may be used to determine the transition from bubbly to slug flow. In addition, the psd may be used to determine slug frequency. Results obtained from statistical analysis results are in agreement with predictions from Taitel et al.'s correlations. Also, they are consistent with our visual observations in the small glass column.

The effect of superficial gas velocity on the power spectra for pressure signals obtained from the batch experiment with SASOL reactor wax (no solids) in the 0.21 m ID column at heights of 0.08 and 1.8 m above the distributor are shown in Figures 6.17 and 6.18, respectively. In the vicinity of the distributor, two characteristic psd peaks are observed (see Figure 6.17). The bimodal distribution may be indicative of the coalescence near the distributor. The intensity of the low frequency peak increases significantly with increasing gas velocity, which implies the formation of larger, less frequent bubbles in the vicinity of the distributor. At a height of 1.8 m above the distributor, a single peak in the psd is observed. The single peak is representative of a stable flow pattern (i.e. stable bubble size). As the gas flow rate is increased from 0.02 to 0.04 m/s, there is a definite shift in the frequency of the psd (12 Hz at 0.02 m/s to 8 - 10 Hz at 0.04 and 0.06 m/s). This shift in the dominant frequency between gas velocities of 0.02 and 0.04 m/s represents the transition from bubbly to the churn–turbulent flow regime.

Figures 6.19 and 6.20 show the effect of height above the distributor on the psd for the same experiment at gas velocities of 0.02 and 0.06 m/s, respectively. At both velocities, the bimodal distribution prevails at heights of 0.08 and 0.6 m. As mentioned above, the bimodal distribution is characteristic of the entry region over which bubble coalescence and breakup occurs. At heights of 1.2 and 1.8 m above the distributor, we no longer observe the bimodal distribution, thus indicating the presence of fully developed flow.
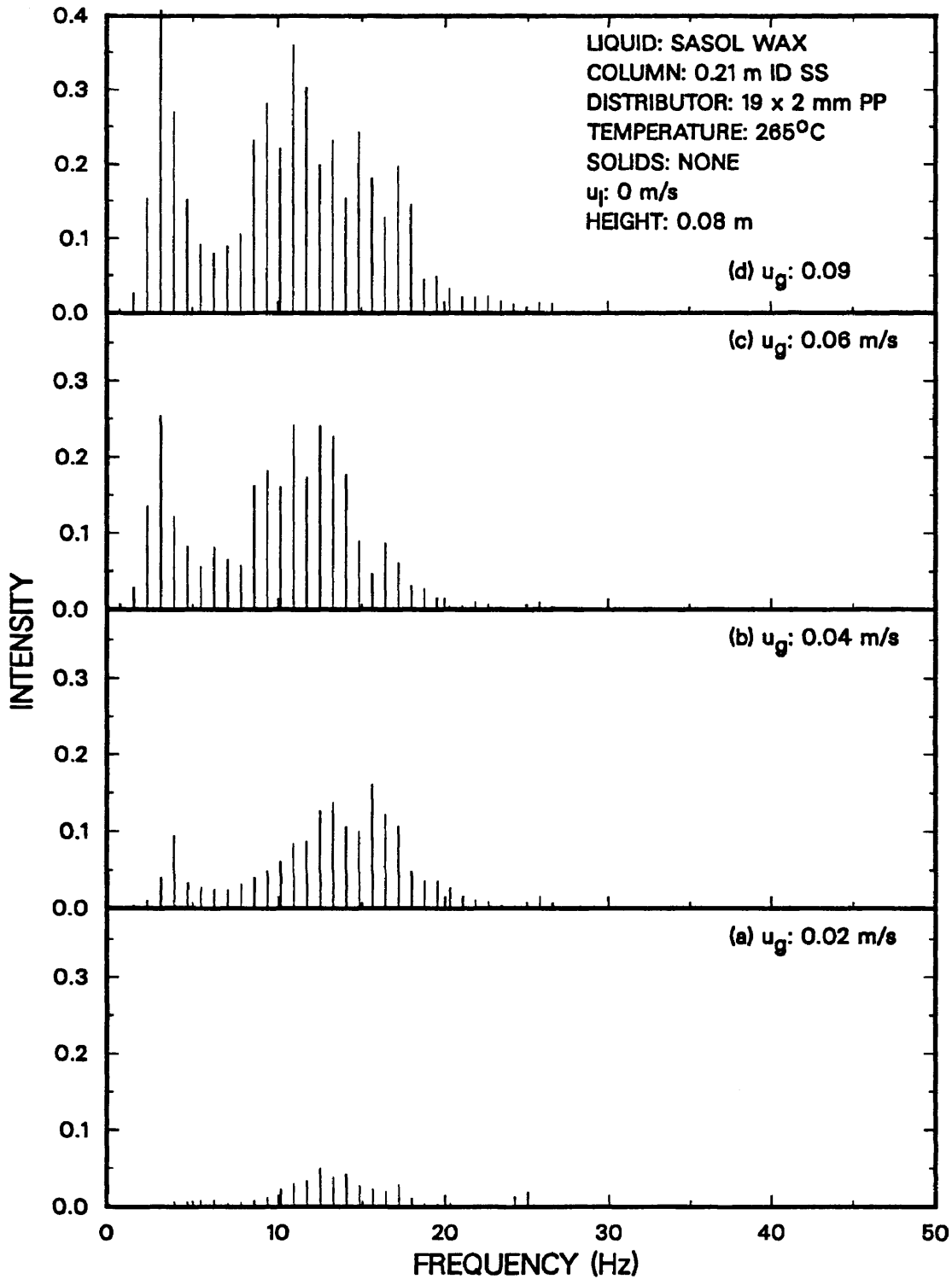
Figure 6.17. Effect of superficial gas velocity on the power spectral density function for pressure fluctuations at the wall (SASOL wax, 265 °C, 0.21 m ID column, u_l = 0.0 m/s, height = 0.08 m).
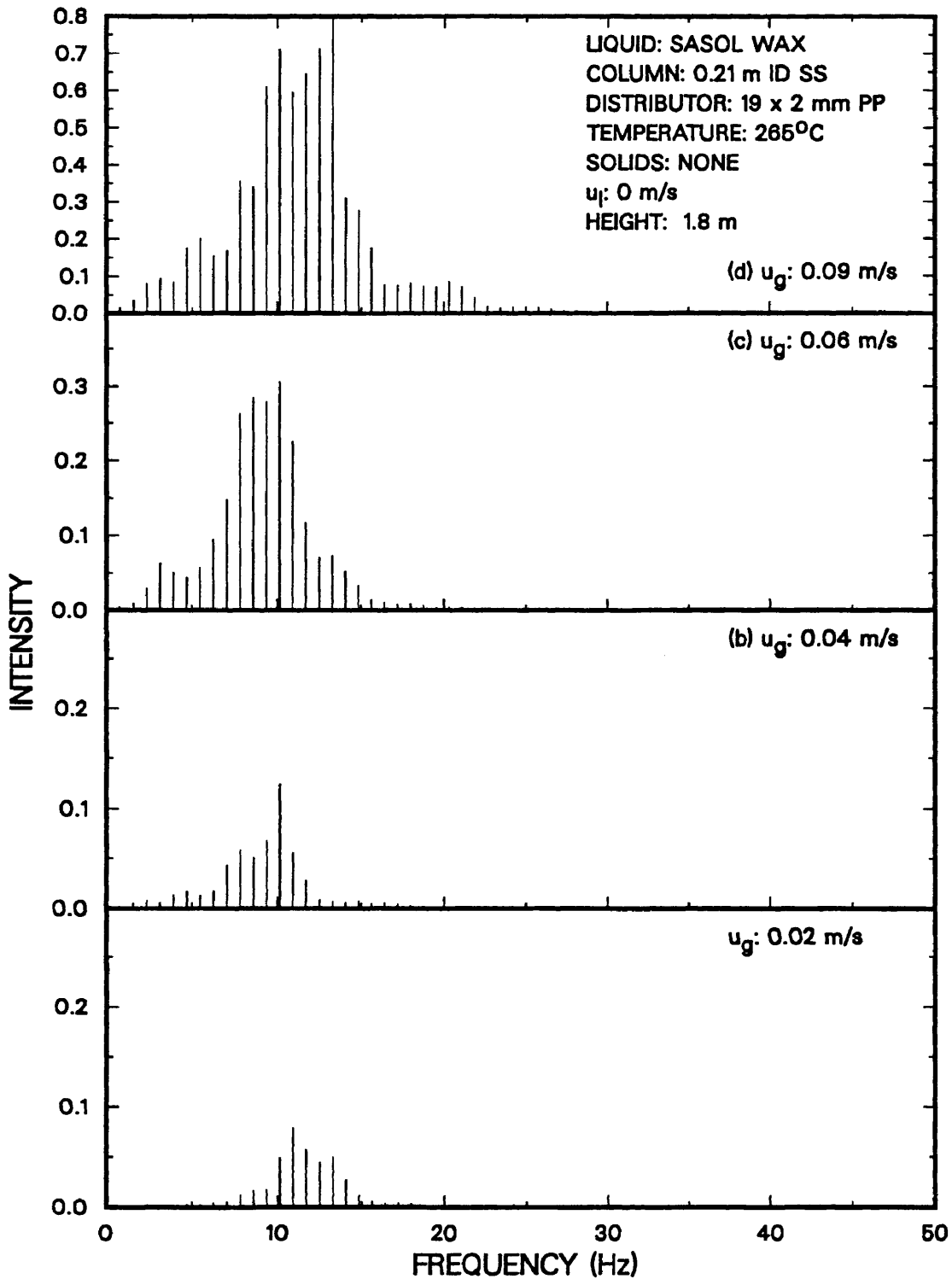
Figure 6.18. Effect of superficial gas velocity on the power spectral density function for pressure fluctuations at the wall (SASOL wax, 265 °C, 0.21 m ID column, u_l = 0.0 m/s, height = 1.8 m).
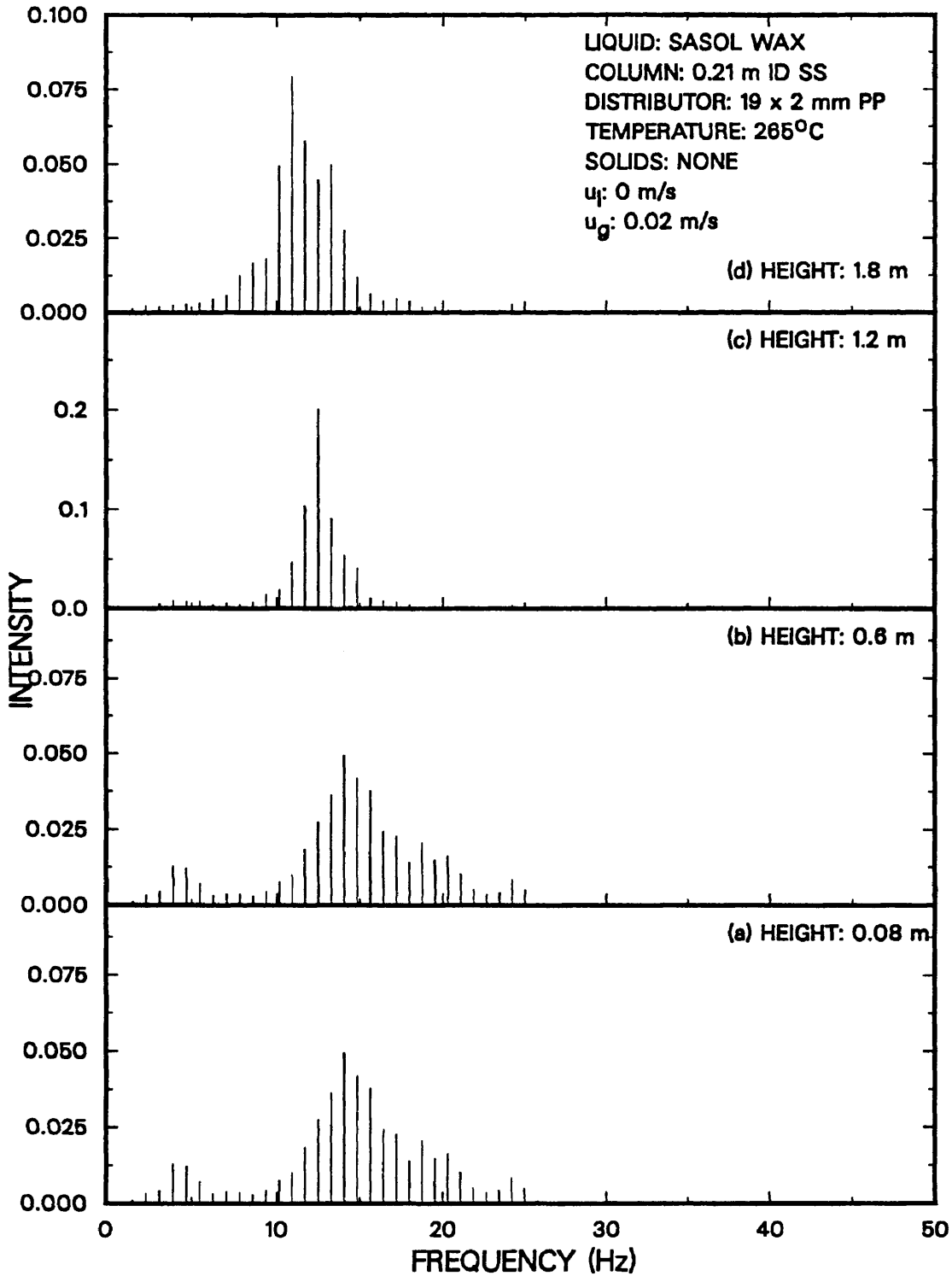
Figure 6.19. Effect of height above the distributor on the power spectral density function for pressure fluctuations at the wall (SASOL wax, 265 °C, 0.21 m ID column, u_l = 0.0 m/s, u_g = 0.02 m/s).
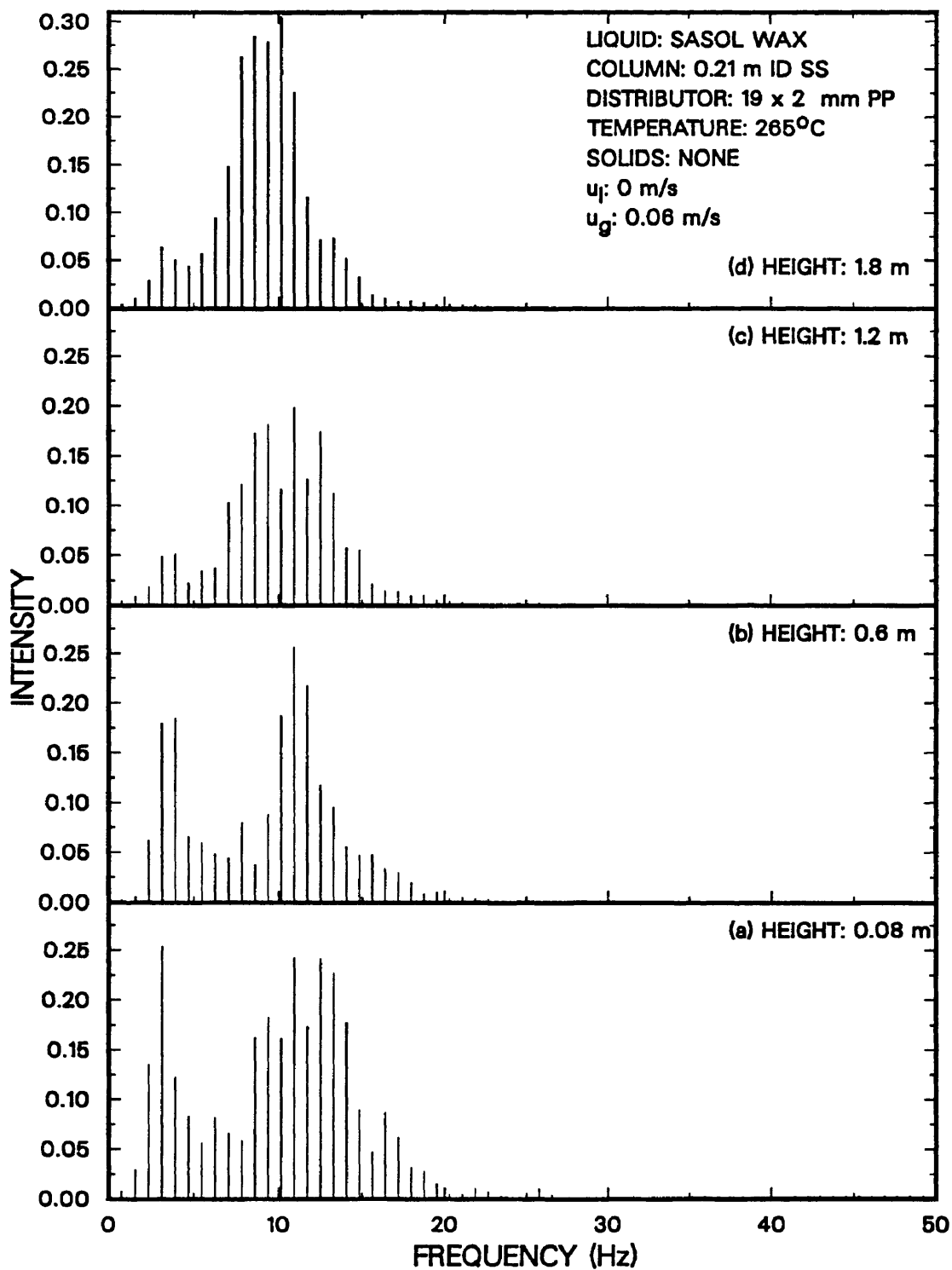
Figure 6.20. Effect of height above the distributor on the power spectral density function for pressure fluctuations at the wall (SASOL wax, 265 °C, 0.21 m ID column, u_l = 0.0 m/s, u_g = 0.06 m/s).

Figure 6.21 shows the effect of superficial gas velocity on the psd of nuclear density gauge fluctuations from the batch experiment with FT–300 wax in the 0.21 m ID column at a height of 1.5 m above the distributor. At a gas velocity of 0.02 m/s, the psd is fairly broad, which indicates the presence of the homogeneous bubbly regime. As the gas velocity is increased, the psd appears to become narrower and there is a shift in the dominant frequency towards the left (i.e. lower frequency). In the homogeneous bubbly regime, there is not a dominant frequency; however, in the churn–turbulent flow regime, large bubbles are produced which pass by the transducer at regular intervals (i.e. the dominant frequency). At a gas velocity of 0.02 m/s the frequency primarily ranges from 6 to 12 Hz; whereas, at gas velocities of 0.04 and 0.08 m/s, the dominant frequency is approximately 6 Hz. This shift in the frequency of the psd represents a transition from the bubbly flow regime to the churn–turbulent flow regime. The transition to the churn–turbulent flow regime in the neighborhood of 0.04 m/s is in agreement with our results obtained using the MSE approach. Also, the transition velocity is within the range of velocities presented by Deckwer et al. (1980).
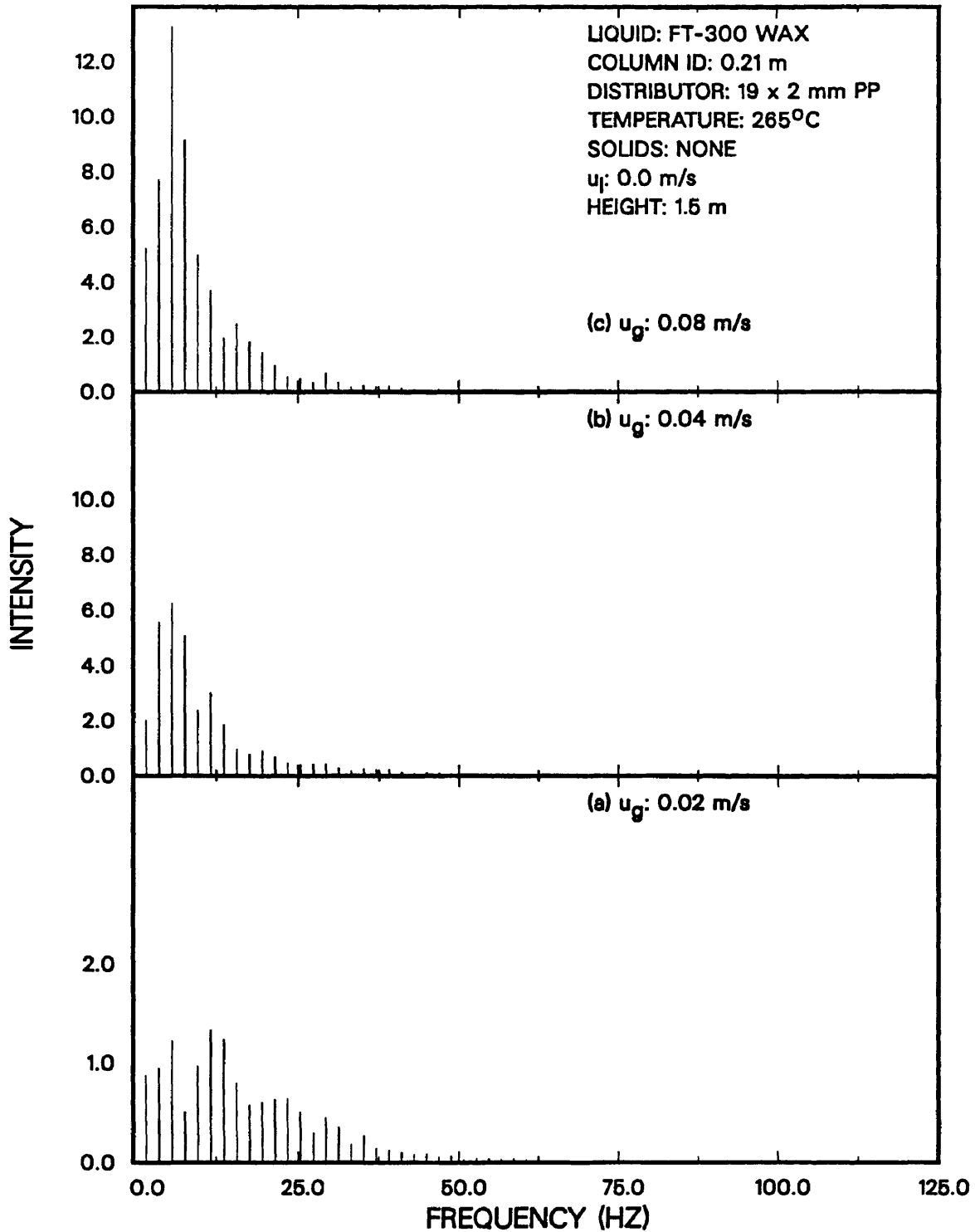
Figure 6.21. Effect of height above the distributor on the power spectral density function for nuclear density gauge fluctuations (FT-300 wax, 265 °C, 0.21 m ID column, Cobalt-60, height=1.5 m).

CHAPTER VII

CONCLUSIONS AND RECOMMENDATIONS

In order to properly design and scale–up a bubble column reactor, both hydrody-
namic and kinetic data are needed. This study has provided some of the hydrodynamic
data which is needed for the design and scale–up of a slurry phase Fischer–Tropsch bub-
ble column reactor. Hydrodynamic studies of direct relevance to the Fischer–Tropsch
process were conducted in both 0.05 m and 0.21 m ID bubble columns using the molten
wax–nitrogen system. In this study, we measured (1) average and axial gas holdup, (2)
axial solids concentration distributions and dispersion coefficients, (3) gas holdup using
a dual energy nuclear density gauge, (4) bubble size distributions, and (5) flow regime
transitions.

Gas Holdup

The effect of gas velocity (0.02 to 0.12 m/s), slurry velocity (0 to 0.02 m/s), solids
type (iron oxide and silica), size (0–5 μm and 20–44 μm) and concentration (0 to 30
wt%), wax type (SASOL and FT–300), distributor type, and column diameter (0.05
and 0.21 m ID) on axial and average gas holdups were measured using conventional
techniques (i.e. pressure measurements/slurry samples). Gas holdup results from this
study show that in the small diameter column FT–300 wax has a tendency to foam
during batch experiments. However, the introduction of a small upward liquid flow
(0.005 m/s) is sufficient to dissipate the foam. The amount of foam produced in the
large diameter column with FT–300 wax during batch experiments was significantly less.
SASOL wax did not foam significantly in either column during batch experiments. The
addition of solids increases the amount of foam (i.e. gas holdup) in the batch mode
of operation, for both FT–300 wax (non–coalescing media) and SASOL reactor wax
(coalescing media), which may be attributed to the poor wettability of the iron oxide
and silica particles used in this study. In the absence of foam, gas holdups obtained in

the small diameter and large diameter columns were similar. Both a perforated plate and bubble cap distributor were used during experiments in the 0.21 m ID column. Gas holdup values obtained with the bubble cap distributor were slightly greater than those obtained with the perforated plate distributor. We believe that the difference in holdups may be attributed to differences in the geometry of the two distributors. Gas holdup increased with height above the distributor for experiments conducted in both columns; however, this was most pronounced during batch experiments in the small diameter column. Average gas holdup data from both two–phase and three–phase experiments were evaluated using non–linear regression to obtain the following empirical correlation for predicting gas holdups:

$$\epsilon_g = 0.24(Fr_g^{0.28}Bo^{0.14}) \tag{7.1}$$

A total of 514 data points from all experiments conducted in both columns (nonfoamy data only) were used to obtain the correlation (MSE = 0.0007).

Axial Solids Concentration Distributions

Axial solids concentration profiles were obtained during experiments conducted in both the 0.05 m and 0.21 m ID columns with $0 - 5$ μm and $20 - 44$ μm iron oxide and silica particles. Solids concentrations of 10, 20, and 30 wt% were employed throughout these studies. The small ($0 - 5$ μm) iron oxide and silica particles were completely suspended in both columns in the batch and continuous modes of operation. However, significant concentration gradients were observed with large ($20 - 44$ μm) particles, particularly iron oxide, in the small diameter column during batch experiments. In the large column, the solids concentration gradient was smaller. The solids distribution became uniform with the introduction of upward slurry velocity (0.005 or 0.02 m/s), since the slurry velocity was greater than the terminal settling velocity of the largest

particles. Axial solids dispersion coefficients were estimated from axial solids concentration profiles obtained in experiments conducted with large solids in both the batch mode and continuous mode (the latter in the large diameter column only) of operation. The axial solids dispersion coefficients in the large diameter column were significantly greater than those obtained in the small diameter column. The following correlation for predicting the particle Pectlet number, which is similar to that presented by Smith and Ruether (1985), was obtained.

$$Pe_p = 8.4 \left[\frac{Fr_g^6}{Re_g} \right]^{0.107} \tag{7.2}$$

The above correlation was developed from data obtained with both large iron oxide and silica particles using both SASOL wax and FT–300 wax.

Due to operational problems with the pump in the small diameter column, experiments with large particles at a superficial slurry velocity of 0.005 m/s were not conducted. Thus, additional experiments are needed to determine the validity of Eq. 7.2 for continuous flow experiments.

Nuclear Density Gauge Measurements

A dual energy gamma–ray densitometer was designed and constructed for the purpose of obtaining phase (i.e. gas, liquid, and solid) fractions in the large diameter column. The sources and detectors were placed on a movable platform so that measurements could be made at various axial and radial locations. Cesium–137 and Cobalt–60 radioactive sources were used. For the (Cesium–137) – (Cobalt–60) system, slight errors in various parameters (e.g. the distance through the column) cause significant errors in the measured phase fractions. This is due to similarities in the absorption coefficients for the various phases associated with the two sources. However, when we treated our three–phase system as a two–phase (slurry/gas) system, the measured volume fractions of gas and slurry were comparable to those obtained using conventional (i.e. DP cells)

techniques. Throughout this work, we encountered problems with pressure transducers becoming "plugged" with wax. Thus, since gas holdup values obtained using the DP cells and nuclear density gauges were similar and there were no major operational problems with the density gauge, we would recommend using a nuclear density gauge (coupled with slurry withdrawal) to measure gas holdup in a slurry bubble column reactor.

Bubble Size Measurements

Sauter mean bubble diameters were measured using the dynamic gas disengagement (DGD) technique. The DGD technique is based on the fact that the volumetric flow rate at which the liquid level decreases once the gas flow is shut–off is equal to the volumetric flow rate at which the bubbles exit the dispersion. In the past, the majority of studies which utilized the DGD technique were conducted in clear columns, and the rate at which the liquid level (or dispersion) dropped was recorded via a VCR/camera system. In this study, we utilized pressure measurements to determine the rate of disengagement. Pressure measurements not only remove some of the subjectivity associated with VCR/camera measurements, but also enables one to determine the effect of axial position on the bubble size distribution. Sauter mean bubble diameters for FT–300 wax were quantitatively similar in both the 0.05 m and 0.21 m ID bubble columns for the range of gas velocities employed in this study. The Sauter mean bubble diameter ranged from approximately 0.9 mm at a gas velocity of 0.02 m/s to a value of 1.4 mm at a gas velocity of 0.12 m/s. Sauter mean bubble diameters for the experiment conducted with SASOL wax (increasing gas velocities, 0.21 m ID column) were similar to those obtained with FT–300 wax. However, for the experiment conducted using a decreasing order of gas velocities, the Sauter mean bubble diameters were slightly higher (e.g. $d_s = 1.7$mm at a gas velocity of 0.12 m/s). For the experiment conducted with SASOL wax in the

0.05 m ID column, the Sauter mean bubble diameters ranged from 1.4 mm (u_g=0.02 m/s) to 2.2 mm (u_g=0.09 m/s).

The DGD technique was also used to obtain bubble size distributions for tap water. A new method for analyzing the disengagement curve obtained during slug flow was developed. The results obtained using the new technique were in excellent agreement with those predicted using correlations presented by Hughmark (1967) and Akita and Yoshida (1974).

Flow Regime Transitions

Statistical analysis of wall pressure and nuclear density gauge fluctuations was used to determine flow regime transitions in both columns. For experiments in the small diameter column, the transition from the bubbly to slug flow regime occurred between gas velocities of 0.04 and 0.06 m/s, regardless of solids concentration or slurry velocity (up to 0.02 m/s). Likewise, in the large diameter column, the transition from the homogeneous bubbling regime to the churn–turbulent regime occurred between gas velocities of 0.04 and 0.06 m/s. In the small diameter column, slugs start forming at a height of 0.6 m above the distributor. The flow regime transitions obtained in this study are in agreement with those predicted using correlations presented by Taitel et al. (1981) and the flow regime map presented by Deckwer et al. (1980).

Future Work

We were successful in completing the majority of our proposed work. Some difficulty was encountered during measurements with the nuclear density gauges. In particular, we were not able to measure the three phase fractions (i.e. gas/liquid/solid) independently using the dual energy gamma–ray densitometer. The problem encountered with the independent measurement of all three fractions is related to similarities in the attenuation coefficients of the Co–60 and Cs–137 sources. It might be possible to use this technique with our system if a lower energy source with sufficient activity is available or

a high ($>$ 10 MeV) energy source is available. With the low energy source one would probably not be able to obtain instantaneous variations in the phase fractions but it might be possible to obtain average values provided measurements are made over an extended period of time.

When we treated our system as a pseudo two–phase system, there was excellent agreement between the gas holdups obtained using the NDG and the DP cells. However, no measurements were made with the nuclear density gauge in the presence of foam (i.e. at the top of the column). Thus, some experiments should be conducted using the nuclear density gauges to determine the accuracy with which holdups can be measured in different flow regimes.

We were unable to estimate the size and rise velocities of large bubbles in the 0.21 m ID column. In order to use the density gauges to estimate the bubble size and rise velocity of large bubbles, the distance between the density gauges should be less than the length of the large bubbles. For the system we employed, the density gauges were placed in parallel, and the distance between the gauges was approximately 0.1 m (limited by the size of the source holders). If the density gauges were placed perpendicular to one another the distance between the gauges could be reduced and one could obtain estimates for the size and rise velocity of the large bubbles using the cross correlation function.

The DGD technique was used in this study to obtain bubble size distributions. While the bubble sizes for wax obtained from this study are comparable to our previous results (Bukur et al., 1987a), more work is needed to verify that the bubble sizes obtained by DGD are representative of the actual bubble sizes. Experiments in which bubbles sizes are measured simultaneously by various techniques (e.g. photography, probes, DGD) are needed to determine whether the DGD technique may be used to accurately determine the bubble size distribution.

Future work in the area of Fischer–Tropsch hydrodynamic studies should be aimed towards transport studies. Mass transfer and heat transfer studies in large diameter slurry phase Fischer–Tropsch bubble columns need to be conducted. Once these data become available, they may be used in conjunction with the results from this study and various kinetic studies to model Fischer–Tropsch slurry bubble column reactors.

NOMENCLATURE

a_s = specific gas–liquid interfacial area, m^2 / m^3

A_i = atomic mass of species i, Chapter III, kg/kmole

Ar = Archimedes number

A_L = cross sectional area of the column occupied by large bubbles, m^2

A_s = cross sectional area of the column occupied by small bubbles, m^2

A_{s_i} = area of region i, defined by Eq. 3.39, m^2

A_{slug} = cross sectional area of a slug, m^2

A_x = cross sectional area of the column, m^2

A_x = cross sectional area of the absorbing media, Chapter III, m^2

a = slope of pressure transducer calibration curve, inches water/volts

b = intercept of pressure transducer calibration curve, inches water

Bo = Bond number

B = number of photons crossing a unit area per unit time

B_o = incident number of photons crossing a unit area per unit time

B_i = number of photons crossing a unit area per unit time for source i

B_{oi} = incident number of photons crossing a unit area per unit time for source i

C_1, C_2 = constants of integration in Eq. 3

C_s = solids concentration, kg/m^3

C_s^B = solids concentration at the bottom of the dispersion, kg/m^3

C_s^f = solids concentration in the feed, kg/m^3

d = distance through the column, m

d_{Bi} = size of bubble i, m

d_c = column diameter, m

d_{col} = column diameter, m

d_i = distance through the column at position i, m

d_p = particle diameter, m

d_s = Sauter mean bubble diameter, m

E_s = axial dispersion coefficient, m^2/s

$f_{d_{ij}}$ = volume fraction of the dispersion between pressure ports i and j

f_{o_i} = fraction of the incident beam passing through phase i

Fr_g = Froude number = $\dfrac{u_g}{\sqrt{gd_{col}}}$

f_s = fraction of the cross sectional area occupied by small bubbles

f_{slug} = fraction of the cross sectional area occupied by slugs

g = gravitational accelerational constant, 9.81 m/s^2

H_{DP} = height of the pressure transducer, m

$H_t(t)$ = height of liquid above the presure transducer at time t, m

$H_t(0)$ = height of liquid above the presure transducer at time t=0, m

h = height, m

h_s = static liquid height, m

h_{exp} = expanded height, m

I = intensity of radiation

I_o = initial intensity of radiation

l_e = entry length, cm

L = expanded height of the dispersion, m

MSE = mean square error, defined by Eq. 2.36

$m_{s\ell}$ = weight of solidified slurry sample, kg

m_1 = weight of structure + sample, kg

m_2 = weight of structure + sample immersed in acetone, kg

N = number of data points

n_i = number of bubbles of size i

psd = power spectral density function, defined by Eq. 15

P = Fourier transform of the autocorrelation function, Eq. 15

$\bar{P}$ = average pressure

P_i = pressure

P_n = probability associated with a Poisson process, defined by Eq. 3.29

Pe_p = particle Peclet number = $\frac{u_g d_{col}}{E_s}$

Q_{slug} = volumetric flow rate of a slug, m^3/s

Q_s = volumetric flow rate small bubbles downward due to a to a slug passing, m^3/s

Q'_s = volumetric flow rate of small bubbles upward due to buoyancy, m^3/s

Q_{liq} = volumetric flow rate of liquid downward due to slugs, m^3/s

Q'_{liq} = volumetric flow rate of liquid downward due to small bubbles, m^3/s

Q_{netliq} = net volumetric flow rate of a liquid downward, m^3/s

r_c = column radius, m

r_{pos_i} = radial position measured from the center of the column, defined by Eq. 3.38, m

S_c = scale factor used in Eq. 3.34

$s_{d_{ij}}$ = specific gvavity of the dispersion between pressure ports i and j

s_ℓ = specific gvavity of the liquid

$s_{s\ell_{ij}}$ = specific gvavity of the slurry between pressure ports i and j

P = pressure, inches water

Re_g = Reynolds number = $\frac{u_g d_{col} \rho_\ell}{\mu_\ell}$

Re_p = particle Reynolds number = $\frac{u_T d_p \rho_\ell}{\mu_\ell}$

RMS = root mean square, defined by Eq. 12

t = time, s

$u = $ lag

$u_{bs} = $ rise velocity of small bubbles, m/s

$u_{bL} = $ rise velocity of large bubbles, m/s

$u_g = $ superficial gas velocity, m/s

$u_\ell = $ superficial liquid velocity, m/s

$u_p = $ hindered settling velocity of particles, m/s

$u_r = $ bubble rise velocity, Eq. 2.28, m/s

$u_{s\ell} = $ superficial slurry velocity, m/s

$u'_{s\ell} = = \frac{u_{s\ell}}{(1-\epsilon_g)}$ in Eq. 4.3, m/s

$u_T = $ terminal rise velocity of a single particle in an infinite medium, m/s

$V_{exp_i} = $ volume of the dispersion, m^3

$V_{g_i} = $ volume of gas in section i, m^3

$V(t) = $ volume of liquid above the pressure transducer at time t, m^3

$V_i = $ volume of component i, defined by Eq. 3.11, m^3

$V_L(t) = $ volume of large bubbles that rise above the pressure transucer at time t, m^3

$V_{liq}(t) = $ volume of liquid displaced during Period I of disengagement, m^3

$V'_{liq}(t) = $ volume of liquid displaced during Period II of disengagement, m^3

$V_o = $ volume of liquid above the pressure transducer at time t=0, m^3

$V_{sb_{between}} = $ volume of small bubbles which leave the dispersion in between the passage of slugs, m^3

$V_{sb_{last}} = $ volume of small bubbles which leave the dispersion during the last period of disengagement, m^3

$V_{sb_{slug}} = $ volume of small bubbles which leave the dispersion during the passage of a slug, m^3

$V_{sb_{total}} = $ total volume of small bubbles which leave the dispersion, m^3

$V_{sb_{between}} = $ volume of small bubbles which leave the dispersion in between the passage of slugs, m^3

V_{sect_i} = volume of section i, m^3

$V_\ell(t)$ = volume of the liquid entering the dispersion at time t, m^3

$V_{s\ell}$ = volume of solidified slurry, defined by Eq. 2.4, m^3

$V_s(t)$ = volume of small bubbles that rise above the pressure transucer at time t, m^3

V_T = total volume of the slurry, m^3

V_{ij} = volume of the slurry in section ij, m^3

w_i = weighting factor, defined by Eq. 3.40

W_{acet} = weight of acetone displaced, defined by Eq. 2.3, kg

We = Weber number, defined by Eq. 2.28

x = dimensionless height above the distributor, Chapter IV, m

x_i = thickness of species i, Chapter III, m

Z_i = atomic number of species i, Chapter III

Greek Letters

Δh_{ij} = height between preessure ports i and j, inches

ΔI = change in intensity of radiation

ΔP_{ij} = pressure drop across ports i and j, inches water

Δt = time interval, sec

Δx = thickness of the absorbing media, m

ϵ_g = average gas holdup

ϵ_{goL} = volume fraction of large bubbles at steady state

ϵ_{gos} = volume fraction of small bubbles at steady state

ϵ_{gs} = volume fraction of small bubbles - non steady state, defined by Eq. 5.29 and 5.41

ϵ'_{gs} = volume fraction of small bubbles - non steady state, defined by Eq. 5.31

ϵ_{gax} = axial gas holdup

$\epsilon_{g_{ij}}$ = gas holdup between pressure ports i and j

ϵ_ℓ = average liquid holdup

$\epsilon_{\ell_{ij}}$ = liquid holdup between pressure ports i and j

ϵ_{meas} = measured gas holdup

ϵ_{pred} = predicted gas holdup

ϵ_{r_i} = radial gas holdup at location i

ϵ_s = average solids holdup

$\epsilon_{s_{ij}}$ = solids holdup between pressure ports i and j

γ_{xx} = autocovariance function

κ_i = Compton scattering coefficient of component i, Chapter III, m^{-1}

μ = mean of the time series, Chapter IV

μ_ℓ = liquid viscosity, Chapter II, kg/m-s

$\mu_{s\ell}$ = slurry viscosity, Chapter II, kg/m-s

μ_i = attenuation coefficient of species i, Chapter III, m^{-1}

μ_{ij} = attenuation coefficient of species i associated with source j, Chapter III, m^{-1}

ω_s = weight fraction of solids

ρ_i = density of the component i, kg/m^3

ρ_{acet} = density of acetone, kg/m^3

ρ_d = density of the dispersion, kg/m^3

ρ_g = density of the gas, kg/m^3

ρ_p = particle density, Eq. 2.28, kg/m^3

ρ_s = density of solids, kg/m^3

$\rho_{s\ell}$ = density of the solidified slurry, kg/m^3

ρ_w = density of solidified wax, kg/m^3

ρ_{water} = density of water, kg/m^3

$\rho_{xx} =$ autocorrelation function

$\sigma_\ell =$ surface tension of the liquid, Eq. 2.28, N/m

$\sigma_i =$ Compton scattering coefficient of component i, Chapter III, m^{-1}

$\tau_i =$ Compton scattering coefficient of component i, Chapter III, m^{-1}

$\Phi_\ell =$ volume fraction of liquid in the slurry

$\overline{\Phi_\ell} =$ average volume fraction of liquid in the slurry

Subscripts

1,2,... $=$ component number

$g =$ gas

$\ell =$ liquid

$s\ell =$ slurry

$s =$ solids

$T =$ total

LITERATURE CITED

Abou–el–Hassan, M.E., "A Generalized Bubble Rise Velocity Correlation," *Chem. Eng. Commun.*, **22**, 243 (1983)

Abouelwafa, M.S.A., and E.J.M. Kendall, "The Measurement of Component Ratios in Multiphase Systems Using Gamma–Ray Attenuation," *J. Phys. E: Sci. Instrum.*, **13**, 341 (1980)

Akagawa, K., H. Hamaguchi, and T. Sakaguchi, "I. Studies on the Fluctuation of Pressure Drop in Two-Phase Slug Flow," *Bulletin of JSME*,**14**, 447 (1971a)

Akagawa, K., H. Hamaguchi, and T. Sakaguchi, "II. Studies on the Fluctuation of Pressure Drop in Two-Phase Slug Flow," *Bulletin of JSME*,**14**, 455 (1971b)

Akagawa, K., H. Hamaguchi, and T. Sakaguchi, "III. Studies on the Fluctuation of Pressure Drop in Two-Phase Slug Flow," *Bulletin of JSME*,**14**, 462 (1971c)

Akita, K., and F. Yoshida, "Bubble Size, Interfacial Area, and Liquid–Phase Mass Transfer Coefficient in Bubble Columns," *Ind. Eng. Chem. Proc. Des. Dev.*, **13**, 84 (1974)

Albal, R.S., Y.T. Shah, N.L. Carr, and A.T. Bell, "Mass Transfer Coefficients and Solubilities for Hydrogen and Carbon Monoxide under Fischer–Tropsch Conditions," *Chem. Eng. Sci.*, **39**,905 (1984)

Attix, F.H., *Radiation Dosimetry, Volume I: Fundamentals*, Academic Press, New York (1968)

Bach, H.F., and T. Pilhofer, "Variation of Gas Holdup in Bubble Columns with Physical Properties of Liquids and Operating Parameters of Columns," *Ger. Chem. Eng.*, **1**, 270 (1978)

Badjugar, M.N., A. Deimling, B.I. Morsi, and Y.T. Shah, "Solids Distribution in a Batch Bubble Column," *Chem. Eng. Commun.*, **48**, 127 (1986)

Bartholemew, R.N., and R.M. Casagrande, "Measuring Solids Concentrations in Fluidized Systems by Gamma–Ray Absorption," *Ind. Eng. Chem.*, **3**, 428 (1957)

Basov V.A., V.I. Markheuka, T. Kh. Melik-Akhnazarov, and D.I. Orochko, "Investigation of the Structure of a Non–Uniform Fluidized Bed," *Int. Chem. Eng.*, **9**, 263 (1969)

Baumgarten, P.K., and R.L. Pigford, "Density Fluctuations in Fluidized Beds," *AIChE J.*, **6**, 115 (1960)

Bernatowicz, H., D. Gansmiller, and S. Wolff, "Final Report for the Development of a Three Phase Fraction Meter for Use at the SRC–1 Facility in Wilsonville, Alabama," Final Report to the Department of Energy for Contract Number DE-AC22-82PC50031 (1987)

Bhatia, V.K., K.A. Evans, and N. Epstein, "Effect of Solids Wettability on Expansion of Gas–Liquid Fluidized Beds," *Ind. Eng. Chem. Proc. Des. Dev.*, **11**, 151 (1972)

Buchholz, R., and K. Schugerl, "Bubble Column Bioreactors," *Europ. J. Appl. Micro.*, **6**, 301 (1979)

Buchholz, R., J. Tsepetonides, J. Steinemann, and U. Onken, "Influence of Gas Distribution on Interfacial Area and Mass Transfer in Bubble Columns," *Ger. Chem. Eng.*, **6**, 105 (1983)

Bukur, D.B., D. Petrovic, and J.G. Daly, "Hydrodynamics of Fischer–Tropsch Synthesis in Slurry Bubble Column Reactors," *Proc. DOE Indirect Liquefaction Contractors' Mtg.*, Houston, TX, 479 (1985)

Bukur, D.B., and V.R. Kumar, "Effect of Catalyst Dispersion on Performance of Slurry Bubble Column Reactors," *Chem. Eng. Sci.*, **41**, 1435 (1986)

Bukur, D.B., J.G. Daly, S.A. Patel, M.L. Raphael, and G.B. Tatterson, "Hydrodynamics of Fischer–Tropsch Synthesis in Slurry Bubble Column Reactors," Final Report to the Department of Energy for Contract Number DE-AC22-84PC70027 (1987a)

Bukur, D.B., D. Petrovic, and J.G. Daly, "Flow Regime Transitions in a Bubble Column with a Paraffin Wax as the Liquid Medium," *Ind. Eng. Chem. Res.*, **26**, 1087 (1987b)

Bukur, D.B., S.A. Patel, and M.L. Raphael, "Hydrodynamic Studies in Fischer–Tropsch Derived Waxes in a Bubble Column," *Chem. Eng. Commun.*,**60**,63 (1987c)

Bukur, D.B., and J.G. Daly, "Gas Hold-up in Bubble Columns for Fischer–Tropsch Synthesis," *Chem. Eng. Sci.*, **42**, 2967 (1987)

Calderbank, P.H., and M.B. Moo-Young, "The Continuous Phase Heat and Mass Transfer Properties of Dispersions," *Chem. Eng. Sci*, **16**, 39 (1961)

Calderbank, P.H., F. Evans, R. Farley, G. Jepson, and A. Poll, "Rate Processes in the Catalyst-Slurry Fischer–Tropsch Reaction," *Catalysis in Practice - Instn. Chem. Engs.*, 66 (1963)

Chan, A.M.C., and S. Banerjee, "Design Aspects of Gamma Densitometers for Void Fraction Measurements in Small Scale Two–Phase Flows," *Nucl. Instr. Meth.*, **190**, 135 (1981)

Clift, R., J.R. Grace, and M.E. Weber, *Bubble Drops and Particles*, Academic Press, New York, 171, 236 (1978)

Cova, D.R., "Catalyst Suspension in Gas Agitated Tubular Reactors," *Ind. Eng. Chem. Proc. Des. Dev.*, **5**, 20 (1966)

Deckwer, W.D., Y. Louisi, A. Zaidi, and M. Ralek, "Hydrodynamic Properties of the

Fischer–Tropsch Slurry Process," *Ind. Eng. Chem. Proc. Des. Dev.*, **19**, 699 (1980)

Deimling, A., B.M. Karandikar, Y.T. Shah, and N.L. Carr, "Solubility and Mass Transfer of CO and H_2 in Fischer–Tropsch Liquids and Slurries," *Chem. Eng. J.*, **29**, 127 (1984)

de Vries, R.J., W.P.M. Van Swaaij, C. Mantovani, and A. Heijkoop, "Design Criteria and Performance of the Commercial Reactor for the Shell Chlorine Process," *Proc. 5th Europ. Symp. Chem. Reaction Eng.*, Amsterdam, B9,59 (1972)

El-Halwagi, M.M., and A. Gomezplata, "An Investigation of Solids Distribution Mixing, and Contacting Characteristics of Gas–Solid Fluidized Beds," *AIChE J.*, **13**, 503 (1967)

Evans R.D., *The Atomic Nucleus*, McGraw–Hill, New York (1955)

Fan, L.S., S. Satija, and K. Wisecarver, "Pressure Fluctuation Measurements and Flow Regime Transitions in Gas-Liquid-Solid Fluidized Beds," Paper 67E presented at AIChE Annual Meeting, San Francisco (1984).

Fan, L.S., *Gas–Liquid–Solid Fluidization Engineering*, Butterworth Publishers, Stoneham, MA (1989)

Fan, L.T., C.J. Lee, and R.C. Bailie, "Axial Solids Distribution in Gas–Solid Fluidized Beds," *AIChE J.*, **8**, 239 (1962)

Fan, L.T., T.C. Ho, S. Hiraoka, and W.P. Walawender, "Pressure Fluctuations in a Fluidized Bed," *AIChE J.*, **27**, 388 (1981)

Farley, R., and D.J. Ray, "Gamma Radiation Absorption Measurements of Density and Gas Holdup in a Three Phase Catalytic Reactor," *Brit. Chem. Eng.*, **9**, 830 (1964)

Gibson, E.J., J. Rennie, and B.A. Say, "The Use of Gamma Radiation in the Study of the Expansion of Gas–Liquid Systems," *Int. J. of Appl. Rad. Iso.*, **2**, 129 (1957)

Gidaspow D., C. Lin, and Y.C. Seo, "Fluidization in Two–Dimensional Beds with a Jet. 1. Experimental Porosity Distributions," *Ind. Eng. Chem. Fundam.*, **22**, 187 (1983)

Glasgow, L.A., L.E. Erickson, C.H. Lee, and S.A. Patel, "Wall Pressure Fluctuations and Bubble Size Distributions at Several Positions in an Airlift Fermentor," *Chem. Eng. Commun.*, **29**, 34 (1984)

Godbole, S.P., M.F. Honath, and Y.T. Shah, "Holdup Structure in Highly Viscous Newtonian and Non–Newtonian Solutions in Bubble Columns," *Chem. Eng. Commun.*, **16**, 119 (1982)

Godbole, S.P., A. Schumpe, Y.T. Shah, and N.L. Carr, "Hydrodynamics and Mass Transfer in Non–Newtonian Solutions in a Bubble Column," *AIChE J.*, **30**, 213 (1984)

Gray, D., M. Lytton, M. Neworth, and G. Tomlison, "The Impact of Developing Technology on Indirect Liquefaction," Final Report to the Department of Energy for Contract Number EF-77-C-01-2738 (1980)

Gupte, K.M., J. Smith, T.M. Leib, and J.C.W. Kuo, "Fischer–Tropsch Bubble Column Hydrodynamics", *Proc. of the Fourth DOE Contractors' Conference on Indirect Liquefaction*, Washington, PA (1984)

Hatate, Y., H. Nomura, T. Fujita, S. Tajiri, N. Hidaka, and A. Ikari, "Gas Holdup and Pressure Drop in Three–Phase Vertical Flows of Gas–Liquid–Fine Solid Particles System," *J. Chem. Eng. Jap.*, **19**, 56 (1986)

Heijnen J.J, and K. Van't Riet, "Mass Transfer, Mixing and Heat Transfer Phenomena in Low Viscosity Bubble Column Reactors," *Chem. Eng. J.*, **28**, B21 (1984)

Hughmark, G.A., "Holdup and Mass Transfer in Bubble Columns," *Ind. Eng. Chem. Pro. Des. Dev.*, **6**, 218 (1967)

Ishigai, S., M. Yamane, and K. Roko, "Measurement of Component Flows in a Vertical Two–Phase Flow by Making Use of the Pressure Fluctuation: Part I," *Bull. of JSME*, **8**, 375 (1965a)

Ishigai, S., M. Yamane, and K. Roko, "Measurement of Component Flows in a Vertical Two–Phase Flow by Making Use of the Pressure Fluctuation: Part II," *Bull. of JSME*, **8**, 383 (1965b)

Jasper, J, "The Surface Tension of Pure Liquid Compounds," *J. Phys. Chem. Ref. Data*, **1**, 841(1972)

Jenkins, G.M., and D.G. Watts, *Spectral Analysis and Its Applications*, Holden Day, San Francisco (1968)

Kara, S., B. Kelkar, Y.T. Shah, and N.L. Carr, "Hydrodynamics and Axial Mixing in a Three–Phase Bubble Column," *Ind. Eng. Chem. Proc. Des. Dev.*, **21**, 584 (1982)

Kato, Y., A. Nishiwaki, T. Fukuda, and S. Tanaka, "The Behavior of Suspended Solid Particles and Liquid in Bubble Columns," *J. Chem. Eng. Jap.*, **5**, 112 (1972)

Kelkar, B.G., S.P. Godbole, M.F. Honath, Y.T. Shah, N.L. Carr, and W.D. Deckwer, "Effect of Addition of Alcohols on Gas Holdup and Backmixing in Bubble Columns," *AIChE J.*, **29**, 361 (1983)

Kelkar, B.G., Y.T. Shah, and N.L. Carr, "Hydrodynamics and Axial Mixing in a Three–Phase Bubble Column," *Ind. Eng. Chem. Proc. Des. Dev.*, **23**, 308 (1984)

Kim, S.D., C.G.J. Baker, and M.A. Bergougnou, "Bubble Characteristics in Three–Phase Fluidized Beds," *Chem. Eng. Sci.*, **32**, 1299 (1977)

Kolbel, H., and M. Ralek, "The Fischer–Tropsch Synthesis in the Liquid Phase," *Catal. Rev. Sci. Eng.*, **21**, 225 (1980)

Krambeck, F.J., A.A. Avidan, C.K. Lee, and M.N. Lo, "Predicting Fluid Bed Reactor Efficiency Using Adsorbing Gas Tracers," Paper Presented at AIChE Annual Meeting, Chicago, (1985)

Kuo, J.C.W., "Two-Stage Process for Conversion of Synthesis Gas to High Quality Transportation Fuels," Final Report to the Department of Energy for Contract Number DE-AC22-83PC60019 (1985)

Lassahn G.D., "Two–Phase Flow Velocity Measurements Using Radiation Intensity Correlation," *ISA Trans.*, **15**, 297 (1975)

Ledakowicz, S., H. Nettelhoff, R. Kokuun, and W.D. Deckwer, "Kinetics of the Fischer–Tropsch Synthesis in Slurry Phase on Promoted Iron Catalyst," *Ind. Eng. Chem. Fundam.*, **23**, 510 (1984)

Lee, C.H., *Dynamics of Bubble Size Distribution and Wall Pressure Fluctuations in Airlift Fermentors,* Masters Thesis, Kansas State University, Manhattan (1983)

Lee, Y.H., Y.J. Kim, B.G. Kelkar, and C.B. Weinberger, "A Simple Digital Sensor for Dynamic Gas Holdup Measurements in Bubble Columns," *Ind. Eng. Chem. Fund.*, **24**, 105 (1985)

Lin, P.Y., and T.J. Hanratty, "Detection of Slug Flow from Pressure Measurements," *Int. J. of Mult. Flow*, **13**, 13 (1987)

Matsui, G., "Identification of Flow Regimes in Vertical Gas–Liquid Two–Phase Flow Using Differential Pressure Fluctuations," *Int. J. of Mult. Flow*, **10**, 711 (1984)

Matsui, G., "Automatic Identification of Flow Regimes in Vertical Two–Phase Flow Using Differential Pressure Fluctuations," *Nucl. Eng. Des.*, **95**, 221 (1986)

Miyazaki, K., K. Isogai, Y. Fujii-e, and T. Suita, "Measurement of Propagation Velocities of Pressure and Void By Cross Correlation Fluctuations in Nitrogen–Water Flow," *J. of Nucl. Sci. Tech.*, **10**, 323 (1973)

Murray P., and L.S. Fan, "Axial Solids Distribution in Slurry Bubble Columns," *Ind. Eng. Res.*, **28**, 1697 (1989)

O'Dowd, W., D.N. Smith, J.A. Ruether, and S.C. Saxena, "Gas and Solids Behavior in a Baffled and Unbaffled Slurry Bubble Column," *AIChE J.*, **33**, 1959 (1987)

Orcutt, J.C., and B. H. Carpenter, "Bubble Coalescence and Simulation of Mass Transport and Chemical Reaction in Gas Fluidized Beds," *Chem. Eng. Sci*, **26**, 1049 (1971)

Ouyang C.J.P., and G.B. Tatterson, "The Effect of Distributors on Two–Phase and Three–Phase Flows in Vertical Columns," *Chem. Eng. Commun.*, **49**, 197 (1987)

Parulekar, S.J., and Y.T. Shah, "Steady State Behavior of Gas–Liquid–Solid Fluidized Bed Reactors," *Chem. Eng. J.*, **20**, 21 (1980)

Patel, S.A., *Investigation of Two–Phase Flow Structures in an Airlift Fermentor*, PhD Dissertation, Kansas State University (1985)

Patel, S.A., J.G. Daly, and D.B. Bukur, "Holdup and Interfacial Area Measurements Using Dynamic Gas Disengagement," *AIChE J*, **35**, 931 (1989)

Patel, S.A., J.G. Daly, and D.B. Bukur, "Bubble-Size Distributions in Fischer–Tropsch Derived Waxes in Bubble Columns," *AIChE J*, **36**, 93 (1990)

Perry, and Chilton, *Chemical Engineers Handbook*, McGraw–Hill, New York (1983)

Peter, S., and M. Weinert, "Uber die Loslichkeit von H_2, CO, CO_2, and Wasserdampf in flussigen Kohlenwasserstoffen," *Z. Physik. Chem.*, **5**, 114 (1955)

Petrick, M., and B.S. Swanson, "Radiation Attenuation Method of Measuring Density of a Two–Phase Fluid," *Rev. of Sci. Instr.*, **29**, 1079 (1958)

Quicker, G., and W.D. Deckwer, "A Further Note on Mass Transfer Limitations in the Fischer–Tropsch Slurry Process," *Chem. Eng. Sci.*, **36**, 1577 (1981)

Rabiger, N., "Die Auswirkung von Feststoffpartikein auf den Gasgehalt in einem von oben begasten Schlaufenreaktor," *Chem. Ing. Tech.*, **57**, 248 (1985)

Reilly, I.G., D.S. Scott, T. De Bruijn, A. Jain, and J. Piskorz, "A Correlation for Gas Holdup in Turbulent Coalescing Bubble Columns," *Can. J. Chem. Eng.*, **64**, 705 (1986)

Rodden, J.B., "Diffusion Coefficients for Several Dilute Solutes in n-Eicosane, n-Octacosane, and Fischer–Tropsch Wax," PhD Dissertation, Texas A&M University (1988)

Rodden, J.B., C. Erkey, and A. Akgerman, "Mutual Diffusion Coefficients for Several Dilute Solutes in n-Octacosane and the Solvent Density at 371–534 K," *J. Chem. Eng. Data*i, **33**, 450 (1988)

Sada, E., H. Kumazawa, C. Lee, and T. Iguchi, "Gas Holdup and Mass Transfer Characteristics in a Three–Phase Bubble Column," *Ind. Eng. Chem. Proc. Des. Dev.*, **25**, 472 (1986)

Sanders, E., S. Ledakowicz, and W.D. Deckwer, "Fischer–Tropsch Synthesis in Bubble Column Slurry Reactors of Fe/K Catalyst," *Can. J. Chem. Eng.*, **64**, 133 (1986)

Sauer, T., and D.C. Hempel, "Fluid Dynamics and Mass Transfer in a Bubble Column with Suspended Particles," *Chem. Eng. Tech.*, **10**, 180 (1987)

Saxena, S.C., D. Patel , D.N. Smith, and J.A. Ruether, "An Assessment of Experimental Techniques for the Measurement of Bubble Size in a Bubble Slurry Reactor as Applied to Indirect Coal Liquefaction," *Chem. Eng. Commun.*, **63**, 87 (1988)

Schumpe, A., and W.D. Deckwer, "Gas Holdups, Specific Interfacial Areas, and Mass Transfer Coefficients of Aerated Carboxymethyl Cellulose Solutions in a Bubble Column," *Ind. Eng. Chem. Proc. Des. Dev.*, **21**, 706 (1982)

Schumpe, A., and A. Grund, "The Gas Disengagement Technique for Studying Gas Holdup Structure in a Bubble Column," *Can. J. Chem. Eng.*, **64**, 891 (1986)

Seo, Y.C., and D. Gidaspow, "An X–Ray–Gamma–Ray Method of Measurement of Binary Solids Concentrations and Voids in Fluidized Beds," *Ind. Eng. Chem. Res.*, **26**, 1622 (1987)

Shah, Y.T., B.G. Kelkar, S.P. Godbole, and W.D. Deckwer, "Design Parameter Estimations for Bubble Column Reactors," *AIChE J*, **28**, 353 (1982)

Shah, Y.T., S. Joseph, D.N. Smith, and J.A. Ruether, "On the Behavior of the Gas Phase in a Bubble Column with Ethanol–Water Mixtures," *Ind. Eng. Chem. Proc. Des. Dev.*, **24**, 1140 (1985)

Smith, D.N., and J.A. Ruether, "Dispersed Solid Dynamics in a Slurry Bubble Column Reactor," *Chem. Eng. Sci.*, **40**, 741 (1985)

Smith, J., K.M. Gupte, T.M. Leib, and J.W.C. Kuo, "Hydrodynamics Studies of Fischer–Tropsch Bubble Column Systems," Paper Presented at the AIChE Summer National Meeting, Philadelphia, (1984)

Sriram, K., and R. Mann, "Dynamic Gas Disengagement: a New Technique for Assessing the Behavior of Bubble Columns," *Chem. Eng. Sci.*, **32**, 571 (1977)

Taitel, Y., D. Bornea, and A.E. Dukler, "Modeling Flow Pattern Transitions for Steady Upward Gas–Liquid Flow in Vertical Tubes," *AIChE J.*, **27**, 1043 (1981)

Thompson, G.J., M.L. Riekena, and A.G. Vickers, "Comparison of Fischer–Tropsch Reactor Systems," Final Report to the Department of Energy for Contract Number DE-AC01-78ET 10159 (1981)

Tsao, T.R., "Results of LaPorte Liquid Phase Methanol PDU Unit," Proc. of Fourth DOE Contractors' Conference on Indirect Liquefaction, Washington, PA (1984)

Vermeer, D.J., and R. Krishna, "Hydrodynamics and Mass Transfer in Bubble Columns Operating in the Churn–Turbulent Regime," *Ind. Eng. Chem. Proc. Des. Dev.*, **20**, 475 (1981)

Weimer, A.W., D.C. Gyure, and D.E. Cough, "Application of a Gamma Radiation Density Gauge for Determining Hydrodynamic Properties of Fluidized Beds," *Powder Tech.*, **44**, 179 (1985)

Ying D.H.S., R. Sivasobramanian, and E.N. Givens, "Gas/Slurry Flow in Coal Liquefaction Processes," Final Report to the Department of Energy for Contract Number Fe–14801–3 (1980)

Zaidi, A., Y. Louisi, M. Ralek, and W.D. Deckwer, "Mass Transfer in the Liquid Phase Fischer–Tropsch Synthesis," *Ger. Chem. Eng.*, **2**, 94 (1979)

Zheng, C., B. Yao, and Y. Feng, "Flow Regime Identification and Gas Holdup of Three–Phase Fluidized Systems," *Chem. Eng. Sci.*, **43**, 2195 (1988)

Zigrand, D.J., and N.D. Sylvester, "An Explicit Equation for Particle Settling Velocities in Solid–Liquid Systems," *AIChE J.*, **27**, 1043 (1980)

APPENDIX A

CLEANING PROCEDURES FOR THE SMALL AND LARGE DIAMETER COLUMNS

The cleaning procedures used for the small and large diameter stainless steel columns are presented in this section. Different cleaning procedures were used in the two columns. The small diameter column was cleaned using toluene; whereas, the large diameter column was cleaned by manually scrubbing the various units.

Cleaning Procedure for Small Diameter Column

The small diameter column was cleaned in a two step process. Since a fraction of the slurry settled in the expansion unit, the expansion unit was opened up and the solidified slurry was removed. Once the slurry was removed, the expansion unit was closed and the second part (i.e. a toluene wash) of the cleaning process was initiated.

A separate storage tank for the toluene was constructed. The storage tank was approximately 23 cm in diameter and 46 cm tall (volume is approximately 19000 cc). The exit line from the toluene storage tank entered the column immediately above the distributor (see Figure A.1). The cleaning procedure may be broken down into the following steps.

1. Add approximately 9000 cc of toluene to the toluene storage tank

2. Heat the entire system (except toluene storage tank) to approximately 80 °C

3. Once at temperature, nitrogen overpressure on the toluene feed tank was used to feed toluene into the column and storage tank (see Figure A.1)

4. Close the valve below the calibration unit (see Figure A.1)

5. Turn on storage tank stirrer

6. Start nitrogen flow to the column (MFM setting 70)

7. As the gas displaces some of the toluene, the toluene flows into the calibration chamber

8. Remain at these conditions for approximately 30 minutes
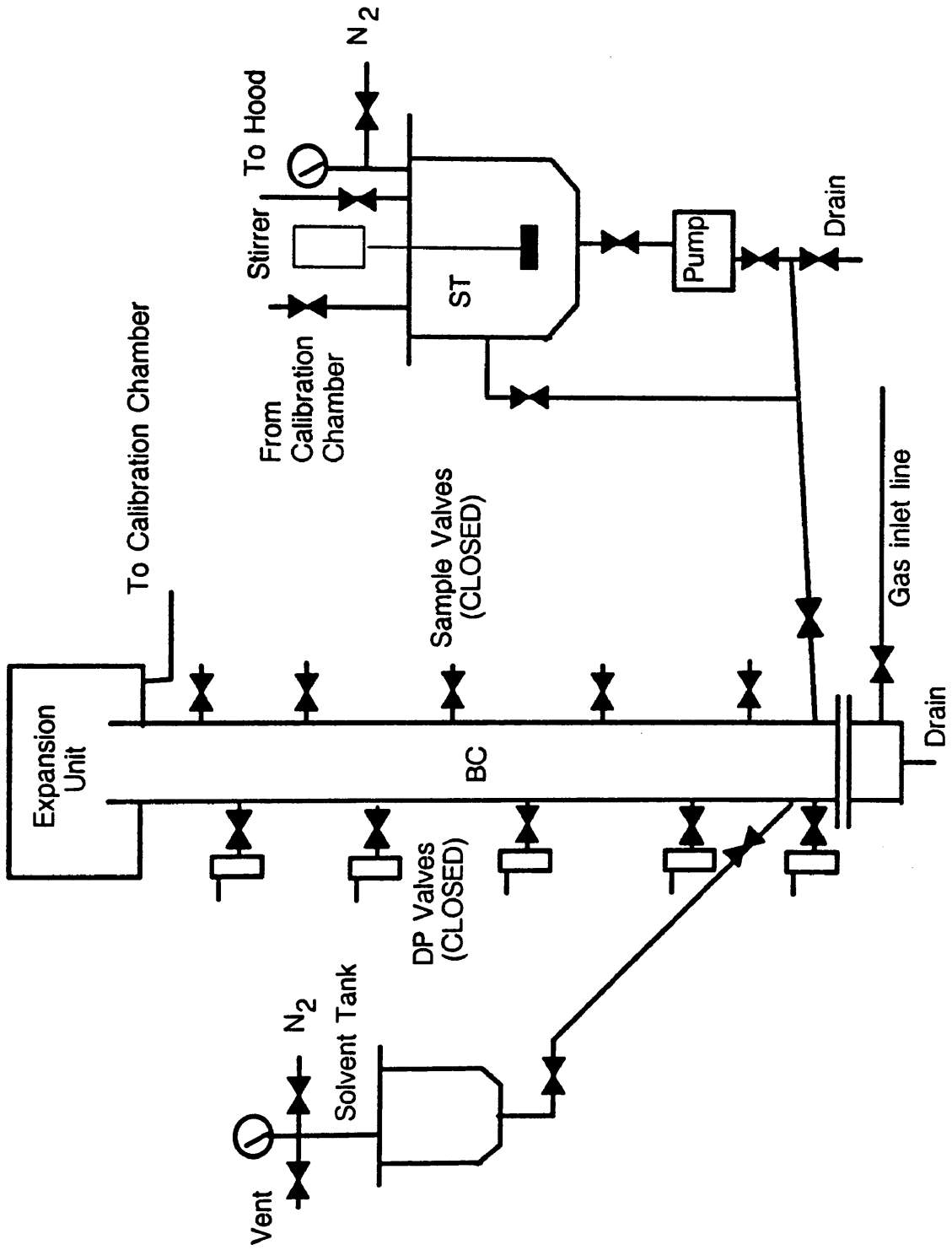
Figure A.1. Schematic diagram of solvent cleaning system for the small diameter column.

9. Turn down nitrogen flow rate to a MFM setting of 10

10. Open valves between the storage tank and the column (see Figure A.1)

11. Apply slight pressure to storage tank using nitrogen to force toluene into the column (see Figure A.1)

12. Once the storage tank is empty, pull a vacuum on the storage tank to remove toluene from the column (see Figure A.1)

13. Repeat steps 11 and 12 three times to clean out slurry inlet line

14. Once all the toluene is in the storage tank, close the valves below the storage tank and open the valve between the calibration unit and the storage tank (see Figure A.1)

15. Reduce the temperature in the storage tank to 50 °C

16. Remove the toluene from the system through the drain valve located below the storage tank (see Figure A.1)

17. Repeat the process

18. Open drain at the bottom of the distributor to remove any toluene that might have weeped through the distributor during the cleaning process (see Figure A.1)

19. Heat entire system to 100 °C

20. Close the drain valve below the distributor (see Figure A.1)

21. Increase nitrogen flow rate to a MFM setting of 70

22. Hold at these conditions for approximately 5 hours to remove any remaining toluene from the system

Cleaning Procedure for Large Diameter Column

Since it would require a substantially greater amount of solvent to clean the large column using the same procedure, we decided to manually clean this system between a series (or batch) of experiments. The four units which we cleaned were the expansion unit, the storage tank, the plenum chamber below the distributor, and the calibration

tank. The storage tank, expansion unit, plenum chamber and calibration tank were cleaned by opening up each unit and removing all wax. The wax was removed by first scraping and then buffing with a wire brush attached to a drill. The distributor was removed and cleaned.

APPENDIX B

DERIVATION OF THE PARALLEL ALIGNMENT MODEL

Derivation of Equation 3.26

Equation 3.26 is derived from Eqs. 3.23, 3.24, and 3.25 as follows:

$$B_1 = B_{o1}[\epsilon_g + \epsilon_\ell \exp(-d\mu_{\ell 1}) + \epsilon_s \exp(-d\mu_{s1})] \qquad (3.23)$$

$$B_2 = B_{o2}[\epsilon_g + \epsilon_\ell \exp(-d\mu_{\ell 2}) + \epsilon_s \exp(-d\mu_{s2})] \qquad (3.24)$$

$$1 = \epsilon_g + \epsilon_\ell + \epsilon_s \qquad (3.25)$$

Substituting Eq. 3.25 into Eqs. 3.23 and 3.24 for ϵ_g yields

$$B_1 = B_{o1}[1 - \epsilon_\ell - \epsilon_s + \epsilon_\ell \exp(-d\mu_{\ell 1}) + \epsilon_s \exp(-d\mu_{s1})] \qquad (A.1)$$

and

$$B_2 = B_{o2}[1 - \epsilon_\ell - \epsilon_s + \epsilon_\ell \exp(-d\mu_{\ell 2}) + \epsilon_s \exp(-d\mu_{s2})] \qquad (A.2)$$

Grouping the terms associated with ϵ_ℓ and ϵ_s together in Eqs. A.1 and A.2 gives

$$B_1 = B_{o1}[1 + \epsilon_\ell \{\exp(-d\mu_{\ell 1}) - 1\} + \epsilon_s \{\exp(-d\mu_{s1}) - 1\}] \qquad (A.3)$$

and

$$B_2 = B_{o2}[1 + \epsilon_\ell \{\exp(-d\mu_{\ell 2}) - 1\} + \epsilon_s \{\exp(-d\mu_{s2}) - 1\}] \qquad (A.4)$$

Multiplying Eq. A.3 by $[\exp(-d\mu_{s2}) - 1]$ and Eq. A.4 by $[\exp(-d\mu_{s1}) - 1]$ and rearranging the terms yields the following expressions

$$B_1 / B_{o1}[\exp(-d\mu_{s2})-1] = [\exp(-d\mu_{s2})-1][1+\epsilon_\ell\{\exp(-d\mu_{\ell1})-1\}+\epsilon_s\{\exp(-d\mu_{s1})-1\}]$$

$$(A.5)$$

$$B_2 / B_{o2}[\exp(-d\mu_{s1})-1] = [\exp(-d\mu_{s1})-1][1+\epsilon_\ell\{\exp(-d\mu_{\ell2})-1\}+\epsilon_s\{\exp(-d\mu_{s2})-1\}]$$

$$(A.6)$$

Subtracting Eq. A.6 from Eq. A.5 yields

$$B_1 / B_{o1}[\exp(-d\mu_{s2})-1] - B_2 / B_{o2}[\exp(-d\mu_{s1})-1] = [\exp(-d\mu_{s2})-1]-[\exp(-d\mu_{s1})-1]$$

$$+\epsilon_\ell[\exp(-d\mu_{\ell1})-1][\exp(-d\mu_{s2})-1] - \epsilon_\ell[\exp(-d\mu_{\ell2})-1][\exp(-d\mu_{s1})-1] \quad (A.7)$$

Dividing Eq. A.7 by $[\exp(-d\mu_{s2})-1]$ yields upon rearrangement

$$(B_1 / B_{o1}) - 1 - \frac{(B_2 / B_{o2} - 1)[\exp(-d\mu_{s1})-1]}{\exp(-d\mu_{s2})-1} =$$

$$+\epsilon_\ell[\exp(-d\mu_{\ell1})-1] - \frac{\epsilon_\ell[\exp(-d\mu_{\ell2})-1][\exp(-d\mu_{s1})-1]}{\exp(-d\mu_{s2})-1} \quad (A.8)$$

Solving Eq. A.8 for ϵ_ℓ yields the following expression for ϵ_ℓ

$$\epsilon_\ell = \frac{(B_1 / B_{o1}) - 1 - \frac{((B_2/B_{o2})-1)(\exp(-d\mu_{s1})-1)}{(\exp(-d\mu_{s2})-1)}}{(\exp(-d\mu_{\ell1})-1) - \frac{(\exp(-d\mu_{\ell2})-1)(\exp(-d\mu_{s1})-1)}{\exp(-d\mu_{s2})-1}} \quad (A.9)$$

which is identical to Eq. 3.26.

Derivation of Equation 3.27

Once ϵ_ℓ is known, ϵ_s may be calculated using either Eq. 3.23 or Eq. 3.24. The following derivation is based on using Eq. 3.24.

$$B_2 = B_{o2}[\epsilon_g + \epsilon_\ell\exp(-d\mu_{\ell2}) + \epsilon_s\exp(-d\mu_{s2})] \quad (3.24)$$

$$1 = \epsilon_g + \epsilon_\ell + \epsilon_s \tag{3.25}$$

Substituting Eq. 3.25 into Eq. 3.24 for ϵ_g upon rearrangement yields

$$B_2 = B_{o2}[1 + \epsilon_\ell\{\exp(-d\mu_{\ell2}) - 1\} + \epsilon_s\{\exp(-d\mu_{s2}) - 1\}] \tag{A.10}$$

Solving Eq. A.10 for ϵ_s yields

$$\epsilon_s = \frac{B_2 / B_{o2} - 1 - \epsilon_\ell[\exp(-d\mu_{\ell2}) - 1]}{[\exp(-d\mu_{s2}) - 1]} \tag{A.11}$$

which is identical to Eq. 3.27 presented in the text.

APPENDIX C

SAMPLE CALCULATION FOR ANALYSIS OF DENSITY GAUGE DATA

Sample calculations are presented for obtaining gas holdups from density gauge measurements. Sample calculations are presented for analysis of three–phase data treating all three phases separately and assuming a pseudo two–phase mixture.

Independent Treatment of the Three Phases

In the following sample calculations, it is assumed that the attenuation coefficients for the various materials and distances through the column, d, at each location for each source have already been determined.

The following sample calculation is for the experiment with 20 wt% $20 - 44$ μm iron oxide particles suspended in FT–300 wax. The sample calculation is based on the data obtained at a gas velocity of 0.08 m/s. The attenuation coefficients are

Cs-137; FT-300 wax $- 0.0555$ cm^{-1}

Cs-137; Iron Oxide $- 0.3910$ cm^{-1}

Co-60; FT-300 wax $- 0.0421$ cm^{-1}

Co-60; Iron Oxide $- 0.2720$ cm^{-1}

And the distances through the column at an axial height of 1.5 m and at radial position 4 (see Figure C.1) are

Cs-137; d_1 $- 19.85$ cm

Co-60; d_2 $- 20.07$ cm

The average gas holdup is determined in a three step process. First, radial gas holdups at each axial position are determined. Then, axial gas holdups are obtained; and finally, average gas holdups are calculated.

<u>Radial Gas Holdups</u>

A slightly modified form of Eq. 3.19 is used to determine the radial holdups. The modified form of Eq. 3.19 is
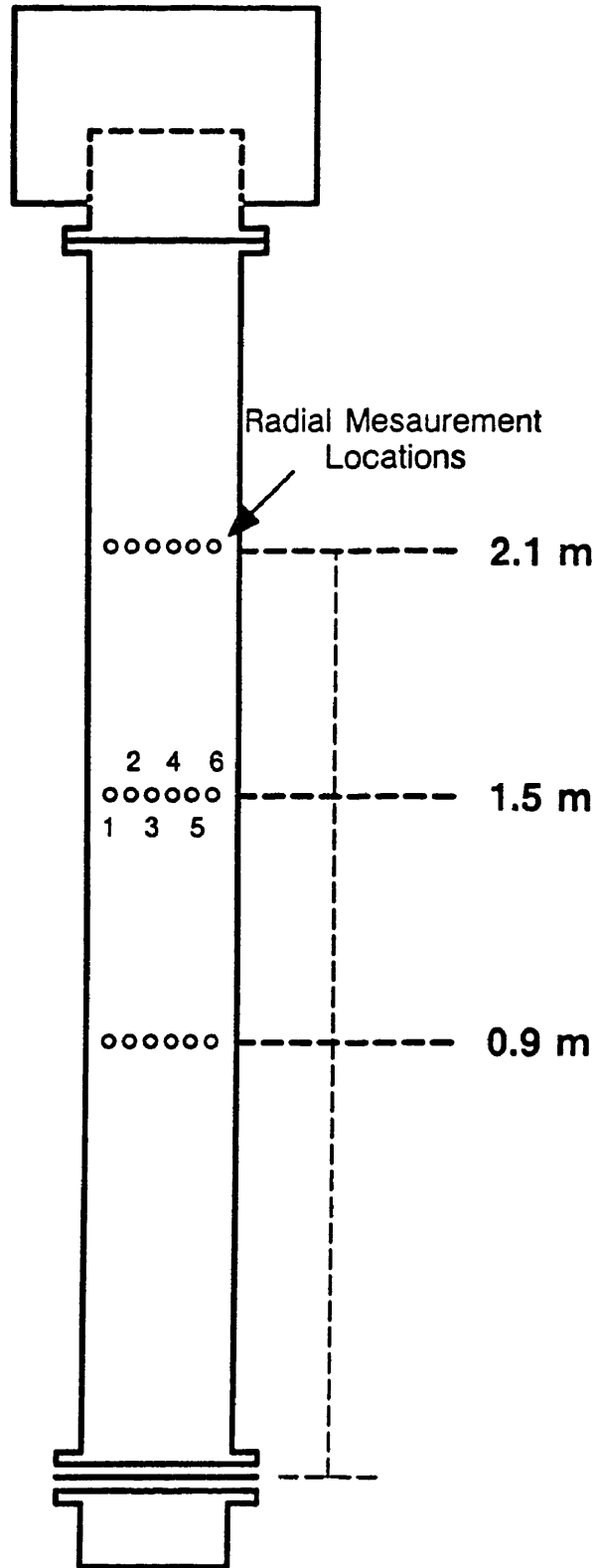
Figure C.1. Schematic diagram of the radial and axial measurement locations.

$$\epsilon_\ell = \frac{\frac{\ln(B_1/B_{o1})\mu_{s2}}{d_1} - \frac{\ln(B_2/B_{o2})\mu_{s1}}{d_2}}{\mu_{\ell2}\mu_{s1} - \mu_{\ell1}\mu_{s2}} \tag{C.1}$$

The only difference between Eq. 3.19 and Eq. C.1 is that the distance through the column for both sources is not the same. The measured empty column count rates at position 4 are

Cs-137; B_{o1} – 2273 c/s

Co-60; B_{o2} – 3981 c/s

and the full column count rates are

Cs-137; B_1 – 815 c/s

Co-60; B_2 – 1818 c/s

The volume fraction of liquid at this position is calculated using Eq. C.1

$$\epsilon_\ell = \frac{\frac{\ln(815/2273)(0.2720)}{19.85} - \frac{\ln(1818/3981)(0.3910)}{20.07}}{(0.0421)(0.3910) - (0.0555)(0.2720)}$$

$$\epsilon_\ell = 0.88$$

Equation 3.15,

$$B_1 = B_{o1}\exp(-d_1(\epsilon_\ell\mu_{\ell1} + \epsilon_s\mu_{s1})) \tag{C.2}$$

may be rearranged to solve for ϵ_s as follows

$$\epsilon_s = \frac{-\ln(B_1/B_{o1})/d_1 - \epsilon_\ell\mu_{\ell1}}{\mu_{s1}} \tag{C.3}$$

Substituting the value of ϵ_ℓ obtained above into Eq. C.3 yields the value of ϵ_s.

$$\epsilon_s = \frac{-\ln(815/2273)/19.85 - (0.88)(0.0555)}{0.3910} = -0.25$$

Thus, knowing ϵ_ℓ and ϵ_s, ϵ_g is calculated from

$$\epsilon_g = 1 - \epsilon_\ell - \epsilon_s \tag{C.4}$$

$$\epsilon_g = 1 - 0.88 - (-0.25) = 0.37$$

The value of ϵ_g is the gas holdup at radial position 4 at an axial height of 1.5 m above the distributor. The same calculation is performed at each of the measurement locations. Once these calculations are performed, the axial gas holdup at each location may be calculated.

Axial Gas Holdups

Axial gas holdups are calculated from radial gas holdups using Eq. 3.41

$$\epsilon_{gax} = \sum_i \epsilon_{r_i} \omega_i \qquad (C.5)$$

The radial gas holdups obtained using the procedure outlined above at a gas velocity of 0.08 m/s and a height of 1.5 m above the distributor are:

Position 1: -0.03

Position 2: 0.19

Position 3: 0.12

Position 4: 0.37 (calculated above)

Position 5: 0.45

Position 6: 0.14

Figure C.1 gives the relative locations of each position. The weight for positions 1 and 6 is 0.11; for positions 2 and 5 is 0.17; and positions for 3 and 4 is 0.22. Knowing the weights and radial gas holdups, the axial gas holdup is calculated from (see Eq. C.5):

$$\epsilon_{gax} = 0.11(0.14 + (-0.03)) + 0.17(0.19 + 0.45) + 0.22(0.37 + 0.12) = 0.23$$

We will assume that at heights of 0.9 m and 2.1 m above the distributor, the axial gas holdups are 0.16 and 0.30, respectively.

Average Gas Holdups

Now, using the three axial gas holdups, there are three ways in which the average gas holdup may be obtained. The simplest approach is to use the average of the three axial gas holdups (see Eq. 3.45), i.e.

$$\epsilon_g = \sum_i (\epsilon_{gax_i}) / 3 \qquad i = 1 \text{ to } 3 \qquad (C.6)$$

Substituting the values of the axial gas holdups into Eq. C.6 yields the following value for the average gas holdup.

$$\epsilon_g = \frac{0.16 + 0.23 + 0.30}{3} = 0.23$$

Another way to calculate the average gas holdup is to divide the expanded height of the slurry into three sections, and based on the volume of the dispersion in each section, calculate the average gas holdup. The gas holdup may be calculated using (see Eq. 3.43)

$$\epsilon_g = \sum_i \epsilon_{gax_i} \frac{h_i}{h_{exp}} \qquad (C.7)$$

where h_i is the height of each section (see Figure 3.15) and h_{exp} is the expanded height. For this experiment, at a gas velocity of 0.08 m/s, the expanded height of the slurry was 2.9 m. The heights of each section are: (1) 1.2 m (corresponds to the measurement made at a height of 0.9 m); (2) 0.6 m (corresponds to the measurement made at a height of 1.5 m); and (3) 1.1 m (corresponds to the measurement made at a height of 2.1 m). These values are substituted into Eq. C.7 together with the values of the axial gas holdups and expanded height to obtain the average gas holdup.

$$\epsilon_g = 0.16(1.2 / 2.9) + 0.23(0.6 / 2.9) + 0.30(1.1 / 2.9) = 0.228$$

And finally, the gas holdup may be estimated by fitting a curve to the axial gas holdup data (i.e. axial gas holdup vs. height) and then integrating across the expanded height

of the bed (see Eq. 3.44)

$$\epsilon_g = \frac{1}{h_{exp}} \int_0^{h_{exp}} \epsilon_{gax} dh \qquad (C.8)$$

For the purpose of this example, axial gas holdups at heights of 0.9 and 2.1 m above the distributor were chosen such that axial gas holdup is a linear function of the height above the distributor. The equation for gas holdup as a function of height based on the axial gas holdups presented above is

$$\epsilon_{gax} = 0.117h + 0.055$$

Substituting the expression for gas holdup as a function of height into Eq. C.8 and integrating yields

$$\epsilon_g = \frac{1}{2.9}[0.117h^2/2 + 0.055h]_0^{2.9} = 0.224$$

Pseudo Two-Phase Treatment

The only difference in the analysis in terms of treating the system as a pseudo two–phase system as opposed to a three–phase system is the procedure used to obtain radial gas holdups. Thus, only this procedure is given in the following sample calculation. Once again, the sample calculation for radial gas holdup is based on the data obtained from the experiment with $20 - 44$ μm large iron oxide in FT–300 wax at a gas velocity of 0.08 m/s. Also, data acquired at a height of 1.5 m above the distributor at radial position number 4 is used.

For this analysis, Eq. 3.37 is used to obtain the radial gas holdup at any given point in the reactor. However, the attenuation coefficient of the liquid is replaced by the attenuation coefficient of the slurry

$$\epsilon_g = 1 + \frac{\ln(B_i/B_{oi})}{d_i\mu_{sl}} \qquad (C.9)$$

where i corresponds to the source (i.e. Co-60 or Cs-137). The absorption coefficient for the slurry (liquid/solid) is estimated by using the solids concentration of the sample withdrawn from the slurry sampling port closest to the measurement location (see Figure 3.13). The weight fraction of solids at a height of 1.5 m above the distributor at a gas velocity of 0.08 m/s was 0.20. The solids density, ρ_s, the wax density, ρ_ℓ, and the attenuation coefficients for the solids and wax, μ_s and μ_ℓ, respectively, are used together with the weight fraction of solids to determine the attenuation coefficient for the slurry (see Eq. 3.30)

$$\mu_{s\ell} = \rho_{s\ell}\left[\frac{\mu_\ell(1-\omega_s)}{\rho_\ell} + \frac{\mu_s(\omega_s)}{\rho_s}\right] \qquad (C.10)$$

where ω_s is the weight fraction of solids in the slurry and $\rho_{s\ell}$ is defined as

$$\rho_{s\ell} = \frac{1}{\frac{\omega_s}{\rho_s} + \frac{(1-\omega_s)}{\rho_\ell}} \qquad (C.11)$$

The attenuation coefficient for the slurry, $\mu_{s\ell}$, may be obtained for both the Cs–137 and Co–60 sources.

The slurry density, $\rho_{s\ell}$, is (Eq. C.11)

$$\rho_{s\ell} = \frac{1}{\frac{0.2}{5.1} + \frac{(1-0.2)}{0.66}} = 0.8 \text{g / cc}$$

and the attenuation coefficient (Cs–137) for the slurry, $\mu_{s\ell}$, is (Eq. C.10)

$$\mu_{s\ell} = 0.8\left[\frac{0.0555(1-0.2)}{0.66} + \frac{0.392(0.2)}{5.1}\right] = 0.0661 \text{cm}^{-1}$$

and for the Co–60 source, the attenuation coefficient is

$$\mu_{s\ell} = 0.8\left[\frac{0.0421(1-0.2)}{0.66} + \frac{0.272(0.2)}{5.1}\right] = 0.0494 \text{cm}^{-1}$$

Next, the gas holdup at the given location may be obtained for each source using Eq. C.9. For the Cs–137 source, the gas holdup at radial position number 4 at a height of 1.5 m (see Figure C.1) is

$$\epsilon_g = 1 + \frac{\ln(815 \, / \, 2273)}{(19.85)(0.0661)} = 0.22$$

and for the Co–60 source

$$\epsilon_g = 1 + \frac{\ln(1818 \, / \, 3981)}{(20.07)(0.0494)} = 0.21$$

<u>Axial and Average Gas Holdups</u>

Gas holdups are calculated from the data obtained at each measurement location, and these holdups are then used to estimate the axial gas holdup at a given height and subsequently the average gas holdup in the column using the procedures described previously.

APPENDIX D

SAMPLE CALCULATION FOR ANALYSIS OF DGD DATA

Sample calculations are presented for obtaining rise velocities, gas holdup of slugs and small bubbles, and Sauter mean bubble diameters for Types 1, 2, and 3 interactive disengagement.

Type 1 Interactive Disengagement

Figure D.1 represents DGD data that would be obtained from a pressure transducer. For simplicity, it is assumed that the first slug disengages at time t = 0 (i.e. $t_{start} = 0$). The DGD curve presented in this example closely resembles the actual DGD data shown in Figure 5.22d. Table D.1 lists the heights and time at each breakpoint assuming that small bubbles disengage in between the passage of slugs. The data has been chosen such that the slope of the disengagement curves during slug disengagement is the same for all slugs (i.e. S_2 = -14.1 cm/s). Likewise, the slope of the disengagement curve between slugs is assumed to be the same (i.e. S_1 = -0.37 cm/s). The slope of the disengagement curve during the last period of disengagement, S_3, is -1.66 cm/s.

For this example, we have assumed that the pressure transducer is located 185 cm above the distributor, and the cross sectional area of the column is 19.635 cm.

Calculations

Determination of Rise Velocities

The first step in analyzing the data is the determination of the rise velocity of the slugs and small bubbles. From Eq. 5.27,

$$u_{bL} = H_{DP} / t_{lastslug} = H_{DP} / t_5$$

the rise velocity of the slugs is

$$u_{bL} = 185 / 4.97 = 30 cm / s$$
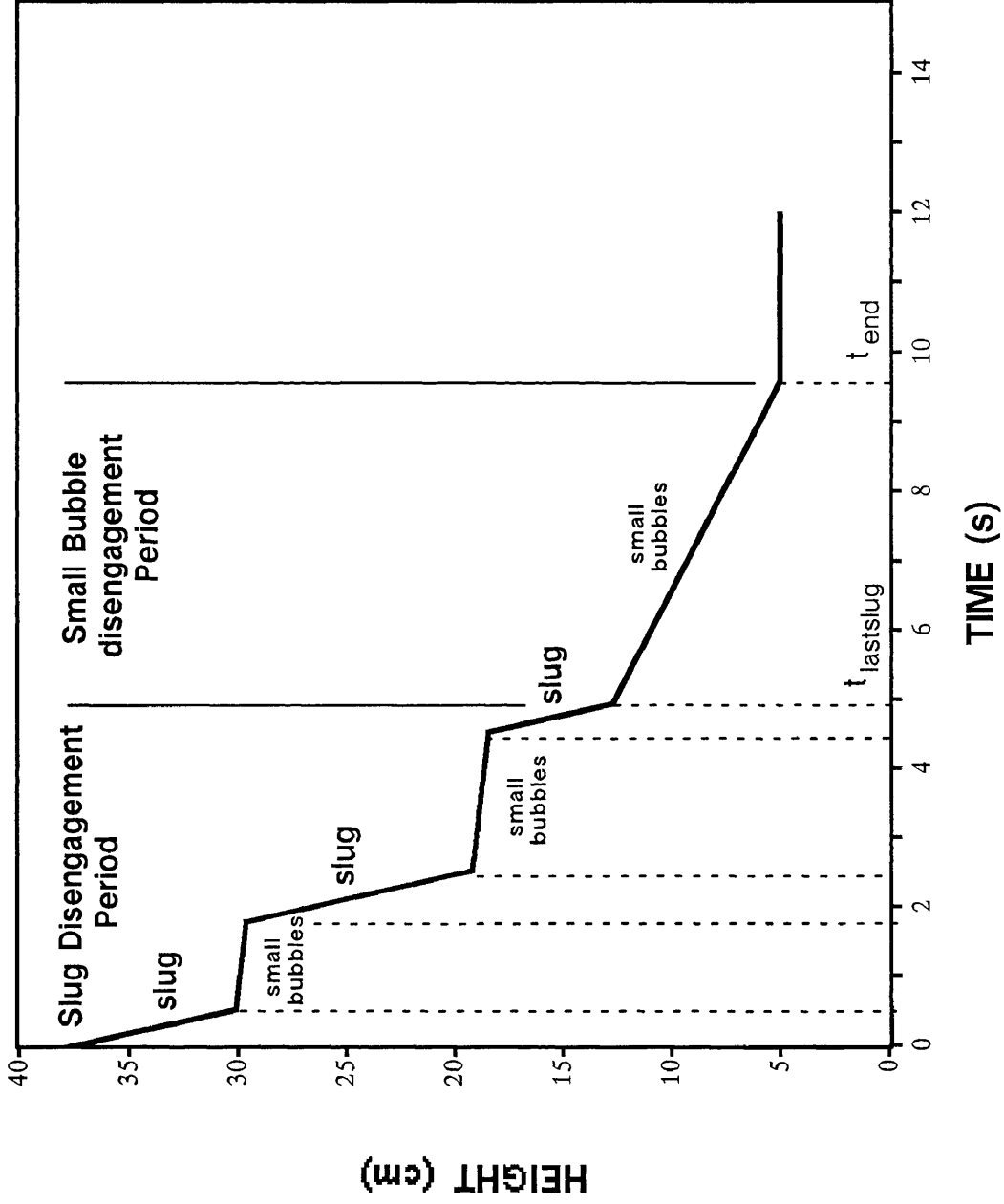
Figure D.1. Dynamic gas disengagement curve for Type 1 interactive disengagement.

Table D.1. Data Points for Type 1 Interactive Disengagement

No.	t (s)	H (cm)	Δ H (cm)	Δ t (s)	Slope (cm/s)
0	0	37.9			
			−8.6	0.545	−14.1
1	0.545	30.2			
			−0.47	1.27	−0.39
2	1.82	29.73			
			−10.43	0.74	−14.1
3	2.56	19.3			
			−0.74	2.0	−0.37
4	4.56	18.6			
			−5.76	0.41	−14.1
5	4.97	12.8			
			−7.70	4.63	−1.66
6	9.6	5.1			

Note: for calculations, S_2 is −14.1, S_1 is −0.37, and S_3 is −1.66

Similarly, the rise velocity of the small bubbles is (see Eq. 5.28)

$$u_{bs} = H_{DP} / t_{end} = H_{DP} / t_6$$

$$u_{bs} = 185 / 9.6 = 19.3 cm / s$$

Determination of ϵ_{gs} During Slug Disengagement

The next quantity that is needed is the volume fraction of small bubbles, ϵ_{gs}, in the dispersion that disengage in between the passage of slugs. It is assumed that this volume fraction also corresponds to the volume fraction of bubbles in the dispersion that is associated with the small bubbles which are forced downward during the passage of slugs. From Eq. 5.29

$$\epsilon_{gs} = \frac{-S_1}{u_{bs}}$$

$$\epsilon_{ga} = \frac{0.37}{19.3} = 0.192$$

Determination of A_{slug}, f_s, and f_{slug}

For Type 1 interactive disengagement, it is possible to determine a value for the cross–sectional area of the slug, A_{slug}. Once this quantity is known, the fraction of the cross sectional area occupied by the slug, f_{slug} and the fraction of the cross sectional area occupied by the dispersion may be determined. From Eq. 5.30, the cross sectional area of the slug is

$$A_{slug} = \frac{A_x(S_2 + u_{bs}\epsilon_{gs})}{-u_{bL}(1 - \epsilon_{gs}) + u_{bs}\epsilon_{gs}}$$

$$A_{slug} = \frac{(19.635)(-14.1 + 19.3(0.0192))}{-30(1 - 0.0192) + 19.3(0.0192)} = 9.28 cm^2$$

The volume fraction of the slug is simply

$$f_{slug} = \frac{A_x - A_{slug}}{A_x}$$

$$f_{slug} = \frac{19.635 - 9.28}{19.635} = 0.53$$

and the volume fraction of the dispersion is

$$f_s = 1 - f_{slug}$$

$$f_s = 1 - 0.53 = 0.47$$

Determination of the Gas Holdup of Small Bubbles in the Dispersion During the Final Period of Disengagement

The last quantity needed before volumes may be calculated in the gas holdup of small bubbles in the dispersion during the final period of disengagement, ϵ'_{gs}. This quantity is defined as (see Eq. 5.31)

$$\epsilon'_{gs} = \frac{-S_3}{u_{bs}}$$

$$\epsilon'_{gs} = \frac{1.66}{19.3} = 0.086$$

Determination of the Total Volume of the Dispersion

The total volume of the dispersion below the pressure transducer, V_T, is (see Eq. 5.32)

$$V_T = H_{DP}A_x$$

$$V_T = (185)(19.635) = 3632.5 cm^3$$

Determination of the Volume of Small Bubbles which Enter the Dispersion Below the Pressure Transducer as the Slugs Exit

Since there are three slugs in this example, all with different lengths, we must determine the volume of each slug. The governing equation for this calculation is (see Eq. 5.33)

$$V_{sb_i} = (u_{bs}f_s - u_{bL}f_{slug})\epsilon_{gs}A_x\Delta t_i$$

For the first slug (i.e. between times of 0 s and 0.545 s)

$$V_{sb_1} = [(19.3)(0.53) - (30)(0.47)](0.0192)(19.635)(0.545) = -0.795 cm^3$$

The "negative" volume implies that bubbles are entering the dispersion below the pressure transducer (i.e. the bubbles are traveling downward). For the second slug (i.e. between times of 1.82 s and 2.56 s)

$$V_{sb_2} = [(19.3)(0.53) - (30)(0.47)](0.0192)(19.635)(0.74) = -1.08 cm^3$$

And finally, for the last slug (between times of 4.56 s and 4.97 s)

$$V_{sb_3} = [(19.3)(0.53) - (30)(0.47)](0.0192)(19.635)(0.41) = -0.598 cm^3$$

Having determined the volume of small bubbles which enters the dispersion below the pressure transducer due to the passage of each slug, the total volume of small bubbles that enter the dispersion is simply the sum of the three individual volumes (see Eq. 5.34)

$$V_{sb_{slug}} = \sum_i V_{sb_i} \qquad i = 1 to 3$$

$$V_{sb_{slug}} = -0.795 - 1.08 - 0.598 = -2.473 cm^3$$

Determination of the Volume of Small Bubbles which Leave the Dispersion in Between the Passage of Slugs

Since there were three slugs, and the first slug disengaged at time t = 0, there will be two periods in between the passage of slugs. The volume of small bubbles which exit the dispersion in between the passage of slugs is given by Eq. 5.35

$$V_{sb_j} = u_{bs} \epsilon_{gs} A_x \Delta t_j$$

During the period between the first two slugs (i.e. between times of 0.545 s and 1.82 s), the volume of small bubbles which exits the system is

$$V_{sb_1} = (19.3)(0.0192)(19.635)(1.27) = 9.24 cm^3$$

And in between the passage of the second and third slugs (i.e. between times of 2.56 s and 4.56 s), the volume of small bubbles leaving the dispersion is

$$V_{sb_2} = (19.3)(0.0192)(19.635)(2) = 14.55 cm^3$$

Thus, the total volume of small bubbles that exit the dispersion in between the passage of slugs is

$$V_{sb_{between}} = \sum_i V_{sb_j} \qquad i = 1 to 2$$

$$V_{sb_{between}} = 9.24 + 14.55 = 23.79 cm^3$$

Determination of the Volume of Small Bubbles which Leave the Dispersion After the Passage of Slugs

The volume of small bubbles which exit the dispersion during the final period of disengagment (i.e. between times of 4.97 s and 9.6 s) is given by Eq. 5.37

$$V_{sb_{last}} = u_{bs} \epsilon'_{gs} A_x \Delta t_{last}$$

$$V_{sb_{last}} = (19.3)(0.086)(19.635)(4.63) = 150.9 cm^3$$

Determination of the Total Volume of Small Bubbles

The total volume of small bubbles which were in the dispersion below the pressure transducer at time t = 0 (i.e. steady state operation) is (see Eq. 5.38)

$$V_{sb_{total}} = V_{sb_{slug}} + V_{sb_{between}} + V_{sb_{last}}$$

$$V_{sb_{total}} = -2.473 + 14.55 + 150.9 = 162.977 cm^3$$

Determination of the Volume Fraction of Small Bubbles at Steady State

The volume fraction of small bubbles in the column (belwo the pressure transducer) at steady state, ϵ_{gos} is simply the total volume of small bubbles, $V_{sb_{total}}$ divided by the total volume of the dispersion below the pressure transducer, V_T (see Eq. 5.39)

$$\epsilon_{gos} = \frac{V_{sb_{total}}}{V_T}$$

$$\epsilon_{gos} = \frac{162.977}{3632.5} = 0.0448$$

Determination of the Total Gas Holdup

In order to determine the gas holdup associated with the slugs, we must first determine the total gas holdup below the pressure transducer. The total gas holdup is simply the total change in height divided by the height of the pressure transducer.

$$\epsilon_g = \frac{H_6 - H_0}{H_{DP}}$$

$$\epsilon_g = \frac{(37.9 - 5.1)}{185} = 0.177$$

Determination of the Volume Fraction of Slugs at Steady State

The volume fraction of slugs at steady state is simply the difference betwee the total gas holdup and the gas holdup of small bubbles at steady state (see Eq. 5.40)

$$\epsilon_{goL} = \epsilon_g - \epsilon_{gos}$$

$$\epsilon_{goL} = 0.177 - 0.0448 = 0.132$$

Determination of the Sauter Mean Bubble Diameter

In order to determine the Sauter mean bubble diameter, we must first calculate the size of both small bubbles and slugs. For simplicity, we will assume that the size of small bubbles is 1.4 mm and the slugs are 50 mm in diameter (i.e. the column diameter). The Sauter mean bubble diameter is calculated using Eq. 5.49

$$d_s = \frac{\epsilon_g}{\sum_{i=1}^{2} \epsilon_{goi} / d_{Bi}}$$

$$d_s = \frac{0.177}{0.0448 / 1.4 + 0.132 / 50} = 5.1 mm$$

Type 2 Interactive Disengagement

For Type 2 interactive disengagement, we assume that no small bubbles disengage in between the passage of slugs. Table D.2 lists the data used for this example. In essence, we have used essentially the same disengagement profile that was used in the first example; except it is assumed that the slope of the disengagement curve in between the passage of slugs, S_2, is 0.

Calculations

The rise velocity of small bubbles and slugs remains the same, i.e. 19.3 and 30 cm/s, respectively. The volume of the dispersion, height of the pressure transducer and cross sectional area of the column are also the same as those used for Type I interactive disengagement, i.e. 3632.5 cm^3, 185 cm, and 19.635, respectively. The slopes of the disengagement curves are approximately -14.8 cm/s (slug disengagement, S_2), and -1.66 cm/s (small bubble disengagement after the last slug disengages, S_3).

Determination of ϵ_{gs} During Slug Disengagement

For Type 2 interactive disengagement, the value of ϵ_{gs} is not as easily determined. In order to calculate ϵ_{gs}, we must assume a value for the fraction of the cross sectional area occupied by the slugs, f_{slug}. Based on our visual observations of slugs in the column, we will assume that f_{slug} is 0.5. This implies that f_s is also 0.5. The volume fraction of small bubbles in the dispersion around the slug is (see Eq. 5.41)

$$\epsilon_{gs} = \frac{S_2 + u_{bL}f_{slug}}{u_{bL}f_{slug} - u_{bs}f_s}$$

$$\epsilon_{gs} = \frac{-14.8 + (30.0)(0.5)}{(30.0 * 0.5 - 19.3 * 0.5)} = 0.037$$

Determination of the Volume of Small Bubbles which Enter the Dispersion Below the Pressure Transducer as the Slugs Exit

Since there are three slugs in this example, all with different lengths, we must determine the volume of each slug. The governing equation for this calculation is (see

Table D.2. Data Points for Type 2 Interactive Disengagement

No.	t (s)	H (cm)	Δ H (cm)	Δ t (s)	Slope (cm/s)
0	0	37.9			
			-7.94	0.545	-14.56
1	0.545	29.965			
			0.0	1.27	0.0
2	1.82	29.965			
			-11.015	0.74	-14.88
3	2.56	18.95			
			0.0	2.0	0.0
4	4.56	18.95			
			-6.15	0.41	-15.0
5	4.97	12.8			
			-7.70	4.63	-1.66
6	9.6	5.1			

Note: for calculations, S_2 is -14.8, S_1 is 0.0, and S_3 is -1.66

Eq. 5.33)

$$V_{sb_i} = (u_{bs}f_s - u_{bL}f_{slug})\epsilon_{gs}A_x\Delta t_i$$

For the first slug (i.e. between times of 0 s and 0.545 s)

$$V_{sb_1} = [(19.3)(0.5) - (30)(0.5)](0.037)(19.635)(0.545) = -2.14 cm^3$$

The "negative" volume implies that bubbles are entering the dispersion below the pressure transducer (i.e. the bubbles are traveling downward). For the second slug (i.e. between times of 1.82 s and 2.56 s)

$$V_{sb_2} = [(19.3)(0.5) - (30)(0.5)](0.037)(19.635)(0.74) = -2.91 cm^3$$

And finally, for the last slug (between times of 4.56 s and 4.97 s)

$$V_{sb_3} = [(19.3)(0.5) - (30)(0.5)](0.037)(19.635)(0.41) = -1.61 cm^3$$

Having determined the volume of small bubbles which enters the dispersion below the pressure transducer due to the passage of each slug, the total volume of small bubbles that enter the dispersion is simply the sum of the three individual volumes (see Eq. 5.34)

$$V_{sb_{slug}} = \sum_i V_{sb_i} \qquad i = 1 to 3$$

$$V_{sb_{slug}} = -2.14 - 2.91 - 1.61 = -6.66 cm^3$$

Determination of the Volume of Small Bubbles which Leave the Dispersion After the Passage of Slugs

The volume of small bubbles which exit the dispersion during the final period of disengagment (i.e. between times of 4.97 s and 9.6 s) is given by Eq. 5.37

$$V_{sb_{last}} = u_{bs}\epsilon'_{gs}A_x\Delta t_{last}$$

$$V_{sb_{last}} = (19.3)(0.086)(19.635)(4.63) = 150.9 cm^3$$

Determination of the Total Volume of Small Bubbles

The total volume of small bubbles which were in the dispersion below the pressure transducer at time t = 0 (i.e. steady state operation) is (see Eq. 5.38)

$$V_{sb_{total}} = V_{sb_{slug}} + V_{sb_{between}} + V_{sb_{last}}$$

$$V_{sb_{total}} = -6.66 + 150.9 = 144.24 cm^3$$

Determination of the Volume Fraction of Small Bubbles at Steady State

The volume fraction of small bubbles in the column (belwo the pressure transducer) at steady state, ϵ_{gos} is simply the total volume of small bubbles, $V_{sb_{total}}$ divided by the total volume of the dispersion below the pressure transducer, V_T (see Eq. 5.39)

$$\epsilon_{gos} = \frac{V_{sb_{total}}}{V_T}$$

$$\epsilon_{gos} = \frac{144.24}{3632.5} = 0.04$$

Determination of the Total Gas Holdup

In order to determine the gas holdup associated with the slugs, we must first determine the total gas holdup below the pressure transducer. The total gas holdup is simply the total change in height divided by the height of the pressure transducer.

$$\epsilon_g = \frac{H_6 - H_0}{H_{DP}}$$

$$\epsilon_g = \frac{(37.9 - 5.1)}{185} = 0.177$$

Determination of the Volume Fraction of Slugs at Steady State

The volume fraction of slugs at steady state is simply the difference betwee the total gas holdup and the gas holdup of small bubbles at steady state (see Eq. 5.40)

$$\epsilon_{goL} = \epsilon_g - \epsilon_{gos}$$

$$\epsilon_{goL} = 0.177 - 0.04 = 0.137$$

Determination of the Sauter Mean Bubble Diameter

In order to determine the Sauter mean bubble diameter, we must first calculate the size of both small bubbles and slugs. For simplicity, we will assume that the size of small bubbles is 1.4 mm and the slugs are 50 mm in diameter (i.e. the column diameter). The Sauter mean bubble diameter is calculated using Eq. 5.49

$$d_s = \frac{\epsilon_g}{\displaystyle\sum_{i=1}^{2} \epsilon_{goi} / d_{Bi}}$$

$$d_s = \frac{0.177}{0.04 / 1.4 + 0.137 / 50} = 5.7 \text{mm}$$

This approach is fairly sensitive to the value of f_{slug} that is used. For example, if we assume that the diameter of the slug is equal to 90 % of the column diameter, then f_{slug} is approximately 0.8 as opposed to 0.5. If we had used a value of 0.8 for f_{slug}, then the Sauter mean diameter would have been 10 mm as opposed to 5.7 mm. Thus, if this approach is used, one must have a good estimate for f_{slug}.

Type 3 Interactive Disengagement

Type 3 interactive disengagement is the simplest of all three. The only information that is needed to determine the volume fraction of small bubbles and slugs is the major breakpoints (i.e. at the end of slug disengagement and at the end of small bubble disengagement).

The volume fraction of small bubbles is simply (see Eq. 5.44)

$$\epsilon_{gos} = \frac{H_t(\text{lastslug}) - H_t(\text{end})}{H_{DP}}$$

$$\epsilon_{gos} = \frac{12.8 - 5.1}{185} = 0.0415$$

The volume fraction of slugs is

$$\epsilon_{goL} = \epsilon_g - \epsilon_{gos}$$

$$\epsilon_{goL} = 0.177 - 0.0416 = 0.135$$

And the Sauter mean bubble diameter is calculated using the same procedure described previously (note: rise velocities, needed to determine bubble sizes, are the same as those previously given)

$$d_s = \frac{\epsilon_g}{\sum_{i=1}^{2} \epsilon_{goi} / d_{Bi}}$$

$$d_s = \frac{0.177}{0.0416 / 1.4 + 0.135 / 50} = 5.5 mm$$